Quantification of metabolic interactions between microorganisms

Dissertation

accepted by the Faculty of
Energy-, Process- and Bio-Engineering of the University of Stuttgart
in partial Fulfilment of the Requirements for the Degree of
Doctor of Natural Sciences (Dr. rer. nat.)

by

Andreas Ulmer

born in Esslingen am Neckar

Supervisor:	Prof. Ralf Takors
Co-Examiner:	Prof. Bas Teusink
Day of Exam:	31st January 2024

Institute of Biochemical Engineering
University of Stuttgart
Year of Publication 2024

The Tables Turned by William Wordsworth

Up! up! my Friend, and quit your books;
Or surely you'll grow double:
Up! up! my Friend, and clear your looks;
Why all this toil and trouble?

The sun, above the mountain's head,
A freshening lustre mellow
Through all the long green fields has spread,
His first sweet evening yellow.

Books! 'tis a dull and endless strife:
Come, hear the woodland linnet,
How sweet his music! on my life,
There's more of wisdom in it.

And hark! how blithe the throstle sings!
He too, is no mean preacher:
Come forth into the light of things,
Let Nature be your Teacher.

She has a world of ready wealth,
Our minds and hearts to bless –
Spontaneaous wisdom breathed by health,
Truth breathed by cheerfulness.

One impulse from the vernal wood
May teach you more of man,
Of moral evil and of good,
Than all the sages can.

Enough of Science and of Art;
Close up the barren leaves;
Come forth, and bring with you a heart
That watches and receives.

Declaration of Authorship

I, Andreas Ulmer, declare that this dissertation titled "Quantification of metabolic interactions in microbial communities" and the work presented in it are my own.
I confirm that:

- This work was done wholly or mainly while in candidature for a research degree at this University.

- Where any part of this dissertation has previously been submitted for a degree or any other qualification at this University or any other institution, this has been clearly stated.

- Where I have consulted the published work of others, this is always clearly attributed.

- Where I have quoted from the work of others, the source is always given. With the exception of such quotations, this dissertation is entirely my own work.

- I have acknowledged all main sources of help.

- Where the dissertation is based on work done by myself jointly with others, I have made clear exactly what was done by others and what I have contributed myself.

Date & Sign

Abstract

Microbial communities provide the potential to support, reorganise, and design complex biological processes. However, interactions among microorganisms have not yet been fully explored. Hence, this work draws a line from the benefits available in microbial communities, over existing techniques studying systems with interacting cells, to a newly developed compartmentalized fermentation system. The further developing food industry, white biotechnology, and sustainability concepts demand new bioprocesses. Thus, understanding microbial interactions, how to quantify molecules exchanged among microorganisms, and the development of techniques with which to analyse microbial communities require further exploration. Biological systems involving one bacterial strain (mono-culture) have been investigated in detail and applied to biotechnology. However, less is understood about systems comprising two (co-culture) or more bacterial strains (community).

The relevant driving issues are how to determine and quantify intra- and intercellular fluxes and which tools can be applied to improve co-culture technology. Different cell strains in a co-culture or microbial community might consume or produce the same molecules, which impedes strain-specific mapping. State-of-the-art methods are not generally applicable to individual analyses of co-cultured bacterial strains. This hinders the establishment of predictive models for microbial interactions due to missing strain-specific data.

Therefore, this dissertation considers three strategies for co-culture analysis. The first outlines ^{13}C-MFA to calculate intra- and intercellular metabolic fluxes. The second strives for strain-specific characterisation of a co-culture after cell inactivation and separation. The third attempts the quantification of strain-specific fluxes in a two-compartment fermentation system.

This leads to the following results:

- Metabolic interactions between *S. thermophilus* and *L. bulgaricus* were quantified under defined conditions. The results showed that amino acid release rates in co-

cultures were not equivalent to the sum of these rates in individual cultures. A genome-scale and a pH-dependent kinetic model of *L. bulgaricus* were created using experimental datasets. Simulations using the kinetic model explained the faster growth of *L. bulgaricus* in a medium containing casein via preferred uptake and enabled the prediction of acidification profiles during cultivation.

- The potential of compartmentalised mathematical models comprising two interlinked metabolic networks to reveal flux distribution was determined. Differences in simulated flux profiles exploiting and ignoring compartment-specific data, such as those of cytosol and mitochondria were investigated. Although cellular analysis provided good estimates of most intracellular fluxes in the two compartments when non-compartment-specific data were derived from IgG1-producing Chinese hamster ovary cells, some fluxes widely differed. Accurate flux estimation of almost all isoenzymes depends on the presence of subcellular labelling information. Hence, compartment-specific ^{13}C analysis is a prerequisite for identifying compartment-specific flux distributions.

- Cells were rapidly heat-inactivated to stop metabolic activity and obtain precise metabolomic data. A developed inactivation device comprised a thin capillary encased in an aluminium block. A retention time of 0.1 s at 160 °C was sufficient to stop metabolic activity of *L. bulgaricus* while maintaining membrane integrity. However, the medium contained casein, which clogged the capillary, rendering this system unsuitable for inactivating lactic acid bacteria.

- The novel compartmentalised cultivation system presented herein enabled the investigation of interactions between two microbial strains at the metabolic level. A membrane separating the two compartments allowed for the exchange of amino acids and peptides between the strains but retained the biomass. The two compartments enabled quantification of strain-specific production and consumption rates of amino acids in interacting *S. thermophilus-L. bulgaricus* co-cultures.

The major topic of this dissertation is the quantification of metabolic interactions between microorganisms, in particular *S. thermophilus* and *L. bulgaricus*. Using several strategies, this work expands theoretical and experimental methods, and applies a new bioprocess. The data led to the conclusion that behavior differs between mono- and co-cultured cells. Hence, understanding co-cultures as well as microbial communities using mechanistic and data-driven modelling requires a basis of experimental data. The methods and results presented herein elevate extant co-culture technology, enable a more detailed picture of intercellular metabolic activity, and promote economic and ecological applications involving the benefits of microbial interactions.

Zusammenfassung

Mikrobielle Gemeinschaften bieten das Potenzial, komplexe biologische Prozesse zu unterstützen, zu reorganisieren und zu entwickeln. Die Interaktionen zwischen den Mikroorganismen sind jedoch noch nicht vollständig erforscht. Daher erstreckt sich diese Arbeit von den Vorteilen, die mikrobielle Gemeinschaften bieten, über bestehende Techniken, die Systeme mit interagierenden Zellen untersuchen, bis hin zu einem neu entwickelten kompartimentierten Fermentationssystem. Die sich weiterentwickelnde Lebensmittelindustrie, die weiße Biotechnologie und Nachhaltigkeitskonzepte suchen nach neuen Bioprozessen. Daher sollen mikrobielle Interaktionen, die Quantifizierung der zwischen den Mikroorganismen ausgetauschten Moleküle und die Entwicklung von Techniken zur Analyse der mikrobiellen Gemeinschaften weiter erforscht werden. Biologische Systeme mit einem Bakterienstamm (Monokultur) sind eingehend untersucht und in biotechnologischen Prozessen angewandt worden. Systeme, die zwei (Kokultur) oder mehr Bakterienstämme (Gemeinschaft) umfassen, werden selten berücksichtigt.

Dabei geht es um die Frage, wie intra- und interzelluläre Flüsse bestimmt und quantifiziert werden können und welche Techniken zur Verbesserung der Kokultur-Technologie eingesetzt werden können. Verschiedene Zellstämme in einer Kokultur oder mikrobiellen Gemeinschaft können dieselben Moleküle aufnehmen oder produzieren, was eine stamm-spezifische Zuordnung erschwert. Methoden, die dem neuesten Stand der Technik entsprechen, sind im Allgemeinen nicht auf individuelle Analysen von kokultivierten Bakterienstämmen anwendbar. Dies erschwert die Erstellung von Modellen zur Vorhersage von mikrobiellen Interaktionen durch fehlende stamm-spezifischer Daten.

In dieser Dissertation werden daher drei Strategien für die Analyse von Kokulturen betrachtet. In der ersten wird die ^{13}C Metabolische Flussanalyse zur Berechnung der intra- und interzellulären Stoffwechselflüsse vorgestellt. In der zweiten wird eine stamm-spezifische Charakterisierung einer Kokultur nach Zellinaktivierung und -trennung angestrebt. Die dritte Strategie versucht die Quantifizierung stamm-spezifischer Flüsse in einem Zwei-

Kompartiment-Fermentierungssystem.

Dies führt zu den folgenden Ergebnissen:

- Die metabolischen Interaktionen zwischen *S. thermophilus* und *L. bulgaricus* wurden unter definierten Bedingungen quantifiziert. Das Ergebnis zeigt, dass die Produktionsraten von Aminosäuren in Kokulturen nicht den Summen dieser Raten in Monokulturen entsprechen. Ein genomisches und ein pH-abhängiges kinetisches Modell von *L. bulgaricus* wurden mit Hilfe von experimentellen Daten erstellt. Simulationen des kinetischen Modells erklärten das schnellere Wachstum von *L. bulgaricus* in kaseinhaltigem Medium durch höhere Aufnahmeraten und ermöglichten die Vorhersage von Ansäuerungsprofilen während einer Kultivierung.

- Um das Verhalten von Kokulturen vorherzusagen, wurde das Potenzial von kompartimentierten mathematischen Modellen, die zwei miteinander verknüpfte Stoffwechselnetzwerke umfassen, zur Entschlüsselung von Flussverteilungen erforscht. Untersucht wurden die Unterschiede zwischen simulierten Flussprofilen, die kompartimentspezifische Daten, wie die des Zytosols und der Mitochondrien berücksichtigen, und solchen, die sie ignorieren. Obwohl die Zellanalyse eine gute Schätzung der meisten intrazellulären Flüsse in den beiden Kompartimenten lieferte, wenn nicht kompartiment-spezifische Daten von IgG1-produzierenden Ovarialzellen des chinesischen Hamsters verwendet wurden, wichen einige Flüsse stark voneinander ab. Die Güte der Flussberechnung fast aller Isoenzyme hängt von vorhandenen Informationen über die subzelluläre Markierung ab. Daher schafft die kompartiment-spezifische ^{13}C-Markierungsanalyse eine Voraussetzung für die Ermittlung kompartiment-spezifischer Flussverteilungen.

- Um präzise Metabolomdaten zu erhalten, wurden Zellen schnell hitzeinaktiviert und dadurch deren Stoffwechselaktivität gestoppt. Eine entwickelte Inaktivierungsvorrichtung bestand aus einer dünnen Kapillare, die von einem Aluminiumblock umschlossen war. Eine Verweilzeit von 0,1 s bei 160 °C genügte, um die Stoffwechselaktivität von *L. bulgaricus* zu stoppen und gleichzeitig die Membranintegrität zu erhalten. Die Verwendung eines Kultivierungsmedium mit Kasein führte jedoch zur Verstopfung der Kapillare. Daher war die Vorrichtung nicht für die Inaktivierung von Milchsäurebakterien geeignet.

- Das hier vorgestellte, neuartige und zwei Kompartimente umfassende Kul-

tivierungssystem ermöglichte die Untersuchung der Interaktionen zwischen zwei Mikrobenstämmen auf der Stoffwechselebene. Eine Membran, die beide Kompartimente trennt, ermöglichte den Austausch von Aminosäuren und Peptiden zwischen den Stämmen und verhindert die Vermischung der beiden Zelltypen. Die beiden Kompartimente ermöglichten die Quantifizierung der stamm-spezifischen Produktions- und Aufnahmeraten von Aminosäuren in interagierenden *S. thermophilus*-*L. bulgaricus* Kokulturen.

Das übergeordnete Forschungsthema dieser Dissertation ist die Quantifizierung der metabolischen Interaktion zwischen Mikroorganismen, im Speziellen von *S. thermophilus* und *L. bulgaricus*. Dies wurde in mehreren Strategien angestrebt, die theoretische und experimentelle Methoden und ein neues Fermentationssystem umfassen. Die Daten führten zu der Schlussfolgerung, dass sich das Verhalten zwischen mono- und kokultivierten Zellen unterscheidet. Um Kokulturen und mikrobielle Gemeinschaften mit Hilfe mechanistischer und daten-basierter Modellierung zu verstehen, bedarf es daher grundlegender experimenteller Daten. Die hier vorgestellten Methoden und Ergebnisse erweitern die bestehenden Arbeiten zu Kokulturen, schaffen ein detaillierteres Bild der interzellulären Stoffwechselaktivität und fördern wirtschaftliche und ökologische Anwendungen, die die Vorteile der mikrobiellen Interaktionen nutzen.

Contents

List of Figures

List of Tables

List of Abbreviations

Da Damkoehler number

HPLC High-performance liquid chromatography

MS Mass spectrometry

SMaa Synthetic medium supplemented with amino acids

SMcas Synthetic medium supplemented with casein

MRS Man–Rogosa–Sharpe

2cs Two-compartment system

LAB Lactic acid bacterium

EPS Exopolysaccharides

GEMs Genome-scale metabolic models

CDW Cell dry weight

BOF Biomass objective function

PPP Pentose phosphate pathway

TCA Trycarboxylic acid

Opp Oligopeptide transport system

MILP Mixed integer linear programming

FVA Flux variability analysis

13C-MFA 13C-metabolic flux analysis

CHO Chinese hamster ovary

ME Malic enzymes

L. bulgaricus *Lactobacillus delbrueckii* subsp. *bulgaricus*

LB *Lactobacillus delbrueckii* subsp. *bulgaricus*

S. thermophilus *Streptococcus thermophilus*

ST *Streptococcus thermophilus*

FBA Flux Balance Analysis

MFA Metabolic flux analysis

SSD Sum of squared differences

CFU Colony forming units

qPCR Quantitative polymerase chain reaction

IU Inactivation unit

HU Heat unit

CU Cool unit

Chapter 1

Introduction

Predictions indicate that 10^{12} microbial species populate the Earth [168]. An immense number of microorganisms have great potential as powerful tools that can enable many applications [57, 64, 155]. Microbial databases provide information about thousands of enzymes that accelerate various chemical reactions [41, 43], and synthetic biology expands and optimises existing cellular systems [48]. However, microorganisms in natural habitats do not live solitary lives. Cells interact with various organisms and shape environments such as water, soil, and animal intestines [171, 306]. Estimates have indicated more numerous bacterial than other cells in humans [257].

Analysing microbial interactions helps to understand fundamental processes such as bacterial communication [19], enables reshaping for gaining health and environmental benefits [332], plays an essential role in a sustainable economy [266, 272], and opens the door to the application of (synthetic) microbial communities to improved biotechnological applications [113]. Consequently, the application potential of two or more interacting microbes [92, 144] in natural and synthetic co-cultures to industrial use has been investigated [33, 181, 261, 313].

Interacting bacteria in natural or synthetic communities might confer benefits over mono-cultures, because the metabolic burden imposed by processes such as gene expression of desirable compounds is divided among them (fig. 1.1) [93, 197, 317]. Furthermore, the distribution of reaction pathways among bacteria is beneficial because specialised cellular compartments satisfy reaction-specific cofactor and precursor requirements [137],
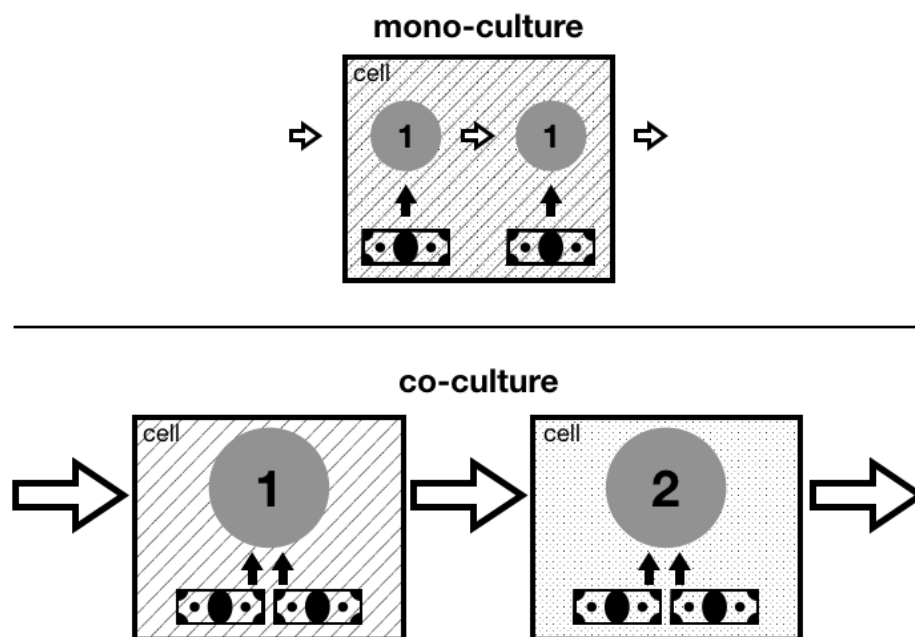
Figure 1.1: Partitioning a reaction cascade comprising cell segments 1 and 2 into different compartments such as bacterial strains, increases metabolic power and establishes advantageous reaction environments that result in increased productivity.

or increase prokaryotic and eukaryotic enzyme activities [330].

Additional advantages, such as reduced control requirements, occur in natural habitats and industrial processes, including interacting microorganisms. For instance, when applied to wastewater treatment, microbial communities [58] are more robust against substrate fluctuations as more metabolic alternatives are available [331]. Their stability is further enhanced by competing interactions between species (fig. 1.2)[50]. Toxic by-products can be immediately degraded by another strain [243], thus increasing the long-term persistence of the process and decreasing amounts of inadvertent products.

Interactions between microorganisms are based on a wide spectrum of chemical molecules [61] that possess huge potential for medical and industrial applications. Deciphering chemically based molecules provides a tool to affect microbial communities for medical purposes and to discover new antibiotics [24, 228, 255]. However, most of these biosynthetic pathways are inactive under mono-culture fermentation conditions [52, 219] and
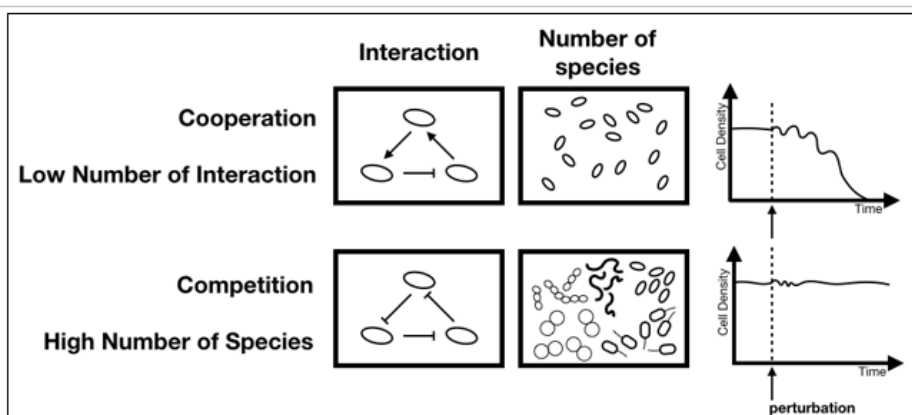
Figure 1.2: The stability of a microbial communities increases with more competitive interspecies interactions and increased numbers of species. Perturbation of a microbial community with insufficient competition or numbers of species (top) and stable responses to perturbation due to sufficient competition or species numbers (bottom). (Adapted from [50])

require co-culture conditions for activation.

The applications involving co-cultures [192, 242] have been extended by recent improvements and include:

- Expansion of strain libraries providing numerous co-culture combinations.

- Discovery of stimulated co-cultured microorganisms that produce antibiotics [24].

- Innovations in synthetic biology enabling designed synthetic co-cultures [95, 151].

- Increased availability of genome-scale models has revealed metabolic potential of many microorganisms [3, 268, 287] and enables reconstruction of metabolic networks in microbial communities [271] to optimise their productivity.

- Enhanced computation power [109] and smartly reduced requirements to compute metabolic models of communities [333].

The rising potential of co-cultures is also indicated by an increase in the number of published reports (fig. 1.3).
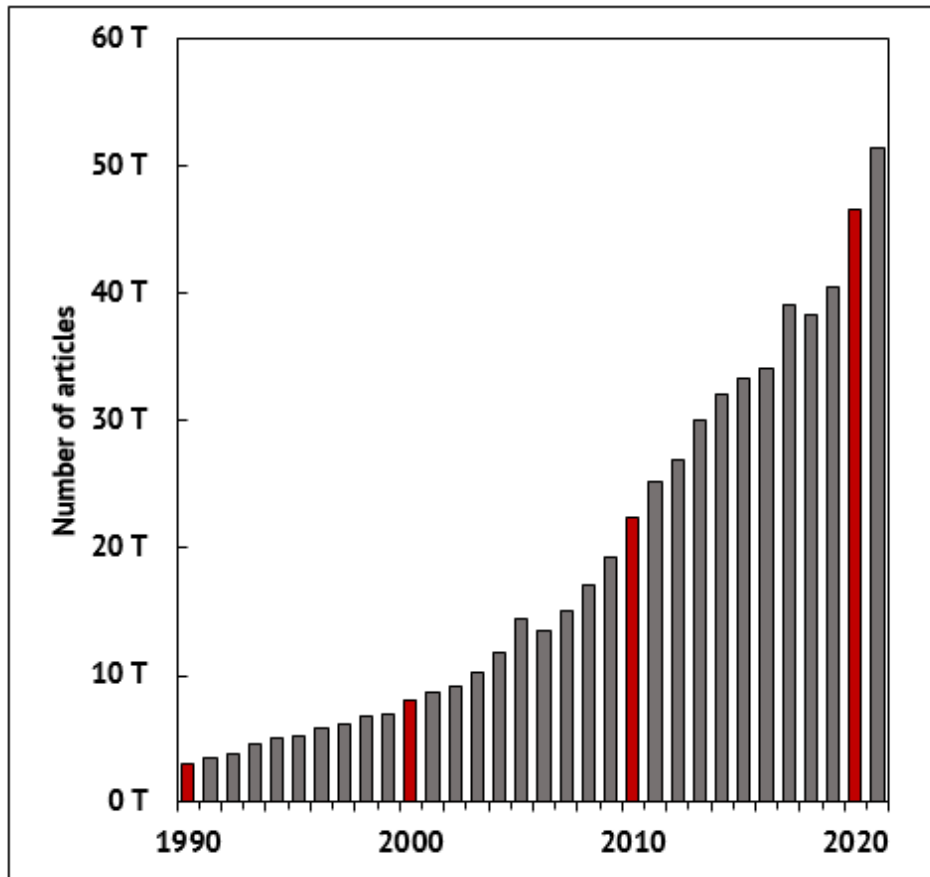
Figure 1.3: Annual increases in numbers of published articles mentioning co-cultures (1990 to 2021). Data were derived from a GoogleScholar search using the terms "co-culture" or "coculture".

1.1 Examples of co-culture processes

Processes that include co-cultures and microbial communities include food, beverage, biogas production, and wastewater treatment [243]. Over the last decade, co-cultures have been applied [71, 82, 210, 298, 324, 334] to produce flavonoids [137], tryptamine [298], 3-amino-benzoic acid [324], caproic acid [117], and anthranilate [191]. These individual co-cultured strains have provided a modular basis for new co-culture combinations, thus reducing the amount of time required for construction, optimisation, and evaluation [305, 324, 330].

1.2 *S. thermophilus-L. bulgaricus* co-cultures

Gram-positive, non-sporulating *L. bulgaricus* and *S. thermophilus* are co-cultured for dairy fermentation [115, 116, 184, 264, 291]. Interactions between these lactic acid bacteria are promoted in food products, such as yogurt, resulting in increased acidification. Various combinations of strains have led to numerous acidification profiles, textures, and tastes. To fully understand molecular exchange between these bacteria in co-cultures requires knowledge of the molecules that they consume and produce [179].

Many *L. bulgaricus* and *S. thermophilus* strains are available. Thus, rapid and reliable methods are needed to characterize strains in mono- and co-cultures; this would pave the way to rational co-culture assembly, fermentation using plant-based substrates [183, 318], and metabolic engineering [122, 124, 297]. Only a small subset of all possible co-culture combinations has been analysed. Thus, comparable experiments quantifying strain-specific rates would lay a foundation for modelling approaches [268] to predict the co-culture properties [105, 108, 110, 271] of *S. thermophilus*, *L. bulgaricus*, and other microorganisms [287].

1.3 Demands of co-culture technology

Several requirements were identified to fully understand and develop the potential of co-cultures (A–E).

(A) The key to realising the potential of co-cultures is the quantification of strain-specific fluxes, enabling the mapping, prediction, and control [174, 229] of highly dynamic co-cultures by mathematical representation [31, 63, 98, 287]. This is difficult to achieve because individual strains in co-cultures often produce or consume the same molecules. Measuring the extracellular concentration profiles does not always reveal strain-specific rates because only cumulated fluxes are measured (fig. 1.4)[251]. Interaction studies have used plating, flow cytometry, and microfluidics [38] to determine the composition of various populations [86, 250]. However, computational approaches rely on strain-specific uptake or consumption rates to reveal flux distribution [268]. Predicting individual growth rates, substrate consumption, and product yields enables the identification of bottlenecks that impede the increased production of target molecules [109, 293]. Furthermore, disclosed and quantified flux distributions are fundamental for metabolic engineering to improve targeted processes [316]. Modelling the molecular basis of interactions by using strain-specific biochemical knowledge and high-throughput molecular data [44] enables the calculation and prediction of molecular exchanges between strains [110].

(B) Efforts in synthetic biology [48] allow for manifold applications of these principles to design new microbial co-cultures [136]. A toolbox of known interacting mechanisms between microorganisms it is essential to design new synthetic co-cultures [176]. However, the identification of further interaction processes can support existing efforts [109, 265, 314] and optimise synthetic co-cultures [95, 278].

(C) Immense libraries of microbial species must be characterised to determine their metabolic potential in co-cultures. Computational methods support the challenging characterisation of all possible combinations [31]. However, they rely on minimum amounts of necessary experiments and data [268]. Such metabolic characterisation of the immense diversity of microbial species [109] opens the door to their potential and enables the smart evolution of co-culture processes.

(D) Maintaining stable coexisting co-culture fermentation is difficult because microorganisms have different growth rates or compete for growth resources, which can result in strain overgrowth [324]. The adjustment of strain-to-strain ratios in co-cultures, particularly during continuous fermentation, is challenging because both strains might be affected. Thus, manipulating population composition is key to co-culture processes [324]. A carefully selected and maintained biomass ratio prevents the washout of a
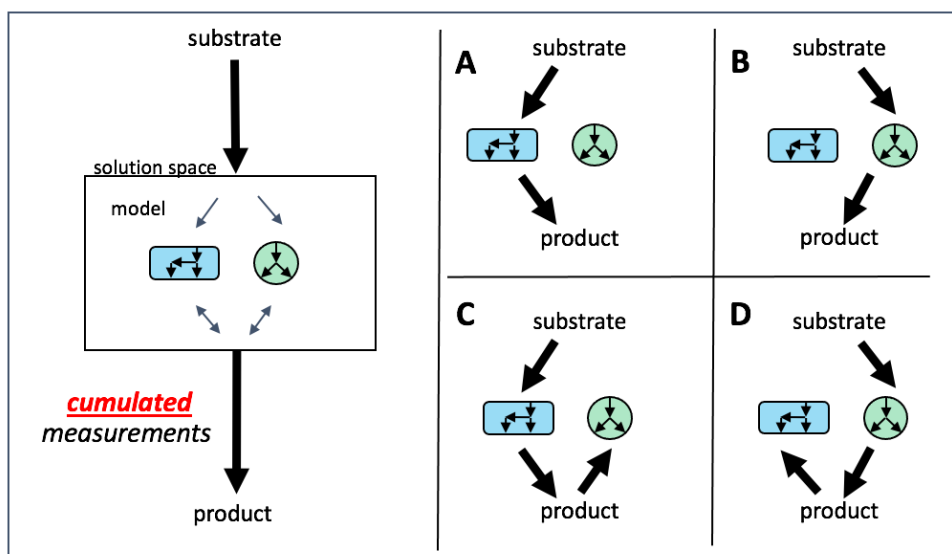
Figure 1.4: Calculation of strain-specific fluxes in co-culture models. Measuring cumulated consumption or production rates to constrain solution space in models is insufficient to calculate strain-specific fluxes as combined substrate uptake or product release is considered. Only strain-specific measurements can reveal individual rates.

strain or the accumulation of intermediates, thus leading to more efficient processes.

(E) To reveal the metabolic activity of microorganisms, uncover interactions between microorganisms, and extend the toolbox of bio-based processes with mono- and co-culture, the performance of reproducible cultivations are fundamental. Especially in co-culture fermentation, protocols and methods for the on-time preparation of all strains are essential. However, they still shows white spots and need to be extended. Well-functioning experimental protocols allow studies of physiological characterisation using genomic, transcriptomic, or proteomic approaches [154, 289, 300]. Profound metabolomic studies serve as a basis for mathematical descriptions such as kinetic or genome-scale models [188].

Three strategies for studying interactions among microorganisms at the molecular level are outlined below to address these needs and gain strain-specific information. Subsequent chapters focus on these strategies and investigate and discuss the realisation using *L. bulgaricus* and *S. thermophilus* as an example.

Table 1.1: Demands to study interactions between microorganisms and to expand applicability of co-culture processes.

	Requirements	Advantages	Chapter
A	Quantification of strain-specific fluxes	Predict, improve, and control co-culture processes	Methods to quantify strain-specific fluxes: chapters 6–8
B	Mechanistic description of interaction processes	Design new synthetic co-cultures	Examples of mechanistic models: chapters 4 and 5. Strategies for co-culture: chapters 6–8
C	Experimental data sets of different co-cultures	Characterize diversity of co-cultures	Datasets of *S. thermophilus*-*L. bulgaricus* co-cultures: chapters 3 and 8. Strain-specific data acquisition: chapters 6–8.
D	Techniques to adjust strain-to-strain ratios	Continuous co-culture fermentation	Co-culture cultivation system: chapter 8
E	Reproducible cultivation conditions for used microorganisms	In-depth metabolomic studies	Experimental methods to cultivate *S. thermophilus* and *L. bulgaricus*: chapters 3 and 7

Right column, chapter: location of information.
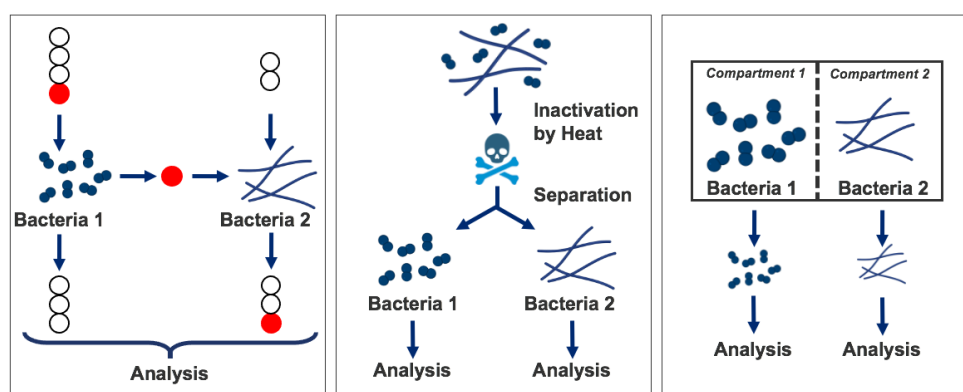
Figure 1.5: Overview of three strategies to reveal strain-specific flux distribution in microbial co-cultures. (Left) ^{13}C Metabolic Flux Analysis based on labelled substrate and product. Circles, carbon atoms. Red circle, one ^{13}Carbon atom. (Center) Cell inactivation and separation to analyse individual strains. (Right) Co-cultures in compartmentalized system enables strain-specific sampling and subsequent analysis. Created with BioRender.com.

1.4 Strategy 1: ^{13}C-Metabolic flux analysis of compartmentalized systems to calculate compartment-specific flux distribution

A sophisticated ^{13}C-MFA [309] was outlined to unravel intracellular flux distribution in co-cultures [322], and its practicability was demonstrated [85, 89] (fig. 1.5, left). However, ^{13}C-MFA might not be universally applicable to all co-culture networks because it contains overlapping metabolic activities [322]. Access to strain-specific measurements can overcome this limitation, but they are difficult to obtain in co-cultures [243]. Chapter 6 describes a ^{13}C-MFA of data comprising two compartments – similar to a co-culture – and highlights the analytical barriers overcome by compartment-specific information. Quantification of stoichiometric networks by ^{13}C MFA does not reveal kinetic information [84, 278, 285], but efforts have been directed towards merging these needs [134, 201, 202]. In addition, information about regulation is lacking. Creating ^{13}C models requires effort and time and ^{13}C labelled substrates can be costly or available only in small amounts.

1.5 Strategy 2: Inactivation, separation and subsequent analysis of individual strains grown in co-culture

A method that consists of cell inactivation, separation, and individual analysis was considered and clarified based on the example of *S. thermophilus* and *L. bulgaricus* to quantify strain-specific flux distribution in co-cultures. As indcated, fig. 1.5, center outlines separation based on morphological differences [269]. Lactic acid bacterial cell inactivation, while simultaneously maintaining cell integrity has not been reported until now. Chapter 7 describes a method for rapidly inactivating *S. thermophilus* and *L. bulgaricus* while maintaining cell integrity.

1.6 Strategy 3: A compartmentalized cultivation system for co-cultures to quantify strain-specific fluxes

Spatially separated co-cultivation enables the sampling of strain-specific information [95], such as intracellular metabolite pools. However, extant microfluidic systems [38, 39, 118], cell culture inserts [120], and cell culture plates [132] do not provide a sufficient volume for analysis. Furthermore, dialysis bioreactors, as reviewed here [221] are promising, but expensive due to the high cost of techniques and media, and assembly is time-consuming, which is a burden when analysing numerous co-cultures. Chapter 8 describes the development and application of a new compartmentalised cultivation system that generates strain-specific information. Continuous cultivation enables strain-specific flux quantification (fig. 1.5, right).

1.7 Alternative strategies for studying interactions among microorganisms

Microdroplets containing individual cells allow high-throughput screening of co-cultures based on extracellular production [114, 279]. Microdroplet production and sorting are inexpensive, but metabolome studies can be impeded by low volumes of droplets and cell numbers.

One type of cells has been immobilised in traps for interaction studies [73]. However, this creates a gradient for the immobilised cell type and does not offer a sufficient biomass for subsequent metabolomics.

Co-cultured cells have been fixed in a hydrogel [6]. However, because gels are not liquid, problems with substrate supply and product allocation can arise, resulting in considerable heterogeneity.

Fluorescence-based sorting enables cell-specific analyses. However, natural co-cultures must first be labelled with fluorescence [239, 260]. This might be possible for synthetic co-cultures, but the expression of fluorescent proteins is a burden on metabolism, and the accumulation of a sufficient biomass for metabolomics might be difficult. Genome editing

is avoided for *S. thermophilus* and *L. bulgaricus* used in organic food production.

1.8 Study objective

The study described herein aimed to quantify flux distribution in co-cultures. Therefore, cultivation methods for *S. thermophilus* and *L. bulgaricus* were developed to enable their growth in mono- and co-cultures. Three strategies were evaluated, discussed, and quantification of flux distributions in interacting *S. thermophilus* and *L. bulgaricus* co-cultures was attempted.

The results will increase physiological understanding and enable co-culture reshaping as well as the use of metabolic engineering to create synthetic co-cultures.

The following chapters illustrate the potential of co-cultures, clarify requirements for co-culture models, describe the development of experimental methods for strain-specific quantification in co-cultures, and present advanced co-culture cultivation technologies.

This dissertation aims to fill four research gaps as outlined in the following section (fig. 1.6).

(i) Chapters 3 to 5, 7 and 8 describe the metabolic potential of *S. thermophilus* and *L. bulgaricus* in mono- and co-cultures determined using experimental methods for reproducible cultivation, biomass determination, metabolite profiling, and strain-specific analysis.

(ii) Chapters 6 to 8 evaluate and discuss these three strategies. Proof-of-concept was attempted to quantify promising flux distribution in interacting co-cultures of *S. thermophilus* and *L. bulgaricus* (chapter 8). This allowed for a deeper understanding, prediction, engineering, and control of co-cultures.

(iii) Chapters 4 and 5 describe a stoichiometric and kinetic model of *L. bulgaricus* to provide computational tools. Chapter 6 describes ^{13}C-MFA in a two-compartment system and outlines limitations associated with analysing intertwined pathways.

(iv) Chapter 8 describes a useful tool for establishing beneficial co-culture processes such as continuous fermentation.
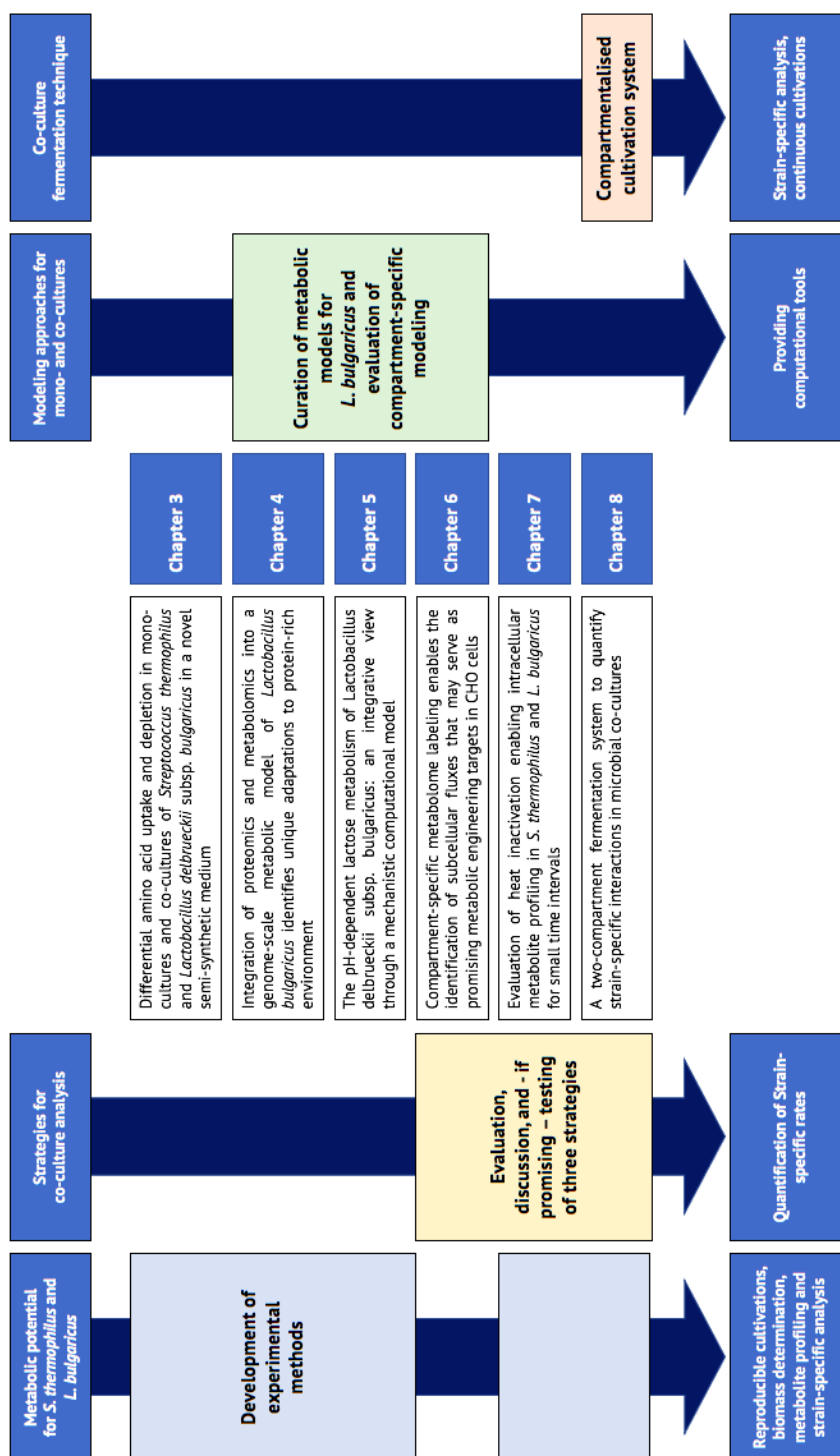
Figure 1.6: Outline of dissertation and assignment of chapters.

Chapter 2

Scientific Background

2.1 Interaction between microorganisms

The cultivation of two different species with a desired interaction targeting their cellular activity is called co-culture. This system comprising two different organisms is composed of intra- and inter-kingdom species, such as bacterial-bacteria, bacterial-fungal, or bacteria-algae species [326]. Microbial communities comprise more than two different organisms and are also called mixed culture, multi-species, or mixed-species consortium. Besides naturally occurring communities, synthetic communities were developed [95]. However, it is difficult to establish a stable and controllable state [189].

The interaction between microbes is favored by the reduced availability of resources such as carbon sources. The interaction results in efficient utilization and consequently an advantage over other non-interacting cells [90]. Also, this might explain why the cultivation of 99.8% of all microbes is not possible in mono-culture [273] indicating their dependence on other microbes [227]. Microorganisms interact through physical contact, signaling molecules, or indirectly by changing the physio-chemical properties of an environment [265].

The interaction can be bi-directional (mutualism, parasitism, competition) or uni-directional (commensalism, amensalism) [133]:

- Mutualism (+/+) (also named symbiosis, cooperation, or proto-cooperation): This interaction results in positive effects for both species. The interaction can be oblig-

atory or facultative. For example, species A consumes a waste product from species B and prevents product inhibition of species B [101, 264].

- Parasitism (+/-): A species benefits from another species while imposing a negative effect. For example, Species A consumes a product of species B and secretes a molecule that is toxic for species B [101].

- Competition (-/-): Two species compete for the same resource such as the same carbon source [101].

- Commensalism (+/0): A species profits from another species without affecting this species. For example, species A consumes a waste product from species B [101].

- Amensalism (-/0): A species affects negatively another species without any benefits. For example, a waste product inhibits the growth of species B [101].

2.2 Application of co-cultures

Co-culture processes can be beneficial by division of labor such as reduced metabolic burden, compartment-specific environments [93, 326], or the secretion of specific products [330]. A co-culture is often not the sum of the included species [314]. Further, co-cultures might overcome inefficiencies or can use complex substrates such as lignocellulose in a more beneficial process [133] [chapter 1].

2.3 Modelling of co-cultures

To understand co-cultures and to apply them in an industrial process, it is important to understand their interaction and to predict their behavior. Therefore, mathematical approaches are necessary. Further, this allows for improving the co-culture systems. Sequencing techniques allow the establishment of genome-scale models [203] and the metabolic potential can be revealed [285], but quantitative data sets are needed to constrain the solution space of these models in more depth [268, 322]. Hence, metabolic models can be used to represent and predict the metabolic fluxes between species. These stoichiometric metabolic models lack kinetic information and regulatory effects reducing the precision of the simulation [276, 285]. Therefore, the development of kinetic models which might later be merged with genome-scale models is still an expanding field [201].

2.3.1 Flux balance analysis (FBA)

Stoichiometric metabolic models based for example on genome-scale reconstructions can be analysed by Flux Balance Analysis (FBA) [205]. Assuming a steady-state of the system, the flux vector can be calculated. To constrain the solution space, measurements such as uptake or production rates, as well as enzymatic capacities can be included as lower and upper bounds of reaction fluxes [234]. Easily, gene knockouts or different conditions such as substrate influx can be simulated. The objective function – such as biomass production – is optimized in an FBA resulting in a specific solution [205].

2.3.2 Community flux balance analysis

A metabolic network comprising different compartments is used to predict fluxes by an FBA [271]. This demands high computational resources because at least two networks are connected [333].

2.3.3 Metabolic flux analysis (MFA)

The MFA calculates fluxes in a fully determined stoichiometric network while the FBA is underdetermined. The additional information to determine a system is gained from measurements, in particular from intracellular measurements gained from an isotopic tracer experiment [10, 309].

2.3.4 ^{13}C metabolic flux analysis (^{13}C-MFA)

The ^{13}C-MFA [309] allows for the calculation of fluxes in cells by using a ^{13}C labelled substrate. The uptake of the substrate, the release of a product, and intermediate metabolite pools are measured. This data set allows the calculation of metabolic reaction rates by using a fully determined (genome-scale) metabolic network. However, ^{13}C-MFA enlarges the metabolic model by the addition of all isotopomers resulting in long computational run times [321].

2.3.5 Isotopes

The isotope ^{13}C is stable and non-radioactive. It has 7 neutrons and therefore, it is heavier than ^{12}C which can be detected by mass spectrometry [196].

2.3.6 Isotopomers

Each carbon atom in a molecule can be a ^{12}C atom or a ^{13}C atom. Each form is called an isotopomer. The number of isotopomers of a molecule is $n = 2^{\,number\ of\ carbon\ atoms}$. For example, glucose has $2^6 = 64$ isotopomers.

2.3.7 Isotopologues

Isotopomers with the same number of labelled atoms have the same weight. Therefore, their mass is the same. All isotopomers with the same mass are called isotopologues.

2.3.8 Stationary and instationary ^{13}C MFA

In both methods, a metabolic steady state is assumed. For a stationary ^{13}C MFA, an isotopic steady state is reached and the isotopomer fractions are measured. For an instationary ^{13}C MFA, the isotopomer fractions are measured without achieving an isotopic steady-state. Hence, several measurements are needed in a short time interval. This is advantageous compared to the stationary ^{13}C MFA because it provides enzyme and reaction kinetic information. Further, the amount of ^{13}C substrate which is required is lower for an instationary ^{13}C MFA compared to a stationary [200, 310].

2.3.9 Implementation of ^{13}C MFA in Matlab

To solve the ordinary differential equations (ODEs) of a metabolic network comprising isotopologues, a numerical approach implemented in Matlab by using the function *ode*45 is useful. The equations describe the change of isotopologue pools. Numerous *for*-loops sum up all equations representing all isotopomers of one metabolite. An isotopologue includes the information on wheater a carbon position is a ^{12}C (expressed with 0), or a ^{13}C (expressed with 1). As result, the simulation is able to calculate over time the isotopomer fractions of each metabolite in a fully determined system based on given fluxes. The

calculated isotopomer fractions are compared with a dataset and the difference between the calculated and the measured values are minimized by using the sum of squared differences (SSD).

2.3.10 Tracer selection

The information which is derived from a ^{13}C MFA experiment depends on the used tracer or tracer mix [55]. A tracer is a substrate containing ^{13}Carbon atoms [196, 321]. In addition, an computational evaluation of different tracers is helpful because the costs of tracers can be very high [30]. However, the selection of an appropriate tracer depends also on the (biological) question, which means for example which flux will be revealed [54]. In general, the choice of the tracer has an impact on the slope in the graph which shows the isotopomer fraction over time. To correctly minimize the SSD, it is beneficial to reach higher slopes [196].

2.4 Cultivation of *L. bulgaricus* and *S. thermophilus*

2.4.1 Milk as a medium for the production of yogurt

Yogurt is conventionally produced from bovine milk. This milk contains approx. 87% water, 5% lactose, 3% fatty acids, 4% protein, and 1% mineral nutrients (g per 100 g milk). The pH is around 6.6 [139, 284]. Freshly collected milk contains a very low titer of bacteria and contamination arise afterward [139]. Pasteurisation and sterilisation of milk decrease the risk of harmful contamination but change the concentrations of milk compounds [284].

2.4.2 B-Milk

In industry and laboratories, B-Milk is often used. The water was removed by a drying process. This hinders the growth of microorganisms and allows them to store B-Milk longer than fresh milk [223]. Further, B-Milk allows more comparable experimental conditions [265].
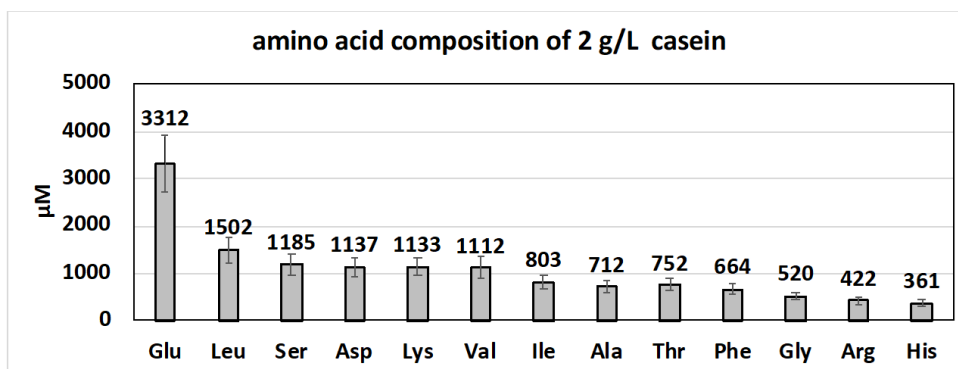
Figure 2.1: Amino acid composition of casein. Numbers above each bar indicate the exact concentration. Adapted from chapter 5.

2.4.3 Milk interferes with analytical methods

The composition of raw milk, pasteurised milk, and B-milk is very complex and variable [265, 284]. Further, Milk contains a high fraction of fatty acids and proteins. This interferes with many sensitive analytical methods such as photometry, high-performance liquid chromatography (HPLC), and mass spectrometry (MS).

2.4.4 The composition of proteins in bovine milk

Bovine milk contains approx. 36 g protein per kg milk. This protein is composed of 29 g casein and 7 g whey protein [139]. The whey protein contains alpha-lactoglobulin, beta-lactoglobulin, immunoglobulin, serum albumin, and protease-peptone [139]. The casein contains alpha-s1-casein, alpha-s2-casein, beta-casein, kapa-casein, and gamma-casein [67, 96, 97, 139, 236]. The classification of these proteins relies on their electrophoretic mobility according to the American Diary Science Association [307]. These proteins form casein-micelles which are stabilized by calcium [78].

2.4.5 The amino acid composition of casein

The fractions of amino acids in the casein were determined (fig. 2.1).

2.4.6 *Lactobacillus bulgaricus*

The *Lactobacillus delbrueckii* subsp. *bulgaricus* (*L. bulgaricus*) is part of the species *Lactobacilli*. It is gram-positive, non-motile, and non-sporulating [68, 102, 292]. The *Lactobacillus delbrueckii* subsp. *bulgaricus* is heterofermentative. However, some Lactobacilli are obligate-homofermentative, facultative-heterofermentative, or obligate-heterofermentative [270]. Medium enriched with CO_2 supports the growth of *L. bulgaricus* [13]. The optimal pH for proliferation and exopolysaccharide production is around 6 [100].

2.4.7 Amino acid metabolism of *L. bulgaricus*

Casein is the main nitrogen source for *L. bulgaricus* cultivated in milk [156] and serves as the source of amino acids. The cell wall-anchored protease PrtB hydrolyses the casein into oligo-peptides [167, 265] and intracellular peptidases hydrolyses the peptides into amino acids (fig. 2.2). The proteolysis of casein is essential for the growth of the high auxotroph *L. bulgaricus* [265]. However, *L. bulgaricus* prefers to consume amino acids from the medium rather than the *de novo* synthesis [329]. Zheng et al. 2012 [329] assume that *L. bulgaricus* is able to synthesize glutamate, glutamine, aspartate, asparagine, lysine, threonine, serine, cysteine, glycine, methionine, and alanine. On the opposite, Kafsi et al. [68] assume that *L. bulgaricus* is not able to synthesize glycine, serine, alanine, and glutamate, as well as, lysine, aspartate, phenylalanine, tyrosine, tryptophan, valine, leucine, isoleucine, histidine, and arginine.

2.4.8 Sugar metabolism of *L. bulgaricus*

The preferred carbon source of *L. bulgaricus* is lactose [47, 68, 100]. Lactose is consumed and hydrolyzed by the beta-galactosidase into glucose and galactose. The glucose is metabolised mainly into lactic acid, and the galactose is exported with a lactose-galactose-antiporter [68].

2.4.9 *Streptococcus thermophilus*

The *Streptococcus salivarius* subsp. *thermophilus* is part of the species *Streptococci* [125, 212]. *S. thermophilus* is homo-fermentative and contains an incomplete pentose-phosphate pathway [212]. *S. thermophilus* produces an exopolysaccharide-matrix which increases the
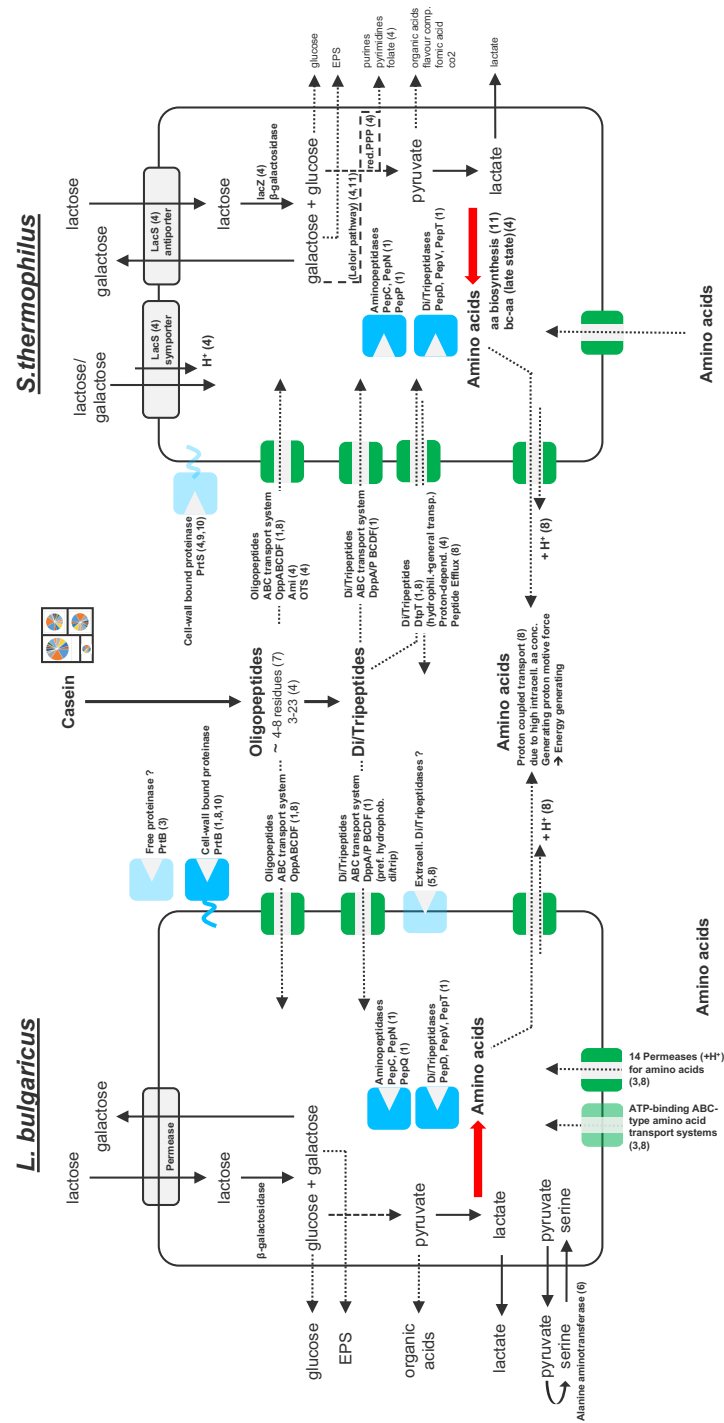
Figure 2.2: The proteolytic system in an *S. thermophilus-L. bulgaricus* co-culture. Casein proteolysis and amino acid biosynthesis was adopted from literature as indicated: (1) [167]; (3) [165]; (4) [179]; (5) [163]; (6) [162]; (7) [150]; (8) [91]; (9) [60]; (10) [49]; (11) [115]

viscosity of the medium [265]. Further, *S. thermophilus* contains a pathway to produce acetaldehyde, which is an important component to establish the "yogurt taste" [212].

2.4.10 Amino acid metabolism of *S. thermophilus*

The cell wall-anchored protease PrtS is present in some *S. thermophilus* to allow hydrolysis of extracellular casein similar to the PrtB in *L. bulgaricus* [167, 265]. Further, intracellular aminopeptidases such as PepC, PepN, and PepM release amino acids from the peptides (fig. 2.2) [167]. *S. thermophilus* is able to synthesise all amino acids, except histidine. glutamine and glutamate, as well as cysteine and methionine, are converted into each other [156, 212, 265]. Methionine, cysteine, and leucine are not essential but promote the growth of *S. thermophilus* [156].

2.4.11 Interaction between *S. thermophilus* and *L. bulgaricus*

The proteolytic activity of *L. bulgaricus* by the peptidase PrtB allows the release of peptides and amino acids from casein which favors the growth of *S. thermophilus*, especially of *S. thermophilus* strains that do not possess the PrtS [49]. On the opposite, *S. thermophilus* releases formate and folate which supports the purine synthesis in *L. bulgaricus* [51, 65, 184, 264]. Further, folate is a cofactor in the biosynthesis of amino acids [265]. *S. thermophilus* produces CO_2 and NH_3 by urease activity from urea [13, 14, 156]. CO_2 is a precursor in the synthesis of aspartate, glutamate, arginine, and for nucleotides [265]. NH_3 increases the pH [13]. Other metabolites which are assumed to be exchanged are pyruvate, long-chain fatty acids, and ornithine [102, 125, 264].

2.4.12 Types of interaction between *S. thermophilus* and *L. bulgaricus*

S. thermophilus and *L. bulgaricus* decrease the pH of the environment which reduces the growth of non-tolerant species for low pH. This indicates amensalism [72]. *S. thermophilus* and *L. bulgaricus* compete for the nitrogen source for example for amino acids, indicating competition [265]. However, the exchange of metabolites between *S. thermophilus* and *L. bulgaricus* might indicate mutualism and protocooperation [265]. In general, the type

of interaction between *S. thermophilus* and *L. bulgaricus* will change according to the metabolic level which is considered.

2.4.13 The effect of interacting *S. thermophilus* and *L. bulgaricus*

The metabolic interaction between *S. thermophilus* and *L. bulgaricus* is mainly found on the level of amino acids, purines, and long-chained fatty acids [264]. This results in increased growth and lactate production [265]. A collectively evolved co-culture of *S. thermophilus* and *L. bulgaricus* showed increased growth rates, lower final pH, faster acidification, and higher biomass compared to an unrelated *S. thermophilus – L. bulgaricus* co-culture [107].

2.5 Analysis of co-cultures

With genome sequencing techniques, it is possible to analyse species composition in microbial communities [289]. However, it is challenging to assign individual characteristics to a single species [26]. Furthermore, it is not possible to make predictions based on knowledge of the individual metabolic behavior of a strain in a community because interactions between species alter their dynamics [176, 313]. Cultivation in mono-culture can provide information on the metabolic capacity of individual strains [243], but not all species can be cultivated in mono-culture [227]. In addition, synthetic co-cultures can provide better insight into the interaction dynamics between microorganisms because they represent a reduced and better defined system [243]. In addition, mathematical models can improve the understanding of co-cultures [31, 287, 333].

2.5.1 Biomass determination

The medium which is used to cultivate lactic acid bacteria traditionally contains proteins such as casein. This impedes the measurement of biomass by the optical density method to some extent [66] or the purification of dry biomass for example by centrifugation [172] because of insoluble material such as casein remains in the pellet. Biomass amount determination by colony forming units (CFU) might be possible but is very time-consuming [172, 299]. Further, cell enumeration might also be possible through real-time quantitative PCR (qPCR) [107, 299]. However, the purification of DNA from lactic acid bacteria is

challenging and a correlation between qPCR enumeration and OD-values was not consistent [107]. Measuring biomass is important for a deeper physiological understanding as well as to create predictive models.

2.5.2 Flow cytometer

A flow cytometer is a multi-parameter analysis with up to 50 000 cells per second and can be used to enumerate cells [237, 299]. The cells flow through a laser beam which scatters the light. From the scattered light, it is possible to distinguish between cells and medium particles such as casein [13, 53]. Further, it is possible to distinguish between different cell types, for example in a co-culture [120, 222, 237]. The data analysis is time-consuming [299] and software tools still show white spots [147].

2.5.3 Analysis of cells by flow cytometry

The flow cytometry data analysis allows us to distinguish between different cell types as well as between viable and dead cells by staining the sample with a dye, for example with propidium iodide [23, 127]. Further, different strains can be enumerated by flow cytometry due to their differences in structure or size [299]. The scattered light will be different for different types of cells, as well as staining can facilitate these differences [238]

2.5.4 Using flow cytometry to estimate biomass in milk

The application of flow cytometry analysis for samples containing milk, casein, or other media with high protein and fat content causes increased background data [104]. For example, casein forms micelles that interfere with data from cells [294]. Therefore, treatment with proteases [104] or chelating agents [13, 182] can reduce the interferences. The proteases hydrolyse the proteins into smaller peptides and the chelating agents bind the calcium ions and disrupt the micelles [34]. Further, a fluorescent labelled antibody that binds specific species can be used [103, 182]. Mathematical analysis of data sets such as automatic classification is often used in biology, for example in gene expression analysis [199]. This is beneficial because manual classification is time-consuming and complicated. The SVM method relies on the maximization of the margin between data sets [320].

Chapter 3

Differential amino acid uptake and depletion in mono-cultures and co-cultures of *Streptococcus thermophilus* and *Lactobacillus delbrueckii* subsp. *bulgaricus* in a novel semi-synthetic medium

The manuscript outlined in this chapter has been accepted and published in *MDPI microorganisms*:

Ulmer, A., Erdemann, F., Mueller, S., Loesch, M., Wildt, S., Jensen, M. L., Gaspar, P., Zeidan, A. A. and Takors, R. (2022). Differential Amino Acid Uptake and Depletion in Mono-Cultures and Co-Cultures of Streptococcus thermophilus and Lactobacillus delbrueckii subsp. bulgaricus in a Novel Semi-Synthetic Medium. Microorganisms, 10(9), 1771. Available at:[https://doi.org/10.3390/microorganisms10091771]

The author of this dissertation, Andreas Ulmer, is first author of this manuscript. Andreas Ulmer planned the study, supervised and participated in the conduction of experiments. Andreas Ulmer supervised and contributed to the development of the cultivation medium and flow cytometry method, created the models, and visualized the results. Andreas Ulmer wrote the original draft of this manuscript.

3.1 Abstract

The mechanistic understanding of the physiology and interactions of microorganisms in starter cultures is critical for the targeted improvement of fermented milk products, such as yogurt, which is produced by *Streptococcus thermophilus* in co-culture with *Lactobacillus delbrueckii* subsp. *bulgaricus*. However, the use of complex growth media or milk is a major challenge for quantifying metabolite production, consumption, and exchange in co-cultures. This study developed a synthetic medium that enables the establishment of defined culturing conditions and the application of flow cytometry for measuring species-specific biomass values. Time courses of amino acid concentrations in mono-cultures and co-cultures of *L. bulgaricus* ATCC BAA-365 with the proteinase-deficient *S. thermophilus* LMG 18311 and with a proteinase-positive *S. thermophilus* strain were determined. The analysis revealed that amino acid release rates in co-culture were not equivalent to the sum of amino acid release rates in mono-cultures. Data-driven and pH-dependent amino acid release models were developed and applied for comparison. Histidine displayed higher concentrations in co-cultures, whereas isoleucine and arginine were depleted. Amino acid measurements in co-cultures also confirmed that some amino acids, such as lysine, are produced and then consumed, thus being suitable candidates to investigate the inter-species interactions in the co-culture and contribute to the required knowledge for targeted shaping of yogurt qualities.

3.2 Introduction

Dairy products have been a part of the human diet since ancient times [178]. Detailed identification and analysis of fermented milk products began in the twentieth century [179]. Efforts are ongoing to develop tools to examine lactic acid bacteria [13, 27, 254, 258]. Yogurt, which is currently an important part of the cuisine of many cultures, will be a crit-

ical dietary component in the future. Therefore, the identification and determination of novel co-culture compositions that impart improved technological and organoleptic properties are active areas of research in the food industry [135]. *Streptococcus thermophilus* and *Lactobacillus delbrueckii* subsp. *bulgaricus* are the key species that drive yogurt production [179]. To meet the changing market demands, there is a need to understand the interaction between *S. thermophilus* and *L. bulgaricus* during milk fermentation and to make use of this knowledge to design improved food products [8]. Despite significant progress in the past, the current state of understanding still shows white spots [179].

In the last 15 years, metabolomics [163, 204] and transcriptomics [115, 116, 264] have been widely applied to understand the physiology of *S. thermophilus* and *L. bulgaricus* in mono-culture and co-culture. Previous studies provide insights into the metabolites exchanged between the strains and elucidated the characteristic gene expression patterns. However, these datasets have provided a limited scope to assign contextual functionalities to metabolites [116, 184, 264].

Screening various combinations of *S. thermophilus* and *L. bulgaricus* strains in co-cultures is a time-consuming and costly process. Thus, only a small subset of all possible combinations and conditions has been investigated. To overcome this limitation, mathematical modelling approaches, such as community flux balance analysis, have been used to predict the performance of co-cultures [31]. Although the mathematical modelling approach enables the estimation of flux distributions in underdetermined systems, a minimum number of experimental measurements is required to limit the solution space. Additionally, the stoichiometry of interactions must be understood for the application of mathematical approaches. Both constraints require reliable and representative experimental datasets as a prerequisite for flux balance modelling [268].

Understanding of the complex metabolic interactions between *S. thermophilus* and *L. bulgaricus*, including the exchange of peptides and amino acids, is currently limited [179]. One key feature is the strong proteolytic activity of *L. bulgaricus*, which enhances the production of peptides and amino acids that become available for *S. thermophilus*, enabling growth [264]. However, some *S. thermophilus* strains exhibit proteolytic activity. Consequently, the question that arises is whether and what differences in this inter-species interaction exist when proteolytic and non-proteolytic *S. thermophilus* are combined with *L. bulgaricus* in co-cultures. Acidification, a marker for lactic acid formation, may serve as an easy-to-follow readout once mono-cultures and co-cultures can be cultured under comparable

conditions. Limited information is available on amino acid production and consumption [163] and potential amino acid depletion, which may trigger amino acid biosynthesis [116, 264].

Milk is traditionally used as a growth medium for *S. thermophilus* and *L. bulgaricus* cultivations in the production of yogurt. *S. thermophilus* and *L. bulgaricus* produce lactic acid from lactose, which imparts an acidic taste and inhibits the growth of microbes, including *S. thermophilus* and *L. bulgaricus* [17,18]. However, milk composition is highly variable. Furthermore, milk comprises several complex ingredients that interfere with the sensitivity of analytical methods, such as High-performance liquid chromatography (HPLC) and Mass spectrometry (MS). Additionally, the acidification of milk leads to an increase in viscosity, which impairs the sensitivity of the analytical methods [240].

To overcome these intrinsic analytical barriers, this study developed a synthetic medium supplemented with amino acids (SMaa) to allow the growth of *S. thermophilus* and *L. bulgaricus* in mono-cultures, which enabled the analysis of individual growth characteristics. The synthetic medium may be supplemented with casein (SMcas) instead of amino acids to investigate the proteolytic abilities of *S. thermophilus* and *L. bulgaricus* in mono-cultures. The medium allows for investigation of the interactions between *S. thermophilus* and *L. bulgaricus* by excluding individual components that are likely to be exchanged. An important effect of the symbiotic relationship between *S. thermophilus* and *L. bulgaricus* is the faster acidification during milk fermentation [31]. Therefore, this study investigated this feature by co-cultivating the strains in SMcas.

This study presents a new medium and comparable datasets of *S. thermophilus* and *L. bulgaricus* in mono-culture and co-culture conditions, providing useful insights into essential amino acid production and consumption. Our results demonstrate that the patterns and levels of amino acid release and consumption in co-cultures are different from those of mono-cultures. These findings are essential for data-driven modelling and testing hypotheses on the induction of basic regulatory mechanisms in cells.

3.3 Materials and Methods

3.3.1 Strains and Cultivation Conditions

Lactobacillus delbrueckii subsp. *bulgaricus* strains (LB.1 = ATCC BAA-365, LB.2, LB.3, and LB.4) were provided by Chr. Hansen A/S and stored at $-70\,°C$ in Man–Rogosa–Sharpe (MRS) (69966 MRS Broth, Sigma-Aldrich Chemie GmbH, Steinheim, Germany) containing 20% (v/v) glycerol. For cultivation, the total cell suspension in the cryotube (1 mL) was transferred into 15 mL of MRS supplemented with $14.3\,\mathrm{g\,L^{-1}}$ lactose and incubated for 6–8 h at $40\,°C$ [100, 166, 224]. After washing twice with 0.9% NaCl solution, the cell pellet was resuspended in 200 μL of 0.9% NaCl to inoculate the preculture containing SMaa. The preculture was cultured at $40\,°C$ and gently stirred with a 10 mm magnetic bar at 400 rpm for 14–18 h until the pH was between 5 and 6.

Streptococcus thermophilus strains (ST.1, ST.2, ST.3, and ST.4 = LMG 18311) were provided by the industrial partner (Chr. Hansen) and stored at $-70\,°C$ in M17 (56156 M-17 Broth, Sigma-Aldrich Chemie GmbH, Steinheim, DE) containing 20% (v/v) glycerol. The cells in the cryotube were washed twice with 0.9% NaCl solution. Then, the cell pellet was resuspended in 200 μL of 0.9% NaCl to inoculate the preculture containing SMaa. The preculture was cultured at $40\,°C$ and gently stirred with a 10 mm magnetic bar at 400 rpm for 2–6 h until the pH was between 5 and 6.

Calculated amounts of biomass from *L. bulgaricus* and *S. thermophilus* precultures were washed twice with 0.9% NaCl solution and the cell pellets were resuspended in 200 μL 0.9% NaCl to inoculate the main culture. The main culture was carried out in SMaa or SMcas as indicated in table 3.1.

The preculture (SMaa) and main culture (SMaa or SMcas) were cultured in crimp-top serum bottles, which were pretreated by flushing with 80% N_2 and 20% CO_2 for 10 min at 400 rpm. Growth was monitored by measuring the optical density (OD) ($\lambda = 600$ nm) using a photometer (Amersham Bioscience, Ultrospec 10 cell density meter) or flow cytometry.

The SM contains all listed compounds, except amino acids and casein. SM supplemented with amino acids (SMaa) contains all listed compounds, except casein. SM supplemented with casein (SMcas) contains all listed compounds, except amino acids.

Table 3.1: Composition of synthetic medium (SM)

Category	Compound	Concentration g L^{-1}	CAS Number
—	Di-potassium hydrogen phosphate	2.5	7758-11-4
	Potassium dihydrogen phosphate	3	7778-77-0
	Sodium acetate	1	127-09-3
	Ammonium citrate tribasic	0.6	3458-72-8
	Manganese sulfate monohydrate	0.02	10034-96-5
	Iron(II) sulfate heptahydrate	0.00132	7782-63-0
	Calcium chloride dihydrate	0.08745	10035-04-8
	Tween 80	1 mL L^{-1}	9005-65-6
	D-Lactose monohydrate	15.75	10039-26-6
	Magnesium sulfate heptahydrate	0.2	10034-99-8
	Urea	0.12	57-13-6
nucleobases	Adenine	0.01	73-24-5
	Guanine	0.01	73-40-5
	Uracil	0.01	66-22-8
	Xanthine	0.01	69-89-6
vitamins	Biotin	0.0002	58-85-5
	Folic acid	0.0002	59-30-3
	Pyridoxal hydrochloride	0.001	65-22-5
	Riboflavin	0.0005	83-88-5
	Thiamine chloride hydrochloride	0.0005	67-03-8
	Nicotinamide	0.0005	98-92-0
	Cyanocobalamin	0.0005	68-19-9
	4-Aminobenzoic acid	0.0005	150-13-0
	D-Pantothenic acid hemicalcium salt	0.004	137-08-6
	DL-6,8-thioctic acid	0.0005	1077-28-7
trace elements	Ammonium molybdate tetrahydrate	0.0000037	12054-85-2
	Cobalt(II) chloride hexahydrate	0.000007	7791-13-1
	Boric acid	0.000025	10043-35-3
	Copper(II) sulfate pentahydrate	0.0000025	7758-99-8
	Zinc sulfate heptahydrate	0.0000029	7446-20-0

	L-Alanine	0.1	56-41-7
	L-Arginine	0.317	74-79-3
	L-Asparagine monohydrate	0.343	5794-13-8
	L-Aspartic acid	0.499	56-84-8
	L-Cysteine hydrochloride monohydrate	0.3	7048-04-6
	L-Glutamic acid	0.331	56-86-0
	L-Glutamine	0.29	56-85-9
	Glycine	0.16	56-40-6
	L-Histidine monohydrochloride monohydrate	0.273	5934-29-2
	L-Isoleucine	0.361	73-32-5
amino acids	L-Leucine	0.6	61-90-5
	L-Lysine	0.351	56-87-1
	L-Methionine	0.119	63-68-3
	L-Phenylalanine	0.34	63-91-2
	L-Proline	0.921	147-85-3
	L-Serine	0.359	56-45-1
	L-Threonine	0.3	72-19-5
	L-Tryptophan	0.102	73-22-3
	L-Tyrosine	0.12	60-18-4
	L-Valine	0.468	72-18-4
casein	Casein	2	9005-46-3

3.3.2 Acidification Measurements

The pH was measured offline using a pH meter (SevenEasy™, Mettler Toledo, Columbus, OH, USA) connected to a pH electrode (InLab Semi-Micro, Mettler Toledo, Columbus, OH, USA).

3.3.3 Medium Preparation

Complex Media

MRS (69966 MRS Broth, Sigma-Aldrich Chemie GmbH, Steinheim, Germany) was dissolved in Milli-Q water and the pH of the medium was adjusted to 6.5 using 2 M NaOH. Then, the medium was filtered using a 0.22 μm filter (ROTILABO®, PVD, Carl Roth GmbH & Co. KG) and sterile polysorbate 80 (CAS-Nr.: 9005-65-6, Sigma-Aldrich Chemie GmbH, Steinheim, Germany) was added according to the manufacturer's instructions. M17 (56156 M17 Broth, Sigma-Aldrich Chemie GmbH, Steinheim, DE) was prepared following the manufacturer's instructions and autoclaved.

Semi-Synthetic Medium

A sterile 5× basal solution containing di-potassium hydrogen phosphate, potassium dihydrogen phosphate, sodium acetate, ammonium citrate, manganese sulfate, iron(II) sulfate, and Tween 80 was prepared as indicated in table 3.1. Sterile lactose, magnesium sulfate, urea, nucleobases, and amino acids were added to the solution. After the pH was set to 6.5 with 1 M HCl, trace elements, vitamins, calcium chloride, and casein were added. The serum bottle was sealed, crimped, and flushed with sterile 80% N_2 and 20% CO_2 for 10 min at 400 rpm. The casein stock solution was prepared in a beaker containing glass beads (3 mm in diameter), which were covered with a thin layer of 200 μL of Tween 80. Next, 100 mL of water containing $0.26 \, \mathrm{g \, L^{-1}}$ $CaCl_2$ was added, and the solution was stirred slowly overnight, followed by autoclaving for 5 min at 121 °C.

3.3.4 Cell Dry Weight (DW)

A glass vial (1 mL, VWR) was dried at 105 °C for at least 36 h, cooled at 20 °C for at least 1 h, and weighed. Aliquots of 1 mL of culture samples in SMaa were washed thrice with Milli-Q water (40 °C) in a 1.5-mL reaction tube (Eppendorf), resuspended in 300 μL

of Milli-Q water, and transferred into a dried glass vial. The reaction tube was rinsed with 200 μL of Milli-Q water, and the water was transferred to the glass vial. The glass vial was dried at 105 °C for at least 36 h, cooled at 20 °C overnight in a desiccator, and weighed to calculate the cell dry weight.

The correlation between optical density, flow cytometry data (events mL^{-1}), and cell dry weight (g$_{DW}$ L^{-1}) was as follows: for LB.1, 1 g$_{DW}$ L^{-1} = 0.17101671 × 10^{-12} events mL^{-1} = 0.2527 × OD$_{600}$ nm; for ST.1, 1 g$_{DW}$ L^{-1} = 0.01970622 × 10^{-12} events mL^{-1} = 0.2075 × OD$_{600}$ nm; for ST.4, 1 g$_{DW}$ L^{-1} = 0.043115 × 10^{-12} events mL^{-1} = 0.243 × OD$_{600}$ nm.

3.3.5 Biomass Measurements Using Flow Cytometry

Samples for flow cytometry analysis were prepared as described previously [13]. The cell suspension (100 μL) was diluted 10-fold with Tris-HCl (1.3 M) EDTA (0.13 M) buffer (pH 8) and incubated for 10 min on a shaker (Eppendorf Thermomixer 5436, Hamburg, Germany) at 1200 rpm and 50 °C. Next, the cell suspension was incubated with 1 x SYBR™Green I nucleic acid gel stain concentrate (Thermo Fisher Scientific, Waltham, MA, USA) for at least 10 min at 20 °C in the dark. The sample was filtered through a filter (Partec CellTrics®30 μM mesh filter size, Sysmex, Germany) into a polystyrene tube immediately before measurements and analysed using a flow cytometer (BD Accuri™ C6; BD Bioscience, Franklin Lakes, NJ, USA) equipped with four fluorescence detectors (FL1 533/30 nm, FL2 585/40 nm, FL3 > 670 nm, and FL4 675/25 nm), two scatter detectors, a blue laser (488 nm), and a red laser (640 nm). Sterile Milli-Q water was used as the sheath fluid. The instrument performance was monitored weekly with BD™ CS&T RUO Beads. The threshold settings, FSC-H 500 and FL1-H 500, a limit of 25 μL, and the slow flow rate of 14 μL/min were used for the analysis of the samples.

The log-transformed FL1-A and FSC-H signals were used to enumerate the total number of events in a sample. The flow cytometry data of the first 10,000 events of the pure medium sample were used for a one-class support vector machine (SVM) classifier implemented in MATLAB® using the command '$fitcsvm$' to identify and remove signal from medium in samples. Additionally, the lower background data were removed using a linear line as the gate, resulting in a cleaned dataset. Linear correlations between cleaned flow cytometric data and the dry weight of cells cultured in SMaa were fitted to the measured data from LB.1, ST1, and ST.4 cultures (figure S8). To determine the transferability of the linear correlation between flow cytometric data and cell dry weight from cells cultured in SMaa to

cells cultured in SMcas, a 1:1 mixture (v/v) of both samples was prepared and measured using flow cytometry. Additionally, each sample was individually analysed using flow cytometry. The calculated sum of the number of cell events cultured in SMaa and the number of cell events cultured in SMcas resulted in the same number of cell events in the measured mixture, indicating transferability (figure S8). Cell dry weight in co-cultures was calculated using the same method with determined transferability (figure S9). The strain-specific cell events of *S. thermophilus* and *L. bulgaricus* in co-culture were estimated using manual classification or SVM classification depending on the pH of the sample (figure S10). Manual classification was achieved by separating the flow cytometry data using a line (the log-transformed FSC-H signal was plotted against the log-transformed FL1-A signal and separated by a linear line). The data points above and below the line represent *L. bulgaricus* and *S. thermophilus*, respectively. Classification of strains in co-culture using SVM was achieved using the log-transformed FSC-H and FL1-A signals of mono-culture datasets. Background data were removed to optimize SVM parameters in MATLAB® using the command *fitcsvm*' (figure S11).

3.3.6 Quantification of Fermentation Products

The culture sample (0.5 mL) was centrifuged for 3 min at $20,000\times$ g and $4\,°C$. The supernatant was stored at $-70\,°C$. Sugars (lactose, glucose, galactose) and organic acids (lactate, succinate, formate) were quantified using the Agilent 1200 series HPLC system equipped with an RI detector [36]. Before analysis, the supernatant was incubated with 4 M NH_3 and 1.2 M $MgSO_4$ solutions, followed by an incubation for 15 min with 0.1 M H_2SO_4 to precipitate phosphate. Isocratic separation was achieved using a Rezex ROA organic acid H (8%) column (300×7.8 mm, 8 μm; Phenomenex) protected by a Phenomenex guard carbo-H column (4×3.0 mm) at $50\,°C$. The HPLC conditions were as follows: mobile phase, 5 mM H_2SO_4 solution; constant flow rate, $0.4\,\text{mL}\,\text{min}^{-1}$. Absolute concentrations were obtained by standard-based external calibration, and rhamnose was used as an internal standard ($1\,\text{g}\,\text{L}^{-1}$) to correct measurement variability. Amino acid concentrations were determined by an Agilent 1200 series instrument (Agilent Technologies) [36]. Bicratic separation was achieved by an Agilent Zorbax Eclipse Plus C18 column (250 by 4.6 mm, 5 μm), which was protected by an Agilent Zorbax Eclipse Plus C18 guard column (12.5 by 4.6 mm, 5 μm). After automatic precolumn derivatization with ortho-phthaldialdehyde, fluorometric detection (excitation at 230 nm and emission at 450 nm) was carried out.

The elution buffer consisted of a polar phase (10 mM Na_2HPO_4, 10 mM $Na_2B_4O_7$, 0.5 mM NaN_3, pH 8.2) and a nonpolar phase (45% [v/v] acetonitrile, 45% [v/v] methanol). The quantification of amino acids was achieved by standard-based external calibration, and 4-aminobutanoic acid was used as an internal standard at 100 μM to correct for analyte variability.

3.3.7 Total Amino Acid Composition in the Supernatant

The culture sample (0.3 mL) was centrifuged for 3 min at 20,000× g and 4 °C. The supernatant was stored at −70 °C. The supernatant (200 μL) was incubated with 300 μL of 32% HCl at 100 °C for 24 h, cooled at 20 °C for at least 1 h, slowly mixed with 490 μL of 6.23 M NaOH, and stored at −20 °C until quantification of amino acid concentrations by HPLC analysis.

3.3.8 Calculation of Amino Acid Production Rates

Individual biomass-specific amino acid production rates q_{aa} [mol g_{DW}^{-1} h^{-1}] were calculated for each amino acid in a differential manner at 1 h intervals. The average biomass c_x [g_{DW} L^{-1}] in the period Δt [h], and the net amount of produced amino acids Δc_{aa} [mol L^{-1}] eq. (3.1) were considered.

$$q_{aa} = \frac{\Delta c_{aa}}{\dfrac{c_{x_1} + c_{x_2}}{2} \cdot \Delta t} \tag{3.1}$$

3.3.9 Fitting of Gaussian Models to pH-Dependent Amino Acid Production Rate

The release of amino acids strongly relies on enzymatic proteolysis. As the proteolytic activity depends on various enzymes with each contributing to an individual optimum pH [150, 235], integral activities may be described by the superposition of Gaussian activity distributions. However, exact values for pH optima were not available. Additionally, de novo biosynthesis may occur, albeit to a minor extent. Consequently, the Gaussian model was considered a suitable proxy for the observed amino acid 'production' profiles.

Parameter regression was achieved by fitting the pH-dependent qaa of the *L. bulgaricus* LB.1 mono-culture (figure S13) using eq. (3.2) [119].

$$q_{aa} = \sum_{i=1}^{n} a_i \cdot e^{-\left(\dfrac{pH - b_i}{c_i}\right)^2} \tag{3.2}$$

where q_{aa} is the amino acid production rate [mol g_{DW}^{-1} h^{-1}]; n is the number of pH optima to fit; and a, b, and c are regression parameters coding for the shape of the curve. MATLAB® was used for fitting. The consideration of a single pH dependency is not always sufficient. Then, overlaying Gaussian models considering two pH optima were used to improve the model prediction quality (figure S13).

3.3.10 Simulation of Amino Acid Concentrations

Changes of biomass, substrate, and product concentrations were described in a process model assuming batch operation modes by balancing biomass (eq. (3.3)), substrate (eq. (3.4)), and product (eq. (3.5)) within the system boundary.

$$\frac{dc_x}{dt} = \mu \cdot c_x \tag{3.3}$$

$$\frac{dc_s}{dt} = -q_s \cdot c_x \tag{3.4}$$

$$\frac{dc_p}{dt} = q_p \cdot c_x \tag{3.5}$$

The amino acid production kinetics were integrated into the process model to predict $c_{aa}(t)$. The simulation time steps Δt considered the mean pH and biomass values as indicated in eq. (3.6).

$$c_{aa} = q_{aa} \cdot c_x \cdot \Delta t = \sum_{i=1}^{n} a_i \cdot e^{-\left(\dfrac{\frac{pH_1 + pH_2}{2} - b_i}{c_i}\right)^2} \cdot \frac{c_{x_1} + c_{x_2}}{2} \cdot \Delta t \tag{3.6}$$

The feasibility of this approach was demonstrated for the mono-culture of *L. bulgaricus* LB.1 (figure S12).

3.3.11 Uncertainty Analysis

Metabolite concentrations, pH, OD, flow cytometric data, and dry weight values were analysed using Microsoft® Excel. Mean and standard deviation were calculated using duplicates and triplicates (STABW.S) in Microsoft® Excel. All experimental results are expressed as the mean of three biological replicates with experimental errors unless otherwise stated.

3.4 Results

3.4.1 Medium Development

The main objectives for preparing the SMcas were as follows: (a) enabling the growth of both species in mono-culture, (b) enabling the growth of both species in co-culture, and (c) potential metabolites that may be exchanged [13, 179, 258], [115, 204], [116, 184] were excluded if growth was not affected. To obtain this medium, previously reported defined growth medium compositions of *S. thermophilus* [47, 156] and *L. bulgaricus* [47, 100] were compiled, resulting in a long list of constituents. This list was further reduced to achieve a lean growth medium to fulfil the demands (a–c). Medium acidification, which mirrors growth-coupled lactate formation, was used as a readout to verify the ability of the strains to grow with different modifications in the medium. Oleic acid, pyruvic acid, formic acid, orotic acid, niacin, spermine, ascorbic acid, thioglycolate, and 2'-deoxyguanosine, which were used in the growth medium by Chervaux et al. [47] but not by Grobben et al. [100], were excluded from the medium because they are not essential for the growth of *L. bulgaricus*. Additionally, we evaluated whether the addition of orotic acid is essential since it was considered to be an important component of the growth medium by Otto et al. [206] and Letort et al. [156]. Growth analysis of *L. bulgaricus* and *S. thermophilus* in the medium lacking orotic acid revealed culture acidification. The omission of biotin, thiamine, aminobenzoic acid, and thioctic acid did not result in the acidification in *S. thermophilus* culture but promoted the acidification in *L. bulgaricus* culture. Furthermore, urea was not excluded from the medium because it has previously been established that it increases the

buffer capacity of the medium [156] and provides carbon dioxide and ammonia [13].

Studies using SMcas revealed the ability of three proteinase-positive S. thermophi-lus (ST.1, ST.2, and ST.3) strains and the four *L. bulgaricus* strains to acidify the medium. The proteinase-negative *S. thermophilus* ST.4 was not able to acidify SMcas and required access to free amino acids provided in SMaa (figure S1).

Protocooperation between *L. bulgaricus* and *S. thermophilus* in co-culture has industrial relevance [179]. Co-culture benefits from the rapid exchange of metabolites, leading to accelerated acidification [264]. The effect of this protocooperation in the co-culture was observed in SMcas in the form of a faster acidification rate and a lower final pH (figure S2).

3.4.2 Growth and Amino Acid Release in *L. bulgaricus* Mono-Culture

L. bulgaricus hydrolyzes amino acids from casein through its cell wall proteinase PrtB, which is complemented by other intracellular and extracellular peptidase activities [49, 116, 164, 264]. Therefore, peptides and free amino acids can be utilized by *S. thermophilus*. Furthermore, amino acid depletion may upregulate amino acid biosynthesis in co-cultures [116, 264]. Hence, a key step in understanding cellular responses to extracellular amino acid depletion is to monitor amino acid release and uptake.

L. bulgaricus LB.1 was cultured in SMcas as a mono-culture. The biomass of the culture increased from 0.05 to 0.6 g_{DW} L^{-1}, whereas the pH decreased from 6.4 to 4.3 (fig. 3.1).

Lactose was consumed, glucose was initially secreted (up to 1.4 mM) and then consumed, and galactose, lactate, formate, and succinate were produced (figure S7) in the culture, in-dicating metabolic activity. The following two patterns of amino acid release were observed (fig. 3.1): accumulation of alanine, serine, lysine, tyrosine, and valine from the beginning of culturing; other amino acids began to increase after 2 h. A previous study suggested that this lag time indicates cellular adaptation to casein through upregulation of proteolytic activity [163]. The initial release of tyrosine, arginine, serine, leucine, and valine indicates active proteolytic activity from the beginning of culturing as they might not be produced de novo from *L. bulgaricus* [102, 264].
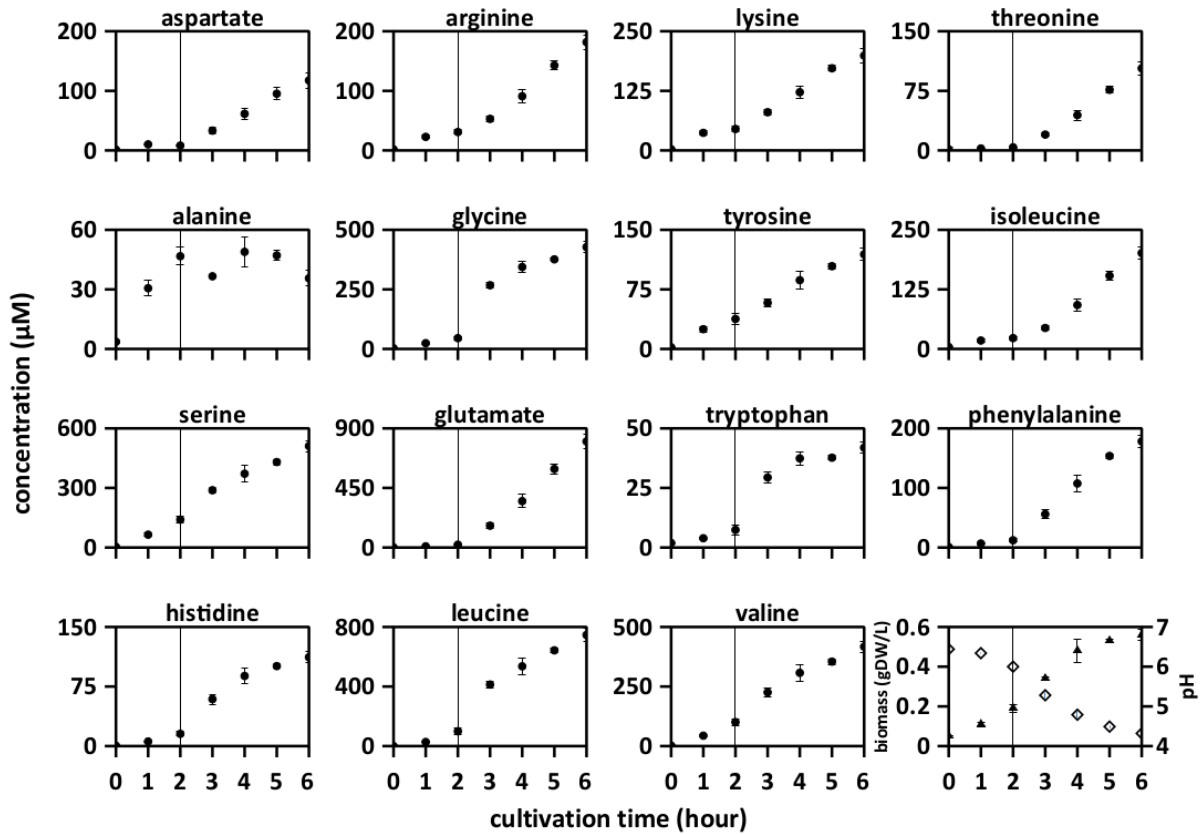
Figure 3.1: Amino acid concentrations were measured in *Lactobacillus bulgaricus* LB.1 culture in synthetic medium supplemented with casein (SMcas). The line indicates a change in increasing amino acid concentration profiles after 2 h. Downright: biomass (triangle) and pH (rhomb) measurements
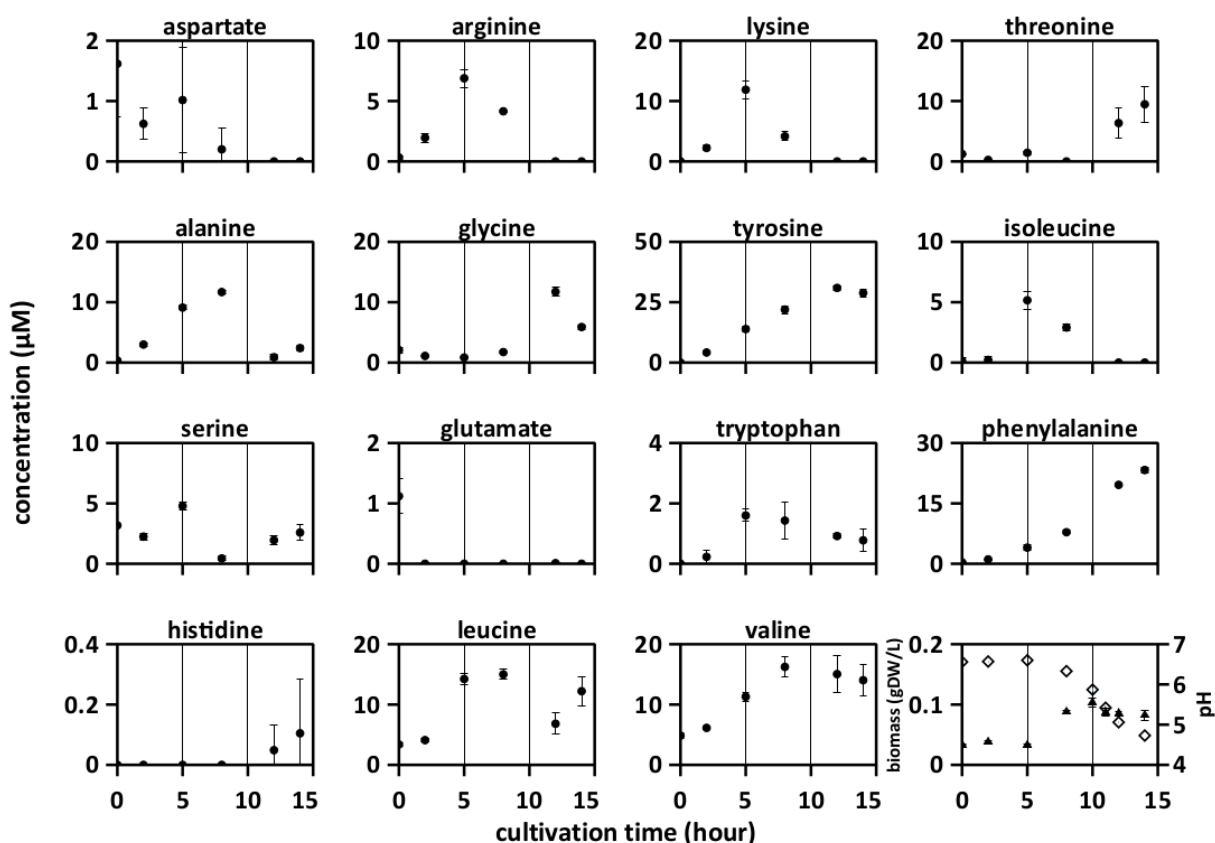
Figure 3.2: Amino acid concentrations were measured in proteinase-positive *S. thermophilus* ST.1 culture in synthetic medium supplemented with casein (SMcas). The lines indicate three phases according to the growth. Downright: biomass (triangle) and pH (rhomb) measurements.

3.4.3 Growth and Amino Acid Release in Proteinase-Positive *S. thermophilus* Mono-Culture

The dynamics of amino acid release and uptake in the proteinase-positive *S. thermophilus* ST.1, amino acid concentrations were measured over a culturing period of 14 h (fig. 3.2).

The following three distinct phases were identified: 0–5 h, increase of some amino acid concentrations but no change in biomass and pH; 5–10 h, acidification, biomass increase, and decrease of some amino acid concentrations while others kept increasing; 10–15 h, acidification, biomass decrease, and uptake and release of amino acids. The concentration of all analysed amino acids increased at some time point. Additionally, the pH decreased from 6.6 to 4.7, whereas the biomass increased from 0.03 g_{DW} L^{-1} to 0.1 g_{DW} L^{-1} (fig. 3.2). Furthermore, 12 out of the 15 amino acids were consumed at some points in time. Moreover,

the concentrations of some amino acids exhibited an oscillating release-consumption-release profile (e.g., serine and leucine). After 12 h, almost all lactose was consumed (30 mM), which was accompanied by the production of large amounts of glucose (22 mM) and lactate (30 mM) (figure S3).

3.4.4 Growth and Amino Acid Release in the Co-Culture of Proteinase-Positive *S. thermophilus* and *L. bulgaricus*

Next, the amino acid concentrations in an *L. bulgaricus* LB.1—proteinase-positive *S. thermophilus* ST.1 co-culture were examined. The strains could grow in both SMcas (fig. 3.1 and fig. 3.2) and SMaa (figure S4 and S6), indicating their ability to utilize casein and free amino acids. As shown in fig. 3.3, the concentration of all amino acids increased during cultivation at some point. The concentrations of aspartate, arginine, lysine, alanine, and isoleucine began to decrease after approximately 2 h. Meanwhile, the decrease in glycine concentration was delayed until 4 h. The following two phases were observed in amino acid release (fig. 3.3), growth, and acidification (fig. 3.4): 0–4 h, pH decreased from 6.4 to 4.7 while the growth of both strains was weak (fig. 3.4); 4–7 h, the biomass of *L. bulgaricus* increased from 0.05 g_{DW} L^{-1} to 0.22 g_{DW} L^{-1}. Additionally, the consumption of 30 mM lactose, the production of 57 mM lactate, and the secretion (up to 10 mM) and uptake of glucose were observed (figure S5).

3.4.5 Growth and Amino Acid Release in the Co-Culture of Proteinase-Negative S. thermophilus and L. bulgaricus

Next, the effects of replacement of proteinase-positive S. thermophiles ST.1 with proteinase-negative *S. thermophilus* ST.4 on the amino acid availability and the nutrient needs in the co-culture with *L. bulgaricus* LB.1 were examined. ST.4 could not grow in SMcas but could grow in SMaa (figures S4 and S6). Therefore, a higher biomass fraction of *S. thermophilus* ST.4 was inoculated to avoid the anticipated overgrow of *L. bulgaricus.*

The fig. 3.4B shows the following three phases: 0–2.5 h, increased biomass of S. thermophilus ST.4; 2.5–4 h, dominant growth of *L. bulgaricus* LB.1; 4–7 h, decreased biomass of *S. thermophilus* ST.4 even as *L. bulgaricus* LB.1 continued to grow. Hence, the presence of *L. bulgaricus* LB.1 enables the growth of *S. thermophilus* ST.4 in SMcas, which is consistent with previous findings [116]. Additionally, 25 mM of lactose was consumed and 58 mM of
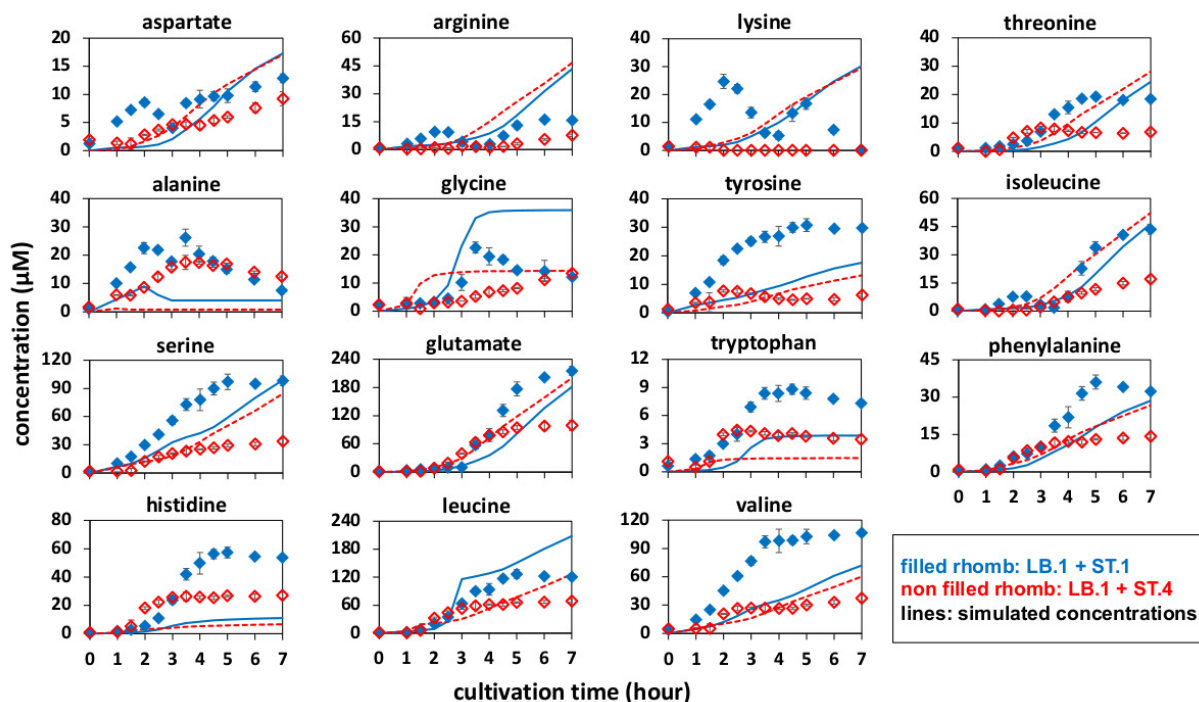
Figure 3.3: Amino acid concentrations in different co-cultures. (filled) *Lactobacillus bulgaricus* LB.1 co-cultured with proteinase-positive *Streptococcus thermophilus* ST.1 in synthetic medium supplemented with casein (SMcas). (non-filled) *L. bulgaricus* LB.1 co-cultured with proteinase-negative *S. thermophilus* ST.4 in SMcas. (line) Simulated amino acid concentration released from *L. bulgaricus* LB.1 in LB.1–ST.1 co-culture. (dashed line) Simulated amino acid concentration released from *L. bulgaricus* LB.1 in LB.1–ST.4 co-culture.

lactate was produced (figure S5). Interestingly, lactose consumption severely slowed down after the growth stop of ST.4, while lactate formation continued. Furthermore, the concentrations of arginine (0–5 h), isoleucine (0–3 h), and lysine (0–7 h) decreased. Overall, the amino acid concentration in the proteinase-negative S. ther-mophilus ST.4—*L. bulgaricus* co-culture was lower than that in the proteinase-positive *S. thermophilus* ST.1—*L. bulgaricus* LB.1 co-culture.

3.4.6 Simulation of Amino Acid Concentrations to Compare Mono- and Co-Culture Cultivations

To indicate the changes in the amino acid profile when *S. thermophilus* was added to the *L. bulgaricus* culture, a Gaussian model of amino acid release dependent on pH and biomass
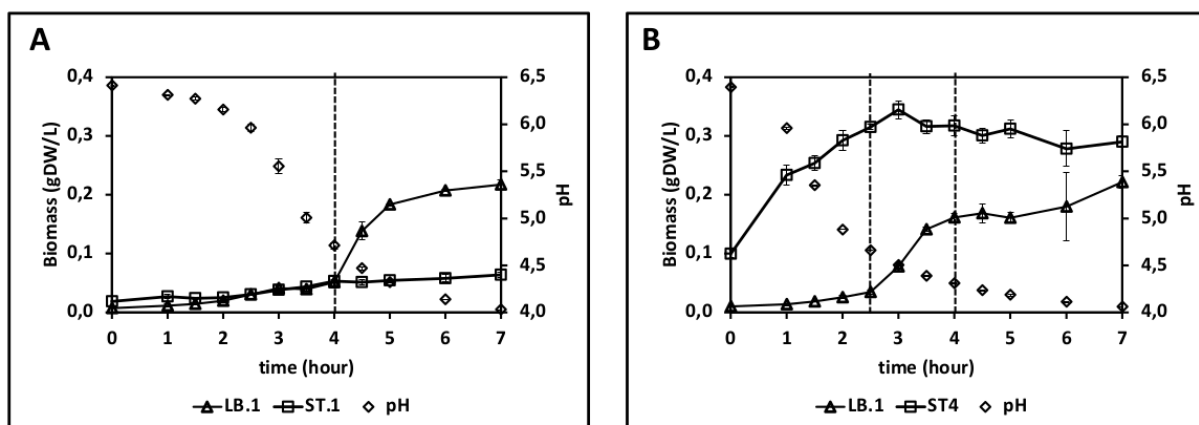
Figure 3.4: Strain-specific biomass profiles measured by flow cytometry and pH measurements in (A) LB.1–ST.1 (initial biomass fraction of 1:2 (LB:ST)) and (B) LB.1–ST.4 (initial biomass fraction 1:10 (LB:ST)) co-cultures in synthetic medium supplemented with casein (SMcas).

was generated (see section 3.3.9). This model enables the simulation of the amount of amino acids released solely from *L. bulgaricus* in co-culture, which could not be identified in the mixed culture. Hence, the comparison between the simulation and measured data will indicate if the amino acid release activity differs between mono-culture and co-culture.

Amino acid profiles of *L. bulgaricus* mono-culture (fig. 3.1) were used to fit the Gaussian q_{aa} models. The fig. 3.3 compares the simulated amino acid profiles of *L. bulgaricus* with the measured amino acid profiles of the co-cultures, reflecting the results of the mixed culture interaction.

Generally, the amino acid concentrations in the proteinase-positive *S. thermophilus* ST.1—*L. bulgaricus* co-culture were higher than those in the simulated amino acid time courses of *L. bulgaricus* in mono-culture, with the exception of glycine and leucine. By way of analogy, fig. 3.3 shows the difference between the measured amino acid concentrations in the *S. thermophilus* ST.4—*L. bulgaricus* co-culture and the simulated amino acid concentrations released from *L. bulgaricus*. Here, most of the measured amino acid profiles, except for alanine, tryptophan, and histidine, were lower than those of the simulated courses. This indicates increased uptake of amino acids, likely via the proteinase-negative *S. thermophilus* ST.4, which can only feed on amino acids and peptides released from *L. bulgaricus* but not from casein.

3.5 Discussion

3.5.1 Amino Acids Are Consumed by *L. bulgaricus* and *S. thermophilus*

In this study, amino acids were consumed by *L. bulgaricus* and *S. thermophilus* cultured in SMcas in both mono-culture (fig. 3.1 and fig. 3.2) and co-culture (fig. 3.3). This is in accordance with [166]. Amino acids were consumed even in the presence of peptide-bound amino acids (table S1). For example, lysine was consumed in the *S. thermophilus* ST.1—*L. bulgaricus* LB.1 co-culture after 4 h (fig. 3.3), although at least 230 μM of lysine bound to proteins and peptides was available (table S1). This indicates that amino acid transporters are active and enable the strains to exchange amino acids that are produced through casein hydrolysis or biosynthesis [125, 329]. Hence, it allows interaction [231, 265, 267]. Additionally, this enables the manipulation of *S. thermophilus* and *L. bulgaricus* cultivations in biotechnological processes by adding amino acids, such as lysine [128].

3.5.2 Amino Acids Can Accumulate in Cultivations with L. bulgaricus and S. thermophilus

L. bulgaricus LB.1 could accumulate all analysed amino acids (fig. 3.1). Some of these amino acids accumulated from the beginning of culturing, indicating basal proteolytic activity although the strain was precultured under SMaa conditions. This suggests that *L. bulgaricus* LB.1 releases more amino acids from casein or/and produces amino acids than it is needed for growth and that amino acids become available for other strains [145]. The accumulation of amino acids indicates that extracellular peptidases are highly active [162], unusable amino acids are separated from peptides to gain posteriorly required amino acids, or proton-coupled amino acid secretion supports the maintenance of intracellular pH during acidification [131]. The poor release of amino acids in a *S. thermophilus* ST.1 cultivation reflects its low activity of peptidases [225, 235].

3.5.3 Differences between Co-Cultures with Different *S. thermophilus* Strains

The proteinase-negative *S. thermophilus* ST.4—*L. bulgaricus* LB.1 co-culture yielded lower amino acid concentrations than the proteinase-positive *S. thermophilus* ST.1—*L. bulgaricus* LB.1 co-culture. This phenotype can be attributed to the increased growth of *S. thermophilus* ST.4 (fig. 3.4), which results in an enhanced demand for amino acids [25]. In addition, this observation is consistent with the lack of protease activity of *S. thermophilus* ST.4 (fig. 3.3). The depletion of arginine, lysine, and isoleucine observed in this study can upregulate peptidases or amino acid biosynthesis, which is consistent with the hypothesis of previous studies [116, 163, 264].

3.5.4 Co-Culture Is Not the Sum of Mono-Cultures

The proteinase-positive *S. thermophilus* ST.1—*L. bulgaricus* LB.1 co-culture yielded higher amino acid concentrations than the simulated concentration of amino acids released from only *L. bulgaricus* LB.1 (fig. 3.3). In particular, histidine was rarely released in the presumably histidine auxotroph *S. thermophilus* ST.1 mono-culture (fig. 3.2) [212] but was detected in high amounts in the *S. thermophilus* ST.1—*L. bulgaricus* LB.1 co-culture. The interaction between the two species may trigger metabolic changes in the strains, resulting in the rearrangement of metabolic fluxes [102, 258, 313]. Future studies must identify these co-culture triggers that serve as stimuli for basic metabolic adjustments.

The amount of amino acid released from the co-culture was higher than the individual sums of the amounts of amino acid released from the mono-cultures. This might be a consequence of an upregulated proteolytic system in *L. bulgaricus* LB.1 and *S. thermophilus* ST.1. Alternatively, individual biosynthetic pathways might be stimulated in co-culture but not in mono-culture [111, 212]. Previous studies have alluded to the up-regulation of histidine biosynthesis [116, 264].

3.5.5 Stimulatory Effects of Branched-Chain Amino Acid (BCAA) Depletion

Previous studies have hypothesized that BCAA availability is limited in the *S. thermophilus*—*L. bulgaricus* co-cultures due to the upregulation of BCAA permease in *L.*

bulgaricus [264] and BCAA biosynthesis in *S. thermophilus* [83, 116, 264]. In this study, the levels of isoleucine, but not those of valine or leucine, were temporarily depleted in the co-cultures (fig. 3.3). Furthermore, the release of BCAA in the *L. bulgaricus* LB.1 mono-culture was similar to that reported in a previous study [163], which revealed that the proteolytic activity of *L. bulgaricus* promotes the excess release of BCAA from casein. In the LB.1 mono-culture, the final concentration of isoleucine (200 μM) was lower than that of valine (417 μM) and leucine (746 μM). This indicated isoleucine as a potential candidate for depletion. Additionally, low concentrations of isoleucine (up to 5 μM), leucine (up to 15 μM), and valine (up to 16 μM) were observed in the protease-positive *S. thermophilus* ST.1 mono-culture, indicating its ability to release BCAA from casein or biosynthesize BCAA [125, 212]. However, the levels of isoleucine, leucine, and valine were lower than those in *L. bulgaricus*. Hence, isoleucine depletion is plausible and may result in the up-regulation of BCAA permease in *L. bulgaricus* and BCAA biosynthesis in *S. thermophilus*, respectively.

3.5.6 Arginine and Lysine Depletion in Co-Cultures

Arginine and lysine concentrations were limited in the proteinase-negative *S. thermophilus* ST.4—*L. bulgaricus* LB.1 co-culture and oscillated in the proteinase-positive *S. thermophilus* ST.1—*L. bulgaricus* LB.1 co-culture (fig. 3.3). Previous studies [115, 264] have reported the upregulation of arginine biosynthesis in *S. thermophilus* co-cultured with *L. bulgaricus*. Hence, our results support the hypothesis that low arginine concentrations might influence physiological responses [14], such as the up-regulation of arginine biosynthesis in *S. thermophilus*.

3.6 Conclusions

In this work, we developed a synthetic medium that supports the growth of the dairy organisms *S. thermophilus* and *L. bulgaricus* in mono- and co-culture, which enables the quantitative monitoring of growth as well as substrate consumption and metabolite production dynamics. Amino acid release profiles in co-culture were not the sum of amino acid release profiles in mono-cultures. Additionally, the amino acid release profiles were not similar in co-cultures with different strain combinations. Amino acid depletion was observed in *S. thermophilus*—*L. bulgaricus* co-cultures, which may provide an explanation

for the induced expression of proteolytic enzymes.

The uptake of several amino acids was observed during growth. Knowledge of co-culture-specific consumption rates for peptide and amino acid uptake along with release rates of amino acids provides a tool for determining yogurt quality and useful insights into cellular fitness for further strain and process optimization. Understanding cellular amino acid needs may enable a quantitative and detailed understanding of interactions in yogurt cultures.

Chapter 4

Integration of proteomics and metabolomics into a genome-scale metabolic model of *Lactobacillus bulgaricus* identifies unique adaptations to protein-rich environment

Chapter not included in the published version

Chapter 5

The pH-dependent lactose metabolism of *Lactobacillus delbrueckii* subsp. *bulgaricus*: an integrative view through a mechanistic computational model

The author of this dissertation, Andreas Ulmer, shares first authorship for the manuscript outlined in this chapter with Tamara Bendig (BioQUANT/COS, Heidelberg University, Heidelberg, Germany). Andreas Ulmer planned and conducted cultivations experiments of *L. bulgaricus* with various substrate conditions and collected samples to quantify biomass, sugars, organic acids, and amino acids profiles. Andreas Ulmer was involved in the interpretation of the computational and wet-lab results. Andreas Ulmer wrote those paragraphs which describe (method section) and present (result and discussion section) the aforemen-

tioned activities. Andreas Ulmer reviewed and edited the manuscript.

5.1 Abstract

The fermentation process of milk to yogurt using *Lactobacillus delbrueckii* subsp. *bulgaricus* in co-culture with *Streptococcus thermophilus* is hallmarked by the breakdown of lactose to organic acids such as lactate. This leads to a substantial decrease in pH - both in the medium, as well as cytosolic. The latter impairs metabolic activities due to the pH-dependence of enzymes, which compromises microbial growth. To quantitatively elucidate the impact of the acidification on metabolism of *L. bulgaricus* in an integrated way, we have developed a proton-dependent computational model of lactose metabolism and casein degradation based on experimental data. The model accounts for the influence of pH on enzyme activities as well as cellular growth and proliferation of the bacterial population. We used a machine learning approach to quantify the cell volume throughout fermentation. Simulation results show a decrease in metabolic flux with acidification of the cytosol. Additionally, the validated model predicts a similar metabolic behaviour within a wide range of non-limiting substrate concentrations. This computational model provides a deeper understanding of the intricate relationships between metabolic activity and acidification and paves the way for further optimization of yogurt production under industrial settings.

5.2 Introduction

Lactobacillus delbrueckii subsp. *bulgaricus* is a homofermentative lactic acid bacterium (LAB) widely used in co-culture with *Streptococcus thermophilus* in the dairy industry. Lactic acid bacteria produce mainly lactic acid as an end product of fermentation. This leads to a remarkable pH drop in the medium [241], while achieving the desired characteristics of yogurt such as acidity, taste and texture [44, 46, 87]. Further, the acidification inhibits the growth of competing bacteria, prevents spoilage, and prolongs the product shelf-life [81]. However, bacteria vary in their ability to maintain growth under acidic stress. Coping with low pH is an essential aspect for survival and productivity, and consequently for the industrial use such as for the choice of starter cultures or probiotics [131]. *L. bulgaricus* reduces the cytosolic pH (pH_c) as a function of the extracellular pH (pH_e) [232, 259, 263]. The reduction in pH causes a decreased catabolic flux and increased rates

for energy consumption, resulting in energy limiting growth conditions [185]. In addition, an acidic pH_e can lead to membrane damage [5], affects the growth rates [45, 186], viability and reduces metabolic activities. *In vitro* studies of enzyme kinetics in *L. lactis* indicate that a reduction of one pH unit to 5, reduces the activity of the glycolytic enzymes by around 50% [69]. The pH does not only alter the protonation state of the functional groups of enzymes, it also affects the equilibrium and kinetics for reactions including protons. For these reasons, it is essential to consider the pH dynamics when investigating the reaction velocities and thermodynamics of metabolism in LAB. While pH is a key factor in metabolism, especially in environments which can reach a pH of 4 or lower [62], it is often overlooked in models. To the authors' current knowledge, no prior computational models exist describing the lactose metabolism of *L. bulgaricus* using pH-dependent kinetics and suitable data is scarce. The change of pH_c in *L. bulgaricus* following an abrupt change in extracellular, more acidic pH_e was already measured (e.g., [149, 262]). However, no study could be found explaining the development of pH_c throughout fermentation, especially not continuously between lag phase and stationary phase and in growing cells. Further, measuring pH_c during batch fermentation and in a changing pH environment experimentally pose challenges difficult to tackle with the available technology. Experimental methods require high cell densities [193], staining [262] or the expression of genetic modified pH sensors [173], which are not always compatible with the experimental design or even food industry regulations. Only a few models consider the effect of inherent acidification and metabolic processes in LAB (e.g., [4, 9, 70]), however, pH_c as a dynamic value impacting the activities of individual glycolytic enzymes has not been incorporated in such models. While pH_c-dependent enzyme kinetics are rarely considered in models of other organisms [170, 187, 295], such models highlight the importance of pH_c in metabolic regulation. Consequently, the influence of pH on glycolytic flux and its impact on growth behaviour is not fully elucidated yet. Understanding pH_c dynamics will contribute to strengthen our knowledge about lactose metabolism and the underlying reason for the incomplete lactose catabolism. Further, such models can be used to stir the fermentation product outcome in terms of acidity and residual lactose concentration. Systems biology approaches to model lactose fermentation with protons as species can help to shed light upon the processes behind lactic acid bacteria metabolism and its interdependence with pH dynamics. In this work, we investigated the lactose metabolism of *L. bulgaricus* using a proton-dependent computational model, wherein pH_c and pH_e were simulated and pH_c implemented into the enzyme kinetics of the glycolytic reactions. In addition, growth changes throughout

batch fermentation were integrated into the kinetic model. We present a proton dependent computational model with predictive power to provide new insights into the central carbon metabolism of *L. bulgaricus* and its intricate dependency with pH levels.

5.3 Materials and Methods

Strain and culture conditions

All experiments were conducted with *Lactobacillus delbrueckii* subsp. *bulgaricus* ATCC®BAA-365 in synthetic medium (SM) under microaerophilic conditions (80% V/V N_2 and 20% V/V CO_2) as previously described in [291] with deviations in the concentration of lactose monohydrate or substitution of the amino acids by casein as indicated in the respective experimental setup. The fermentation to measure extracellular metabolites was performed without pH control, using an initial pH of 6.3, SM containing 2 g/L casein (Sigma-Aldrich Chemie GmbH, #9005-46-3, Steinheim, Germany) as a substitute for the amino acids and 43.85 mM lactose a constant fermentation temperature of 40°C and stirring with 500 rpm. The SM for maintenance and experiments to determine the cytosolic volume contained 21 g/L lactose monohydrate (58.3 mM) and amino acids.

Biomass and dry weight quantification

The biomass was quantified using flow cytometry as described in [291].

Optical density and correlation to total cellular volume

Growth was determined spectrophotometrically in SM containing amino acids and 15 g/L lactose by measuring the optical density at 600 nm in biological triplicates. To evaluate the cytosolic volume, ten images of the cell suspension per time point were captured in two biological replicates during the time course using a bright-field light microscope with a 400-fold magnification in Bürker-Türk counting chambers. The area occupied by cells per image was determined in Fiji (Version 1.52p, [249, 253]). Cell segmentation was performed using the machine learning tool Trainable Weka Segmentation [11] with default settings and the Particle Analyser implemented in Fiji. Only particles smaller than 10^{-7} mm^2 and a circularity lower than 0.7 were considered. The volume of all cells within the culture was calculated using eq. (5.1) assuming a cylindrical cell shape. The volume of each

particle n was calculated as the product of the respective area A_n of particle n, π and the respective secondary axis of a fitted ellipse, depicting the width of the particle M_n. The volumes of all particles were summed up for each image k, representing the cellular volume in $2{,}5 \cdot 10^{-4}\,\mathrm{mm}^3$ medium.

$$\sum_{k=1}^{n} V_k = A_n \cdot \pi \cdot \frac{M_n}{4} \tag{5.1}$$

The mean of two samples per time point with the 10 technical replicates per sample was used to calculate the volume. The linear relationship between OD_{600} and the total cytosolic volume shown calculated using this method was used to convert OD_{600} values to cytosolic volume.

Quantification of metabolites

The concentrations of extracellular metabolites were measured using high-performance liquid chromatography (HPLC). The concentration of carbohydrates (lactose, glucose, galactose, lactate) was measured in cell-free supernatants using the Agilent 1200 series HPLC system with a RI detector. The isocratic separation was achieved by a Rezex ROA organic acid H (8%) column (300 by 7.8 mm, 8 μm; Phenomenex) protected by a Phenomenex guard carbo-H column (4 x 3.0 mm) maintained at 50°C. 5 mM H_2SO_4 was used as mobile phase with a constant flow rate of 0.4 mL min^{-1}. To precipitate phosphate, the supernatants were treated with 4 M NH_3 and 1.2 M $MgSO_4$ solutions and incubated with 0.1 M H_2SO_4 before the experiment. Rhamnose was used as internal standard at 1 g/L to correct for measurement variability. The quantification of amino acids was conducted with an Agilent 1200 series instrument (Agilent Technologies, Santa Clara, USA). Separation was achieved by an Agilent Zorbax Eclipse Plus C_{18} column (250 x 4.6 mm, 5 μm) which was protected by an Agilent Zorbax Eclipse Plus C_{18} guard column (12.5 x 4.6 mm, 5 μm). After automatic precolumn derivatization with ortho-phthaldialdehyde, fluorometric detection (excitation at 230 nm and emission at 450 nm) was carried out. The elution buffer consisted of a polar phase (10 mM Na_2HPO_4, 10 mM $Na_2B_4O_7$, 0.5 mM NaN_3, pH 8.2) and a nonpolar phase (45% [vol/vol] acetonitrile, 45% [vol/vol] methanol). Quantification of amino acids was achieved by using 4-aminobutanoic acid as internal standard at 100 μM to correct for analyte variability.

Preparation of cell extracts

The enzyme activity was assayed using a modified protocol by Goel et al. [94] with cell pellets harvested in prior at mid-log phase and stored at -80°C until further use. The frozen pellet was resuspended in cell lysis buffer (50 mM HEPES (Sigma, #H4034), pH 7.5, 2 mM MgCl$_2$ (Sigma, #M2670) and 1x Halt^{TM} Protease Inhibitor-Cocktail (Sigma, #78425) and disrupted with the the FastPrep-24^{TM} 5G cell homogenizer (MP Biomedicals) immediately according to Goel et al. [94]. Then, the cell extract was diluted with the same amount of cell lysis buffer and diluted with a serial dilution (1:2, 1:4, 1:8, 1:16, 1:32). The protein concentration was measured in three diluted cell extract samples using the bicinchoninic acid assay (Pierce^{TM} BCA, Protein Assay Kit, Thermo Scientific, #23225) according to the manufacturer's instructions.

Evaluation of enzyme activity

The enzyme activity was measured by following spectrophotometrically changes in concentration of NAD(P)H at 340 nm. The method to determine the enzymatic activity was based on the protocols of Goel et al [94] with modifications. The enzyme activity was measured in *in vivo*-like assay buffer containing: 0.1 M MES (Applichem, #A0689), 0.4 M glutamic acid potassium salt (Fluka, #49601), 0.05 M sodium chloride (Merck, #1.06404), 0.001 M K$_3$PO$_4$ (Fluka, #60495), 1:10-diluted metals given in supplementary material and the respective reaction specific compounds stated in table 5.1. The pH of each solution was adjusted to 5.25, 5.5, 6.0 and 6.5, respectively, at 30°C. The activities were measured in triplicates using excess amounts of substrate, co-substrate and, if required, coupling enzymes. To ensure non-rate-limiting conditions and to capture dilution rate where the enzyme activity scaled linearly with the enzyme concentration, the assay was performed using six different dilutions. The NAD(P)H formation or consumption as monitored at 340 nm using a Multiskan^{TM} FC Microplate-Photometer (Thermo Scientific, #11590685). The data was evaluated in Python 3.7.1. . The script determined the slope of the linear part of the progress curve over time and determined the range where the enzyme velocity scaled linear with the used amount of cell extract using the random sample consensus (RANSAC) algorithm [214] with a threshold of 20% of the median absolute deviation to determine outliers. The slope of the inliers was corrected by the base activity by subtracting the slope of the control without cell extract. The corrected slope was divided by the respective dilution and the mean of all corrected slopes of inliers was used as final value.

Table 5.1: **Reaction specific compounds for the *in vivo*-like assay buffer**. The given concentrations refer to the final concentrations in the assay.

Enzyme	EC	Reaction Specific Compounds	Based on
PFK	2.7.1.11	ATP: 5 mM, NADH: 0.3 mM; MgSO4: 7 mM; Phosphocreatine: 80 mM; Creatine Kinase (EC: 2.7.3.2): 30 µg/mL, Aldolase (EC: 4.1.2.13): 2 U/mL; G3PDH (EC: 1.1.1.8): 4 U/mL, TPI (EC: 5.3.1.1): 5 U/mL. **Start**: F_6P: 20 mM	[209]
GAPD	1.2.1.12	ADP: 3 mM; NAD^+: 5 mM; KH_3PO_4: 50 mM; PGK (EC: 2.7.2.3): 14.5 U/mL; $MgSO_4$: 5 mM, Cysteine: 5 mM. **Start**: G3P: 10 mM	[94]
PYK	2.7.1.40	ADP: 3 mM; NADH: 0.3 mM; $MgSO_4$: 5 mM; $F_{1,6}BP$: 5 mM; LDH (EC: 1.1.1.27): 10 U/mL. **Start**: PEP: 6 mM	[94]
LDH	1.1.1.27	NADH: 0.3 mM; $F_{1,6}BP$: 3 mM; $MgSO_4$: 2 mM. **Start**: PYR: 20 mM	[94]

Computational approaches for model construction

The computational model was constructed using a system of ODEs. The model was build using COPASI 4.36 (Build 260) [126]. The rate laws were formulated in accordance with Liebermeister and Klipp's convenience kinetics [161] and mass action. The reaction stoichiometries were taken from literature or KEGG [140, 141, 142]. The model was parameterized using parameter ranges for the parameter estimation task in COPASI corresponding to the minimum and maximum value of the respective glycolytic enzyme occurring in the class of bacteria in SABIO-RK [315] or from Bar & Even et al. [18], if SABIO-RK had only a few listed values. Parameters were estimated with the Parameter Estimation Task in COPASI, using Particle Swarm (swarm size 50, standard deviation for an alternative ending of 10^{-6}), based on the experimental data. Equilibrium constants K_{eq} were estimated in a range between 0.5 to 100. Some parameter ranges were adjusted iteratively to fit the experimental data. The effect of the pH on the enzyme activities was included by adding a pH-dependent scaling factor to the respective rate laws by multiplying the V_{max} by the respective pH_c-dependent factor F_{E, pH_c} in eq. 5.9 as a Global Quantity.

Determination of the buffer capacity

The parameters of the cytosolic buffer system were estimated by the parameter estimation function in COPASI. The buffer system was modeled employing the equations of Anderson et al. [9], with the deviation that only three buffers for the cytosol and medium, respectively, were used. The initial values for all buffer systems were implemented with initial conditions for the protonated buffer bh to assure an equilibrium of the buffer compounds at time point 0 (eq. 5.2).

$$[bh_0] = \frac{k_1 \cdot [h_0] \cdot [b_{total,\,0}]}{k_2 + k_1 \cdot [h_0]} \tag{5.2}$$

Retrieving pH profiles

In order to implement the effect of pH_c, the enzyme activity of every glycolytic enzyme is adjusted by pH_c using eq. 5.9 with pH as a function of the cytosolic concentration of protons (eq. 5.3). The values for the pH profile was retrieved by experimental measurements as stated above or taken from literature. The reference of the pH profiles is given in table A4. All values were normalized to the maximal value in the respective data set. As the model was in mmol/L, the pH was calculated by eq. (5.3), respectively for the cytosolic and pH_e. The parameters of eq. 5.9 for every enzyme were estimated using the Parameter Estimation function in COPASI. Only literature pH profiles from enzymes with a sequence similarity in terms of chemical similarity of $< 65\%$ was used. The sequence similarity was calculated by the alignment function of UniProt [20].

$$pH = -(log_{10})\frac{[h]}{1000} \tag{5.3}$$

5.4 Results

In this work, we developed a model of *L. bulgaricus*, which links the extracellular pH (pH_e) with the cytosolic pH (pH_c) and its impact on glycolytic activity. The model can predict acidification profiles and residual amounts of lactose for various cultivation conditions. To accommodate the impact of pH on enzymatic activity, we constructed a kinetic model that includes the lactose metabolism of *L. bulgaricus*, as described in section 1. In section 2, we

depict the measured substrate conversion of glycolytic enzymes across multiple pHs to couple pH_c and enzyme activities. We additionally developed a machine learning based image analysis approach to estimate cytosolic volume from flow cytometry measurements. The influence of pH on the enzyme kinetics and the increase in total cytosolic volume was integrated into the model in section 3. Section 4 describes further parameterization processes and model validation with additional data sets not used for parameterization. Lastly, we used the model to predict the final pH of cultures at various lactose concentrations.

5.4.1 Setup of *L. bulgaricus* Model Reactions

The stoichiometric reactions required for the metabolism of lactose were selected based on literature. Our model consists of import reactions for the uptake of carbohydrates, the respective anaerobic catabolism and export of lactic acid, the degradation of casein to peptides and amino acids, to generate energy and finally, a cytosolic buffer system to control cytosolic acidity. We grouped protonated and unprotonated species except for the buffer systems (eq. (5.5)).

Carbohydrate uptake

Our model includes two import systems for lactose (lcts_e): an antiporter with galactose (gal) and a symporter with protons (h_e) via the lactose permease LacS (LACS, TC: 2.A.2.2.1) [77, 130, 304]. The symport reaction accounts for the kick start of lactose uptake while the antiport reaction is used predominantly to sustain the majority of lactose uptake in later stages [220]. No functional phosphoenolpyruvate:lactose phosphotransferase system (PTS) for the lactose uptake was reported [121], therefore we omitted a phosphoenolpyruvate:lactose PTS. We integrated a reversible glucose uptake reaction with the phosphoenolpyruvate:glucose (pep:glu) PTS (GLUpts) [121] and two symport reactions exporting and importing equimolar amounts of glucose called GLUe and GLUi, respectively.

Lactose catabolism

The uptaken lactose is irreversibly split into glucose (glu) and galactose (gal) by the β-galactosidase LacZ (LACZ, EC: 3.2.1.23). This hydrolysis is non-competitively inhibited by
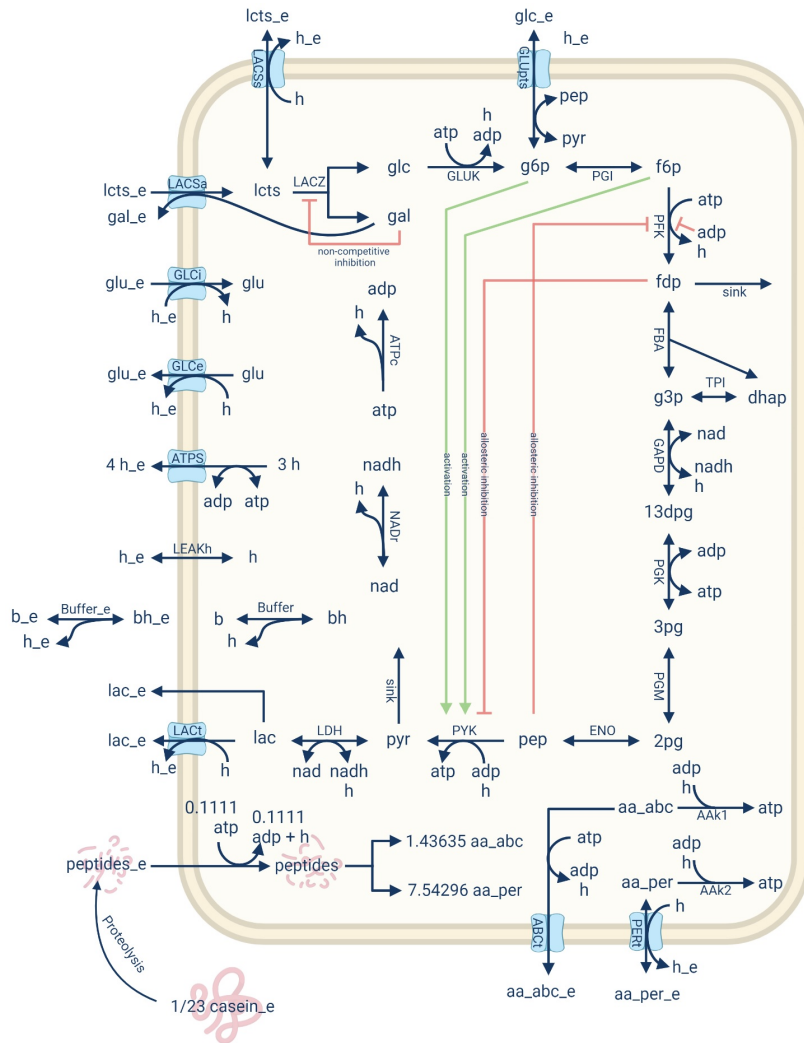
Figure 5.1: **Illustration of the reactions in the kinetic model.** The model represents the relevant reactions for the glucose metabolism of *L. bulgaricus* ATCC BAA-365. The green arrows indicate an activating effect, and the red arrows represent an inhibitory impact of the compound. The cytosolic compartment is growing. The reactions to correct the concentrations of the three cytosolic buffers bh and b, adenosine phosphates (ATP and ADP) and nicotinamide adenine dinucleotides (NAD$^+$ and NADH) by the growth rate were not implemented in the figure. The buffer system is depicted as one reaction in this figure, while it was modelled with three identical reactions with different pKs.

glucose and galactose [194], however, the competitive effect of glucose is rather negligible. Therefore, we did not implement the inhibitory effect of glucose and considered only the impact of galactose. The majority of galactose is extruded by LacS and the glucose moiety is further metabolized to pyruvate (pyr) by glycolytic enzymes and eventually reduced to

lactate [68, 121, 296].

Regarding glycolysis, glucose is degraded to lactate through eleven reactions, all modelled as pH_c-dependent. Further, we account for the regulatory mechanisms acting upon phosphofructokinase (EC: 2.7.1.11) and pyruvate kinase (EC: 2.7.1.40). Phosphofructokinase is inhibited by ADP and phosphoenolpyruvate (pep) [209]. Pyruvate kinase is inhibited by fructose 1,6-bisphosphate (fdp) and activated by glucose 6-phosphate (g6p) and fructose 6-phosphate (f6p) [32] (see reaction PYK in fig. 5.1). In the lower branch of glycolysis, pyruvate is oxidized to lactate (lac), which is excreted by a lactate-proton symporter LACt and a leak reaction, as the membrane is permeable to undissociated lactic acid [42]. Undisccociated lactic acid is present to a small extent at pH values between 5.5 and 6.5. NADP-dependent non-phosphorylating glyceraldehyde-3-phosphate dehydrogenase (EC:1.2.1.9) was neglected in our model, as we could not observe any activity under our experimental setting (fig. A14). To include side branches of glycolysis related with catabolism, two sink reactions were implemented: one for fructose-1,6-diphosphate (fdp) and one for pyruvate (pyr).

Casein degradation and amino acid catabolism

L. bulgaricus BAA-365 possesses a powerful proteolytic system to degrade casein into peptides and eventually amino acids [163, 165]. Albeit *L. bulgaricus BAA-365* has lost the arginine deiminase pathway and glutamate decarboxylase [68], some amino acids can be decarboxylated or catabolized and used in the carbon cycle, thus supplying additional ATP [215]. For example, aspartate can be converted in two reactions to phosphoenolpyruvate, which can be used in glycolysis. Aspartate can be synthesized from other amino acids such as asparagine or glutamine [111, 329], making other amino acids available for ATP production as well. To ensure that amino acids are available in our model, we implemented a simplified version of proteolysis, where casein is degraded into peptides followed by cytosolic breakdown into amino acids. At the end of the proteolytic pathway, the amino acids are catabolized in an irreversible reaction that generates ATP, as exemplarily shown in eq. 5.4.

$$\text{aa} + \text{adp} + \text{h}^+ \longrightarrow \text{atp} \tag{5.4}$$

We lumped the amino acid into two groups based on the transport mechanisms described by Zheng et al. [329]: reversible transport via a permease or irreversible export by an ATP-binding cassette (ABC) transporter. Arginine, asparagine, aspartate, glutamate, glutamine and glycine were included in the second group, and thus grouped as abc. Alanine, histidine, isoleucine, leucine, lysine, phenylalanine, serine, threonine, tryptophan, tyrosine and valine were allowed to diffuse via permeases and were grouped as per. In this model, we did not include cysteine, serine and threonine. The stoichiometric coefficients for all reactions were calculated based on previously published data [290] and a genome-scale metabolic reconstruction of *L. bulgaricus*. For each amino acid, we determined the experimental and the predicted secretion rate. Then, we calculated experimental and predicted amino acid yields using the secretion rates and the specific growth rate predicted by the model (pFBA). The algorithm selected uses an iteratively process to adjust the amino acid stoichiometry until the experimental and predicted yield match.

Cytosolic acidity control and buffer system

Weak organic acids, such as lactic acid, as well as other compounds are acting as an internal buffer system, which contribute to pH buffering. We generically consider this contribution by an estimated buffer capacity in the model. This lumped buffer capacity is modelled in a similar way as in to the model of Andersen et al. [9] and consists of a buffer system for the cytosolic and extracellular compartment, respectively. Each buffer system contains three stepwise distributed protonation reactions with different pKs. Every reaction is modelled using reversible mass action and consists of a buffer (bh), which can be deproneated to the unprotonated buffer b and the proton h (eq. 5.5). Additionally, leak flux for protons was included in the model [175], and implemented as a reversible flux of protons between the extracellular and cytosolic compartments.

$$b + h^+ \rightleftharpoons bh \tag{5.5}$$
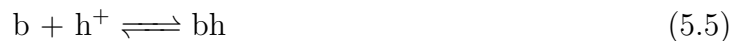
5.4.2 pH-dependent enzyme activity and total cytosolic volume

pH-dependency of enzymes

In our model, the activities of every glycolytic enzyme with the addition of LACZ and LDH are modulated by pH_c. To achieve this, we fitted pH-dependent activity values we

obtained from literature and experiments (tab. A2) to a bell-shaped algebraic function (eq. 5.9). The values determined in this work were obtained by measuring the substrate conversion rates of enzymes using cell lysate in *in vivo*-like buffer at pH 5.25, 5.5, 6.0 and 6.5. Although this pH range only allowed an extrapolation of the relative activity for pHs beyond this range, existing literature confirmed our work for PFK [153] and PYK [32] in *L. bulgaricus* and for GAPD in *L. lactis* [69].

All enzymes showed the highest activity at a neutral pH around 7, and we consistently observed a substantial decrease in enzyme activity at lower pH values. The enzyme activity of most enzymes decreased at pH 6 by approximately 50% relative to activity at pH 7 (fig. 5.2). It can be assumed that pH_c is maintained above 6 if the pH_e is higher than 5 [262].

Increase of cytosolic volume

As *L. bulgaricus* proliferates during the process of fermentation, the total volume in which lactose can be metabolized increases. For this reason, our model comprises a volume growth function describing the time-dependent volume changes of cytosol derived from biomass measurements. The cytosolic volume was fitted to eq. (5.6). The extracellular volume was assumed by subtracting the cytosolic volume from the total fermentation volume of 0.05 L eq. (5.7).

$$V_{t,\,c} = \frac{b \cdot t^n}{t^n + k^n} \tag{5.6}$$

$$V_{t,\,e} = 0.05 - V_{t,\,c} \tag{5.7}$$

5.4.3 Model construction

The metabolic network given in section 1 is translated into a kinetic model based on ordinary differential equations (ODEs). The reaction rates of enzymatically catalyzed reactions were predominantly described using convenience kinetics [161], as exemplarily shown in eq. 5.8 for a reversible reaction with one substrate S and one product P. The changes in apparent enzyme activity caused by pH were included by the pH-dependent algebraic function $F_{E,\,pH}$ (eq. 5.9). Non-enzymatic reactions are implemented using mass
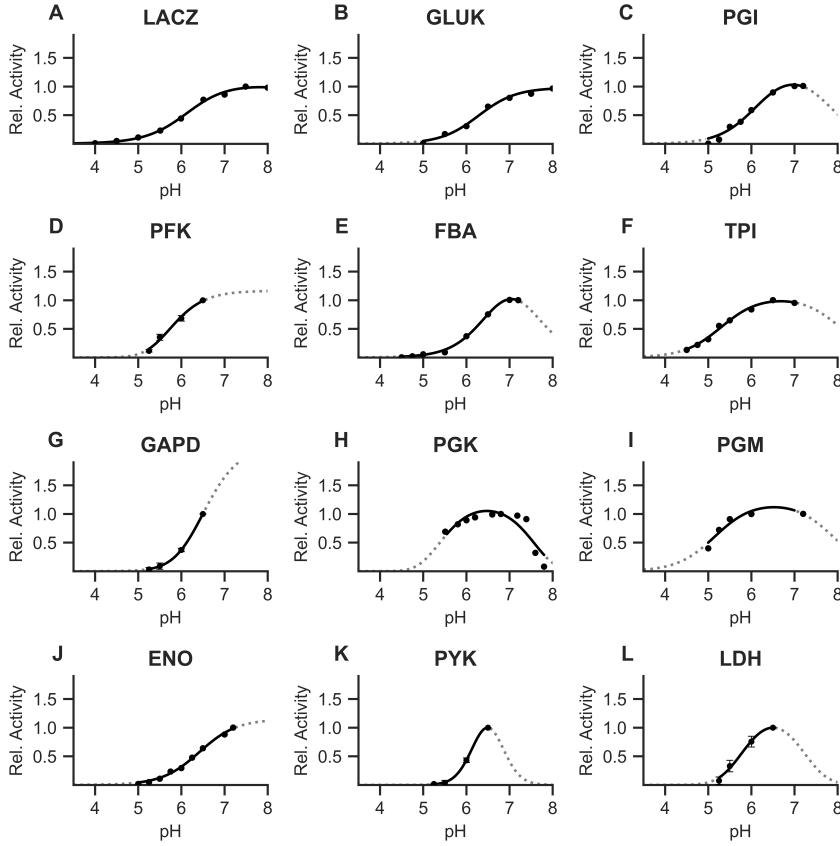
Figure 5.2: **Enzyme activities of the glycolytic enzymes report different pH dependencies.** The activities of the respective enzymes in D, G, K and L were measured in *in vivo*-like assay buffer at pH 5.25, 5.5, 6.0 and 6.5. The other profiles were retrieved from literature. The black part of the curve lies within the range of measurements. The dotted grey lines are extrapolated based on the measured values fitted to an algebraic function. The activity of each pH profile was normalized to the highest value within the dataset. (A) β-galactosidase LACZ [194], (B) Glucokinase GLUK [99], (C) Glucose-6-phosphate isomerase PGI [69], (D) Phosphofructokinase PFK, (E) Fructose-1,6-bisphosphate aldolase FBA [69], (F) Triosephosphate isomerase TPI [69], (G) Glyceraldehyde-3-phosphate dehydrogenase GAPD, (H) Phosphoglycerate kinase PGK [29], (I) Phosphoglycerate mutase PGM [69], (J) Enolase ENO [69], (K) Pyruvate kinase PYK, (L) Lactate dehydrogenase LDH.

action as rate law. A schematic overview of the model is given in fig. 5.1.

$$S \underset{k_{-1}}{\overset{k_1}{\rightleftharpoons}} P, \quad v = F_{E,pH_c} \cdot \frac{(V_{max} \cdot k_{M,P}) \cdot ([S] \cdot k_{eq} - [P])}{k_{eq} \cdot (k_{M,S} \cdot k_{M,P} + [S] \cdot k_{M,P} + [P])} \tag{5.8}$$

$$\text{with } F_{E,pH_c} = \left(\frac{k_{opt}}{1 + 10^{k_1 - pH_c} + 10^{pH_c - k_2}} \right)^n \tag{5.9}$$

5.4.4 Measurement and simulation of glycolytic metabolites

Parameter estimation.

We cultivated *L. bulgaricus* in synthetic medium (SM) with casein to obtain time-dependent data for pH_e, lactose, glucose, galactose, lactate and amino acids, as well as biomass measurements. This dataset, excluding biomass, was added to the parameter estimation task in COPASI [126] to estimate parameter values in our model. Additionally, to avoid solutions with parameter sets where the pH_e drops below 3.65 or becomes higher than 8, we defined an ODE which increases if pH_e is outside of this range and added the minimization of this function to the parameter estimation task. Having a well-parameterized model, we can estimate the dynamics of pH_c. The simulations with the parameterized model are in good agreement with the experimental data for lactose, lactate, glucose and galactose (fig. 5.3 A to D). The dynamics for pH_e were reproduced well for the first four and last two hours of the time course, however, the model overestimates pH_e for time points 5 and 6 hours slightly by 0.4 pH units (fig. 5.3E). The model shows a continuous metabolization of lactose with an increase in the concentrations of lactate and galactose. The decrease of lactose can be divided in four stages (fig. 5.3A). During the lag phase and the early exponential phase, lactose is consumed very slowly. Then, during the exponential phase, lactose is consumed with a high rate, followed by a lower rate with a linear behavior in the transition and early stationary phase. After approximately 14 hours, a sudden stagnation in the concentrations of lactose, lactate, galactose, and in pH_e becomes apparent. By the end of the time course, 30 mM of lactose were approximately consumed. Glucose differs from the other curves in its dynamics (fig. 5.3C). In the first 2.5 hours, glucose accumulates to 1 mM and then drops to 0 mM. Only after 24 hours, the concentration increases again reaching 0.22 mM. The model resembles the peak of glucose concentration within the first hours, however, the concentrations at 24 and 26 hours were lower by approx. 0.15 mM in the simulation (fig. 5.3C).
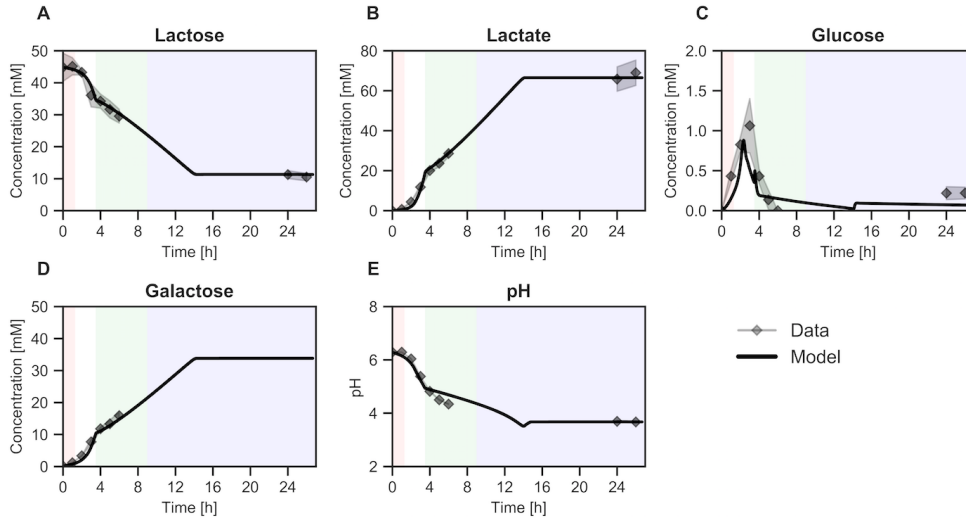
Figure 5.3: **Metabolic profiles of extracellular metabolites and pH.** Shown are the experimental values (squares) of a batch fermentation in SM with an initial concentration of 45 mM lactose and casein measured in triplicate the standard deviation shown as a transparent error band and the calculated concentrations after the model was fit to the experimental data (solid line) of (**A**) extracellular lactose, (**B**) lactic acid, (**C**) glucose, (**D**) galactose and (**E**) extracellular pH. Growth phases are color-coded in the background. Red: lag-phase, white: exponential phase, green: transition phase, blue: stationary phase

Glycolytic flux and cytosolic pH

This model incorporates dynamic changes in pH_c. Therefore, we measured substrate conversion rates *in vitro* in different pH environments (fig. 5.2) and implemented pH-dependent kinetic equations (eq. 5.8 and 5.9). The resulting parameterized model allows to gain a better understanding of the changes in pH_c during cultivation and interdependence between pH_c, glycolytic flux and carbohydrate metabolism. Hereafter, we will use the flux through the PYK as representative for the glycolytic flux because it is the last step to pyruvate followed by lactate production.

Figure 5.4A shows the change of pH_c and glycolytic flux for PYK during a batch fermentation in SM with initially 45 mM lactose and casein. According to this, we identified four phases: an active phase between 0 and 3.5 hours with increasing glycolytic flux and a decreasing pH_c from 7.6 and 6.9 marked in red in fig. 5.4A. This phase includes the highest extracellular acidification rate (fig. 5.3E) and biomass increase (fig. 5.4B). After 3.5 hours, a short and radical transition phase occurs where pH_c drops to 5.9, while
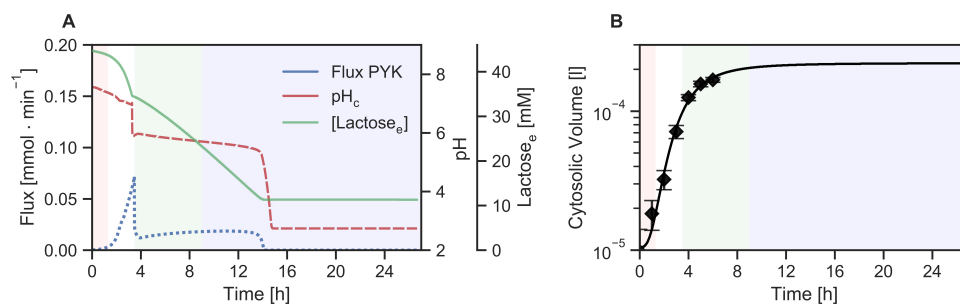
Figure 5.4: **Glycolytic flux in dependence of cytosolic pH.** (**A**) Simulated time course for the glycolytic flux, represented by the flux of PYK (blue), pH_c (red) and extracellular lactose (green). (**B**) Total intracellular volume in Litre (L) in dependence of model time. The solid line gives the model value while the dots represent the mean of three experimentally determined values. Growth phases are color-coded in the background. Red: lag-phase, white: exponential phase, green: transition phase, blue: stationary phase.

the glycolytic flux regresses. Then, a long stationary phase follows for about 11 hours indicated by a steady low glycolytic flux and a small decrease of pH_c from 5.8 to 5.4, depicted in green. Interestingly, enzymes of the upper branch of glycolysis are strongly affected in their activity by this reduction in pH, while enzymes such as PGK, PGM, PYK, and LDH are less affected and do not show a steep decline in their relative activity (fig. A7). Thereafter, approx. 14 hours after the start of fermentation, pH_c again drops to 2.7, glycolytic flux ceases and depletion of lactose stops. The consequent stop of lactose metabolization can be explained by inactivation of all glycolytic enzymes (fig. A7), as pH_c rapidly drops to 2.7 (fig. 5.4A). Further, fig. 5.4A indicates two main states for glycolytic activity: a high glycolytic flux at pH_c above 6.9 (within the first 3.5 hours) or a reduced glycolytic flux during pH_c between 5.8 to 5.0 (3.5 to 14 hours).

Quantification of predictive power

To determine the predictive power of the model, the batch fermentation experiments were repeated with altered concentrations of initial lactose. We increased the initial lactose concentration to 60 mM to investigate any effects of high lactose concentrations on lactate production and we decreased it to 30 mM to achieve complete consumption of lactose. All three initial lactose concentrations lead to a glucose peak of 1 mM at 3 hours after inoculation and a rapid depletion afterward. With 30 and 45 mM initial lactose, glucose maintains

a concentration close to 0 mM, while, intriguingly, glucose accumulates to 1.5 mM with an initial lactose concentration of 60 mM (fig. 5.5C). Next, the initial values for lactose in the previously parameterized model were adjusted to the respective initial concentration of the experiments and the simulation outcomes were compared to the experimental data as shown by the blue, black and red curves in fig. 5.5. The simulations predict a similar behavior in terms of dynamics for lactose, lactate, glucose, galactose and pH_e. Difference between the simulated and the measured data set were found for the simulation with a high initial lactose concentration (60 mM), particularly, in the final glucose concentration. Overall, the model can simulate the correct acidification profile for all initial lactose concentrations which supports its predictive power based in pH-dependency (fig. 5.5E). As predicted by the model, substrate limitation occurs at around 30 mM lactose.
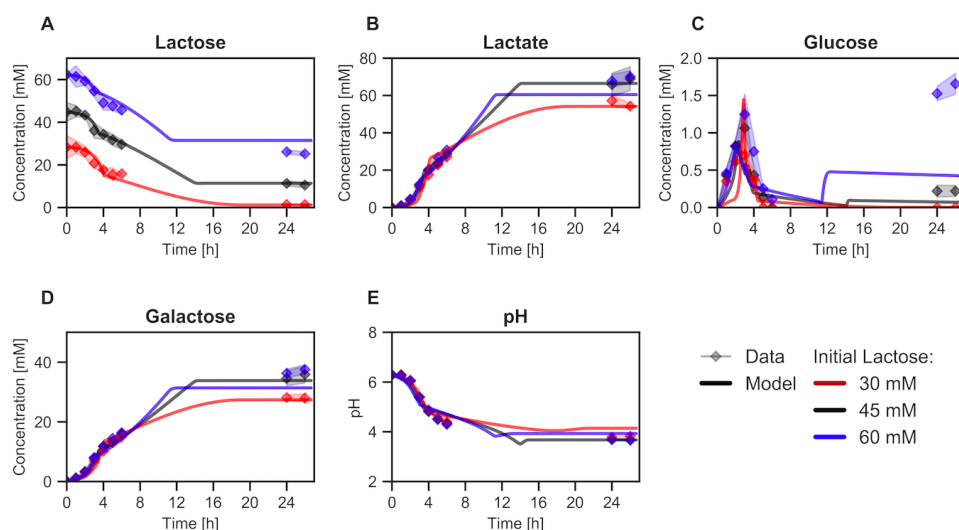
Figure 5.5: **Prediction of metabolic behavior with different initial concentrations of lactose at pH 6.3.** The concentration of (**A**) extracellular lactose (**B**) lactic acid, (**C**) glucose, (**D**) galactose and pH_e was measured at pH 6.3 with 30 mM (blue), 45 mM (red) and 60 mM (black) initial lactose. The dots with the standard deviation shown as a transparent error band are the experimentally determined concentrations measured in tree biological replicates. The lines are model predictions based on the parameterized model shown in fig. 5.3.

Prediction of pH as a results of various lactose concentrations.

Our aim was to predict the final pH_e of cultivation with *L. bulgaricus*. Therefore, we developed and parameterized a model which could reproduce several experiments. Next,

we used this model with a wide range of initial lactose concentrations to predict pH_e after 24 hours. Fig. 5.6A shows the pH value after 24 hours from simulations with initial lactose concentration from 0 to 80 mM. We found that an initial lactose concentration of 41 mM results in the lowest pH of 3.6. A lower initial lactose concentration results in a higher pH as less lactose depletion occurs. Interestingly, an increase of initial lactose concentration above 41 mM results in a slightly increased pH of up to 4.1. Similar dynamics can be observed for the production of lactic acid in fig. 5.6B. As expected, to gain an excess of lactose above 1 mM after 24 h, the initial lactose concentration must be at least 30 mM. The maximal consumed lactose (33.7 mM) and maximal produced lactic acid (67.2 mM) occurs at 41 mM initial lactose concentration.
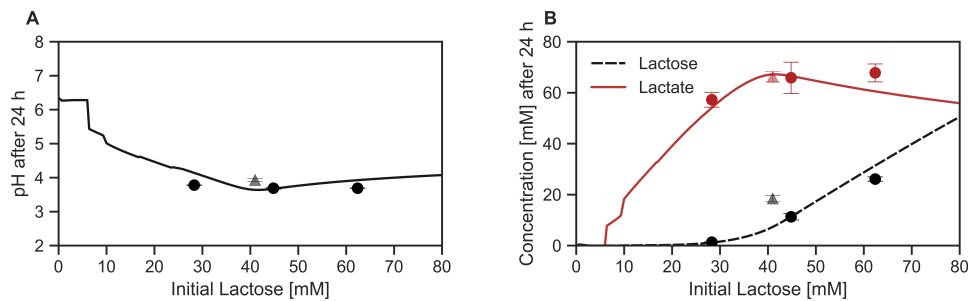
Figure 5.6: **Prediction of final pH, lactose concentration and lactate concentrations after 24 hours with different initial concentrations of lactose.** pH_e (**A**) extracellular lactose and extracellular lactic acid (**B**), respectively. The lines are model predictions based on the parameterized model shown in fig. 5.3. The squares are the mean of three independent experiments with the respective standard deviation shown in fig. 5.5. The results from a fourth experiment (grey or light red triangle) were added with a different experimental set-up: Pre-culture conditions were SM with casein instead of amino acids, and main culture contained 5 g/L casein.

5.5 Discussion

In contrast to most other bacteria, LAB thrive in acidic environments. Fermentation processes by LAB can cause a dramatic drop in pH_e leading to outcompeting other microbes and preservation of foods. Although *L. bulgaricus* maintains a more alkaline cytosolic environment in comparison to the medium, its pH_c is decreasing in co-dependence to the environmental pH_e and can potentially reach values below 6 as the pH of the medium

declines [232, 259, 263]. As enzyme activities are pH-dependent, changes in pH_c affect the catabolic flux. The resulting impact is often neglected in metabolic models and including pH_c is a step towards more physiologically accurate approach to the study of metabolism and eventually the production of high-quality fermented dairy products.

General methodology

In this study we introduced an approach to account for changes in cellular volume during batch cultivation. Since the total volume changes at least 10-fold, this drastically changes the uptake and release of metabolites and protons in the culture. To our knowledge, this is the first time that a mechanistic biochemical model of intracellular processes in microbial batch culture has been integrated with volume growth. Only in the context of vertebrate cells - human brain cells - we found one example integrating volume changes and intracellular behaviour [226]. In addition, we included protons as an independent species in our model - something that has been done in the context of LABs before (e.g., [9]), albeit rarely. Another new insight is further offered, as we took measured pH dependent enzyme activities into account, which hasn't been done before for studying batch cultures and LABs. Generally, we know of only one study on skeletal muscle metabolism [295] that takes measured pH dependencies of enzyme activities into account and one study that used simplified forms of computed pH dependency in a model of *Clostridium acetobutylicum* [187]. The drastic changes in pH during fermentation of LAB, and especially *L. bulgaricus*, emphasize the importance of considering pH and its impact on metabolism.

Modeling pH and its impact on metabolism During fermentation, protons are intrinsically produced in metabolic reactions e.g., upon the usage of ATP, while other reactions such as e.g., the pyruvate kinase consume protons. In our model, those protons are considered as an independent species, which can further impact enzyme activities due to pH-dependent V_{max} values. The pH-activity profiles implemented in $_{max}$ (fig. 5.2) demonstrate that the resulting changes in pH_c affect the activities of the different glycolytic enzymes in distinct ways. According to our data, enzymes in *L. bulgaricus* which are less sensitive to pH variation in terms of their activity are e.g., PGK, PGM, and especially TPI. TPI and PGM maintain around 10% of their activity even at pH 4.2 compared to pH 6.5, while the other enzymes function at approximately 2% (fig. 5.2). Thus, TPI and PGM are still capable to potentially maintain a high metabolic flux. In contrast, enzymes which catalyze the often flux controlling reactions are more affected by pH, such as PYK, GLUK, FBA,

halting glycolysis at a lower pH_c. When pH_c reached values lower than 5.5, the glycolytic flux diminishes and even converges to 0 $mmol \cdot min^{-1}$, if pH_c becomes lower than 5, as depict in fig. 5.4A. The structure of the rate laws in our model is limited for pH-mediated changes in activity, however neglecting effects of changing enzyme concentrations, since these are kept constant throughout simulation. The results of Even et al. [69] suggest an increase in enzyme synthesis for many glycolytic enzymes at lower pH values for *L. lactis* in steady-state, indicating a compensation mechanism. So far, it is unclear in which manner *L. bulgaricus* changes enzyme concentrations during batch cultivation. Including the changes in enzyme concentration during acidification could help to increase the predictive power of the model further.

pH_c and growth phases

Maintaing glycolytic flux is necessary for bacterial growth and ultimately, the survival of the population. Our model showed that *L. bulgaricus* can maintain a low glycolytic flux at acidic pH_c down to 5.5 and that the pH_c needs to be above 5.5 to enable enzyme activity and therefore, glycolytic flux. According to our model, pH values between 5.5 and 5.0 occurred at the late stationary phase (Fig. 5.4B). Those predictions are consistent with existing research indicating that lactic acid production diminishes rapidly at pH values below 6 in permeabilized cells [13] and pH_c 4.7 as the limit for growth [186]. Fig. 5.4B revealed a drop in pH_c after 13 hours, which stops the activity of all enzymes and explains the incomplete lactose metabolism and growth arrest. However, the model predictions about the drop in pH_c at this time point and abruptness may be inaccurate, as we have a gap in data between 6 and 24 hours and due to the lack of such data reported in literature. Nevertheless, the model findings depict the observation that *L. bulgaricus* starts to fail maintaining the gradient between pH_c and pH_e after the beginning of the stationary phase [233]. Our model could demonstrate how the continuous metabolic acidification ultimately leads to the collapse of the pH gradient and inactivation of cytosolic enzymes. Accurate predictions of this behaviour require time-course data of cytosolic metabolites and could further give insights into the impact of organic acid accumulation, which is also suspected to cause growth arrest [40, 245].

Different lactose concentrations and their impact on metabolic behavior

Another industrially relevant aspect in yogurt making is the effect of substrate concentration on the product outcome, such as product yield and acidity. To validate our model, we cultivated *L. bulgaricus* with different substrate concentrations and measured the pH_e, carbohydrates and biomass. As shown in fig. 5.5, the metabolic behaviour with different initial concentrations of lactose followed similar dynamics - in our model and in the experimental data. Regardless of the non-limiting substrate concentration, metabolic inhibition occurred, which suggests an internal effect. This internal effect can be explained by the diminishing pH_c depicted by our model. As our model reproduced the experimental data well without changing parameter values, we applied our model to a parameter scan with a range of initial lactose concentrations to simulate pH_e and remaining lactose concentration after 24 hours of batch fermentation. The results in fig. 5.6 point out that approximately 33 mM lactose were consumed, independent of the initial lactose concentration. The lowest pH_e was obtained with an initial concentration of 41 mM lactose. A decrease or - interestingly - an increase of initial lactose concentration provoked a higher pH_e after 24 hours. As the acidity of yogurt is an essential parameter for taste and consumer acceptance, this model can be applied to optimize the fermentation condition to achieve a desired product outcome.

Conclusion

In summary, our model allows the simulation of pH_c and the computation of biotechnologically relevant parameters like external pH and residual lactose as a function of the initial lactose concentration. Moreover, this study provides valuable insights into how activity of enzymes and their inactivation by the internal pH_c changes the metabolic activity of the cell culture. The model simulation illustrated that metabolic activity continuously acidifies the cytosol. Once a threshold of a pH below 5.5 is reached, the metabolic activity regressed, with the consequence of growth arrest. Thus, the model can be used for the optimization of batch cultures of *Lactobacillus delbrueckii* subsp. *bulgaricus* and can be used as starting point for more complex questions like modeling co-cultures with *Streptococcus thermophilus* during yogurt cultivation. This can lead to a deep understanding of growth inhibition under non-limiting substrate conditions and e.g., to obtain a milder yogurt with a higher pH_e or less residual lactose for lactose intolerant customers.

Chapter 6

Compartment-specific metabolome labeling enables the identification of subcellular fluxes that may serve as promising metabolic engineering targets in CHO cells

The author of this dissertation, Andreas Ulmer, shares first authorship for the manuscript outlined in this chapter with Andy Wiranata Wijaya (Institute of Biochemical Engineering, University of Stuttgart, Stuttgart, Germany). Andreas Ulmer and Andy Wiranata Wijaya contributed equally to the development of the ^{13}C MFA code and implementation in Matlab. Andreas Ulmer was involved in the interpretation of the computational results. Andreas Ulmer reviewed and edited the manuscript.

6.1 Abstract

^{13}C labeling data are used to calculate quantitative intracellular flux patterns reflecting *in vivo* conditions. Given that approaches for compartment-specific metabolomics exist, the benefits they offer compared to conventional non-compartmented ^{13}C flux studies remain to be determined. Using compartment-specific labeling information of IgG1-producing Chinese hamster ovary cells, this study investigated differences of flux patterns exploiting and ignoring metabolic labeling data of cytosol and mitochondria. Although cellular analysis provided good estimates for the majority of intracellular fluxes, half of the mitochondrial transporters, and NADH and ATP balances, severe differences were found for some reactions. Accurate flux estimations of almost all iso-enzymes heavily depended on the sub-cellular labeling information. Furthermore, key discrepancies were found for the mitochondrial carriers v_{AGC1} (Aspartate/Glutamate antiporter), v_{DIC} (Malate/H+ symporter), and v_{OGC} (α-ketoglutarate/malate antiporter). Special emphasis is given to the flux of cytosolic malic enzyme (v_{ME}): it could not be estimated without the compartment-specific malate labeling information. Interesting enough, cytosolic malic enzyme is an important metabolic engineering target for improving cell-specific IgG1 productivity. Hence, compartment-specific ^{13}C labeling analysis serves as prerequisite for related metabolic engineering studies.

6.2 Introduction

^{13}C metabolic flux analysis (^{13}C MFA) is a key tool for quantitative analysis in systems metabolic engineering. First, applications dealt with prokaryotic cells [309], but the technique was also applied for eukaryotes, such as yeast [79, 312], fungi [328], mammalian [1, 138, 274, 283], and plant [8] cells. Among others, prokaryotes and eukaryotes differ in cellular compartmentation, which is particularly important when using ^{13}C MFA. In eukaryotes, compartmentation is essential since each cellular compartment fulfils different functions [2]. Even multi-compartment isozymes exist that serve different purposes. For example, Chinese hamster ovary (CHO) cells comprise cytosolic and mitochondrial malic enzymes (MEs) with different NAD+ and NADP+ regeneration capacities, thereby fulfilling diverse catabolic and anabolic needs [138].

Metabolic compartmentation must be considered when performing ^{13}C MFA [2]. There are two levels of complexity; on the one hand, subcellular metabolic models should be used

to enable proper *in silico* predictions. On the other hand, *in vivo* compartment-specific metabolome data should be available to allow data-driven studies. Nicolae et al. (2014) and Pfizenmaier and Takors (2016) provided evidence for the importance of subcellular stoichiometric models for estimating fluxes in CHO cells [180, 195, 217]. Regarding the latter, Matuszczyk et al. (2015) applied compartment-specific metabolomics in CHO outlining that cytosolic ATP pools are considerably larger than their mitochondrial counterparts [180]. Later, Junghans et al. (2019) continued investigating mitochondrial and cytosolic metabolic patterns under different cultivation conditions. They found that pool sizes differed between cytosol and mitochondria for all conditions [138].

Given that subcellular metabolomics are very laborious [138, 180] the question arises what differences may occur if ^{13}C flux analysis is based on whole-cell metabolomics instead of compartment-specific measurements. In other words, whether the additional lab-efforts justify the information gain of subcellular studies. Alternative approaches such as superimposing the patterns of two independent ^{13}C experiments using labeled glucose and labeled glutamine also aim to decipher subcellular flux distributions [274]. However, they rely on glutamine synthase deficient cells whereas the suggested subcellular metabolomics approach may be universally applicable.

Given that labeling dynamics in metabolite pools expressed by the ^{13}C labeling turn-over ($\tau_{13\,C}$) are a key information for quantifying fluxes, influencing factors may be considered. Two factors, pool size of metabolite i and net labeling flux j through this pool exist [37]. Either factor may change when a system's analysis shifts from simplifying single to realistic multi-compartment analysis. Differences in $\tau_{13\,C}$ may occur originating from individual pool sizes and fluxes inside the compartments. In theory, the same metabolite in different compartment might present a different labeling dynamic providing that the metabolite turn-over time is different. Thus, resulting on a different labeling dynamics ($\tau_{13\,C}$).

Exploiting the unique subcellular labeling dataset of Junghans et al. (2019), this study investigated whether subcellular labeling information is crucial to obtain the correct compartment-specific flux patterns [138]. Flux distributions considering and ignoring subcellular metabolite labeling were performed using CHO as the showcase. This study investigated whether significant differences exist using whole-cell and compartment-specific metabolic information.

6.3 Materials and Methods

This study was based on published metabolome and ^{13}C isotopologue data [8]. In particular, the ^{13}C dataset covering the first 24 h was used to focus on the exponential growth phase.

6.3.1 Cell culture and experimental set-up

The CHO DP-12 cell line (ATCC©CRL-1445TM) was cultivated in a suspension with TC-42 medium (Xell AG, Bielefeld, Germany) supplemented with 42 mM D-glucose, 6 mM L-glutamine, and 200 mM methothrexate. Precultures were cultivated in pre-sterilized disposable shake flasks (Corning Inc., NY, USA) with culture volume ranging from 125 mL to 1 L at an initial viable cell density (VCD) of 0.4×10^6 cells/mL in a humidified shaking incubator (Infors HT Minitron, Infors GmbH, Einsbach, Germany) at 37 °C, 150 rpm, and 5% saturated CO_2. Bioreactor cultivations were performed in a two-fold parallel CellFerm Pro bioreactor system (DASGIP, Eppendorf, Germany) equipped with pitched blade impellers and a process control system. Bioreactor cultivations were started with a VCD of about 0.4×106 cells/mL, temperature was set to 37 Celsius and agitation to 150 rpm. Additionally, the dissolved oxygen content was controlled using an amperometric electrode (Mettler-Toledo Inc., Columbus, OH, USA) at 40%. The pH was measured with a conventional pH probe (Mettler-Toledo Inc., Columbus, OH, USA) and maintained at 7.1 using 1 M Na_2CO_3 or CO_2 gassing. Carbon labeling experiments were performed in the same setup using [U-^{13}C$_6$]-D-glucose as a carbon tracer with an average isotopic ratio of 25% [U-^{12}C$_6$]- and 75% [U-^{13}C$_6$]-D-glucose. Experiments were performed as biological duplicates. In addition to carbon labeling experiments, bioreactor cultivations with [U-^{12}C$_6$]-D-glucose were performed using the same conditions for metabolome profiling.

6.3.2 Extracellular and intracellular analytics

VCD was monitored with a 12 h interval with Cedex XS, an offline cell counting system (Innovatis AG, Bielefeld, Germany). Extracellular D-glucose and L-lactate were monitored offline with LaboTRACE, an amperometric biosensor system (Trace Analytics GmbH, Braunschweig, Germany). Extracellular antibody (IgG$_1$) concentrations were measured using ELISA as reported previously [15]. Extracellular amino acid concentrations were quantified with reversed-phase chromatography (Agilent 1200 Series, Agilent Technolo-

gies, Waldbronn, Germany) [8]. Sampling for metabolomics was performed using differential fast filtration [8, 13]. Then, processed samples were analysed regarding metabolome quantification using an Agilent 1200 HPLC system coupled with an Agilent 6410B (Agilent Technologies, Waldbronn, Germany) triple quadrupole mass spectrometer equipped with an electrospray ion source. Analytical sample preparation and methodology were conducted as reported previoysly [8, 16].

6.3.3 ^{13}C metabolic flux analysis

Isotopic non-stationary ^{13}C MFA was performed in MATLAB 2018a (The MathWorks, Inc., MA, USA). Before performing ^{13}C MFA, measured ^{13}C labeling distributions were corrected for natural stable isotope abundances [17]. Parameter optimization was conducted using MATLAB least square optimization fmincon function in combination with GlobalSearch and MultiStart algorithm in a multi-core computing machine [18]. The first derivative of each isotopomer balance was solved using MATLAB Ordinary Differential Equations ode15s solver. The study used the metabolic and carbon-atom transition model in the previous study [8]. Details of the model are indicated in Table S1 (Supplementary Material S1) and are displayed in Figure 1.

Metabolite balancing

The two-compartment CHO-cell model comprises the stoichiometric matrix S (Supplementary Material S1, Table S1) consisting of m metabolites and n reactions ($m \times n$). The following cell-specific rates [pmol cell^{-1} h^{-1}]were defined: q for cellular uptake and secretion rates, k as inter-compartment transport, and v as compartment-specific reaction. The balance of metabolite i participating in reaction j localized externally, in cytosol, or in mitochondria was described by Equations 1 and 2.

$$\frac{d_{C_{i,\text{ex}}}}{dt} = Q_{i,\text{feed}} + q_i c_X \tag{6.1}$$

$$\frac{d_{c_{i,\text{in}}}}{dt} = \left(-q_i - k_i + \sum_{j=1}^{n} v_j\right) \cdot c_x = 0 \tag{6.2}$$

Where c_i denotes the concentration of metabolite i [mol L^{-1}], c_x denotes VCD [cell L^{-1}], t denotes time [h], and Q_i,feed denotes the feed-rate of metabolite i [pmol L^{-1} h]. The process

model describing the batch cultivation is given in Equation 1 and allows the estimation of q for metabolite i by time-series analysis of extracellular concentrations c_i.

Therefore, the metabolic steady-state was defined as mirrored in the constraint, $\frac{dc_{c,\text{intracellular}}}{dt} = 0$ which is a prerequisite for ^{13}C flux analysis. Both stationary and non-stationary labeling patterns were analysed, originating from the metabolic steady-state condition.

Metabolic flux analysis

MFA was performed using the metabolic network S considering the following constraints: (i) pool sizes of cytosolic and mitochondrial metabolites were in a steady-state and (ii) the entire system was (over)-determined because of the ample ^{13}C labeling information.

Fluxes were estimated according to:

$$v = \begin{pmatrix} S \\ M \end{pmatrix}^{-1} \begin{pmatrix} 0 \\ [q_{\text{meas}}\ p] \end{pmatrix} \tag{6.3}$$

Where M is the measurement matrix containing the stoichiometric coefficients of q_{meas} (measured rates [pmol cell^{-1} h^{-1}]) and p contains the estimated fluxes using mass-isotopomer data [pmol-1 cell h-1]).

Isotopomer balancing and bidirectional reactions

Isotopomer balancing was applied to mathematically describe the incorporation of ^{13}C tracers into intracellular metabolite carbon skeletons [19 – 20]. Isotopomer balances for intracellular metabolites are according to eq. (6.4).

$$\frac{d(\mathbf{C}_i\mathbf{I_i})}{dt} = \sum_{j=1}^{N} \left[\alpha \begin{pmatrix} 0 \\ \otimes \\ k=1 \end{pmatrix} \left(\sum_{m=1}^{n} \mathbf{IMM}_{k \to m} \right) \mathbf{I}_k \right) r_j + 1 - \alpha)(v_i r_j \mathbf{I}_i) \right]$$

$$\text{with}$$

$$\alpha = \begin{cases} 1, & \text{if} v_{ij} > 0 \\ 0, & \text{else} \end{cases} \tag{6.4}$$

where the isotopomer transition from reactant k to product m is described by $\mathbf{IMM}_{k \to m}$. Furthermore, Equation [5] was used to describe labeling dilution by extracellular pools (L-lactate, L-glutamate, L-aspartate, and L-alanine).

$$
\begin{aligned}
\frac{d(\mathbf{I}_{i,\text{ex}})}{dt} &= \frac{1}{c_{1,ex}} \left[\overline{c_X} \left(q_{i,\text{ex}} \cdot \mathbf{I}_{i,\text{in}} - q_{i,\text{ex}} \cdot \mathbf{I}_{i,\text{ex}} - \frac{dc_{i,\text{ex}}}{dt} \mathbf{I}_{i,\text{ex}} \right) \right] \\
\text{with} & \\
\overrightarrow{q}_{i,\text{ex}} &= \beta_i \cdot q_{i,\text{ex}}^{\text{net}} \\
\overleftarrow{q}_{i,\text{ex}} &= \overrightarrow{q}_{i,\text{ex}} - q_{i,\text{ex}}^{\text{net}}
\end{aligned}
\tag{6.5}
$$

Exchange fluxes were defined for each reversible biochemical reaction [21 – 22] according eq. (6.6).

$$
\begin{aligned}
\overrightarrow{v}_j &= \beta_j \cdot v_j^{\text{net}} \\
\overleftarrow{v}_j &= \overrightarrow{v}_j - v_j^{\text{net}}
\end{aligned}
\tag{6.6}
$$

Parameter estimation and uncertainty

Parameter (flux) estimation was achieved by fitting the simulated mass isotopomer distribution (MID) to the measured *in vivo* MID as presented in eq. (6.7).

$$
\min f(\theta) = \sum \left(\frac{\text{MID}_i^{\text{sim}} - \text{MID}_i^{\text{exp}}}{\sigma_i} \right)^2
\tag{6.7}
$$

Cytosolic and mitochondrial MIDs were defined for subcellular studies. Non-compartmented analysis considered that no subcellular measurements were available. Instead, only entire cell labeling patterns should exist. Consequently, compartment-specific information was merged again, applying eq. (6.8).

$$
\text{MID}_i^{\text{com}} = \text{MID}_i^{\text{cyt}} \cdot f + \text{MID}_i^{\text{mit}} \cdot (1 - f)
\tag{6.8}
$$

Where f denotes the molar fraction of metabolite i in the cytosol. During simulations, f was treated as an optimization parameter for those metabolites presented in both compartments; pyruvate, citrate, α-ketoglutarate, malate, alanine, aspartate, asparagine, and glutamine. Accordingly, f serves as an alternate indicator for the importance of considering compartments properly. Furthermore, flux estimation was achieved by fitting the

measured non-compartment metabolome data with calculated MID using eq. (6.9).

$$\min f(\theta) = \sum \left(\frac{\text{MID}_i^{\text{comb}} - \text{MID}_i^{\text{exp}}}{\sigma_i} \right)^2 \tag{6.9}$$

A χ^2 statistical test was used to assess goodness of fit as described in eq. (6.10).

$$
\begin{aligned}
\chi^2 &= \sum \frac{\left(x^{\text{sim}} - x^{\text{exp}}\right)^2}{\sigma_i} \\
dof &= (n - p) \\
\chi^2 &\leq \chi^2_{(1-\alpha, dof)}
\end{aligned}
\tag{6.10}
$$

Parameter uncertainty is essential to evaluate the flux differences including versus excluding compartment-specific data. Conventional parameter uncertainty estimates make use of the local calculation of the Jacobian matrix as a linearized proxy for variance. However, this approach only shows poor performance if a complex and non-linear set of equations should be analysed, as it is the case in this ^{13}CMFA study. Thus, confidence intervals of each parameter (fluxes) were estimated using the chi-square (χ^2) statistics, which works best for non-linear equations [23] as demonstrated by Antoniewicz et al. (2006). The method relies on the assumption that the minimized variance-weighted sum of squared residuals is χ^2 distributed. Thus, the residual difference evaluating the global optimum and fixing one parameter is χ^2 distributed with one degree of freedom.

6.3.4 Statistical analysis

The significant differences between the two analyses were assessed using Welch's *t*-test for unequal variances [24].

6.4 Results

Prior to the ^{13}C MFA studies, a metabolic network model was formulated (Supplementary Material S1). First the structural identifiability and calculability of the network was assessed applying well established methodologies (Supplementary Material S4). Next, the identifiability of distinct fluxes was checked by simulating intracellular ^{13}C labeling patterns assuming pool sizes measured by Junghans et al. (2019). Results presented in the

appendix indicate the good identifiability of intracellular fluxes which motivated us to continue the study by analysing real labeling patterns and flux distributions.

In the study by Junghans et al. (2019), CHO-DP12 cells were cultivated in a bioreactor to investigate three distinct growth scenarios; (I) exponential growth with no (carbon and nitrogen) limitation; (II) moderate growth with L-glutamine depletion and L-asparagine saturation; and (III) stationary phase with severe nitrogen limitation [138]. However, the current study regarding the impact of subcellular ^{13}C data only covers the exponential growth phase during the first 24 h. This period is typically investigated *in vitro* because labeling and cultivation conditions can be controlled easily, giving accurate results regarding flux distributions and cell-specific productivities [1, 283]. Furthermore, additional cultivation study data investigating the same cell line and process conditions was used for broadening the data set of subcellular versus cellular ^{13}C metabolomics for flux analysis (see Supplementary Material S6). The summary of all estimated intracellular fluxes is provided in Supplementary Material S2.

6.4.1 Cell growth and carbon labeling studies

During the exponential growth phase, cells grew with 0.025 ± 0.001 h^{-1}. Carbon and nitrogen sources were constantly consumed, and metabolic byproducts were steadily released with constant specific rates (Supplementary Material S1, Table S2). D-Glucose was consumed as a major carbon source while L-glutamine and L-asparagine served as primary nitrogen sources. Additionally, the Warburg effect [301] was observed, showing a glucose-to-lactate ratio of 0.93 mol$_{D-glucose}$/mol$_{L-lactate}$. ^{13}C carbon labeling was introduced by the addition of 75% [U-^{13}C$_6$]-D-glucose after 2.5 days, revealing no phenotypic changes, i.e., no alterations of cellular metabolism.

6.4.2 ^{13}C metabolic flux analysis using compartment-specific metabolome data

^{13}C MFA was performed using compartment-specific metabolome data reflecting subcellular pools of cytosol and mitochondria together with isotopomer profiles of the said compartments. Flux estimations were performed at least 100 times with randomized input values and rational boundary values for each parameter (Supplementary Material S2). Finally, the chi-square tests achieved 228.87, which served the statistical constraint of 232.92

on a 95% significance level.

Glycolysis and PPP

High glycolytic (0.112 ± 0.017 pmol cell^{-1} h^{-1} of hexokinase) and extremely low PPP fluxes (0.008 ± 0.001 pmol cell^{-1} h^{-1} of G6P dehydrogenase) were found. The latter accounted for 6.68% of the D-glucose consumed. These observations are in agreement with the findings of Ahn and Antoniewicz (2011), who performed ^{13}C MFA in adherent CHO-K1 cells [1]. Additionally, approximately 15% (0.016 ± 0.002 pmol cell^{-1} h^{-1}) of intracellular G6P was continuously in exchange with endogenous glycogen.

***in vivo* mitochondrial shuttle**

Glycolytic carbon fueled into mitochondria via two transport mechanisms; 77% entered via the mitochondrial pyruvate carrier (MPC1/2) and 23% via a putative l-alanine transporter. MPC1/2 showed the highest mitochondrial transport activities while other transporters exchanged compounds for different purposes; (i) mitochondrial citrate carrier (citrate/-malate antiporter; 0.049 ± 0.002 pmol cell^{-1} h^{-1}) served as a citrate exporter to provide cytosolic acetyl-CoA for the *de novo* lipid biosynthesis pathway; (ii) the malate-aspartate shuttle comprising 2-oxoglutarate carrier (α-ketoglutarate/mal antiporter) and aspartate-glutamate carrier (aspartate/glutamate antiporter), which is often described as an indirect NADH shuttle because imported malate is oxidized to oxaloacetate, releasing NADH, fulfilled a different function; malate was net exported from mitochondria to fuel cytosolic ME.

Cytosolic malic enzyme and NADPH production

NADPH is a key electron donor for anabolic pathways and is essential for monoclonal antibody biosynthesis. Templeton et al. (2013) and Ahn and Antoniewicz (2011) suggested MEs as key NADPH producers in CHO cells [1, 283]. This hypothesis was further confirmed via compartment-specific flux analysis by Junghans et al. (2019) [138]. Cytosolic ME (ME$_{cyt}$) was identified as the primary provider serving NADPH needs. Compartment-specific ^{13}C MFA estimated that about 86% of the NADPH requirement was fulfilled by ME$_{cyt}$ (0.09 ± 0.01 pmol cell^{-1} h^{-1}).

6.4.3 ^{13}C Metabolic flux analysis using non-compartmented metabolome data

An additional ^{13}C MFA was performed to investigate the importance of distinct sub-cellular information to elucidate proper *in vivo* subcellular flux patterns. analysing the merged data (eq. (6.6)) via ^{13}C MFA yielded a chi-square value of 140.12 on the 95% confidence level, which was accepted as a good fit (with 154.30 as the χ^2 statistical threshold on 95% confidence interval). This study was performed using the same model consisting of 42 intracellular biochemical reactions. Figure 6.2A provides the comparison of intracellular flux distributions estimated with (left) and without (right) sub-cellular information. The related single-compartment key fluxes and iso-enzymatic rates are depicted as bar plots in fig. 6.2B and fig. 6.2C. Notably, the term 'iso enzymes' encodes fluxes connecting the same substrates and products but localized in different compartments.

Biochemical reactions localized in a single compartment

fig. 6.2 (b, c left) shows fluxes of biochemical reactions that exist in one compartment (cytosol or mitochondria) only. Most of them revealed similar results irrespective of whether compartment-specific information was used (black) or not (grey). Figure 6.3b demonstrates the case the metabolome pools and the respective fluxes were the same for both studies, yielding a similar τ_{13C}. This is also true for citrate synthase v_{CS}, although identifiability was poor. Similar results were observed for cytosolic-based reactions: pyruvate carboxylase (v_{pc}) and PEP carboxykinase (v_{pepck}) (fig. 6.2(c)). These single-compartment reactions possessed the particularity of utilizing the same metabolites but in different compartments (fig. 6.1). In this particular case, no statistically sound difference between v_{pc} and v_{pepck} was found, most likely because compartment-specific OAA values lacked.

Iso-enzymatic reactions localized in different compartments

Special emphasis is laid on the so-called iso-enzymatic reactions of fig. 6.2(c right) that catalyze similar conversions in different compartments. The fluxes of malate dehydrogenase (v_{mdh}), ME (v_{me}), aspartate amino-transferases (v_{ast}), and alanine amino-transferases (v_{alt}) are localized in cytosol and mitochondria, respectively. Of the eight iso-enzymes analysed, seven conversion rates were significantly different. The only exception is the mitochondrial malate dehydrogenase ($v_{mdh,mit}$) which revealed statistical similarity although
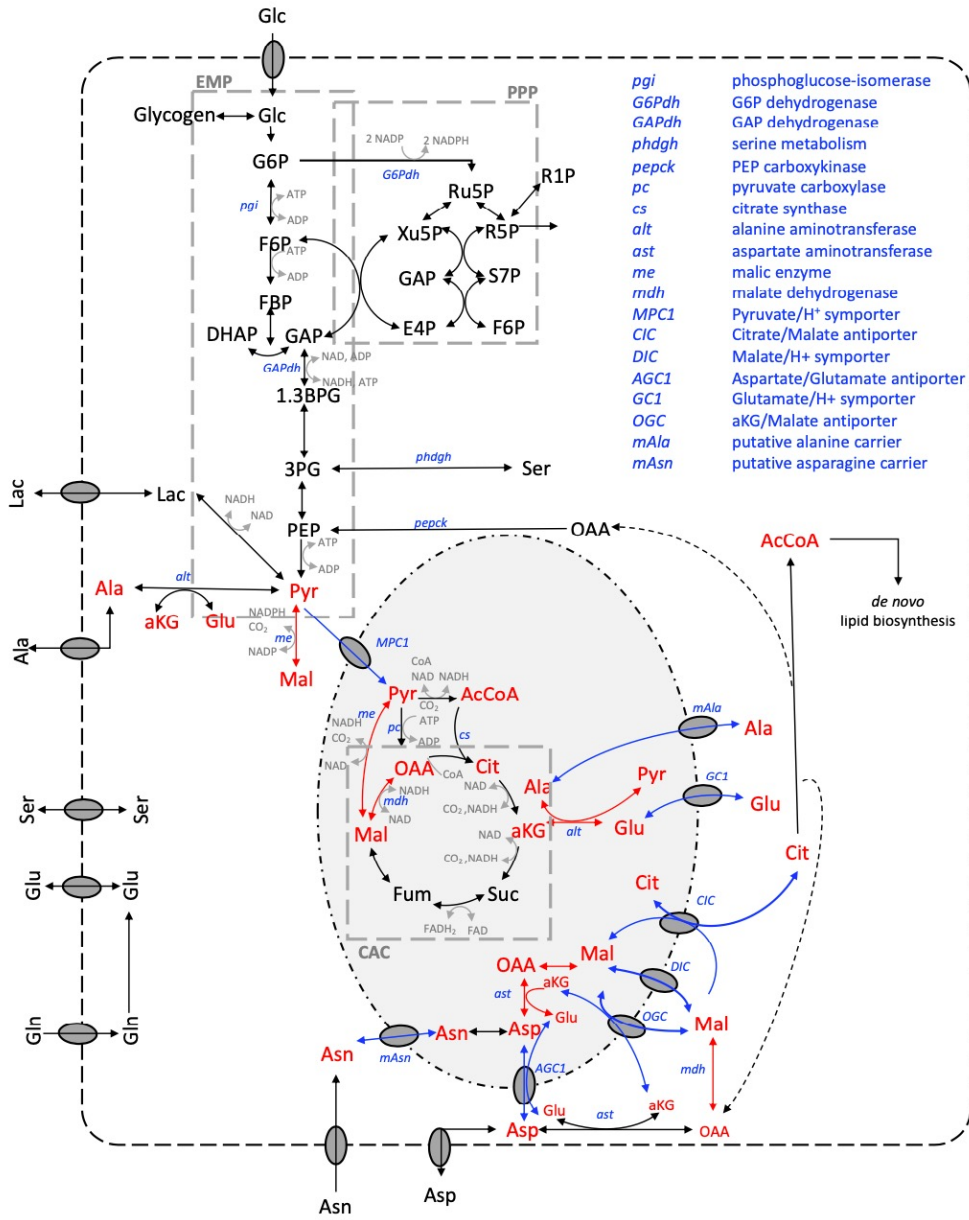
Figure 6.1: Metabolic model of CHO cells used in this study (modified figure from [138]). Arrow coloring indicates the localization of biochemical reactions as follows: black encodes single compartment; red encodes multi-compartments; and blue encodes inter-compartment transporters. Additionally, multi-compartment metabolites are indicated in red.

Figure 6.2: (a) Intracellular flux distribution estimated using compartment-specific (left) and non-compartmented data (right); (b) fluxes of biochemical reactions involving single-compartment metabolites; (c) fluxes of biochemical reactions involving multi-compartment metabolites; and (d) mitochondrial carrier fluxes estimated with compartment-specific and non-compartmented data (* indicates significance $p < 0.05$).

Figure 6.3: Cell-specific production of monoclonal antibodies in CHO cells (modified from Junghans et al., 2019 [138])

fluxes even reversed. On contrary, the cytosolic malate dehydrogenase ($v_{mdh,cyt}$) also disclosed flux reversion but with a sound statistical identifiability. Non-compartmented data were not able to properly reflect real fluxes of the amino-transferases (v_{ast}), namely alanine amino-transferases (v_{alt}) and aspartate amino transferases (v_{ast}). The analysis of whole-cell data resulted in flux overestimation compared to compartment-specific analysis. Notably, the substrate aspartate occurred in cytosol and mitochondria and is a key player of the aspartate-malate shuttle. Moreover, alanine was involved in the co-transport of glycolytic carbon into mitochondria with the MPC1/2. In this case, proper localization and labeling information of the compound is key to estimate fluxes correctly. Additionally, severe bias was observed for fluxes of both malic enzymes (v_{me}) as displayed in fig. 6.2(c right). By trend, ^{13}C flux estimations using non-compartmented data identified significantly lower (about 30%) cytosolic $v_{me,cyt}$ than the non-compartmented data. Regarding mitochondria, the opposite was found. The finding for v_{me} using non-compartmented data is consistent with the observations of Ahn and Antoniewicz (2011) and Templeton et al. (2013) who also performed ^{13}C MFA with cellular data [1, 283]. Importantly, cytosolic ME activity via $v_{me,cyt}$ was identified as a key supplier for NADPH needed for IgG production in CHO cells (Junghans et al., 2019) [138].

Mitochondrial metabolite carriers

Comparing shuttle activities using sub-cellular and cellular labeling information reveals significant differences for half of the inter-compartment transporters, namely the aspartate/glutamate antiporter (v_{AGC1}), malate carrier (v_{DIC}), α-ketoglutarate/malate antiporter (v_{OGC}), and the putative alanine carrier (v_{mAla}) (fig. 6.2d). Similar to the identification of aspartate amino-transferases, the proper identification of v_{AGC1} depends on the labeling turnover τ_{13C} of Asp in both compartments. Missing compartment-specific measurements lead to the different shuttle fluxes, which are also 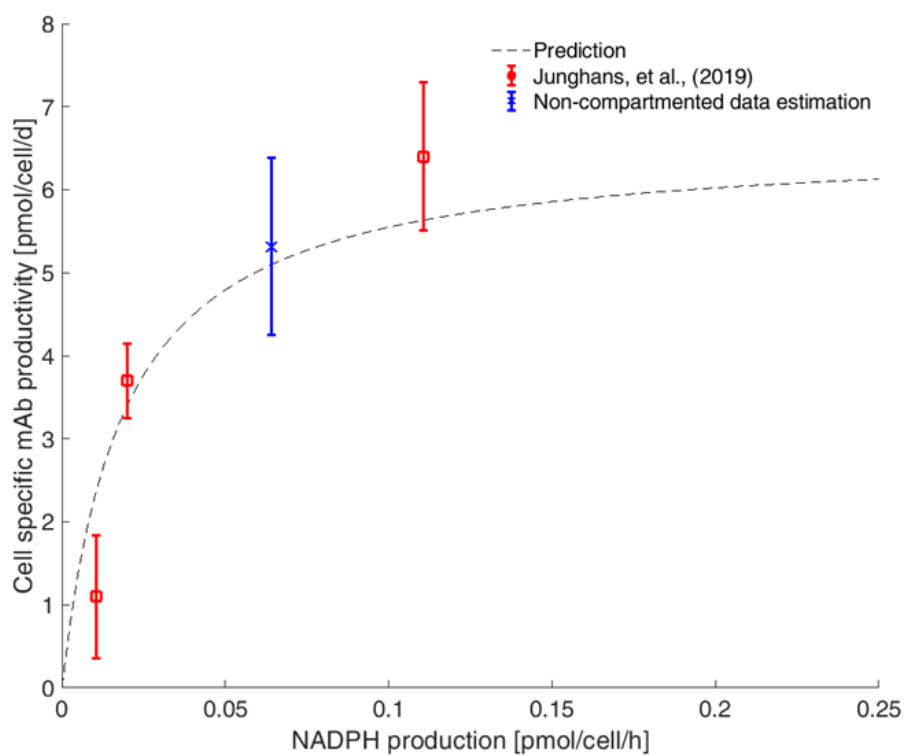reflected in the biased flux v_{ast}. The same scenario also holds true for the putative alanine carrier (v_{mAla}) and the corresponding reactions (alanine amino-transferases; v_{alt}). Shuttle estimations regarding v_{DIC} and v_{OGC} using non-compartment-specific data contradict flux calculations using compartment-specific information estimation. The sub-cellular labeling information of malate is essential to get accurate flux estimates. Interestingly, the flux estimation of putative asparagine carrier (v_{mAsn}) was not biased by the use of whole-cell labeling data only. This may reflect that v_{mAsn} heavily depends on the measured L-asparagine uptake rate (q_{Asn}) irrespective of the existence of additional subcellular information.

Estimated cytosol-mitochondrial fraction (f factor)

Using eq. (6.8), f factors were estimated for each metabolite and compared with the measurements of Junghans et al., (2019) (table 6.1) [138]. As indicated, all estimated cytosolic fractions (f) were poorly identified with pyruvate showing the smallest difference of 8.59% only. On average, 59.71% difference was found compared to the real labeling fraction. Notably, the best estimates of pyruvate and asparagine also enabled improved flux values for the corresponding biochemical reactions, e.g. $v_{MPC1/2}$, v_{pdh} for pyruvate, and v_{asns}, v_{mAsn} for asparagine.

Table 6.1: Complete list of estimated and measured cytosolic fractions of subcellular metabolites used for ^{13}C MFA.

Metabolites	Cytosolic fraction (f)		% difference (measurement as the reference value)
	Estimated	Measurement (Junghans et al., 2019)	
Mal	0.100	0.829	87.9
Pyr	0.910	0.838	8.59
aKG	0.100	0.714	85.99
Cit	0.995	0.489	103.48
Glu	0.373	0.827	54.90
Ala	0.100	0.840	88.1
Asn	0.717	0.805	10.48
Asp	0.500	0.809	38.20

Cellular NADH and NADPH production

table 6.2 shows a comparison of NADH and NADPH production via compartment-specific analysis and neglection of sub-cellular data. Neglecting sub-cellular data, NADPH production is underestimated by approximately 25%. This reflects the 30% underestimation

of cytosolic vME when cellular and not subcellular data are used. In the case of NADH and ATP, the utilization of different datasets disclosed only minor differences. NADH and ATP fluxes were overestimated by 9% and 14% for non-compartmented data, respectively.

Table 6.2: Comparison of NADH, ATP, and NADPH net production rates in compartment-specific analysis and whole-cell analysis (values presented in pmol cell^{-1} h^{-1}).

	NADH	ATP	NADPH
Compartment-specific	0.55692	0.22752	0.10577
Non-compartmented	0.60815	0.25914	0.07924

Challenging the key statements by an additional data set

To investigate whether or not the observed flux characteristics may be specific for the data sets used, additional data of cultivations with the same cell line, cultivation conditions, and analytical tools was used. Figure S6-1:S6-3 (Supplementary Material S6) outlines that very similar key messages are obtained analysing the new data set: Glycolytic fluxes are fairly similar irrespective whether subcellular or cellular ^{13}C metabolomics is used. On contrary, fluxes for cytosolic malate dehydrogenase and malic enzyme differ statistically significant depending on the granularity of metabolic labeling resolution. The same holds true for shuttle activities such as DIC, GC1, and OGC which is in agreement with the results derived from the other data sets.

6.5 Discussion

This study challenges the information gain when performing ^{13}C MFA with compartment-specific metabolome data compared to exploiting cellular labeling information not distinguishing between cytosol and mitochondria.

fig. 6.2 outlines the complexity of the interactions. A group of fluxes (v_{pgi}, v_{GAPdh}, v_{G6Pdh}, and v_{phdgh}) located in a single compartment (here: cytosol) disclose equal values irrespective of the analytical approach selected. Interestingly, this also holds true for v_{cs}, located in mitochondria, primarily due to poor flux identifiability. Furthermore, v_{pepck} and v_{pc} revealed such high flux variances that no distinction could be found whether cellular or subcellular

^{13}C data were used. Apparently, both reactions depend on cytosolic (OAA$_{cyt}$) and mitochondrial oxaloacetate (OAA$_{mit}$). They act at the interphase of the two compartments and rely on proper sub-cellular measurement information (τ_{13C}) for correct identification. Distinct OAA measurements were not available in the current study due to challenging analytical access to the compound. Accordingly, flux estimations might be biased by the quality of OAA pool estimations.

Additionally, some other fluxes should be interpreted with great care, too. This holds particularly true for mitochondrial malate dehydrogenase ($v_{mdh,mit}$) and the pyruvate carrier v_{MPC1}. Both disclose large error bars rendering a discrimination between cellular versus subcellular approaches hardly possible (fig. 6.2(c,d)). Flux imprecisions reflect the lack of reliable CO_2 evolution rates (q_{CO_2}) and CO_2 labeling profiles. The whole-cell (cellular) flux estimation failed to estimate the mitochondrial and cytosolic fluxes of the amino-transferases v_{alt} and v_{ast}. This may reflect that those fluxes heavily depend on the compartment-specific labeling information of alanine and aspartate. Not providing this information by using whole-cell labeling data leads to the large discrepancies given in fig. 6.2(c).

Almost all mitochondrial carrier fluxes were poorly estimated when using non-compartmented data. Inaccurate estimations of v_{AGC1} and v_{mAla} are also reflected by the results of v_{ast} and v_{alt}. Additionally, the poor estimation of the malate carriers v_{DIC} and v_{OGC} depended on v_{me}. In general, fluxes of transporters and bioreactions heavily relied on the labeling dynamics measured in the related metabolites. Regarding v_{MPC1}, the reduced shuttle activity based on non-compartmented data reflects the missing malate exported into cytosol (fig. 6.2(d)).

To check whether the additional use of labeled glutamine (Ahn and Antoniewicz, 2013) [274] might have achieved similar subcellular flux resolutions as the compartment-specific analysis, simulations were performed using U-^{13}C$_5$-L-glutamine (Supplementary Material S3). Interestingly, without information about compartment-specific metabolomics, cytosolic ^{13}C signals obtained from simulations are pretty similar to those of the whole-cell. This is mainly due to the relatively low information gain with respect to the key mitochondrial metabolites malate and aspartate. Compartment-specific labeling information and turnover of the latter are decisive to resolve activities of mitochondrial transporters.

In general, most of the flux estimations using either non-compartment or compartment data led to similar values. Even global cell qualifications, such as rates of total ATP

formation and NADH production, were similar. However, two main findings should be considered:

1. Often, cellular analysis achieved similar flux estimations as subcellular studies by fitting measured cytosolic labeling fractions for the sake of estimating pool sizes properly (table 6.1). In other words, flux optimization algorithms adapted cytosolic and mitochondrial pool sizes to complement missing labeling information. However, the simulated pool size readouts were strongly misleading.

2. Among the fluxes with the largest discrepancies is the cytosolic ME v_{me}. Remarkably, this flux was found to be a promising metabolic engineering target to maximize the formation of heterologous proteins by improved NADPH supply [138]. Accordingly, exact estimation is a prerequisite for proper strain engineering. Figure 6.3 illustrates that even the result of non-compartment data analysis still fits to the subcellular kinetics published in Junghans et al. (2019). Whether or not experimentalists may have identified this enzyme as a metabolic engineering target remains open and is a matter of qualitative discussion rather than quantitative target identification [138].

To date, the compartment-specific analytical approach of Matuszczyk et al. (2015) [180] has shown its suitability for multiple metabolomic studies investigating CHO cells under *in vivo*-like conditions [21, 22, 138, 216, 218, 301, 303]. The latter is enabled by fast and standardized metabolism inactivation. Furthermore, data quality essentially relies on the quantitative access to internal standards, such as G6P/F6P (in cytosolic space) and cis-aconitate (in mitochondrion) to correct for mitochondrial leakage. In general, fast metabolic inactivation, standardized sample processing and use of internal standards are prerequisites for any compartment-specific metabolomics approach that might be used in future applications.

6.6 Conclusions

Investigating the need for using subcellular ^{13}C labeling data, the study revealed that non-compartmented data enabled to identify most fluxes involving single compartment metabolites. Besides, half of the mitochondrial shuttle fluxes and global properties, such as ATP and NADH formation, were fairly well estimated without requiring further subcellular labeling information. However, there is a number of sensitive fluxes that could only be identified properly if compartment-specific pool information was used. Among those

were mitochondrial shuttles that rely on alanine, aspartate and malate. Furthermore, key metabolic engineering targets, such as the cytosolic ME flux for NADPH formation, were severely underestimated using (total) cellular data. This may disguise their role as promising metabolic engineering target if non-compartmented pool analysis is performed, only. The finding underlines the necessity to apply subcellular data for flux estimation, not only to quantify cytosolic/mitochondrial shuttle activities but also to identify metabolic engineering targets and obtain valid values for real pool sizes.

Chapter 7

Evaluation of heat inactivation enabling intracellular metabolite profiling in *S. thermophilus* and *L. bulgaricus* for small time intervals

The author of this dissertation, Andreas Ulmer, is the sole author of the manuscript presented in this chapter.

7.1 Abstract

The determination of substrate conversation rates of enzymes in microorganisms is a piece of important information to gain more insight into cell activity as well as to create predictive models. Exposing cells to heat can stop metabolic activities enabling the determination of intracellular metabolite concentrations and subsequently enzymatic activities by using a labelled substrate. To maintain cell integrity which is essential for further analysis such as fractionating co-cultures into individual strains, a new heat treatment method was developed. The established inactivation unit consists of a thin capillary encased by an aluminium block allowing applied temperatures to at least 200°C. Heat-treated cells (*S. thermophilus* and *L. bulgaricus*) were analysed for alterations in intracellular metabolite pools as well as metabolite leakage into the extracellular matrix. The enzyme activity of LDH was determined to illustrate reduced substrate conversion and constant pool size after heat inactivation. A retention time of 0.1 s at 160 °C was found for *L. bulgaricus* to be

promising to stop metabolic activity while maintaining membrane integrity.

7.2 Introduction

In order to obtain precise flux distributions and enzyme turnover rates in microorganisms, intracellular metabolite pool sizes are essential [247]. The turnover of these metabolite pools is within milliseconds [280] demanding a fast inactivation without disturbing the pool size [123, 248, 302]. Several inactivation methods such as using cold methanol [148] or fast centrifugation [280] were developed. However, treating *L. bulgaricus* with cold methanol results in not reproducible results (Ulmer, personal communication), and fast centrifugation takes several seconds to minutes allowing pool changes, especially in glycolysis.

The inactivation unit (IU) presented is adaptable to methods that demand fast inactivation of metabolism and is suitable for applications such as continuous cultivations with unlimited sample volume. Further, dynamic experiments are possible due to fast inactivation (within seconds). However, the oxygen supply is reduced in connection and in the IU.

To prevent changes in intracellular metabolite pool size, the objective was to reduce enzyme activity and leakage of molecules by reduced cell membrane integrity. To monitor enzyme activity in cells, LDH was chosen. LDH reduces pyruvate to lactate while NADH is oxidized. The decrease of NADH over time was monitored at $\lambda = 340$ nm. LDH activity was examined and used to demonstrate cellular activity. Further analytic methods to point out cellular activity were growth and propidium iodide staining to demonstrate damage to the cellular membrane, and quantification of metabolite pool sizes in various set-ups indicating leakage [123].

7.3 Methods

7.3.1 Cultivation conditions

Cultivation of *L. bulgaricus* and *S. thermophilus* was adapted from [291]. *Lactobacillus delbrueckii* subsp. *bulgaricus* (LB.1 = ATCC BAA-365) was received from an industrial supplier and stored at $-70\,°C$ in MRS (Man et al. 1960) (pH 6.5) containing 20% (vol/vol) glycerol until use. MRS (69966 MRS Broth, Sigma-Aldrich Chemie GmbH, Steinheim, DE) was solved in deionized water, pH adjusted at 6.5 with 2 M NaOH, and

filtrated (ROTILABO, PVD, 0,22 μm, Carl Roth GmbH & Co. KG). Then, 0.5 mL sterile polysorbate 80 (CAS-Nr.: 9005-65-6, Sigma-Aldrich Chemie GmbH, Steinheim, DE) was added. The cells from the cryo tube (volume = 1 mL) were transferred into 15 mL MRS supplemented with additional 14.3 g/L lactose and incubated for 6-8 h at 40 °C. After two wash steps (with 0.9% NaCl solution), the preculture was inoculated containing synthetic medium with amino acids (SMaa) and stirred (400 rpm) at 40 °C for 14-18 h until pH was between 6 and 5.

Streptococcus thermophilus (ST.1) was received from an industrial supplier and stored at -70 °C in M17 (56156 M17 Broth, Sigma-Aldrich Chemie GmbH, Steinheim, DE) (pH 6.5) containing 20% (vol/vol) glycerol until use. M17 was prepared according to the manufactures description and autoclaved. The cells from the cryo tube were washed twice with 0.9% NaCl solution and preculture was inoculated containing synthetic medium with amino acids and stirred (400 rpm) at 40 °C for 2-6 hours until pH was between 6 and 5. Calculated amounts of cells from *L. bulgaricus* and *S. thermophilus* precultures were washed twice in 0.9% NaCl solution and the main culture was inoculated containing amino acids or casein as indicated. Preculture and main culture were cultivated in crimp-top serum bottles pretreated by flushing with 80% N_2 and 20% CO_2 for 10 min and 400 rpm. Growth was monitored by optical density ($\lambda = 600$ nm) with a photometer (Amersham Bioscience, Ultrospec 10 cell density meter) or by flow cytometry (chapter 3).

7.3.2 Medium preparation

A sterile 5x basal solution was prepared containing di-potassium hydrogen phosphate, potassium dihydrogen phosphate, sodium acetate, ammonium citrate, manganese sulfate, iron(II) sulfate, and Tween80 as indicated in table 3.1. Then sterile lactose, magnesium sulfate, urea, nucleobases, and amino acids – if required – were added. After pH was set to 6.5 with 1 M HCl, trace elements, vitamins, calcium chloride, and casein – if required – was added. The serum bottle was sealed, crimped, and flushed with sterile 80% N_2 and 20% CO_2. Casein stock solution was prepared in a beaker containing glass beads (3 mm diameter) which were covered with a thin layer of Tween 80. After casein powder was mixed with beads, 100 mL containing 0.26 g/L $CaCl_2$ was added and the solution was stirred slowly overnight followed by autoclaving carefully for 5 min at C121 °C.

7.3.3 Lactate dehydrogenase activity assay

The pellet of inactivated cells was used to determine the enzymatic activity of LDH according to a modified protocol from [94].

7.3.4 Cell lysis

An aqueous solution of HEPES (0.05 mol/L) was prepared and pH was set to 7.5 using 5 M KOH. $MgCl_2$ (0.2 mol/L) was prepared. HaltTM Protease Inhibitor (ThermoScientific, Waltham, USA) and $MgCl_2$ were diluted 1:100 with HEPES buffer before use.

7.3.5 Medium salt solution

Compounds (table 7.1) were disolved in MiliQ water.

7.3.6 Master Assay Buffer

Compounds (table 7.2) were disolved in MiliQ water and pH was set to 6.5.

7.3.7 Cell lysis

Cell pellets were dissolved in 500 μL lysis buffer on ice. After the addition of 0.5 g glass beads (diameter = 100 μM), the cells were disrupted in a homogenizer (precellys 24, Bertin Instruments, Frankfurt, Germany) with a speed of 5000 rpm, 3 bursts of 20 s. The suspension was centrifuged (15 min, 4°C, 20 000 g) and diluted in lysis buffer (1:2, 1:4, and 1:8). Subsequently, the enzyme activity was measured.

7.3.8 LDH Assay

To determine the lactate dehydrogenase activity, the following (table 7.3) reagent assay was used.

The fructose-1,6-bisphosphate stock solution was prepared by solving 121.8 mg of D-Fructose 1,6-bisphosphate trisodium salt in 1 mL MiliQ water. Pyruvate stock solution was prepared by solving 20 mg of Pyruvate Monosodium in 10 mL.

Table 7.1: Medium salt solution

compound	stock concentration	dilution factor	final concentration	for 10 mL 1x medium-salt
(NH4)6Mo7O24x4H2O		1000x	0,0037 mg/L	10 uL TES (ulmer2022a)
CoCl2x6H2O		1000x	0,007 mg/L	10 uL TES (ulmer2022a)
H3Bo3		1000x	0,025 mg/L	10 uL TES (ulmer2022a)
CuSO4 x 5H2O		1000x	0,0025 mg/L	10 uL TES (ulmer2022a)
ZnSO4x7H2O		1000x	0,0029 mg/L	10 uL TES (ulmer2022a)
MnSO4 x H2O (ulmer2022a)	1 g/L	50 x	0,02 g/L	200 uL
FeSO4 x 7 H2O (ulmer2022a)	0,33 g /L	froozen 500x	0,066 mg/L	20 uL
CaCl2 x 2 H2O (ulmer2022a)	5 g/L	50 x	0,1 g/L	200 uL
MgSO4x7H2O (ulmer2022a)	20 g/L	100 x	0,2 g/L	100 uL

Table 7.2: Master Assay Buffer

compound	concentration [mol L^{-1}]
2-morpholin-4-ylethanesulfonicacid monohydrate	0.2
Potassium glutamate	0.8
Tri-potassiumsulfate monohydrate	0.002
Sodium chloride	0.1

Table 7.3: LDH Assay

compounds	volume [μL]
Master Assay buffer	150
CDM salt solution	30
MgSO4 stock solution ((ulmer2022a)	1.2
Fructose-1,6-bisphosphate stock solution	3
NADH stock solution (15 mM)	6
Adjust pH to 6.1 with 1 M HCl and incubate at 30°C for 10 min	
MiliQ-water	74.8
Measure baseline	
Pyruvate stock solution	30

Subsequent to the assay, the 0.3 mol/l fructose-1,6-bisphosphate, 0.015 mol/L NADH, and 0.2 mol/L pyruvate stock solutions were prepared. Then, 5 μL of pure or diluted sample was transferred in a 96-well plate and 265 μL of reagent mix was added. After 2 min, the baseline was measured at $\lambda = 340$ nm for 20 min. Then 30 μL pyruvate stock solution was added and LDH activity was followed at $\lambda = 340$ nm. LDH activity was determined by considering the slope of measured absorption. The relative enzyme activity was calculated by considering cell pellet samples of cells without heat treatment.

7.3.9 Determination of extra- and intracellular metabolite pools

(a) Cell suspension (12 mL) from cultivation in crimp-top serum bottles was centrifuged (3 min, 4°C, 20 000 g) using three 5 mL Eppendorf tubes (0030119401, Eppendorf, Germany). Cell pellets and supernatant were immediately separated and frozen in liquid nitrogen and stored at -70°C. (b) After cell inactivation in the inactivation unit, the cell suspension was centrifuged (3 min, 4°C, 20 000 g). Cell pellets and supernatant were immediately separated and frozen in liquid nitrogen and stored at -70°C. For metabolite extraction, pellets were supplemented with 120 μL 100 μM Norvalin to correct for analyte variability, boiled at 95°C for 4 minutes, and immediately centrifuged for 20 minutes at 20 000 g and +4°C. All supernatants were filtered (Centrifugation Units ROTI Spin, MINI-3, Carl Roth, Germany) and stored at -70°C. The metabolite concentration was measured on an Agilent 1200 HPLC system coupled with an Agilent 6410B triple quadrupole mass spectrometer (MS-QQQ) using an electrospray ion source (ESI). Chromatographic separation was achieved according to [282]. The metabolite pool concentration was quantified in some samples by the addition of defined amounts of analyte standards into the reaction mixture. Data analysis was performed with the MassHunter B.05.00 software (Agilent Technologies).

7.3.10 Construction of the aluminium-inactivation unit

An aluminium cube (40 or 60 mm) was cut in half and a small furrow was engraved between both halves to insert the capillary. The aluminium cube was placed on a heat plate. The temperature of the aluminium block was monitored by a temperature sensor inserted in the aluminium block. The cooling unit comprises a tube immersed in a water-ice bath. Cells suspension was filled into a syringe pump (HSW HENKE-JECT 20 ml, Henke Sass Wolf, Tuttlingen, Germany) and injected into the IU by a syringe pump (Spritzenpumpe
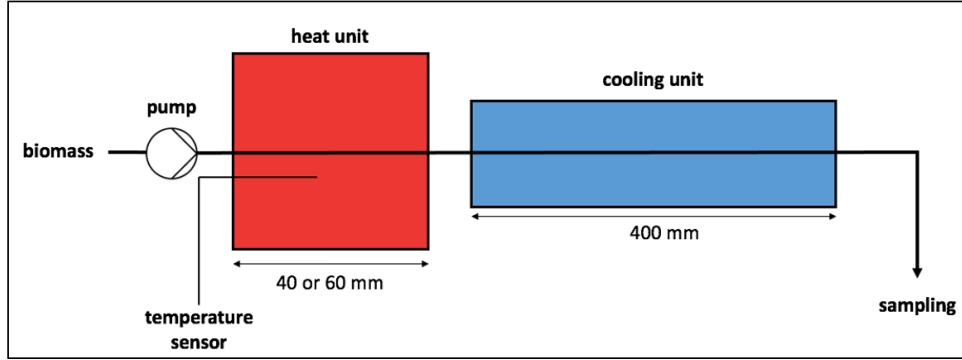
Figure 7.1: Drawing of the aluminium-inactivation unit with an aluminium block used as heat unit and an attached cooling unit.

LA-30, HLL Landgraf Laborsysteme, Langenhagen, Germany) (fig. 7.1).

7.3.11 Characterization of the inactivation unit

The radius of the fused silica capillary was $r_{capillary,inner} = 0.27mm$, and with an indicated length $l_{capillary}$. The heat Q [J] and the heat flow dQ/dt through the area A of the capillary into the fluid in the capillary were calculated according to eq. (7.1). The heat which exits the capillary was determined by eq. (7.2).

$$\dot{Q}_1 = -m_{fluid} \cdot c_{p,fluid} \cdot \frac{\partial \vartheta_{fluid}}{\partial t} \tag{7.1}$$

$$\dot{Q}_2 = \alpha \cdot A \cdot (\vartheta_{fluid} - \vartheta_{applied}) \tag{7.2}$$

$$\alpha = \frac{-ln \frac{\vartheta_{fluid,out} - \vartheta_{applied}}{\vartheta_{fluid,in} - \vartheta_{applied}} \cdot \rho_{fluid} \cdot c_{p,fluid} \cdot \dot{V}_{fluid}}{2 \cdot \pi \cdot r_{capillary,inner} \cdot l_{capillary}} \tag{7.3}$$

In eqs. (7.1) and (7.2), m is the mass of the fluid in the capillary; c_p is the heat capacity ($c_p = 4190 J \cdot K^{-1} \cdot Kg^{-1}$); t_{fluid} is the temperature of the fluid; $t_{applied}$ is the applied temperature in the water bath or in the aluminium block.; and α the heat transfer coefficient. The temperature difference ∂t_{fluid} was replaced by (t_{fluid} - $t_{applied}$) and eqs. (7.1) and (7.2) were equated assuming constant heat transfer coefficient α. The flow rate was included by an

expansion of the equation with $m \cdot t^{-1} = \rho \cdot V \cdot t^{-1}$ ($\rho = 0.997 \ kg \cdot L^{-1}$). This allows the calculation of the heat transfer coefficient α (eq. (7.3)) by measuring the temperature of the fluid.

7.3.12 Dependency of reaction rate constant from temperature

The relation between the reaction rate constant k and the temperature T is provided by equation eq. (7.4) [275] where B is a pre-exponential factor, E_a is the standard reaction enthalpy [J/mol], and R is the universal gas constant.

$$k = B \cdot e^{\frac{E_a}{R \cdot T}} \tag{7.4}$$

7.4 Results

7.4.1 Dynamics in intracellular pool size during cultivation of *L. bulgaricus*

L. bulgaricus was studied in a (semi-) synthetic medium containing casein (fig. 7.2). This allowed profound analysis and a deeper understanding of the original casein habitat. Intracellular poolsizes of *L. bulgaricus* were measured during cultivation in crimp-top serum bottles at three time points. The cell suspension was centrifuged, and the cell pellet was separated from the supernatant and boiled for metabolite extraction (see methods). Figure 7.3 reveals that the upper glycolysis, particularly the fructose-1,6-bisphosphate pool was enriched during cultivation. Only malate and succinate were found, whereas alpha-ketoglutarate, fumarate, and citrate were not found. The very high intracellular concentration of succinate ($91.5 \ \mu mol/g_{DW}$) is intriguing. Thus, using centrifugation and boiling to extract metabolites allowed to quantify intracellular pool sizes in *L. bulgaricus*. However, centrifugation takes several seconds to minutes allowing pool changes, especially in glycolysis.
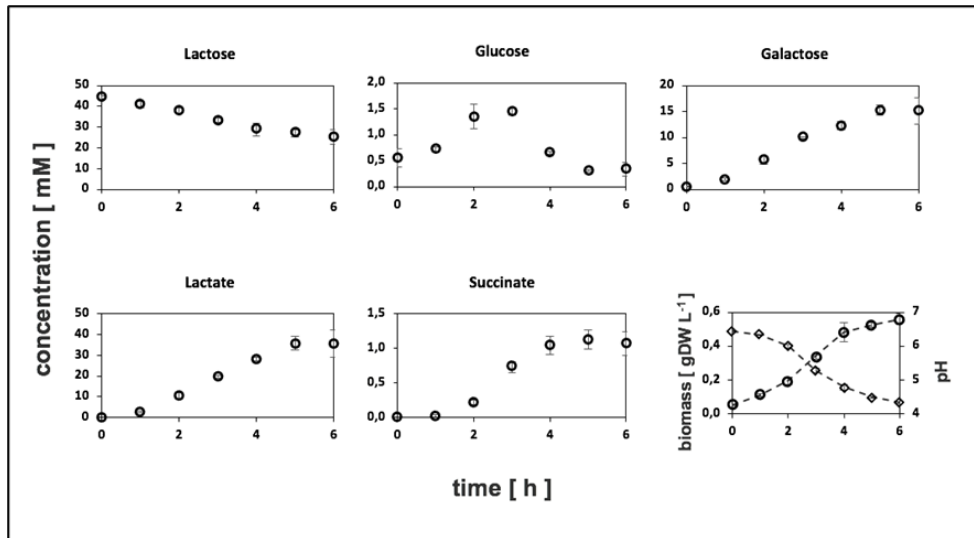
Figure 7.2: Concentration profiles of sugars and organic acids were measured in extracellular matrix in *L. bulgaricus* LB.1 cultivation containing (semi-) synthetic medium supplemented with casein using crimp-top serum bottle. Downright: biomass (circle) and pH (rhomb) measurements.

7.4.2 Using an inactivation unit to stop the metabolic activity and allow strain separation

The method using centrifugation of cell suspension enabled intracellular metabolomics (fig. 7.3), however, it might change the intracellular pool size because the centrifugation step takes minutes whereas (glycolytic) enzymes convert metabolite pools in seconds [281]. Subsequent steps such as density-gradient centrifugation [269] to separate different strains of a co-culture collected in the pellet might also change the cellular state. Thus, initially cell inactivation by using the inactivation unit (fig. 7.4) without demolishing the cell membrane might overcome this limitation.

7.4.3 Leakage of intracellular metabolites

It was assumed that the treatment of cells with the IU might enable fast cell inactivation, but also decrease the stability of the cellular membrane [123]. An unstable membrane might facilitate an increased diffusion of intracellular metabolites to the environment as well as the invasion of staining molecules into the cell [294]. To quantify whether intracellular metabolite pools might leak into the extracellular matrix, phosphoenolpyruvate (PEP) amounts were monitored in the supernatant after cells were treated in IU (m). This might
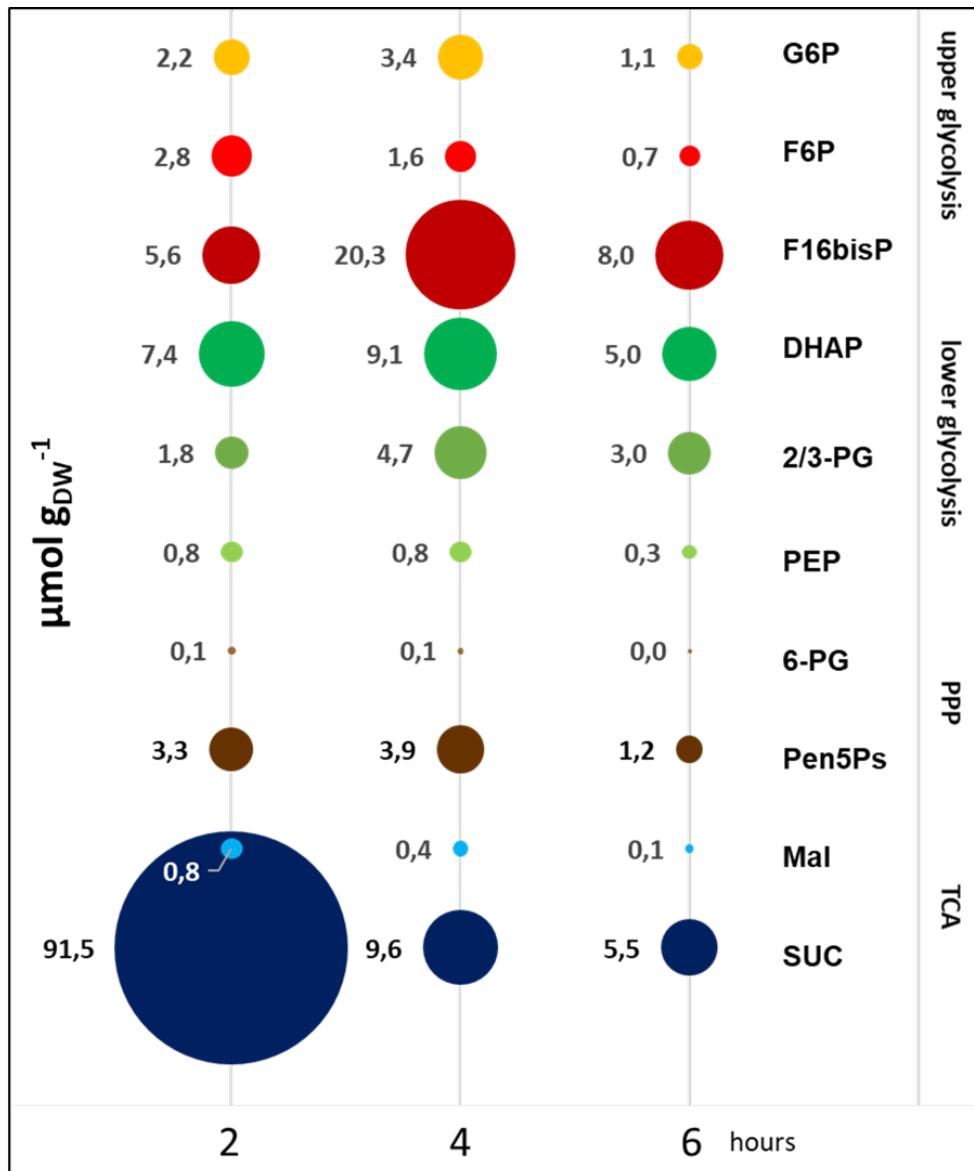
Figure 7.3: Dynamic intracellular poolsizes during cultivation of *L. bulgaricus* in a crimp-top serum bottle. Cells were harvested by centrifugation and boiled for metabolite extraction. Each circle represents the aligned poolsize of a metabolite in $\mu mol/g_{DW}$. Top to bottom illustrates the metabolic sections glycolysis, pentose-phospate-pathway (ppp) and tricarbon-cycle (TCA). G6P: glucose-6-phosphate; F6P: fructose-6-phosphate; F16bisP: fructose-1,6-bisphosphate; DHAP: dihydroxy-acetone-phosphate; 2/3-PG: 2,3-bisphosphoglycerate; PEP: phosphoenolepyruvate; 6-PG: 6-phospho-gluconate; Pen5Ps: pentose-5-phosphate; Mal: malate; Suc: succinate.
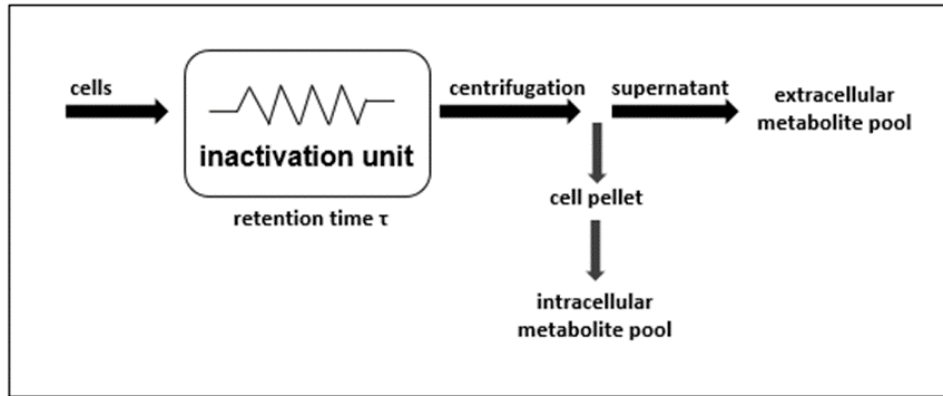
Figure 7.4: Experimental set-up of inactivation unit. Cells cultivated in a crimp-top serum bottle were transferred into syringe pumpe and injected into the capillary integrated in the inactivation unit. Subsequent centrifugation separates cells and cultivation broth.

uncover if leakage is present.

As indicated in fig. 7.5, a retention time longer than 0.3 s at 95°C results in a strong increase of leakage for *S. thermophilus*. Here, the extracellular PEP concentration is almost equal to the extracellular PEP concentration after heat treatment of cells at 95°C for 5 minutes.

7.4.4 Detection of intracellular metabolites in the intracellular matrix

To uncover the effects of IU treatment on cells, the intracellular metabolite pools were examined in *L. bulgaricus* (fig. 7.4). Alterations of the intracellular concentrations might be due to (i) increased enzyme activity facilitation conversion, or (ii) leakage through membrane breaking. However, previously presented leakage in *S. thermophilus* of intracellular PEP into the extracellular matrix (fig. 7.5) indicates that leakage is present. To intracellular metabolite pools of eight metabolites were measured for various retention times at 95°C (fig. 7.6).

The measurement of intracellular metabolite reveals that pools in *L. bulgaricus* decreased with longer exposure to 95°C (fig. 7.6). The reduction of intracellular pool size might be due to leakage as shown in fig. 7.5 for *S. thermophilus*. To exclude the impact of heat treatment at 95°C on intracellular pools, the retention time should be shorter than 0.17 s
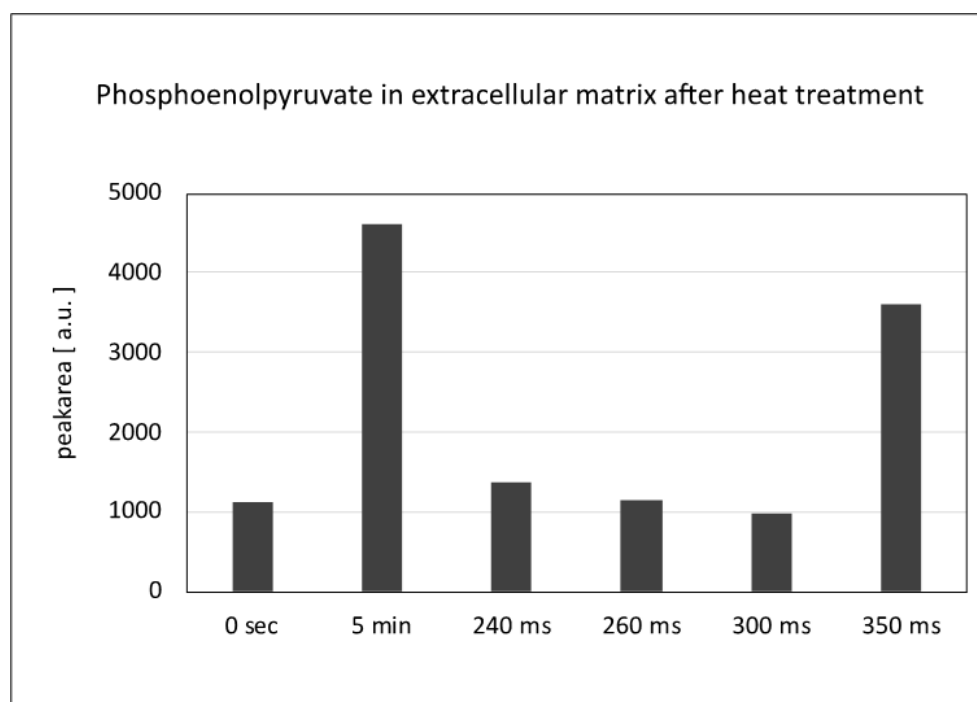
Figure 7.5: Concentration of intracellular phosphoenolpyruvate in extracellular matrix after treatment in water-IU at different retention times (applied temperature was 95°C). The retention time of 5 minutes was achieved by boiling cell suspension and not by using the water-IU. *S. thermophilus* ST.1 was used.
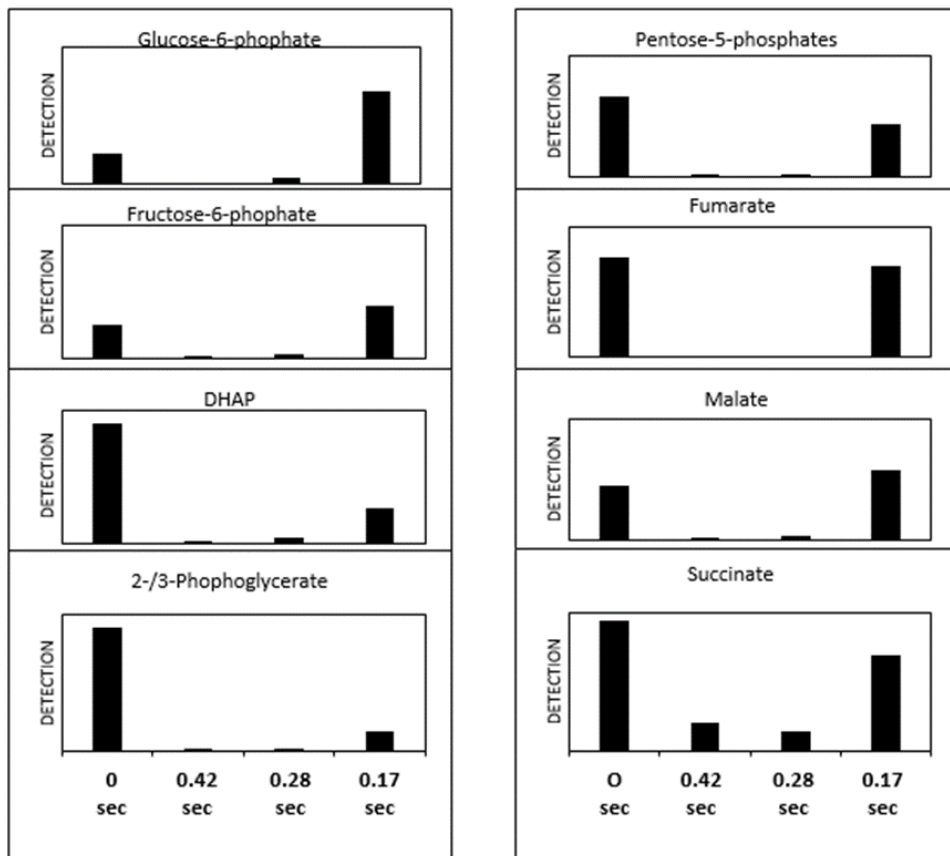
Figure 7.6: Intracellular metabolite pools in *L. bulgaricus* after treatment in IU with different retention times (applied temperature was 95°C).

(fig. 7.6).

7.4.5 Results of existing water-IU

To summarize previous results presented in [123] and the experiments outlined in this dissertation, fig. 7.7 illustrates time frames for retention times to constrain experimental set-up enabling successful cell inactivation. Different objectives such as reduced enzyme activity or intact membrane were chosen to allow sophisticated intracellular metabolome analysis.

The conclusion from fig. 7.7 is, that IU as presented in [123] with a temperature of 95°C was not suitable for demanded inactivation of cells. For example, a retention time of 0.3 s will inhibit the growth of *L. bulgaricus* for 24 h, but not completely inactivate enzyme activity.

7.4.6 From water-inactivation unit (water—IU) to aluminium-inactivation unit

To meet the requirements of unaltered intracellular metabolite pools after heat treatment, the above-mentioned water-IU was adjusted. One possibility was to increase the temperature of the heat unit (HU). This introduces more energy in a shorter time interval to the cells and promotes enzyme inactivation assuming that eq. (7.4) was adapted for enzyme inactivation. The increased temperature might also cause damage to the membrane. Contrasting, another option might be to increase the exposure time to the temperature in the HU. This will lead to damage to the membrane as shown in fig. 7.7. Therefore, the construction of the IU was changed: the HU attached to a water bath was exchanged by an aluminium block encasing the HU and allowing a temperature above 95°C.

7.4.7 Simulation of temperature profiles in heat unit

To indicate the exposed (maximum) temperature of a cell in an IU, the temperature profile was simulated in Matlab.
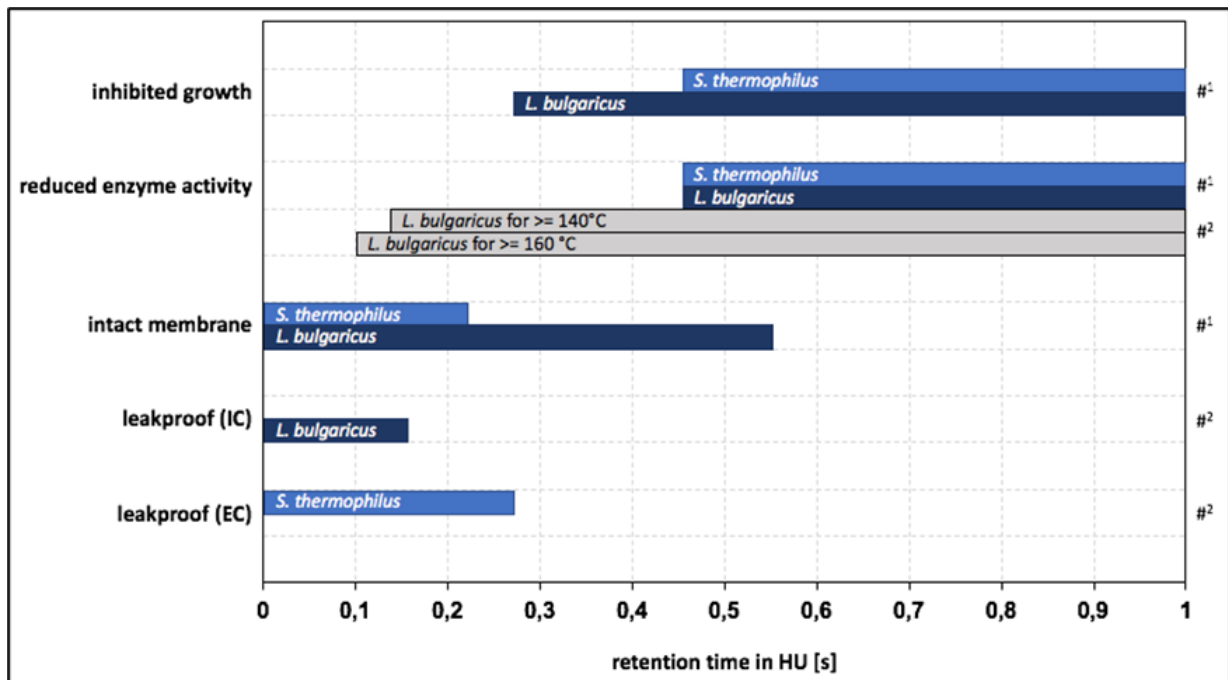
Figure 7.7: Constrains of potential retention times in a heat unit to allow intracellular metabolome analysis. Filled (blue) bars: Retention times from IU with 125 mm heatunit at 95°C. Gray bars: Retention times from from IU with 60 mm heat unit (upper bar) or 40 mm heat unit (lower bar) and various temperature between 120°C to 170°C. At least one measurement was used to extrapolate a bar assuming that result holds true for longer or shorter retention times, respectively. Heat treated cells were analysed for growth recovery for 24 hours, for lactate dehydrogenase activity (reduced enzyme activity indicates reduction of at least 80%), for intact membrane by propidium iodid staining, for sucesful detection of intracellular metabolites (IC), or for detection of intracellular metabolites in extracellular matrix (EC). Source: #1: [123]; #2: this dissertation.
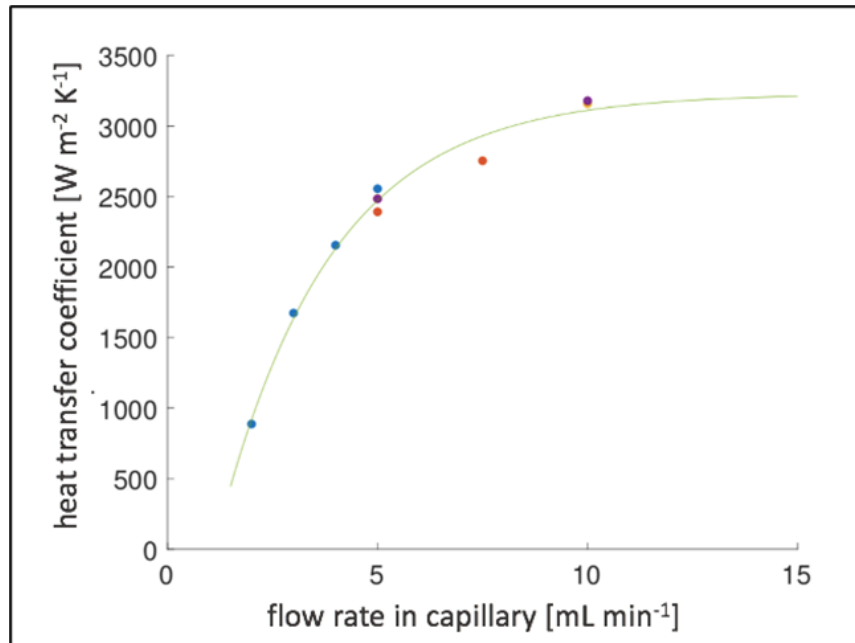
Figure 7.8: Determination of heat transfer coefficient alpha. The temperature of the fluid in the capillary attached to a water-IU (125 mm, 95°C, water [123] was determined for various flow rates.

7.4.8 Calculation of heat transfer coefficient

The heat transfer coefficient α in a water-IU adjusted with 125 mm HU at 95°C [123] was determined and revealed dependency between α and the flow rate (fig. 7.8). This allows the simulation to set α in accordance with the flow rate. Changing this setup to an aluminium-IU as presented below might impact α. The thermal conductivity of aluminium is much higher than water provoking a change of α. An adjustment of the applied temperature from 95°C to 160°C will also impact α. Both effects were not considered in the simulation code.

7.4.9 Enzyme inactivation in IU

The simulated temperature profile (fig. 7.9) of a water-IU (applied temperature 95°C) with a retention time of 0.42 sec resulted in decreased enzyme activity of 80% (fig. 7.7). Cells were exposed to the maximum temperature of 85°C (fig. 7.9). This indicated that at 85°C the metabolization of intracellular pools is strongly reduced due to reduced enzyme activity. Therefore, the requirement of the aluminium-IU was to reach a temperature of
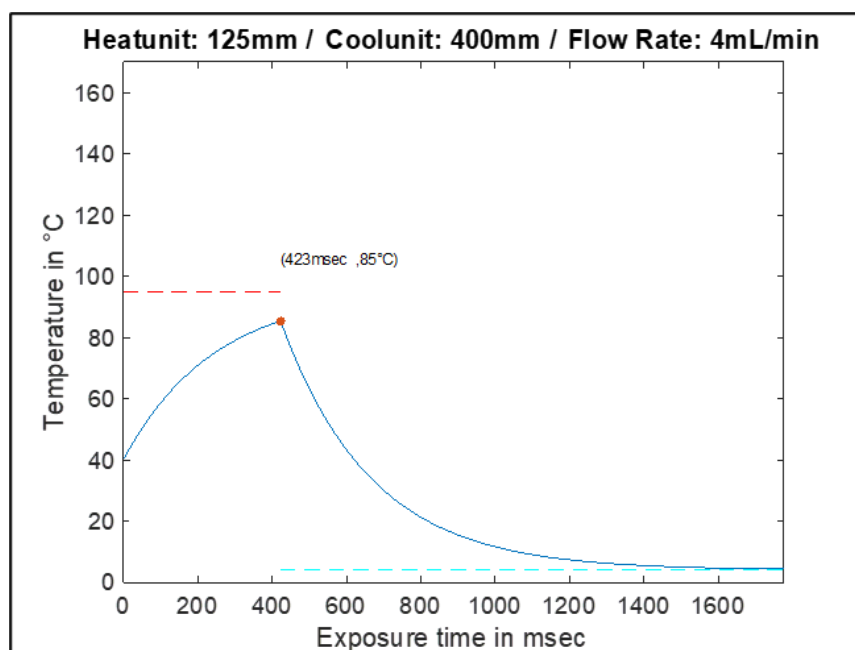
Figure 7.9: Simulated temperatur profil of the water-IU (HU: 125 mm; CU: 400 mm; flow rate: 4 mL/min; retention time: 0.42 s). With this set-up, enzyme inactivation was achieved (adapted from [123]).

at least 85°C while reducing the exposure (retention) time in the HU.

7.4.10 Construction of the aluminium-IU

An aluminium-IU was constructed with 60 mm length and the applied temperatures were between 120-160°C (see methods). From the simulation was assumed that the enzymatic activity should be reduced for an applied temperature higher than 130°C reaching an exposure temperature of 85°C (fig. 7.10).

The measured enzyme activity revealed that treatment in the aluminium-IU (60 mm) with an applied temperature higher than 140°C was sufficient to reduce the enzyme activity from 100% to 20% (fig. 7.10B). An applied temperature of 140°C results in a maximal temperature of 91°C (fig. 7.10A) and was assumed to be sufficient for inactivation of the most enzyme activity (fig. 7.9).

Further, the aluminium-IU enabled to apply temperatures above 160°C and decreased enzyme activity was already observed at 140°C. Therefore, we decreased the size of the aluminium-IU from 60 mm to 40 mm to reduce the residence time at high temperatures

Figure 7.10: (A) Simulated temperature profil in the aluminium-IU with a length of 60 mm (HU) and 400 mm (CU). The flow rate was 5 mL/min resulting in a retention time of 0.1 s. The applied temperatures were 120°C, 130°C, 140°C, 150°C, and 160°C. The maximum (exposure) temperature reached in HU is indicated in the figure. (B) Relative enzyme activity of LDH after treatment in the IU. *L. bulgaricus* was cultivated accordung to methods. Cells were harvest in preculture and resuspended in 0.9% NaCl to OD 0.1. Flow rate of pump was 5 mL/min which results in an retention time of 0.16 sec in the HU. The length of the HU was 60 mm and the applied temperature between 120°C and 160°C as indicated. After treatment in the IU, cells were harvested by centrifugation and LDH activity was determined as indicated in the method section. Error bar were calculated from two treatments with the IU.
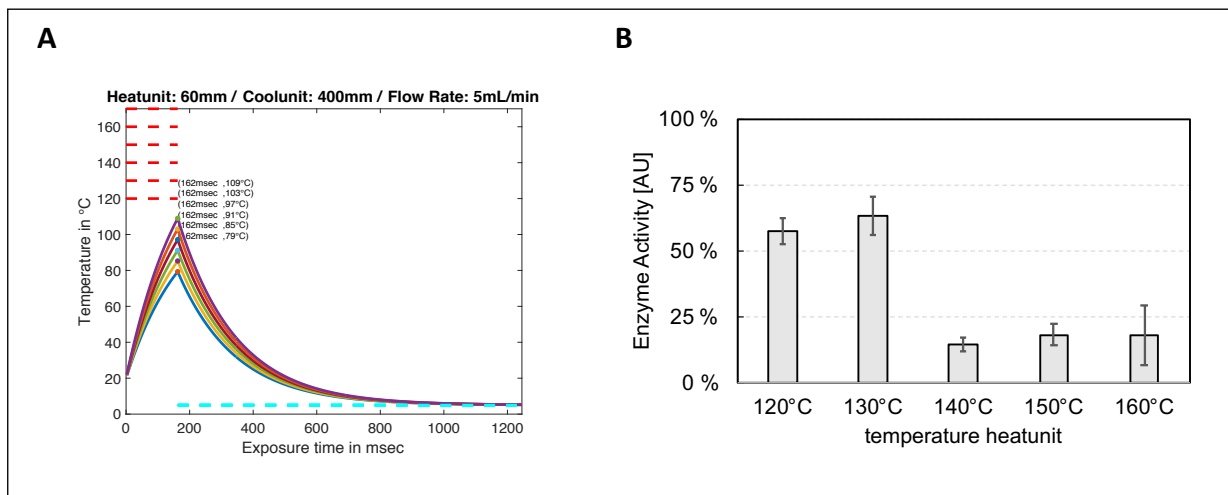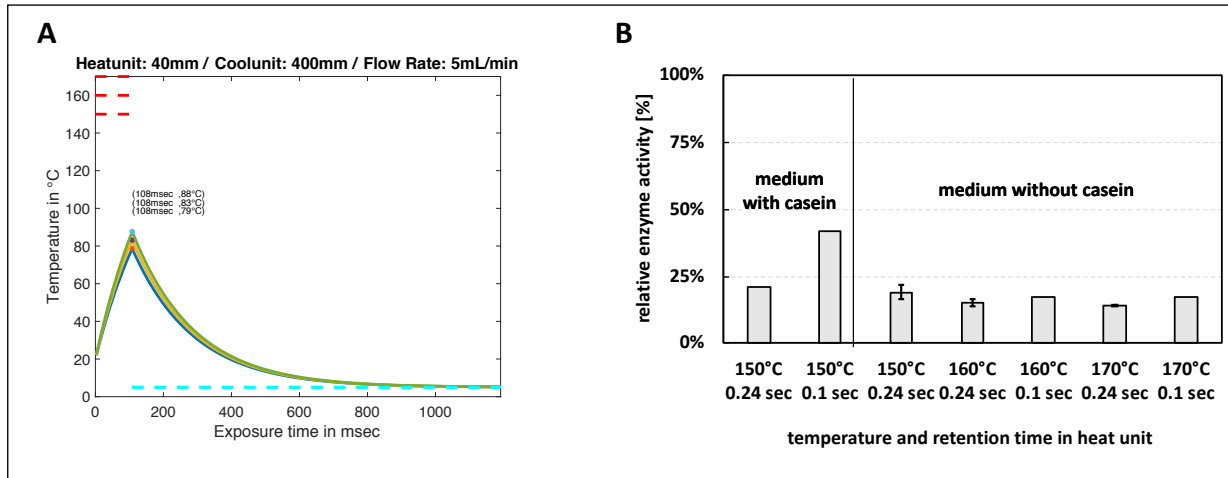
Figure 7.11: (A) Simulated temperature profil in the aluminium-IU with a length of 40 mm (HU) and 400 mm cooling unt (CU). The flow rate was 5 mL/min. The applied temperatures were 150°C, 160°C, and 170°C. (B) Relative enzyme activity of LDH after treatment in the IU. *L. bulgaricus* was cultivated accordung to methods. Cells were harvest from main culture containing medium with casein or medium with amino acids. The flow rate was 2 or 5 mL/min resulting in different retention times as indicated. The applied temperatures were 150°C, 160°C, and 170°C. After treatment with with the IU, cells were harvested by centrifugation and LDH activity was measured indicated in the method section. Error bar were calculated from two treatments with the IU.

reducing assumed damage to the cellular membrane. The simulation of the temperature profile pointed out that a maximum temperature of 83°C is achieved for the 40 mm aluminium-IU when 160°C was applied (fig. 7.11).

As fig. 7.11B indicates, enzymatic activity is decreased by 80% when temperatures above 160°C were applied in a 40 mm aluminium-IU with a retention time of 0.24 s. Using casein in the medium was only possible for samples treated at 150°C. In all experiments with a medium containing casein, the capillary was quickly clogged and IU had to be repaired. Only a small sample volume was inactivated before clogging.

7.5 Discussion

Precise analysing of intracellular metabolite pools after stopping metabolization is only possible when enzyme activity is reduced and the cellular membrane is active preventing changes in pool size and leakage for a given time range. This does not imply that cells are

dead indicating that long-term proliferation might be still possible after treatment in the HU.

As indicated in fig. 7.7, the reduction of enzyme activity and membrane integrity was achieved by a water-IU (applied temperature was 95°C, HU length was 120 mm). However, no setup was sufficient to meet all demands simultaneously (suppressed growth, sufficient enzyme inactivation, and membrane integrity). To overcome this limitation, an aluminium-IU was developed to apply higher temperatures to rapidly inactivate enzyme activity while preventing long residence times in HU (fig. 7.7, gray bars). Thus, results presented in Figures figs. 7.10 and 7.11 indicate for *L. bulgaricus* that a retention time of 0.1 seconds at 160°C was sufficient for cell inactivation and might strive for cell membrane integrity as indicated in figs. 7.5 and 7.6.

Using a medium with casein caused clogging of the capillary. Therefore, the IU was not suitable to inactivate lactic acid bacteria grown in a medium containing casein. However, a medium containing casein is a prerequisite to quantify the interaction between *S. thermophilus* and *L. bulgaricus*.

Chapter 8

A two-compartment fermentation system to quantify strain-specific interactions in microbial co-cultures

The author of this dissertation, Andreas Ulmer, is first author of the manuscript outlined in this chapter. Andreas Ulmer supervised and participated in the development of the two-compartment system. Andreas Ulmer planned the studies and participated in the experiments. Andreas Ulmer conducted data analysis, implemented process model, and evaluated results.

8.1 Abstract

To fulfil the growing interest in investigating microbial interactions in co-cultures, a novel two-compartment bioreactor system was developed, characterised, and implemented. The system allowed for the exchange of amino acids and peptides via a polyethersulfone membrane that retained biomass. Further system characterisation revealed a Bodenstein number of 18, which hints at backmixing. Together with other physical settings, the existence of unwanted inner-compartment substrate gradients could be ruled out. Furthermore, the study of Damkoehler numbers indicated that a proper metabolite supply between compartments was enabled. Implementing the two-compartment system (2cs) for growing *Streptococcus thermophilus* and *Lactobacillus delbrueckii* subs. *bulgaricus*, which are microorganisms commonly used in yogurt starter cultures, revealed only a small variance between the one-compartment and two-compartment approaches. The 2cs enabled the quantification of the strain-specific production and consumption rates of amino acids in an interacting *S. thermophilus–L. bulgaricus* co-culture. Therefore, comparisons between mono- and co-culture performance could be achieved. Both species produce and release amino acids. Only alanine was produced de novo from glucose through potential transaminase activity by *L. bulgaricus* and consumed by *S. thermophilus*. Arginine availability in peptides was limited to *S. thermophilus'* growth, indicating active biosynthesis and dependency on the proteolytic activity of *L. bulgaricus*. The application of the 2cs not only opens the door for the quantification of exchange fluxes between microbes but also enables continuous production modes, for example, for targeted evolution studies.

8.2 Introduction

Interactions between bacteria are common in ecology [171, 306] and involve complex mechanisms that are not yet fully understood [56]. Analysing these natural consortia is important because it improves our understanding of fundamental processes, such as bacterial communication [19]; enables community reshaping to gain health and environmental benefits [332]; and opens the door for the application of (synthetic) microbial consortia in biotechnological applications [113]. Consequently, thorough studies have been performed to investigate the application potential of interacting microbes [92, 144], leading to the development of natural and synthetic co-cultures for industrial use [33, 181, 261, 313].

Microbial interactions allow for a reduction in individual metabolic burden and are considered beneficial for metabolic productivity. For instance, one strain may provide essential nutritional components to another strain and vice versa [197]. Furthermore, the advantages of cofactor and precursor availability may be created for one microorganism if biosynthetic pathways are shared between two strains [137]. In some cases, increased enzyme activity is also observed [330]. Pande et al. [208] provided experimental evidence for the anticipated benefits and studied the growth performance of a synthetic co-culture that relied on the exchange of essential amino acids. Indeed, the growth of the co-culture outperformed that of the mono-culture in the 24 h experiment. Furthermore, the co-culture was stable despite the presence of non-cooperating cells. Smartly sharing metabolic activity between mutually dependent strains yields improvements in biomass production [93, 277, 288, 325]. Driven by the promising potential of microbial consortia for biotechnological applications, here, whether the toolbox for experimental analyses is already complete or should be complemented with novel devices to elucidate strain interactions inside consortia was evaluated. In particular, the following research trends are anticipated to benefit strongly from knowledge of quantitative exchange fluxes among interacting bacteria, which may be measurable in dedicated devices:

- Computational approaches are being steadily extended to unravel and predict interactions between bacteria [88, 152, 319]. To improve the simulation results, data from quantitative experiments providing strain-specific information—in particular, strain-specific growth rates, metabolite production, and consumption rates—are essential to validate model qualities, as indicated previously [17, 31, 106, 268, 323].

- Synthetic co-cultures should be rationally assembled to achieve the desired targets. This demands knowledge of individual uptake and production rates inside co-cultures for fine-tuning the metabolite exchange rates to prevent bottlenecks in supply and the accumulation of intermediates [74, 298].

- Adaptive evolution experiments have been used to improve the performance of strains [16, 256] and have been adapted for co-culture systems [146, 244, 327]. However, to select them for the jointly increased growth of co-cultures, individual adjustments may be necessary, such as the implementation of individual dilution rates to prevent overgrowth and washout scenarios.

Consequently, to meet the demands for strain-specific quantification in co-cultures and to extend co-culture cultivation techniques, several approaches have been developed in recent

years: One approach to obtaining strain-specific rates in co-cultures without disturbing metabolic activities is ^{13}C metabolic flux analysis [322]. To increase the accuracy of estimated fluxes in co-cultures, elegant methods have already been presented by Gebreselassie et al. [85] based on ^{13}C-labelled amino acids, and Ghosh et al. [89] used labelled peptides. These methods are restricted to specific metabolic networks or require specific experimental conditions. Interestingly, even higher flux-resolution patterns may be obtained when applying compartment-specific metabolomics [311]. These observations have shed some light on the potential to unravel exchange fluxes between interacting compartments, each hosting different species of a bacterial consortium.

Alternatively, strain-specific information may be obtained by separating the cells of a co-culture after harvesting. If the cell morphology differs significantly, centrifugation may be an appropriate separation approach [269]. However, this is a time-consuming procedure and is, consequently, prone to changes in intracellular states because of ongoing enzymatic activities [69]. The latter may be prevented by the application of proper cell inactivation technologies, which thus far are still missing. Furthermore, related approaches call for the individual development and optimisation of protocols, making them difficult to transfer to other co-cultures.

Other approaches utilise the spatial separation of interacting strains, as reviewed previously [95]. Often, such experimental settings are miniaturised, allowing the verification of multiple synthetic constructs in a parallel manner, thereby restricting sampling volumes. Examples include microfluidic systems [38, 39, 118] and cell culture plates [132]. Our own studies have indicated that a culture sample of approximately 100 µL is the minimal amount required to quantify the biomass correctly. An additional 100 µL of the supernatant is likely necessary to quantify the metabolites. Hence, the sophisticated and quantitative analysis of interacting cells requires larger reaction volumes than those provided by microfluidic and well-plate approaches. Alternatively, dialysis bioreactors [221] may be applied to cultivate co-cultures in two compartments. However, they incur rather high operational and investment costs and may appear somewhat oversized for studying multiple co-cultures in parallel. To address these limitations, this study aimed to develop a device for co-culture analysis that provides strain-specific information independent of metabolic activity and phenotype. Systematic strain evaluation was enabled by offering a sufficient sampling volume for extensive analysis, and the device was designed to allow quick assembly.

To this end, a compartmentalised fluid system that allowed the growth of two metabolite-

exchanging strains was developed and applied. A strain-specific analysis of growth, production, consumption rates, and intracellular metabolite pools was undertaken. Reflecting the importance of co-cultures in yogurt production, the usability of the system was showcased by investigating the anaerobic interaction between *Streptococcus thermophilus* and *Lactobacillus delbrueckii* subs. *bulgaricus.*

The metabolic activities of the strains are linked to each other: the proteolytic system of *L. bulgaricus* comprises the extracellular proteinase PrtB [49] and intracellular peptidases [162], enabling the strain to gain amino acids from casein, which is likely the reason why the strain loses de novo biosynthetic capacities for many amino acids from sugar [165]. The non-proteolytic proteinase-negative strain *S. thermophilus* benefits from this relationship as it consumes peptides and amino acids from *L. bulgaricus* [212, 264]. The proteolytic system of *S. thermophilus* consists of intracellular and extracellular peptidases [7, 179, 235], which hydrolyse the peptides supplied by *L. bulgaricus.* Peptide and amino acid transporters have been predicted [125, 235] and belong to the ABC binding cassette family [7]. Consequently, amino acids are released from *S. thermophilus*, as measured here [156, 160, 166]. These lactic acid bacteria are used in industrial processes, such as yogurt and bulk chemical production [177, 286], but their interactions are not yet fully understood [179].

8.3 Materials and Methods

8.3.1 Medium Conditions

The synthetic medium (SM) for cultivation (table S1 in Supplementary Materials) was chosen from a previous study [291]. SM containing lactose is indicated as SM + lactose, and SM containing glucose is indicated as SM + glucose. SM containing casein is denoted as SMcas, and SM containing amino acids is denoted as SMaa.

8.3.2 Strain Cultivation

Lactobacillus delbrueckii subsp. *bulgaricus* ATCC BAA-365 and *Streptococcus thermophilus* LMG 18311 were received from Chr. Hansen A/S (Horsholm, Denmark). Precultures and cultivations were performed in crimp-top serum bottles, as described previously [291]. If predefined dilutions were to be installed in cultivations using crimp-top serum bottles, the

related medium was removed and replaced with fresh medium every hour.

For cultivations in two-compartment systems (2cs), precultures were prepared as previously described [291]. Calculated amounts of biomass from one or several precultures were washed twice with 0.9% NaCl solution, and the cell pellets were resuspended in the medium to inoculate each compartment.

8.3.3 Biomass Quantification via the Optical Density Method

Biomass was monitored by optical density ($\lambda = 600$ nm) using a photometer (Amersham Bioscience, Ultrospec 10 cell density meter) by applying the biomass/optical density correlation from a previous study [291]. The pH was measured off-line with a pH meter (SevenEasy^{TM};, Mettler Toledo, Columbus, OH, USA) connected to a pH electrode (In-Lab Semi-Micro;, Mettler Toledo, Columbus, OH, USA).

8.3.4 Biomass Quantification via Flow Cytometry

Samples were processed with Tris-HCl (1.3 M) EDTA (0.13 M) pH 8 buffer; stained with 1X SYBR^{TM} Green I nucleic acid gel stain concentrate (Thermo Fisher Scientific, Waltham, MA, USA); analysed with the flow cytometer BD Accuri^{TM} C6 (BD Biosciences-US) equipped with four fluorescence detectors (FL1 533 / 30 nm, FL2 585 / 40 nm, FL3 > 670 nm, and FL4 675 / 25 nm), two scatter detectors, a blue laser (488 nm), and a red laser (640 nm); and correlated to biomass concentration c_x (g_{DW} L^{-1}), as described previously [291].

8.3.5 Membrane Unit

A membrane unit with two layers was built from polycarbonate to allow the integration of a polyethersulfone (PES; poly(oxy-1,4-phenylsulphonyl-1,4-phenyl)) membrane (pore size 0.2 μm, 15407-47-MIN, Sartorius, Goettingen, Germany) or a polyamide (PA) membrane (pore size 0.2 μm, 25007-47-N, Sartorius, Goettingen, Germany).

8.3.6 Vessel Bioreactor System

Two vessels (50 mL, 101116;, Glasgeraetebau Ochs Laborfachhandel e.K., Bovenden, Germany) were connected to the membrane unit using Teflon tubes (inner diameter, 3 mm)

and stirred. Each side was equipped with a mixing pump (Watson-Marlow 101U/R) to circulate the cultivation broth between the vessels and the membrane unit. The vessels and membrane units were maintained at 40 °C. The vessels and tubes were sterilised via autoclaving, and the membrane unit was sterilised via immersion in 70% (v/v) ethanol for 1 h. The sterile assembled vessel bioreactor system was filled with sterile medium as indicated and warmed up to the cultivation temperature. The biomass was then introduced, and samples were collected using a sterile needle and syringe at the vessel openings.

8.3.7 Tube Bioreactor System

The inlets and outlets of the membrane unit were connected to tubes equipped with a feed and harvest unit. The mixing pump (Watson-Marlow 101U/R) was equipped with a PharMed®-tube (Saint-Gobain, Courbevoie, France) with an outer diameter of 4.8 mm, inner diameter of 1.6 mm, and a length of 18 cm, resulting in a volume of 0.4 mL. An additional connecting tube (Rotilo-silicon tube; Carl Roth GmbH + Co. KG, Karlsruhe, Germany) between the inlet and outlet had an inner diameter of 1.5 mm and a length of 31 cm, which resulted in a volume of 0.5 mL. The feed and harvest tubes had inner diameters of 1 mm. The particles in the membrane unit were removed using 70% (v/v) ethanol followed by washing with sterile Milli-Q water. The tubes and membranes were sterilised via autoclaving. After connecting the tubes and the membrane unit, the cells were seeded into the system by flushing the cell suspension through the feed until the air was removed. Subsequently, the membrane unit and tubes (without the tubes in the mixing pump) were immersed in water at 40 °C to ensure optimal cultivation conditions.

8.3.8 Continuous Cultivation in the Tube Bioreactor System

Each compartment in the tube bioreactor system was equipped with a feed inlet and an outlet to harvest the cultivation suspension for installing individual dilution rates. Syringe pumps (Landgraf Laborsysteme LA100;, Landgraf Laborsysteme, Langenhagen, Germany) were used to ensure feeding to each compartment. To enable accurate harvesting, one outlet was equipped with a drawing syringe pump (LA100; Landgraf Laborsysteme LA100, Langenhagen, Germany), whereas the other outlet allowed the free outflow of the cultivation medium. The harvest was collected for 1 h in an ice-cooled syringe or bottle. A new syringe and bottle were then connected to the harvest for the next sampling. The samples

were analysed for biomass via flow cytometry or centrifuged (3 min, 14,000 rpm, 4 °C), and the supernatant was stored at -70 °C for further analysis.

8.3.9 Metabolite Balancing

The eq. (8.1) depicts the mass balance for metabolite i which may enter one compartment via diffusion and feed (8.1), may be produced (or consumed) in the reaction volume V_R, and leaves the compartment via efflux-indexed production. Considering equal reaction volumes in each compartment, eq. (8.2) (process model) was derived as follows:

$$\frac{dm_i}{dt} = \dot{m}_{i,feed} - \dot{m}_{i,out} + \dot{m}_{i,diffusion} + \dot{m}_{i,production} \tag{8.1}$$

$$\frac{dc_i}{dt} = D \cdot (c_{i,feed} - c_i) + k_i \cdot (c_{i,connected\ compartment} - c_i) + Q_i \tag{8.2}$$

where m_i (kg) denotes the mass of metabolite i; t (h) denotes the time; c_i (mol L^{-1}) denotes the concentration of metabolite i in the balanced compartment; $c_{i,connected\ compartment}$ (mol L^{-1}) denotes the concentration of metabolite i in the connected compartment; D (h^{-1}) denotes the dilution rate; $c_{i,feed}$ (mol L^{-1}) denotes the concentration of metabolite i in the feed; k_i (h^{-1}) denotes the transport coefficient for diffusion in the membrane unit; and Q_i (mol L^{-1} h^{-1}) denotes the metabolic productivities (i.e., the production or consumption of metabolite i). As indicated, k_i denotes the trans-membrane transport coefficient resulting from the driving concentration profile between connected compartments. To exploit the experimental data, Equation 2 was discretised for the time intervals t_2 - t_1. The metabolic productivity $Q_{i,1}$ in compartment 1 was calculated by Equation 3, and the metabolic productivity $Q_{i,2}$ in compartment 2 was calculated by Equation 4. Indexes 1, 2, t_1, and t_2 code for the compartments and time points (h), respectively.

$$Q_{i,1} = \frac{c_{i,1,t_2} - c_{i,1,t_1}}{t_2 - t_1} - D_1 \cdot c_{i,1,feed} + D_1 \cdot \frac{c_{i,1,t_1} + c_{i,1,t_2}}{2} - k_i \cdot \left(\frac{c_{i,2,t_1} + c_{i,2,t_2}}{2} - \frac{c_{i,1,t_1} + c_{i,1,t_2}}{2} \right)$$
$$\tag{8.3}$$

$$Q_{i,2} = \frac{c_{i,2,t_2} - c_{i,2,t_1}}{t_2 - t_1} - D_2 \cdot c_{i,2,feed} + D_2 \cdot \frac{c_{i,2,t_1} + c_{i,2,t_2}}{2} - k_i \cdot \left(\frac{c_{i,1,t_1} + c_{i,1,t_2}}{2} - \frac{c_{i,2,t_1} + c_{i,2,t_2}}{2} \right)$$
$$(8.4)$$

Hence, the biomass-specific activity q_i (mol g_{DW}^{-1} h^{-1} L^{-1}) for amino acid i was calculated by dividing the metabolic productivity Q_i by the biomass c_i. If ^{13}C-labelled amino acids were used, the related production and consumption terms Q_i^{13} were estimated as follows:

$$\frac{dc_{i,1}^{13}}{dt} = D_1 \cdot (c_{i,1,feed}^{13} - c_{i,1}^{13}) + k_i \cdot frac^{13} \cdot \left(c_{i,2}^{total} - c_{i,1}^{total} \right) + Q_{i,1}^{13} \tag{8.5}$$

where c^{13} denotes the concentration (mol L^{-1}) of the fully ^{13}C-labelled isotopologues; c^{total} denotes the total concentration of an amino acid irrelevant to its labelling pattern. For non-labelled amino acids, the sum of $m + 0$ plus the natural $m + 1$ background of isotopologues was considered. $frac^{13}$ (molar ^{13}C concentration divided by total molar concentration) denotes the fully ^{13}C-labelled isotopologue fraction of an amino acid pool either in compartment 1 (if $c_{i,1} > c_{i,2}$) or compartment 2 (if $c_{i,2} > c_{i,1}$).

8.3.10 Reaction Rate Constant Of Metabolite Productivity

The consumption rate constant $k_{consumption,i}$ (h^{-1}) for amino acids was derived from the productivity Q_i for each amino acid concentration c_i according to eq. (8.6).

$$k_{consumption,i} = \frac{Q_i}{c_i} \tag{8.6}$$

8.3.11 Determination of amino acid transport coefficients in the membrane unit

To determine the transport coefficient k_i, the feed and harvest flows were disconnected, and compartment 1 was filled with 65 mL of various concentrations of amino acids (pH 6.5), whereas compartment 2 was filled with 65 mL of Milli-Q water. A constant mixing pump rate of $r_{pump} = 10$ mL min^{-1} was installed in each compartment. Samples (0.5 mL) were taken from each bioreactor after 0, 5, 10, 15, 20, 25, and 30 min or 0, 5, 15, and 30 min, and amino acid concentrations were quantified using HPLC. The process model of eq. (8.2) is

simplified to eq. (8.7) for compartment 1, and k_i was identified as the least-square estimate in MATLAB® (R2020a) (code S1 in Supplementary Materials).

$$\frac{dc_{i,1}}{dt} = -\frac{dc_{i,2}}{dt} = k_i \cdot (c_{i,2} - c_{i,1}) \tag{8.7}$$

8.3.12 Determination of the Bodenstein Number

To determine the Bodenstein number (Bo) in the membrane unit, bromothymol blue solution with a pH of 7.5 (KK19.3;, Carl Roth GmbH & Co. KG, Karlsruhe, Germany) was pumped through each side of the membrane unit at a typical cultivation mixing pump rate of 3.7 mL min^{-1}. Subsequently, 15 µL of 2 M HCl tracer was pulsed into one side of the membrane unit, leading to a colour change. The experiment was recorded using video. Then, one image of the outlet was decomposed into squares for colour analysis using '*imread*' from MATLAB®. As the red *r*-values showed maximum variability, related intensities were applied for the mixing studies. The average residence time (τ) and its variance (σ^2) were calculated after the pulse perturbation, as defined by a previous study [157]. To characterise the degree of mixing in the membrane unit, the *Bo* was extracted from τ and σ^2 (eq. (8.8)):

$$\frac{\sigma^2}{\tau^2} = \frac{2}{Bo} + \frac{8}{Bo^2} \tag{8.8}$$

8.3.13 Calculation of the Damkoehler Number

The Damkoehler number (Da) is a dimensionless mass balance that was adapted to indicate whether amino acid consumption in a compartment encountered limitations due to low amino acid supply by membrane transport [59]. Da_I (*dimensionless*) was calculated for each amino acid iI in a compartment between two subsequent data points (t_1 and t_2) when amino acid consumption and transport in the membrane unit into the compartment were present. A homogeneous distribution of amino acids in the compartment was assumed. Da considered amino acid decrease by consumption (Q_i) and washout by dilution (D). An increase in amino acid concentration in a compartment was expected from transport across the membrane (see XXX Section 3.6.6.)Figure 7). *Da* depicts the quotient between Q_i, D for washout, and the transport rate in the membrane unit for an amino acid i as follows:

$$Da_{i,t_1-t_2} = Da_{consumption} + Da_{dilution} = \frac{-Q_{i,t}}{k_i \cdot g_{i,t_1-t_2}} + \frac{D \cdot c_{i,t_1-t_2}}{k_i \cdot g_{i,t_1-t_2}} \tag{8.9}$$

Trans-compartment concentration gradients g_i (mol L^{-1}) were estimated by considering the arithmetic mean (Δc) of the concentrations between time points (t_1 and t_2) according to eq. (8.10).

$$g_i = \Delta c_{i,connected\ compartment,t_1-t_2} - \Delta c_{i,t_1-t_2} \tag{8.10}$$

The pool turnover rate ($k_{membrane\ unit}$ (h^{-1}) of metabolite pools in the membrane unit with the volume $V_{membrane\ unit}$ (L) imposed by the circulation of the fermentation broth with a mixing pump adjusted to the rate rmixing pump (litre/min) was calculated as follows:

$$k_{membrane\ unit} = \frac{r_{mixing\ pump}}{V_{membrane\ unit}} \tag{8.11}$$

8.3.14 Quantification of extracellular metabolites

Sugar and lactate concentrations were measured with an isocratic Agilent 1200 series HPLC system (Agilent Technologies, Santa Clara, CA, USA) equipped with a Phenomenex guard carbo-H column (4 × 3.0 mm) and a Rezex ROA organic acid H (8%) column (300 × 7.8 mm, 8 μm; Phenomenex) maintained at 50 °C [291]. Separation was achieved with 5 mM H$_2$SO$_4$ with a constant flow rate of 0.4 mL min^{-1}. Samples were pretreated for the precipitation of abundant phosphate by the addition of 4 M NH$_3$ and 1.2 M MgSO$_4$ solution followed by incubation with 0.1 M H$_2$SO$_4$. Absolute concentrations were obtained by standard-based external calibration and normalisation with L-rhamnose as the internal standard. The amino acid concentrations were determined using an Agilent 1200 series instrument (Agilent Technologies, Santa Clara, CA, USA) [291]. Separation was achieved with an Agilent Zorbax Eclipse Plus C18 column (250 by 4.6 mm, 5 μm), which was protected by an Agilent Zorbax Eclipse Plus C18 guard column (12.5 by 4.6 mm, 5 μm), according to a previously established method [112]. After automatic pre-column derivatisation with ortho-phthaldialdehyde, fluorometric detection (excitation at 230 nm and emission at 450 nm) was performed. The elution buffer consisted of a polar phase (10 mM Na$_2$HPO$_4$, 10 mM Na$_2$B$_4$O$_7$, 0.5 mM NaN$_3$, and pH 8.2) and a non-polar phase (45% (v/v) acetonitrile and 45% (v/v) methanol). The quantification of amino acids was

achieved via standard-based external calibration and using 4-aminobutanoic acid as an internal standard at 100 μm to correct for analyte variability.

8.3.15 Quantification of Extracellular And Intracellular Metabolites

For extracellular metabolite quantification via LC-MS / MS, the samples were centrifuged at 20,000 × g for 3 min at 4 °C, and the supernatant was stored at −70 °C. The samples were then filtered (Centrifugation Units ROTI®Spin, MINI-3; Carl Roth GmbH & Co. KG, Karlsruhe, Germany, Carl Roth) and mixed (1:1 v/v) with methanol to precipitate the remaining particles. Biomass samples for intracellular metabolome analysis via LC-MS / MS were centrifuged at 4,500 × g for 3 min and 4 °C, washed with 0.9% (w/v) sodium chloride solution, centrifuged at 20,000 × g for 3 min at 4 °C, and the pellet was stored at −70 °C. For metabolite extraction, the pellets were supplemented with 120 µL of 100 μm norvalin to correct for analyte variability, boiled at 95 °C for 4 min, and immediately centrifuged for 20 min at 20,000 × g and 4 °C. The supernatants were filtered (Centrifugation Units ROTI®Spin, MINI-3; Carl Roth GmbH & Co. KG, Karlsruhe, Germany, Carl Roth) and stored at −70 °C. The metabolite concentrations in the samples were measured using an Agilent 1200 HPLC system coupled with an Agilent 6410 B triple quadrupole mass spectrometer using an electrospray ion source. Chromatographic separation was achieved according to a previously described method [282]. The metabolite pool concentration was quantified by adding defined amounts of analyte standard to the reaction mixture. Data analysis was performed using MassHunter B.05.00 software (Agilent Technologies), and peaks of isotopologues containing ^{13}C were checked for interference by comparing samples of cultivation from ^{12}C and ^{13}C substrates.

8.3.16 Determination of Amino Acid Composition in Casein

First, 32% HCl (200 μL) was slowly added to casein solution (200 μL), vortexed, and incubated at 100 °C for 24 h. After cooling at 18 °C (1 h), 490 μL of 6.23 mM NaOH was slowly added. The samples were stored at −20 °C until HPLC was used to quantify the amino acid concentrations.
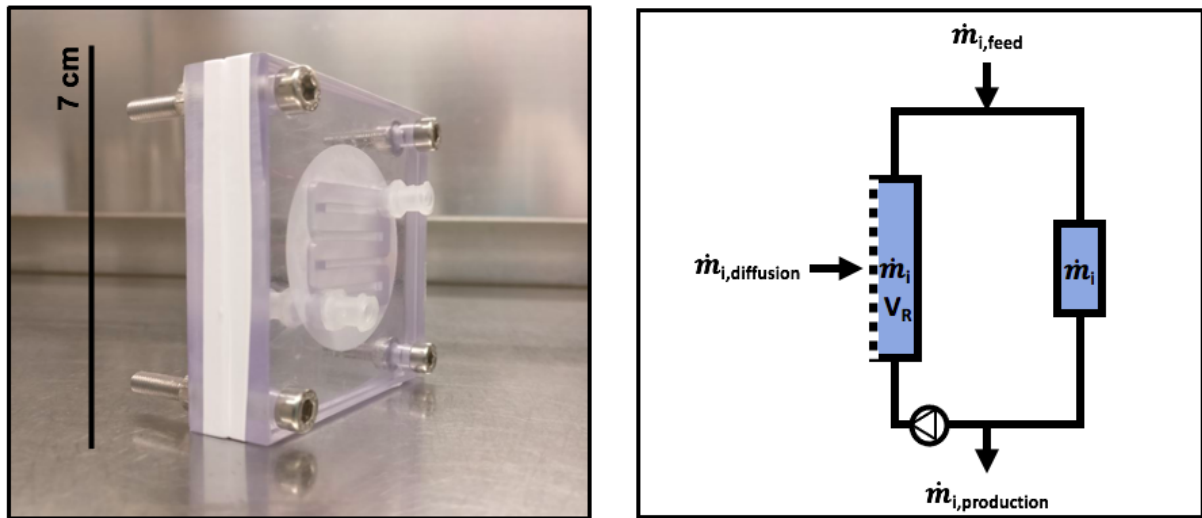
Figure 8.1: (**left**) Image of the membrane unit. The inlet and outlet of the channel were connected to vessels or tubes to allow the circulation of cells. Two polycarbonate elements were used to clamp a semi-permeable membrane that was aligned and fixed. (**right**) Mass balance of a compartment with inflow (feed), outflow (harvest), and diffusion flows in the membrane unit. The mixing pump allowed the circulation of the cultivation broth within the compartment.

8.3.17 Uncertainty Aanalysis

The measured data were analysed using Microsoft®Excel. The mean and standard deviation were calculated using duplicates and triplicates (STABW.S) using Microsoft®Excel.

8.4 Results

8.4.1 Design of the Membrane Unit

Membrane Unit Characteristics

The channels in the membrane unit (see Materials) were located next to each other and were separated by the membrane (fig. 8.1). This setting enabled the diffusion of metabolites, such as amino acids, but retained the cells. The channel in the membrane unit had a length of approximately 166 mm and volume of approximately 2.7 mL. The inserted membrane area was approximately 6.7×10^{-4} m^2.

Amino Acid Transport in the Membrane Unit

A PES or PA membrane was used to determine the amino acid transport coefficient (k_i) between the two vessels connected by the membrane unit. Three independent experiments were performed. Each experiment contained all of the amino acids. For each experiment, another initial amino acid concentration was set between 150 and 3,200 μM (table S2 in Supplementary Materials). The k_i for amino acid i was estimated based on all three experiments (for example, see $k_{alanine}$ in figure S1 in Supplementary Materials). The membrane unit equipped with a PES membrane showed a higher mean transport coefficient ($k = 0.36 \pm 0.03\ h^{-1}$) compared to a membrane unit equipped with a PA membrane ($k = 0.09 \pm 0.01\ h^{-1}$) (figure S2 in Supplementary Materials). Therefore, PES membranes were used in this study. Whether the power input by the mixing pump may bias k_i values by affecting the supply or removal of molecules in the membrane unit was considered. Given a mixing pump rate of $r_{pump} = 10$ mL min^{-1}, the average pool turnover rate in the membrane unit was approximately $k_{membrane\ unit} = 222\ h^{-1}$ on one side of the membrane unit. Considering that the maximum transport coefficients were approximately $k = 0.4\ h^{-1}$, the fraction of molecules exchanged by diffusion in the membrane unit was $f_{diffusion} = k\ /\ k_{membrane\ unit} = 0.02\%$. In other words, 99.98% of all the molecules in one compartment of the membrane unit was exchanged via pumping. Reducing r_{pump} to 3.7 mL min^{-1} increased $f_{diffusion}$ to 0.05%, which was still considered to be a low value. Hence, the k_i was barely affected by the pumping rates used in this study.

8.4.2 Design of the 2cs

The presented 2cs was designed to investigate metabolic interactions in a co-culture. This system enabled the characterisation of individual strains by calculating strain-specific rates and quantifying intracellular metabolite pools. As shown in (fig. 8.2), the experimental setup comprised a central membrane unit separating compartments 1 and 2 that may or may not embed an additional vessel section.

8.4.3 Vessel Bioreactor System: Set-up and Growth Experiment

The vessel bioreactor system comprised two vessels connected by a membrane unit. Each compartment was filled with 61.9 mL of cultivation broth (fig. 8.2A). To evaluate growth behaviour, compartment 1 was filled with SM + lactose and inoculated with *S. thermophilus*,
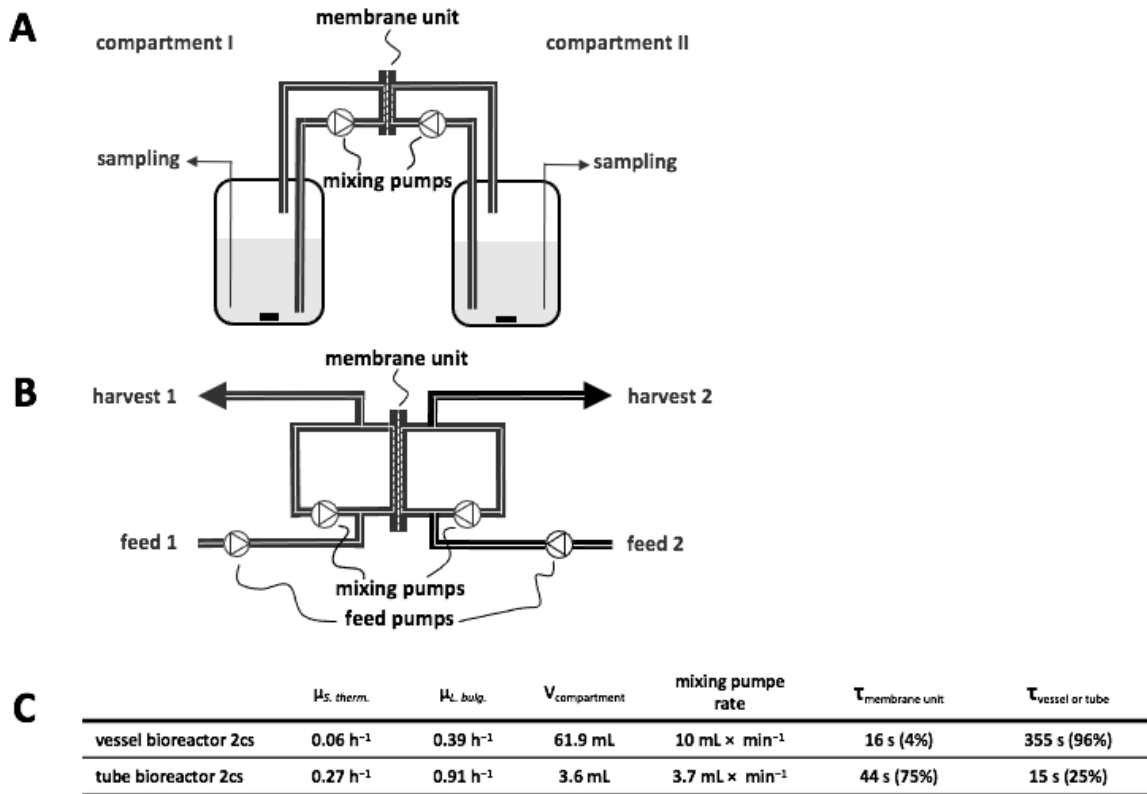
Figure 8.2: (**A**) Diagram of a vessel bioreactor system. The vessels were connected to the membrane unit, and circulation of medium in each compartment was achieved by mixing pumps. (**B**) Diagram of a tube bioreactor system. The inlets and outlets of the membrane unit were connected by tubes, and circulation of medium in each compartment was achieved by mixing pumps. Additionally, attached tubes for feeds and harvests allowed sampling and continuous cultivation by using feed pumps for each compartment. (**C**) Technical parameters and results of co-cultivations in respective two-compartment systems (2cs) with *Lactobacillus delbrueckii* subs. *bulgaricus* in synthetic medium (SM) containing casein and lactose and *Streptococcus thermophilus* in SM containing lactose. Strains were cultivated in co-culture in the 2cs, enabling exchange of metabolites, and strain-specific growth rates were determined from biomass measurements (figure S4 and S5 in Supplementary Materials). V, volume.

whereas compartment 2 contained *L. bulgaricus* in SMcas + lactose. The biomass ratio in the 2cs at inoculation was $1: 2.75$ ($g_{DW}{}^{LB}: g_{DW}{}^{ST}$). This experimental setting was chosen to investigate whether the non-proteolytic *S. thermophilus* cultivated in compartment 1 benefited from metabolite exchange with the proteinase-positive *L. bulgaricus* cultivated in compartment 2. Notably, proteinase-negative *S. thermophilus* was not able to grow in SMcas + lactose as a pure culture (figure S3 in Supplementary Materials). Consequently, the strain crucially relied on *L. bulgaricus*, which released amino acids and peptides from casein that further diffused through the membrane. Considering the geometries and mixing pump rate of 10 mL min^{-1} in each compartment, the estimated cellular residence time was 355 s in the vessel and 16 s in the membrane unit. Cultivation studies revealed a growth rate of $\mu = 0.39$ h^{-1} for *L. bulgaricus* and $\mu = 0.06$ h^{-1} for *S. thermophilus* (figure S4 in Supplementary Materials). This observation is the first evidence that amino acids and peptides are released from *L. bulgaricus* and that they diffuse into compartments containing *S. thermophilus*. However, the growth of *S. thermophilus* is nutrient-limited.

8.4.4 Tube Bioreactor System

To increase the growth rate of *S. thermophilus*, the vessels were removed from the vessel bioreactor system, leading to a simplified tube bioreactor system design (fig. 8.2B). Accordingly, the compartment volume reduced from 61.9 to 3.6 mL, increasing the volume fraction in the membrane unit to 74% (instead of 4% in the vessel bioreactor system). By analogy, the membrane-to-compartment ratio improved from 11 m^{-1} in the vessel bioreactor system to 186 m^{-1} in the tube bioreactor system. In other words, the residence time of amino acids and peptides inside the membrane unit increased from 4% to 74% of the total cycling time. Again, similar experimental conditions were chosen for the first vessel bioreactor system tests; namely, the cultivation of *S. thermophilus* in compartment 1 with SM + lactose and of *L. bulgaricus* in compartment 2 with SMcas + lactose. The mixing pump rate was reduced to 3.7 mL min^{-1}. Dilution rates of $D = 0.14$ h^{-1} were installed in each compartment, resulting in mean residence times of 7.1 h per compartment. The feed medium was equivalent to the medium in the compartments (SM + lactose for feeding into compartment 1 and SMcas + lactose for feeding into compartment 2). The biomass ratio in the 2cs at inoculation was $1: 0.7$ ($g_{DW}{}^{LB}: g_{DW}{}^{ST}$). As expected, the growth of *L. bulgaricus* and S. thermophiles was $\mu = 0.91$ h^{-1} and $\mu = 0.27$ h^{-1}, respectively (figure S5 in Supplementary Materials). For both strains, the growth rates were higher than those

in the studies using the vessel bioreactor system.

8.4.5 Comparison Between Bacterial Growth in Serum Bottles and in the Tube Bioreactor System

To further characterise the growth of a co-culture in the tube bioreactor system (two-compartments), a crimp-top serum bottle (one-compartment) was additionally inoculated in parallel to the experiment described in section 8.4.4. The crimp-top serum bottle contained SMcas + lactose (50 mL) inoculated with the same biomass concentrations of *S. thermophilus* and *L. bulgaricus* and was diluted at the same dilution rate of D = 0.14 h^{-1}. A defined volume was removed each hour and replaced with new SMcas + lactose medium, imitating the continuous process conditions in the tube bioreactor system described in section 8.4.4. Biomass was determined via flow cytometry at each harvest of the tube bioreactor system and in the crimp-top serum bottle. Then, the cell events of both compartments of the tube bioreactor system were summed up. It was not possible to measure the strain-specific biomass in a one-compartment bottle. As depicted in figure S6 in Supplementary Materials, the growth of the co-culture in the one-compartment bottle approach was fairly similar to the added-up biomass course in the tube bioreactor system for the first 2 h. Then, exponential growth continued in the tube bioreactor system while the growth rate slowed down in the one-compartment system, finally leading to 3.2×10^7 events mL^{-1} compared to 4.1×10^7 events mL^{-1} in the tube bioreactor system. Apparently, the tube bioreactor system approach was beneficial for the growth of the co-culture.

8.4.6 Determination of Strain-Specific Rates in Co-Culture

To demonstrate the applicability of the tube bioreactor system for identifying exchange rates of metabolites, proteinase-negative *S. thermophilus* and proteinase-positive *L. bulgaricus* were cultivated using medium containing ^{13}C glucose in the tube bioreactor system. The goal of the experiments was to determine the strain-specific release and consumption of amino acids in the interacting co-culture. Furthermore, experiments were performed to determine whether the released amino acids originated from casein or were synthesised *de novo* from sugar.

Dynamic Cultivation Tests in the Tube Bioreactor System

L. bulgaricus was cultivated in one compartment of the tube bioreactor system containing SMcas + ^{13}C glucose. In the connected compartment, proteinase-negative *S. thermophilus* was cultivated in SM + ^{13}C glucose. The experiments were designed such that dynamic growth conditions were set, which were individually adapted to the kinetics of each strain. The biomass ratio in the 2cs at inoculation was $1:4.4$ ($g_{DW}{}^{LB}:g_{DW}{}^{ST}$). After 2 h of cultivation in the tube bioreactor system, the operational mode switched to continuous fermentation. Pumps feeding the medium with the same composition as the related compartment were started, together with the harvest pump. For the compartment with *S. thermophilus*, a dilution rate of $D = 0.34$ h^{-1} was set to avoid the anticipated overgrowth of the said strain with respect to *L. bulgaricus*. For the latter, a dilution rate of $D = 0.07$ h^{-1} was set to prevent fast washout. After 8 h, that is, 24 h after the start of the experiments, the biomass of each compartment was collected for intracellular metabolite analysis. During the continuous mode period, a mean growth rate of $\mu = 0.05$ h^{-1} for *S. thermophilus* and an intermediary maximum of $\mu = 0.1$ h^{-1} between 1 and 3 h were observed (figure S7 in Supplementary Materials). This indicated the growth of *S. thermophilus*, which is only possible in the presence of amino acids or peptides supplied by *L. bulgaricus* (figure S3 in Supplementary Materials). Therefore, amino acids and peptides must have diffused between the compartments and enriched the medium of *S. thermophilus* (fig. 8.3). Additionally, the pH dropped in the *S. thermophilus* compartment from 6.5 to 5.5, and lactate production was measured, which revealed the metabolic activity of *S. thermophilus*, *L. bulgaricus*, or both (figure S8 in Supplementary Materials). Growth and pH were not measured in compartments containing *L. bulgaricus*. Throughout the continuous mode (8 h), *S. thermophilus* and *L. bulgaricus* were replaced 2.7- and 0.6-fold, respectively. In other words, the system did not run under a hydrodynamic steady state. Accordingly, the derived kinetics may serve as operational conditions, demonstrating the feasibility of this approach.

Calculation of Strain-Specific Rates

In co-culture, proteinase-negative *S. thermophilus* consumed peptides and amino acids provided by *L. bulgaricus* to satisfy its nitrogen demand. A previous study using similar strains and experimental conditions [291] demonstrated that co-cultures of *L. bulgaricus* and *S. thermophilus* released and consumed amino acids (as aspartate, arginine, alanine, lysine, isoleucine, and glycine). Consequently, tracking these components may open the

door for the identification of strain-specific dynamics and to gain further insight into the interactions of the strains.

The strength of the 2cs is that it allows the calculation of strain-specific amino acid rates by the individual analysis of sample concentrations (table S3 in Supplementary Materials). As shown in (fig. 8.4), positive values indicate amino acid release regardless of the precursor origin, that is, casein or glucose, whereas negative numbers correlate with amino acid consumption. By trend, both strains released amino acids during the first 3 h before metabolic productivity declined or even before consumption occurred. In particular,*L. bulgaricus* released amino acids (table S3 in Supplementary Materials) based on its high proteolytic activity. Glutamate, aspartate, and alanine were only produced by *L. bulgaricus* and consumed by *S. thermophilus* during the first 3 h. Another exception was methionine, which was consumed by both strains in the continuous mode.

Biomass-Specific Activity of *S. thermophilus* in Mono- and Co-Cultures

To gain a deeper understanding of amino acid metabolism in *S. thermophilus*, amino acid productivity has often been studied and modelled [212, 231]. However, only strain- and biomass-specific measurements may enable detailed metabolic flux distributions in co-cultures [268], thereby linking mono- and co-culture models [98, 230]. Figure 8.5 compares the amino acid productivity of *S. thermophilus* in a mono-culture grown on SMaa + lactose with the performance when co-cultivated with *L. bulgaricus* in the tube bioreactor system on SMcas + glucose (as shown in fig. 8.4). Most amino acids were released by *S. thermophilus* in the co-culture, indicating the uptake of peptides as well as intracellular and extracellular peptidase activity [125] compared to the mono-culture condition, where amino acids were almost entirely consumed. Similar to the mono-culture activities, glutamate and aspartate were consumed by *S. thermophilus* in the co-culture. This is remarkable, as peptide-bound glutamate and aspartate are available (fig. 8.3) but are not preferred. Apparently, *S. thermophilus* prefers consumption rather than replenishing its demand via the hydrolysis of peptides or interconversion through transaminases [12, 14]. Methionine was consumed by *S. thermophilus* in the co-culture, but uptake was limited by low methionine concentrations (fig. 8.3), which might indicate an insufficient supply [231].
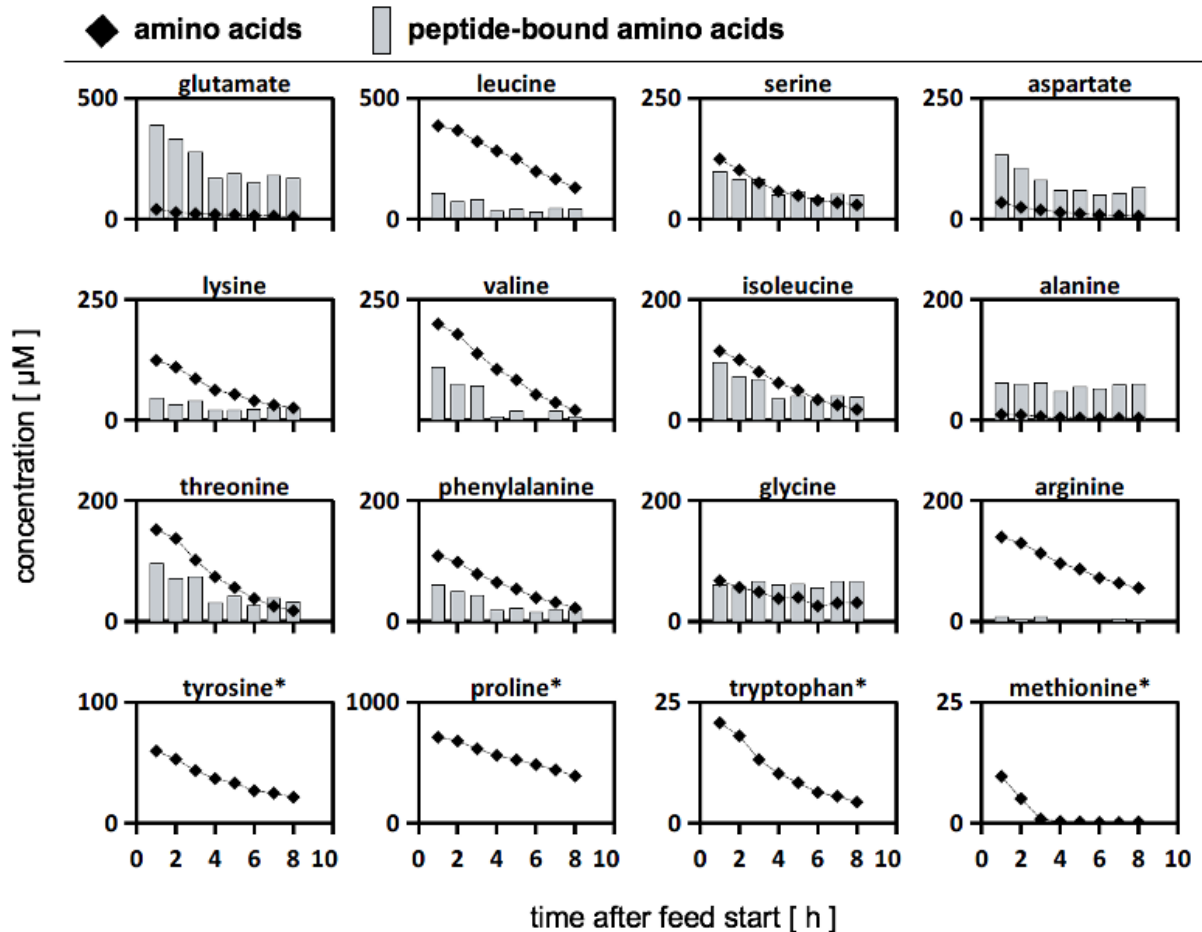
Figure 8.3: Amino acid profiles in the compartment containing *Streptococcus thermophilus* during co-cultivation with *Lactobacillus delbrueckii* subs. *bulgaricus* in the tube bioreactor system. (**rhomb**) Extracellular amino acid concentrations (µM) in the compartment containing *S. thermophilus* during the continuous mode. (**bars**) Extracellular peptide-bound amino acid concentrations (µM) in the compartment containing *S. thermophilus* during the continuous mode. *S. thermophilus* was cultivated in co-culture with *L. bulgaricus* in the tube bioreactor system containing synthetic medium (SM) with casein and glucose in the *L. bulgaricus* compartment and SM with glucose in the *S. thermophilus* compartment. *Profile data for these peptide-bound amino acids not measured.

Figure 8.4: Metabolic productivity of *Lactobacillus delbrueckii* subs. *bulgaricus* (**rhomb**) and *Streptococcus thermophilus* (**triangle**) cultivated in the tube bioreactor system as a co-culture. Positive values indicate the release or production of amino acids; negative values indicate the uptake of amino acids. Strains were cultivated in a tube bioreactor system containing synthetic medium (SM) with casein and glucose in the *L. bulgaricus* compartment and SM with glucose in the *S. thermophilus* compartment. Amino acids were sorted in rows according to the mol-fraction in casein, except tyrosine, proline, tryptophan, and methionine.
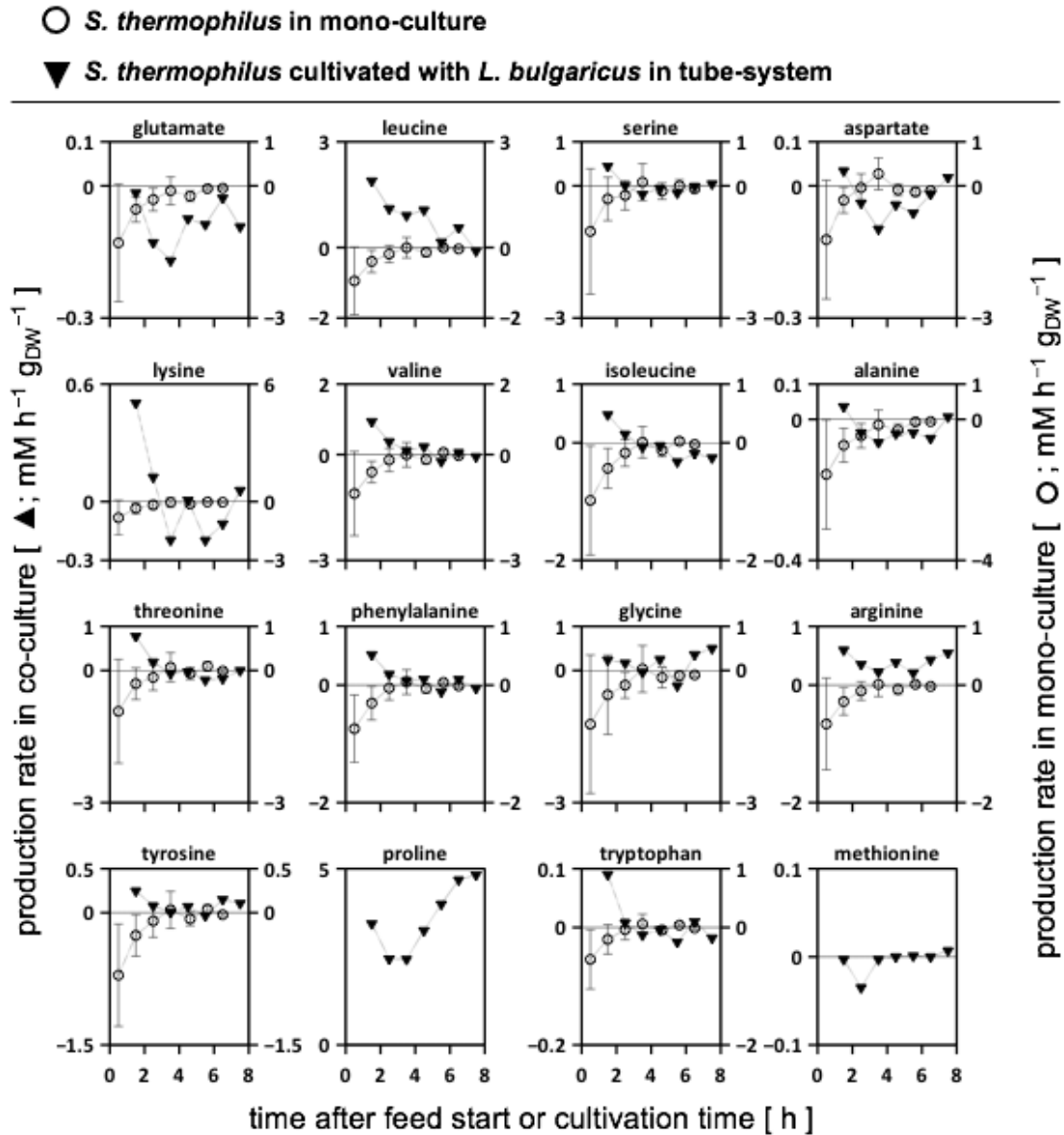
Figure 8.5: Biomass-specific activity of *Streptococcus thermophilus*. Amino acid production or consumption rates of *S. thermophilus* bridging amino acid productivity in mono-culture and co-culture. (**Filled**) *S. thermophilus* grown in co-culture with *Lactobacillus delbrueckii* subs. *bulgaricus*. Strains were cultivated in a tube bioreactor system containing synthetic medium (SM) with casein and glucose in the *L. bulgaricus* compartment and SM with glucose in the *S. thermophilus* compartment. (**Non-filled**) *S. thermophilus* grown in a crimp-top serum bottle containing SM with amino acids and lactose (modified from [291]). Amino acids were sorted in rows according to mol-fraction in casein, except tyrosine, proline, tryptophan, and methionine.

## Analysis of Extracellular ^{13}C Alanine Enrichment

Concentrations of extracellular amino acid isotopologues were measured to determine the origin of the amino acids. Low fractions of labelled aspartate, tyrosine, and threonine were detected ($< 1\%$). Only the alanine pool ($mol\,L^{-1}$) was enriched with up to 50% ^{13}C alanine (fig. 8.6), which was mirrored by intracellular labelling patterns in both strains (figure S9 in Supplementary Materials). This observation highlighted the relevance of *de novo* alanine biosynthesis from (labelled) sugars. The strain-specific production and consumption rates for ^{13}C alanine were calculated (eq. (8.2)) using the process model (fig. 8.6A). Balancing revealed that alanine was produced *de novo* by *L. bulgaricus* at a maximum rate of 5 μM $\times$ h^{-1}, whereas *S. thermophilus* mainly consumed the amino acids (fig. 8.6B).

Alanine Exchange Between the Compartments

The diffusion flux of ^{13}C alanine across the membrane was calculated. Figure S10 in Supplementary Materials shows a ^{13}C alanine flux from the compartment containing *L. bulgaricus* to the compartment containing *S. thermophilus* between 2 and 7 h. This indicated that *L. bulgaricus* provided *de novo*-produced alanine to *S. thermophilus* because *S. thermophilus* consumed alanine within this time range (fig. 8.6).

Calculation of Damkoehler Numbers

To further investigate the metabolite dynamics in the continuous experiments, Damkoehler numbers were calculated for each amino acid (fig. 8.7). In essence, the terms for amino acid consumption and washout were compared with trans-membrane amino acid transport rates, leading to $Da_{consumption}$ and $Da_{dilution}$, respectively (table 8.1). Accordingly, $Da <$ 1 indicated a faster amino acid supply than depletion, and this was the opposite for $Da >$ 1, whereas $Da = 1$ represented an equilibrium between depletion and supply. The calculation of the Da terms $Da_{consumption}$ and $Da_{dilution}$ (eq. (8.9)) illustrated their individual importance for the total Da term.

The analysis of Da_{total} time courses for the compartment containing *S. thermophilus* revealed that Da_{total} data were > 1 (fig. 8.8A) for all amino acids, irrespective of the time interval. By trend, the highest Da_{total} values were observed after 5 h, with alanine being the only exception. Consequently, most amino acids showed greater concentration decreases than their supply from the compartment containing *L. bulgaricus*. This scenario was only
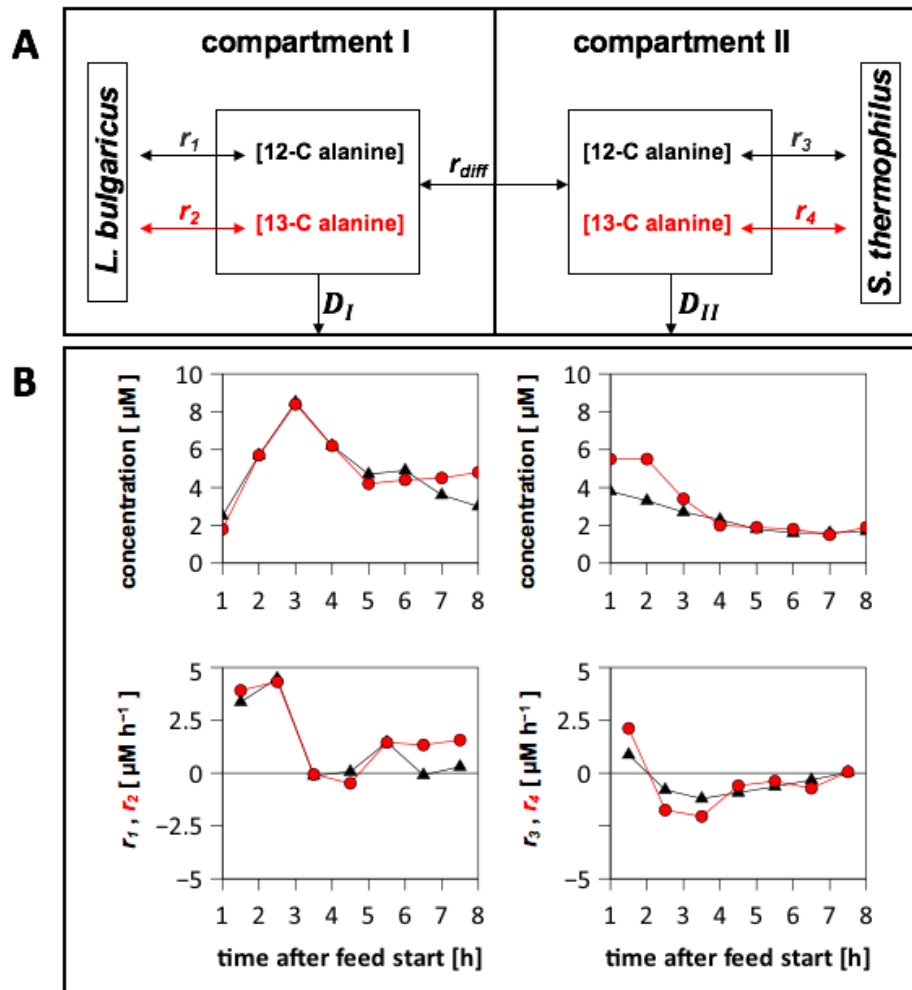
Figure 8.6: Alanine production and consumption of *Streptococcus thermophilus* and *Lactobacillus delbrueckii* subs. *bulgaricus* cultivated in the tube bioreactor system. (**A**) Illustration of alanine pools in the tube bioreactor system. r_1 and r_3 are the production and consumption rates of non-labelled alanine; r_2 and r_4 are the production and consumption rates of ^{13}C alanine; r_{diff} is the diffusion rate of alanine in the membrane unit according to concentration differences; and D is the dilution rate in compartment 1 or compartment 2. (**B**) Compartment 1 was filled with *L. bulgaricus* and synthetic medium (SM) with casein and ^{13}C glucose. Compartment 2 was filled with *S. thermophilus* and SM with ^{13}C glucose. Concentrations of non-labelled (triangle) and ^{13}C alanine (circle) were measured via LC-MS. Strain-specific rates were calculated by balancing each compartment. Positive rates: production; negative rates: consumption.

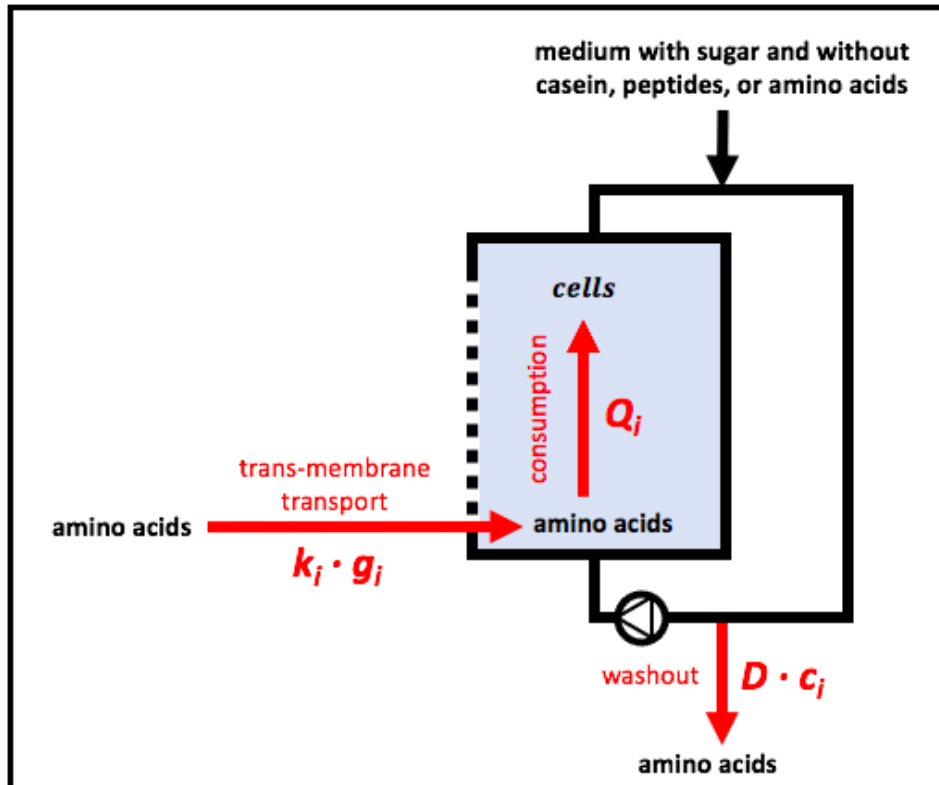Figure 8.7: Illustration of terms to estimate the Damkoehler number (Da) during the continuous mode. Trans-membrane transport provided amino acids; *Streptococcus thermophilus* or *Lactobacillus delbrueckii* subs. *bulgaricus* consumed amino acids; and the continuous mode provoked amino acid washout. The initial concentration for some amino acids was above zero at the start of the continuous mode.

Table 8.1: Comparison of mass balance terms for amino acids in the compartment containing *Streptococcus thermophilus*

mean amino acid consumption	$-Q_i$	$3.0 \pm 2.8 \ \mu M \times h^{-1}$
mean amino acid dilution	$D \times c_i$	$11.4 \pm 10.1 \ \mu M \times h^{-1}$
mean trans-membrane amino acid influx	$k_i \times g_i$	$5.5 \pm 3.8 \ \mu M \times h^{-1}$
mean change in amino acid concentration	$dc_i \ / \ dt$	$13.5 \pm 13.6 \ \mu M \times h^{-1}$
amino acid feed (feed medium without amino acids)	$D \times c_{i,feed}$	$0 \ \mu M \times h^{-1}$
Damkoehler term for consumption	$Da_{consumption}$	0.6 ± 0.4
Damkoehler term for dilution	$Da_{dilution}$	2.3 ± 2.1
Damkoehler number	Da_{total}	2.9 ± 2.3

S. thermophilus was co-cultivated with *Lactobacillus delbrueckii* subs. *bulgaricus* in the tube bioreactor system containing synthetic medium (SM) with glucose in the *S. thermophilus* compartment and SM with casein and glucose in the *L. bulgaricus* compartment.

enabled by the already high concentrations of these amino acids within the compartments at the start of the continuous experiment (fig. 8.3). In the case of alanine, sugar-derived biosynthesis became more important as the experiment lasted longer. figure 8B discloses the individual contributions of $Da_{dilution}$ and $Da_{consumption}$ for the calculation of the total Da number Da_{total} showcasing the compartment of *S. thermophilus*. $Da_{dilution}$ was larger than $Da_{consumption}$, outlining that the decrease in amino acid concentrations was predominately caused by the washout of amino acids ($D = 0.34 \ h^{-1}$) and not by their consumption ($k_{consumption} = 0.15 \pm 0.16 \ h^{-1}$) (fig. 8.7).

8.5 Discussion

8.5.1 Process Characterisation

The fluid behaviour in the membrane unit can be described by $Bo = 18$ (figure S11 in Supplementary Materials). This indicated that axial molecular diffusion and additional backmixing effects were present [157]. Given that Bo represents the ratio between convective flow and axial backmixing (dispersion), one may estimate that a non-optimum plug-flow pattern exists inside the channels with approximately 5% backmixing. Backmixing increased the average residence time of elements inside the membrane unit. However, 5% is far too low to create substrate gradients inside the compartment, as consumption
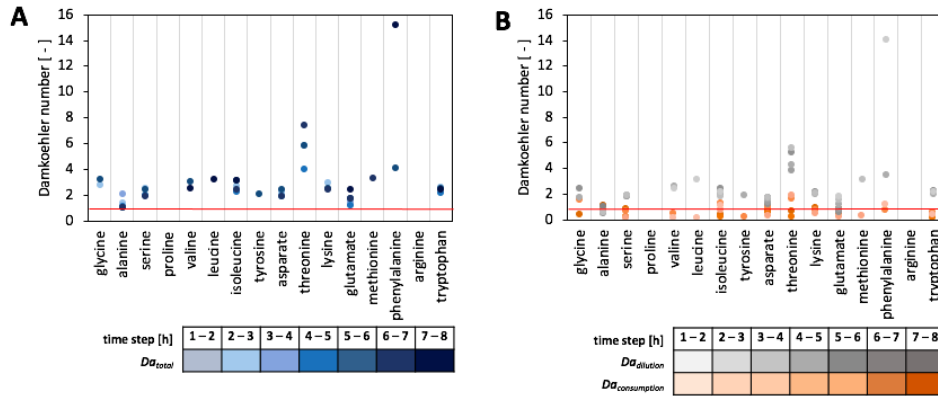
Figure 8.8: Damkoehler numbers (Da_I) of individual amino acids. (**A**) $Da_{total} = Da_{dilution}$ + $Da_{consumption}$ in the compartment containing *Streptococcus thermophilus*. (**B**) $Da_{dilution}$ + $Da_{consumption}$ separated in the compartment containing *S. thermophilus*. Strains were cultivated in the tube bioreactor system, and Da was calculated for each hour of continuous cultivation. Da numbers were only calculated if amino acid uptake was present within 1 h. The red line indicates Da = 1.

rates are much lower than the sum of trans-membrane transport (table 8.1). To investigate whether the diffusion process of metabolites in the membrane unit might result in limitations, such as the supply of amino acids from *L. bulgaricus* to *S. thermophilus*, Damkoehler numbers were estimated according to (crefeq:2cs9. As almost all Da_{total} values were > 1, indicating stronger amino acid withdrawal than supply, cellular growth predominately relied on the amino acids that were released at the beginning of the continuous experiment or those that were already present before the start (fig. 8.3). However, the key readouts regarding amino acid dependencies could be deduced. Nevertheless, future experimental settings may reduce the dilution rate D as the key parameter for washout, which would significantly reduce the available amino acid amount per compartment (fig. 8.7).

8.5.2 Difference Between Cultivation in the serum Bottle and in the Tube Bioreactor System

The growth of the co-culture in the serum bottle and in the tube bioreactor system was compared to study the potential impacts of hampered cell-to-cell interactions. Metabolic interactions could be delayed because of diffusion-limited metabolite exchange, and missing cell-to-cell contact may create secondary responses [28]. Interestingly, 33% more cell

events, that is, the proxy for cell growth, were found in the tube bioreactor system, which might have been the result of delayed acidification (figure S6 in Supplementary Materials). Like amino acids, lactate needs to cross the membrane unit via diffusion, which decelerates acidification dynamics in the connected compartment while maintaining beneficial pH conditions for growth.

8.5.3 Strain-Specific Amino Acid Release and Consumption In the Tube Bioreactor System

Both strains released and consumed amino acids when cultivated in a tube bioreactor system in continuous mode (fig. 8.4). During the first 3 h, both strains mainly released amino acids. Subsequently, amino acids were released and consumed. Only methionine was entirely consumed during the continuous mode. These findings quantified, for the first time, to our knowledge, the amino acid production and consumption rates in an interacting co-culture of *L. bulgaricus* and *S. thermophilus* and highlighted their dynamics. Consequently, the amino acid transport demonstrated for both strains and their impact on proton gradient and energy metabolism must be taken into account to fully understand the cellular physiology in the co-culture [169]. The production and consumption of amino acids by both strains fulfilled the requirements for bidirectional amino acid exchange between the strains and allowed the manipulation of the co-culture by amino acid additions, such as methionine [231]. The amino acid consumption and production rates for *S. thermophilus* during co-cultivation with *L. bulgaricus* in the tube bioreactor system were compared with those of previously published data [291] for *S. thermophilus* during mono-culture growth (fig. 8.5). Basically, *S. thermophilus* released amino acids in co-culture to some extent (fig. 8.5), although these amino acids were available (fig. 8.3), indicating the uptake of peptides or amino acid synthesis (except glutamate, aspartate, and methionine). In contrast, *S. thermophilus* grown under mono-culture conditions only consumed amino acids (fig. 8.5). The dataset of this study confirmed the previously published simulated metabolic activities [231] of different *S. thermophilus* strains grown on various amino acid sources. The predicted amino acid fluxes were mostly within the same ranges as those presented in fig. 8.5. The measurements revealed the dynamics in the amino acid production and consumption of *S. thermophilus*, indicating the importance of extending the model when used for co-culture simulations [98, 143, 230].

Generally, the mutual release of almost all amino acids in an *L. bulgaricus–S. thermophilus*

co-culture specified, for the first time, that both strains contribute to increasing amino acid concentrations in the medium and the enhanced current understanding of their metabolic activity. *L. bulgaricus* provided not only peptides but also—equally to *S. thermophilus*—amino acids to the co-culture, especially at the beginning of cultivation. At the end of the cultivation period, amino acid consumption occurred, indicating a switch between amino acid release and consumption.

Previous studies have revealed the upregulation of arginine biosynthesis genes in *S. thermophilus* [116, 231, 264], although arginine deficiency did not occur [231]. Consequently, here, it was hypothesised that arginine might serve as a precursor for ornithine or polyamine [116, 231]. However, their low extracellular concentrations did not support the idea that arginine biosynthesis might have additional functions as a precursor [231]. The measurement of peptide-bound arginine in the compartment containing *S. thermophilus* revealed low arginine content (fig. 8.3). Thus, arginine upregulation may be caused by limiting arginine supply. In the compartment containing *S. thermophilus*, only 0.5% (after 8 h of continuous experiment) of all the analysed peptide-bound amino acids were arginine molecules (fig. 8.3). In contrast, the arginine fraction of casein represented 3% of the total casein-bound amino acids in a comparable experiment (figure S12 in Supplementary Materials). This observation may indicate that either *L. bulgaricus* prefers the release of peptides from casein with low arginine content or that *S. thermophilus* favours the consumption of arginine-containing peptides. In either case, *S. thermophilus* likely faced arginine limitations during co-cultivation with *L. bulgaricus*. This observation supports the findings of previous studies [116, 264] where an upregulation of arginine biosynthesis occurred in *S. thermophilus*.

Because ^{13}C glucose was used as a substrate in the medium, it was possible to distinguish between non-labelled amino acids hydrolysed from casein and ^{13}C amino acids synthesised from glucose. Measurements of the extracellular medium indicated that alanine, aspartate, tyrosine, and threonine were produced *de novo* from glucose. However, only the alanine pool was enriched with high amounts of ^{13}C alanine (fig. 8.6). A higher ^{13}C alanine concentration was measured in the *L. bulgaricus* compartment than in the compartment containing *S. thermophilus*. Metabolite balancing revealed that *L. bulgaricus* produced ^{13}C alanine, while *S. thermophilus* consumed ^{13}C alanine (fig. 8.6). This supported the hypothesis that *L. bulgaricus* might have an alanine transaminase [162] providing alanine to supply *S. thermophilus* or even serving as a signal molecule for *S. thermophilus* to indicate the presence of *L. bulgaricus*.

8.6 Conclusions

A new compartmentalised cultivation system was developed and established to unclose strain-specific metabolomics and the subsequent calculation of the production and consumption rates of strains grown in co-culture. This enabled the generation of experimental data for sophisticated models that allow comprehensive insight into cellular processes in co-cultures at a strain-specific level. Although the cultivation system was characterised by the spatial separation of cells, the adequate exchange of molecules, such as peptides and amino acids, was enabled. The experimental setting provided a sufficient volume for comprehensive sampling. The small size of the system reduced the preparation time and cost. However, only anaerobic cultivations were installed, to date. It is noteworthy that fairly similar growth characteristics were achieved in the compartmentalised approach compared to the one-pot co-cultivation approach.

The functionality of the system was demonstrated using an *S. thermophilus–L. bulgaricus* co-culture, indicating that both strains released and consumed amino acids. In addition, cultivation was performed using ^{13}C glucose to quantify amino acid production and consumption rates, as well as the *de novo* biosynthesis of amino acids, indicating alanine transaminase activity in *L. bulgaricus* and exchange with *S. thermophilus*.

This setup allowed the characterisation of interacting microorganisms and clarified the interaction fluxes between them, allowing the rational design of co-cultures. Using the compartmentalised system for the continuous cultivation of co-cultures opens the field for advanced co-culturing; for example, by applying technology for targeted evolution studies.

Chapter 9

Conclusion

This dissertation presents experimental (chapters 3 to 5, 7 and 8) and theoretical (chapters 4 and 5) studies of the lactic acid bacteria *S. thermophilus* and *L. bulgaricus*. The outcomes contribute to an advanced mechanistic understanding of mono- and co-cultures. Strategies to quantify strain-specific flux distributions in co-cultures are also described (chapters 6 to 8).

9.1 Exploring the metabolic potential of *L. bulgaricus* and *S. thermophilus* in mono- and co-culture

A protocol for *L. bulgaricus* was developed to facilitate co-culture with *S. thermophilus* and achieve reproducible experimental results (chapter 3). It presents conclusive instructions for the timely preparation of both strains to render them ready for co-culture. A rapid and simple method based on flow cytometry was established to trace biomass profiles in cells co-cultured in medium containing casein that provokes high turbidity. This enabled a trained Support Vector Machine (SVM) to calculate biomass weight in 100 μL samples within 1 h. Correlations between flow cytometry data and biomass weight were established (chapter 3) that coupled physical characteristics with physiological aspects and enabled straightforward monitoring and control of cultivation [190, 222]. A (semi-) synthetic medium also enabled analyses such as high-performance liquid chromatography (HPLC) and mass spectrometry (MS), because the load of complex molecules was reduced, and the viscosity of the medium minimally changed during acidification. The medium allowed the

precise quantification of compounds produced or consumed by the strains and facilitated metabolic activity modelling at the species level. The medium allowed the exchange, omission, or further addition of compounds, enabling curation of an *L. bulgaricus* model (chapter 4) and studies of the dependence of acidification profiles on the initial substrate concentration (chapter 5).

The established medium and cultivation protocol for *S. thermophilus–L. bulgaricus* co-cultures allowed biomass tracking, pH measurement, and amino acid, sugar, and organic acid profiles during cultivation. The findings revealed that:

- Amino acids were released and consumed from co-cultured *S. thermophilus* and *L. bulgaricus.*

- Some amino acids such as arginine became depleted.

- Alanine was exchanged.

- the kinetics of amino acid and biomass concentration profils in co-culture were not the sum of the mono-culture kinetics for *S. thermophilus* and *L. bulgaricus.*

- The pH decreased faster in co-, than mono-cultures.

These results suggested that amino acid uptake and release should be considered in physiological models, such as the pH-dependent kinetic model of *L. bulgaricus* (chapter 5). The intracellular pH affecting the activity of most enzymes was dynamically implemented in the model of *L. bulgaricus* (chapter 5) based on proton-dependent reactions such as amino acid transport. Experimental data were used to parameterise and refine the model, which enabled the prediction of intra- and extracellular pH as a function of the metabolised substrate and the optimisation of fermentation processes. An initial lactose concentration of 41 mM led to the lowest pH of 3.6 after 24 h. A simulation revealed that changes in the initial lactose concentration increased the pH and altered the remaining lactose. An extracellular pH < 5.5. obviously reduced cytosolic pH and enzyme activities, thus changing metabolic activity. Hence, this kinetic model is a powerful tool for knowledge-driven bioprocess optimisation and will contribute to the development of advanced co-culture modelling approaches [230].

The experimental data allowed the curation of a genome-scale model of *L. bulgaricus*

(chapter 4) that is useful in the dairy industry [286] to deepen understanding of the gastrointestinal microbiota [211] and develop of L bulgaricus-*S. thermophilus* co-culture models.

In summary, the (semi-) synthetic medium, reproducible cultivation protocols, and modelling approaches to *L. bulgaricus* have enabled extensive studies and represent a significant step in the rational design of co-cultures with *S. thermophilus* for food production. In a wider context, the workflow will render co-cultures accessible for mechanistic studies and reveal their potential for future applications.

9.2 Strategy 1: ^{13}C-Metabolic flux analysis of compartmentalized systems to calculate compartment-specific flux distribution

Metabolic flux analysis using a ^{13}C-labelled substrate was taken into consideration to analyse intra- and intercellular processes in co-cultures qualitatively and quantitatively. A ^{13}C-MFA code was implemented in Matlab (chapter 6)[129]. The number of equations was significantly reduced to simplify stoichiometric network implementation. Only one equation was required for each molecule to compute all isotopomers. Like interacting prokaryotic co-cultures, metabolites are exchanged between two compartments in eukaryotic cells comprising cytosol and mitochondria. The results of the ^{13}C-MFA based on compartment-specific metabolome data were compared with total labelling information that did not distinguish between the compartments. All fluxes were correctly identified only when pool information was compartment-specific (chapter 6). Hence, revealing flux distribution in co-cultured *S. thermophilus–L. bulgaricus* using ^{13}C-MFA in one-pot cultivation was not suitable because both strains had similar metabolic activities such as the uptake of lactose as a substrate or amino acid release preventing strain-specific metabolomics (chapter 3).

This strategy is relevant because it might enable the calculation of strain-specific fluxes without disturbing specific co-cultures. It is a fast and simple method without additional experimental setups that can characterise many different strain combinations using avail-

able stoichiometric models [3, 268, 287]. Analysis of ^{13}C-flux has potential in co-culture systems that produce individual metabolites by straightforward monitoring exometabolome profiles [309]. Determination of inter- and intracellular ^{12}C/^{13}C-ratios enable more precise results, assuming that metabolite pools can be assigned to each strain (chapter 6) and expand the scope of extant methods [85, 89].

9.3 Strategy 2: Inactivation, separation and subsequent analysis of individual strains in co-culture

Chapter 7 describes cell inactivation using heat which quickly stopped metabolic activity and maintains cell membrane integrity. This is a first step towards strain-specific insight into metabolic activities in co-cultures such as the rapid conversion of intracellular metabolite pools. The cell inactivation might allow a subsequent separation step to fractionate individual strains, enabling strain-specific analysis. A retention time in increments of 0.1 s to 160 °C was promising to halt metabolic activity of *L. bulgaricus*. This resulted in > 80% inactivation of intracellular LDH activity while possibly suppressing intracellular metabolite leakage (chapter 7). This method paved the way to metabolomic measurements [198] in millisecond intervals for *L. bulgaricus* and eventually for *S. thermophilus* in mono-cultures. Using casein as a crucial substrate to favour interactions in co-cultured *L. bulgaricus-S. thermophilus* was incompatible with this setup, as casein in the medium clogged the thin capillary.

Heat inactivation (chapter 7) is relevant because the determination of intracellular metabolite conversion is key to gaining a deeper mechanistic understanding of product formation, such as organic molecules or amino acids. In particular, the high turnover rates of glycolytic enzymes responsible for initial substrate degradation are challenging parameters (chapter 5) [198]. Thus, heat inactivation will enable stopping and monitoring substrate conversion within 0.1 s. Measuring enzyme activity, membrane integrity, and metabolite pools seems promising for evaluating cell inactivation. Incrementally increasing temperatures for inactivation might briefly increase enzyme activity and change metabolite pools. Temperature profiles of inactivation units were calculated and rational adjustments of the

applied temperature and retention time were enabled using a simulation. The presented heat inactivation method is suitable for studies under anaerobic conditions. Compounds in culture media such as casein that clog capillaries, are incompatible with the setup. A wider capillary diameter requires further validation for successful metabolic inactivation. Combining cell inactivation, separation, and ^{13}C-MFA might lead to analyses of microbial communities without disturbing cellular activity.

9.4 Strategy 3: A compartmentalized cultivation system for co-cultures to quantify strain-specific fluxes

A compartmentalized cultivation system was developed to quantify strain-specific fluxes in a co-culture system (chapter 8). Performance was compared between mono- and co-cultured *S. thermophilus* and differences in amino acid production and release of *S. thermophilus* were clarified between axenic growth and co-culture with *L. bulgaricus.* The amino acid production and consumption rates of co-cultured *L. bulgaricus* and *S. thermophilus* were quantified for the first time using the compartmentalized system. Both strains produced and released amino acids. Alanine was produced de novo from glucose by a possible transaminase activity of *L. bulgaricus* and consumed by *S. thermophilus.* Arginine availability in peptides was limited to *S. thermophilus*, indicating active biosynthesis and dependence on the proteolytic activity of *L. bulgaricus.*

The relevance of the compartmentalized cultivation system is the ability to reveal strain-specific metabolomics and subsequently calculate the production and consumption rates of co-cultured strains. This enables the generation of experimental data for sophisticated models that provide comprehensive insight into cellular processes in co-cultures at the strain-specific level. The cultivation system was applicable because molecules such as peptides and amino acids were adequately exchanged using a PES membrane. Technical characterisation using Damkoehler numbers indicated an appropriate metabolite supply between the compartments, thus clarifying adequate molecular exchange between the strains. The experimental setting provided a sufficient volume for sampling and subsequent analytical approaches. The system is applicable to anaerobic cultivation and re-

duces preparation time and costs. Growth characteristics were comparable between two-, and one-compartment co-culture. The compartmentalised system facilitates continuous co-culture and opens the field for beneficial co-culture fermentation and targeted evolution studies.

9.5 Summary of strategies for co-culture analysis

Table 9.1: **Strategy 1: ^{13}C-Metabolic flux analysis of compartmentalized systems to calculate compartment-specific flux distribution** (chapter 6)

Strengths

- Identification of individual fluxes without disturbing the co-culture

- Fast characterization of various co-cultures testing numerous combinations

- Minimal demand for fermentation techniques saving time and costs

- Large number of existing stoichiometric models support this strategy

Weaknesses

- Overlapping stoichiometric networks in the co-culture weaken or prevent strain-specific quantification , for example in *L. bulgaricus - S. thermophilus* co-cultures

- Network information comprising the intra- and intercellular stoichiometry is required

- ^{13}C-MFA in co-cultures neglects kinetic and regulatory information

- ^{13}C-labelled substrate might be costly

- Construction of a stoichiometric model containing ^{13}C-labelling information is laborious

Opportunities

- Easy method to screen various co-cultures combinations for individual metabolic activity

- Integration of existing methods based on labelling information of amino acids [85] or peptides [89] might increase accuracy

- Transfer of method to microbial communities might be possible

Table 9.2: **Strategy 2: Strain-specific characterisation of co-cultures after inactivation and separation** (chapter 7)

Strengths

- Cell inactivation within milliseconds enables determination of fast enzyme activity

- Measurements of enzyme kinetics and metabolomic activity in situ without disturbing co-culture

- Sophisticated prediction of inactivation processes by simulation enables rational adjustment of parameters such as inactivation temperature or retention time

Weaknesses

- Cell separation demands individual protocol optimization and prevent transferability to other strains

- Studying interaction in *L. bulgaricus - S. thermophilus* co-cultures using casein was incompatible with this set-up as casein clogged thin capillary

- Only anaerobic conditions possible

- Heat might briefly increase enzyme activity that changes metabolite pools

Opportunities

- Transfer of method to microbial communities might be possible

Table 9.3: **Strategy 3: Quantification of strain-specific fluxes in two-compartment system and subsequent mass balancing** (chapter 8)

Strengths	
	• Straightforward measurement of strain-specific information enables precise quantification of amino acid production and consumption in co-cultured *L. bulgaricus-S. thermophilus*
	• Simple cultivation (short preparation; inexpensive)
	• Easy to adapt to other fermentation conditions and co-cultures
Weaknesses	
	• Direct cell-cell contact is impeded by membrane
	• Hampered diffusion of molecules between strains
	• Anaerobic cultivation conditions of membrane unit
Opportunities	
	• Combinable with ^{13}C-MFA
	• Continuous co-cultivation
	• Targeted evolution studies

Chapter 10

Outlook

The methods and strategies, as well as the theoretical and experimental descriptions provided herein give deep insights into *S. thermophilus*, *L. bulgaricus*, their interactions and present a toolbox for advanced co-culture technology. The results indicated that the application of a (semi-) synthetic medium, two-compartment system, biomass determination by flow cytometry, and quantitative ^{13}C-flux analysis could reveal exchanged molecules in other co-cultures. Furthermore, quantified interactions between microorganisms will enable the support, recovery, and design of novel co-cultures, as well as microbial communities involved in natural or biotechnological processes.

Further steps could merge the model approaches described in chapters 4 and 5 into a comprehensive mathematical representation of yogurt cultivation and use the data in chapters 3 to 5 and 8 to prioritise studies of exclusive co-cultures based on their strain-specific features. Furthermore, non-mechanistic data-driven analysis using flow cytometry chapter 3 might refine predictive simulation by implementing additional data.

The experimental methods described in chapters 3 and 8 enable the characterisation and classification of lactic acid bacteria accumulated in libraries, providing promising co-culture combinations for improved dairy products or alternatives such as plant-based foods [183, 318].

Further steps using the two-compartment system (chapter 8) might enable the cultivation of microorganisms in the presence of another strain while maintaining individual access, which is of interest to single-strain characterisation or antibiotic discovery [24].

The three strategies described herein can serve as a starting point for the design of favourable synthetic co-cultures [95, 151].

In future:

- The modular assembly of co- and multi-strain cultures might be a powerful approach [324] to increase the efficiency of processes such as the production of target compounds. Techniques such as the two-compartment system described in chapter 8 will contribute to the development of advantageous strain modules and reveal favourable cultivation conditions.

- The two-compartment system (chapter 8) allows for the directed laboratory evolution [256] of interacting co-cultures with improved capabilities [15, 16, 146, 324] such as increased biomass or product formation, based on the principles described in chapter 1. Recent experimental settings for adaptive coevolution [146, 244] require the transfer of co-cultures to a new medium and might result in the overgrowth or extinction of a strain. The two-compartment system enables long-term continuous evolution by applying individual strain parameters, such as dilution rates, to each strain.

- Traditional multi-strain cultures, such as those applied to wastewater remediation, have low dynamics, as they are similar to natural multi-strain processes that require low control [50, 331]. Phenotypic diversification [246] or a reduction in the number of strains requires increased process control (fig. 1.2) [308]. Because analytical tools to monitor and control phenotypically diverse co-cultures have rarely been reported [246]. Chapter 3 describes flow cytometry analysis of co-cultures, and chapter 8 describes direct access to individual strains in co-cultures. Fast and precise measurements of population composition and individual technical parameter settings enable advanced process control of co-cultures or even individual strains in co-cultures [250]. Variables such as pH, temperature, biomass ratio, feed, and dilution rates can be easily controlled and predicted, thus counteracting process fluctuations, increasing process stability, and enhancing co-culture efficiency.

The analysis and application of microbial interactions might contribute to diverse fields. For example, microorganisms in soil contribute to crop growth and remediate environmental contamination [132]. These microbial communities protect plants against disease and supply them with nutrients [252]. Thus, harnessing the potential of bioactive microbes [75] and understanding their interactions might help to stabilise soil microorganisms, contribute to resilience against climate change, and sustain high yields [252].

Wastewater remediation is supported by the removal of unwanted substances [58]. Microorganisms can more sustainably degrade such substances that could then be chemically degraded, or target compounds such as hydrogen might be produced [159]. Studies of these microbial communities might increase the efficiency of these degradative approaches and identify stabilising additives that prevent process fluctuations caused by undefined wastewater [213].

The human gastrointestinal system is colonised by many microbial communities [35]. A stable and balanced gut microbiome is essential to human health [76]. A deeper understanding of microorganisms and their interactions is key [35] to opening the door to health-promoting therapies [76] and evaluating changes in community composition due to variations in diet or antibiotics [80].

10.1 Co-culture processes in bio-based industry

The development of new co-culture processes (chapter 1) is accompanied by the consideration of alternatives, such as mono-culture fermentation [207]. Reducing the use of expensive substrates [334] and minimising purification steps [243] in co-culture processes will lead to a more sustainable and bio-based industry [266, 272, 324]. In addition to profitable process conditions (chapter 3) and optimal control (chapter 8), co-culture fermentation can also contribute to biotransformation [158].

Chapter 11

Author contributions and funding

11.1 Author contributions

Any of the attached published manuscripts (chapters 3, 6 and 8) were prepared in co-authorship with other researchers as indicated in the following paragraphs.

Research paper: Differential amino acid uptake and depletion in mono-cultures and co-cultures of *Streptococcus thermophilus* and *Lactobacillus delbrueckii* subsp. *bulgaricus* in a novel semi-synthetic medium.

The author of this dissertation, Andreas Ulmer, is first author of this manuscript. Andreas Ulmer planned the study, supervised and participated in the conduction of experiments. Andreas Ulmer supervised and contributed to the development of the cultivation medium and flow cytometry method, created the models, and visualized the results. Andreas Ulmer wrote the original draft of this manuscript.

Research paper: A two-compartment fermentation system to quantify strain-specific interactions in microbial co-cultures.

The author of this dissertation, Andreas Ulmer, is first author of the manuscript. Andreas Ulmer supervised and participated in the development of the two-compartment system. Andreas Ulmer planned the studies and participated in the experiments. Andreas Ulmer

conducted data analysis, implemented process model, and evaluated results.

Research paper: Compartment-specific metabolome labeling enables the identification of subcellular fluxes that may serve as promising metabolic engineering targets in CHO cells.

The author of this dissertation, Andreas Ulmer, shares first authorship for the manuscript with Andy Wiranata Wijaya (Institute of Biochemical Engineering, University of Stuttgart, Stuttgart, Germany). Andreas Ulmer and Andy Wiranata Wijaya contributed equally to the development of the ^{13}C MFA code and implementation in Matlab. Andreas Ulmer was involved in the interpretation of the computational results. Andreas Ulmer reviewed and edited the manuscript.

11.2 Contributions to other publications not shown in this dissertation

Loghmani, S.; Zitzow, E.; Koh, G.; **Ulmer, A.**; Veith, N.; Grosseholz, R.; Rossnagel, M.; Loesch, M.; Aebersold, R.; Kreikemeyer, B.; Fiedler, T. and Kummer, U. All driven by energy demand? Integrative comparison of the metabolism of Enterococcus faecalis wildtype and a glutamine synthase mutant. Microbiology Spectrum 2022, 10(2). Available at:
https://journals.asm.org/doi/abs/10.1128/spectrum.02400-21

Hundsdorfer, L.; Loesch, M.; **Ulmer, A.**; and Takors, R. Characterization of lactic acid bacteria for yogurt production. Chem Ing Tech 2020, 9(92), p.1222–1223. Available at:
https://doi.org/10.1002/cite.202055066

11.3 Supervision and Funding

Chapter 12

Bibliography

[1]   Ahn, Woo Suk and Antoniewicz, Maciek R. "Metabolic flux analysis of CHO cells at growth and non-growth phases using isotopic tracers and mass spectrometry". In: *Metabolic Engineering* 13 (5 2011). ISSN: 10967176. DOI: 10.1016/j.ymben.2011.07.002.

[2]   Ahn, Woo Suk and Antoniewicz, Maciek R. "Towards dynamic metabolic flux analysis in CHO cell cultures". In: *Biotechnology Journal* 7 (1 2012). ISSN: 18606768. DOI: 10.1002/biot.201100052.

[3]   Aite, Méziane et al. "Traceability, reproducibility and wiki-exploration for "à-la-carte" reconstructions of genome-scale metabolic models". In: *PLoS Computational Biology* 14 (5 May 2018). ISSN: 15537358. DOI: 10.1371/journal.pcbi.1006146.

[4]   Åkerberg, C. et al. "Modelling the influence of pH, temperature, glucose and lactic acid concentrations on the kinetics of lactic acid production by Lactococcus lactis ssp. lactis ATCC 19435 in whole-wheat flour". In: *Applied Microbiology and Biotechnology* 49.6 (1998), pp. 682–690. ISSN: 1432-0614. DOI: 10.1007/s002530051232. URL: https://doi.org/10.1007/s002530051232.

[5]   Alakomi, H. L. et al. "Lactic Acid Permeabilizes Gram-Negative Bacteria by Disrupting the Outer Membrane". In: *Applied and Environmental Microbiology* 66.5 (May 2000), pp. 2001–2005. DOI: 10.1128/aem.66.5.2001-2005.2000. URL: https://doi.org/10.1128/aem.66.5.2001-2005.2000.

[6]   Albrecht, Dirk R. et al. "Probing the role of multicellular organization in three-dimensional microenvironments". In: *Nature Methods* 3.5 (2006), pp. 369–375. ISSN: 15487091. DOI: 10.1038/nmeth873.

[7]   Alexandraki, Voula et al. "Comparative Genomics of Streptococcus thermophilus Support Important Traits Concerning the Evolution, Biology and Technological

Properties of the Species". In: *Frontiers in Microbiology* 10.December (2019), pp. 1–24. ISSN: 1664302X. DOI: `10.3389/fmicb.2019.02916`.

[8] Allen, Doug K., Shachar-Hill, Yair, and Ohlrogge, John B. "Compartment-specific labeling information in 13C metabolic flux analysis of plants". In: *Phytochemistry* 68 (16-18 2007). ISSN: 00319422. DOI: `10.1016/j.phytochem.2007.04.010`.

[9] Andersen, Ann Zahle et al. "The metabolic pH response in Lactococcus lactis: An integrative experimental and modelling approach". In: *Computational Biology and Chemistry* 33.1 (2009), pp. 71–83. ISSN: 1476-9271. DOI: `https://doi.org/10.1016/j.compbiolchem.2008.08.001`. URL: `http://www.sciencedirect.com/science/article/pii/S1476927108001096`.

[10] Antoniewicz, Maciek R. "13C metabolic flux analysis: Optimal design of isotopic labeling experiments". In: *Current Opinion in Biotechnology* 24.6 (2013), pp. 1116–1121. ISSN: 09581669. DOI: `10.1016/j.copbio.2013.02.003`. URL: `http://dx.doi.org/10.1016/j.copbio.2013.02.003`.

[11] Arganda-Carreras, Ignacio et al. "Trainable Weka Segmentation: a machine learning tool for microscopy pixel classification." In: *Bioinformatics (Oxford, England)* 33 (15 Aug. 2017), pp. 2424–2426. ISSN: 1367-4811. DOI: `10.1093/bioinformatics/btx180`.

[12] Arioli, Stefania et al. "Aspartate biosynthesis is essential for the growth of Streptococcus thermophilus in milk, and aspartate availability modulates the level of urease activity". In: *Applied and Environmental Microbiology* 73.18 (2007), pp. 5789–5796. ISSN: 00992240. DOI: `10.1128/AEM.00533-07`.

[13] Arioli, Stefania et al. "Streptococcus thermophilus urease activity boosts Lactobacillus delbrueckii subsp. bulgaricus homolactic fermentation". In: *International Journal of Food Microbiology* 247 (2017), pp. 55–64. ISSN: 18793460. DOI: `10.1016/j.ijfoodmicro.2016.01.006`. URL: `http://dx.doi.org/10.1016/j.ijfoodmicro.2016.01.006`.

[14] Arioli, Stefania et al. "The relevance of carbon dioxide metabolism in Streptococcus thermophilus". In: *Microbiology* 155.6 (2009), pp. 1953–1965. ISSN: 13500872. DOI: `10.1099/mic.0.024737-0`.

[15] Bachmann, Herwig et al. "Evolutionary engineering to enhance starter culture performance in food fermentations". In: *Current Opinion in Biotechnology* 32 (2015), pp. 1–7. ISSN: 18790429. DOI: `10.1016/j.copbio.2014.09.003`. URL: `http://dx.doi.org/10.1016/j.copbio.2014.09.003`.

[16] Bachmann, Herwig et al. "Experimental evolution and the adjustment of metabolic strategies in lactic acid bacteria". In: *FEMS microbiology reviews* 41.1 (2017), S201–S219. ISSN: 15746976. DOI: 10.1093/femsre/fux024.

[17] Bajic, Djordje and Sanchez, Alvaro. "The ecology and evolution of microbial metabolic strategies". In: *Current Opinion in Biotechnology* 62 (2020), pp. 123–128. ISSN: 18790429. DOI: 10.1016/j.copbio.2019.09.003. URL: https://doi.org/10.1016/j.copbio.2019.09.003.

[18] Bar-Even, Arren et al. "The Moderately Efficient Enzyme: Evolutionary and Physicochemical Trends Shaping Enzyme Parameters". In: *Biochemistry* 50.21 (May 2011), pp. 4402–4410. DOI: 10.1021/bi2002289.

[19] Bassler, Bonnie L. "Small talk: Cell-to-cell communication in bacteria". In: *Cell* 109.4 (2002), pp. 421–424. ISSN: 00928674. DOI: 10.1016/S0092-8674(02)00749-3. eprint: NIHMS150003.

[20] Bateman, Alex and al., Maria-Jesus Martin et. "UniProt: the universal protein knowledgebase in 2021". In: *Nucleic Acids Research* 49.D1 (Nov. 2020), pp. D480–D489. DOI: 10.1093/nar/gkaa1100.

[21] Becker, Max et al. "Perfusion cultures require optimum respiratory ATP supply to maximize cell-specific and volumetric productivities". In: *Biotechnology and Bioengineering* 116 (5 2019). ISSN: 10970290. DOI: 10.1002/bit.26926.

[22] Becker, Max et al. "The less the better: How suppressed base addition boosts production of monoclonal antibodies with Chinese hamster ovary cells". In: *Frontiers in Bioengineering and Biotechnology* 7 (APR 2019). ISSN: 22964185. DOI: 10.3389/fbioe.2019.00076.

[23] Bensch, Gerald et al. "Flow cytometric viability assessment of lactic acid bacteria starter cultures produced by fluidized bed drying". In: *Applied Microbiology and Biotechnology* 98.11 (2014), pp. 4897–4909. ISSN: 14320614. DOI: 10.1007/s00253-014-5592-z.

[24] Bertrand, Samuel et al. "Metabolite induction via microorganism co-culture: A potential way to enhance chemical diversity for drug discovery". In: *Biotechnology Advances* 32.6 (2014), pp. 1180–1204. ISSN: 07349750. DOI: 10.1016/j.biotechadv.2014.03.001. URL: http://dx.doi.org/10.1016/j.biotechadv.2014.03.001.

[25] Beshkova, Dora M et al. "Production of Amino Acids by Yogurt Bacteria". In: *Biotechnology Progress* 14.6 (1998), pp. 963–965. DOI: https://doi.org/10.1021/

bp980082j. URL: https://aiche.onlinelibrary.wiley.com/doi/abs/10.1021/bp980082j.

[26] Biggs, Matthew B. et al. "Metabolic network modeling of microbial communities". In: *Wiley Interdisciplinary Reviews: Systems Biology and Medicine* 7.5 (2015), pp. 317–334. ISSN: 1939005X. DOI: 10.1002/wsbm.1308. arXiv: 15334406.

[27] Blasche, Sonja et al. "Metabolic cooperation and spatiotemporal niche partitioning in a kefir microbial community". In: *Nature Microbiology* 6.2 (2021), pp. 196–208. ISSN: 20585276. DOI: 10.1038/s41564-020-00816-5. URL: http://dx.doi.org/10.1038/s41564-020-00816-5.

[28] Bolotin, Alexander et al. "Complete sequence and comparative genome analysis of the dairy bacterium Streptococcus thermophilus". In: *Nature Biotechnology* 22.12 (2004), pp. 1554–1558. ISSN: 10870156. DOI: 10.1038/nbt1034.

[29] Bourniquel, Aude A. and Mollet, Beat. "Purification and characterization of the 3-phosphoglycerate kinase from the thermophile Lactobacillus delbrueckii subsp. lactis". In: *International Dairy Journal* 12.9 (2002), pp. 723–728. ISSN: 0958-6946. DOI: https://doi.org/10.1016/S0958-6946(02)00069-9. URL: http://www.sciencedirect.com/science/article/pii/S0958694602000699.

[30] Bouvin, Jeroen et al. "Multi-objective experimental design for 13C-based metabolic flux analysis". In: *Mathematical Biosciences* 268 (2015), pp. 22–30. ISSN: 0025-5564. DOI: https://doi.org/10.1016/j.mbs.2015.08.002. URL: https://www.sciencedirect.com/science/article/pii/S0025556415001480.

[31] Branco dos Santos, Filipe, Vos, Willem M. de, and Teusink, Bas. "Towards metagenome-scale models for industrial applications-the case of Lactic Acid Bacteria". In: *Current Opinion in Biotechnology* 24.2 (2013), pp. 200–206. ISSN: 09581669. DOI: 10.1016/j.copbio.2012.11.003. URL: http://dx.doi.org/10.1016/j.copbio.2012.11.003.

[32] Bras, G. Le and Garel, J.R. "Pyruvate kinase from Lactobacillus bulgaricus: Possible regulation by competition between strong and weak effectors". In: *Biochimie* 75.9 (Jan. 1993), pp. 797–802. DOI: 10.1016/0300-9084(93)90130-k.

[33] Brenner, Katie, You, Lingchong, and Arnold, Frances H. "Engineering microbial consortia: a new frontier in synthetic biology". In: *Trends in Biotechnology* 26.9 (2008), pp. 483–489. ISSN: 01677799. DOI: 10.1016/j.tibtech.2008.05.004. arXiv: 1503.05043.

[34] Broyard, Camille and Gaucheron, Frederic. "Modifications of structures and functions of caseins: a scientific and technological challenge". In: *Dairy Science and Technology* 95.6 (2015), pp. 831–862. ISSN: 1958-5594. DOI: 10.1007/s13594-015-0220-y. URL: https://doi.org/10.1007/s13594-015-0220-y.

[35] Bucci, Vanni and Xavier, Joao B. "Towards predictive models of the human gut microbiome". In: *Journal of Molecular Biology* 426.23 (2014), pp. 3907–3916. ISSN: 10898638. DOI: 10.1016/j.jmb.2014.03.017.

[36] Buchholz, Jens et al. "Platform engineering of corynebacterium glutamicum with reduced pyruvate dehydrogenase complex activity for improved production of l-lysine, l-valine, and 2-ketoisovalerate". In: *Applied and Environmental Microbiology* 79.18 (2013), pp. 5566–5575. ISSN: 00992240. DOI: 10.1128/AEM.01741-13.

[37] Buescher, Joerg M et al. "A roadmap for interpreting 13C metabolite labeling patterns from cells". In: *Current Opinion in Biotechnology* 34 (Aug. 2015), pp. 189–201. ISSN: 0958-1669. DOI: 10.1016/J.COPBIO.2015.02.003. URL: https://www.sciencedirect.com/science/article/pii/S0958166915000221?via%3Dihub.

[38] Burmeister, Alina and Grunberger, Alexander. "Microfluidic cultivation and analysis tools for interaction studies of microbial co-cultures". In: *Current Opinion in Biotechnology* 62 (2020), pp. 106–115. ISSN: 18790429. DOI: 10.1016/j.copbio.2019.09.001.

[39] Burmeister, Alina et al. "A microfluidic co-cultivation platform to investigate microbial interactions at defined microenvironments". In: *Lab on a Chip* 19.1 (2019), pp. 98–110. ISSN: 14730189. DOI: 10.1039/c8lc00977e.

[40] Carpenter, C. and Broadbent, Jeff. "External Concentration of Organic Acid Anions and pH: Key Independent Variables for Studying How Organic Acids Inhibit Growth of Bacteria in Mildly Acidic Foods". In: *Journal of food science* 74 (Feb. 2009), R12–5. DOI: 10.1111/j.1750-3841.2008.00994.x.

[41] Caspi, Ron et al. "The MetaCyc database of metabolic pathways and enzymes and the BioCyc collection of Pathway/Genome Databases". In: *Nucleic Acids Research* 42.D1 (Jan. 2014). ISSN: 03051048. DOI: 10.1093/nar/gkt1103.

[42] Cássio, F, Leão, C, and Uden, N van. "Transport of lactate and other short-chain monocarboxylates in the yeast Saccharomyces cerevisiae." In: *Applied and Environmental Microbiology* 53.3 (1987), pp. 509–513. DOI: 10.1128/aem.53.3.509-513.1987.

[43] Chang, Antje et al. "BRENDA, the ELIXIR core data resource in 2021: New developments and updates". In: *Nucleic Acids Research* 49.D1 (Jan. 2021), pp. D498–D508. ISSN: 13624962. DOI: 10.1093/nar/gkaa1025.

[44] Chen, Chen et al. "Role of lactic acid bacteria on the yogurt flavour: A review". In: *International Journal of Food Properties* 20.sup1 (2017), S316–S330. ISSN: 1094-2912. DOI: 10.1080/10942912.2017.1295988. URL: https://doi.org/10.1080/10942912.2017.1295988.

[45] Chen, Shiwei et al. "Influence of Lactic Acid on Cell Cycle Progressions in Lactobacillus bulgaricus During Batch Culture". In: *Applied Biochemistry and Biotechnology* (2020). ISSN: 15590291. DOI: 10.1007/s12010-020-03459-8.

[46] Cheng, H. "Volatile flavor compounds in yogurt: a review". In: *Crit Rev Food Sci Nutr* 50.10 (2010), pp. 938–50. ISSN: 1040-8398. DOI: 10.1080/10408390903044081.

[47] Chervaux, Christian, Ehrlich, S. Dusko, and Maguin, Emmanuelle. "Physiological Study of Lactobacillus delbrueckii subsp. bulgaricus Strains in a Novel Chemically Defined Medium". In: *Society* 66.12 (2000), pp. 5306–5311.

[48] Church, George M. et al. "Realizing the potential of synthetic biology". In: *Nature Reviews Molecular Cell Biology* 15.4 (2014), pp. 289–294. ISSN: 14710080. DOI: 10.1038/nrm3767. URL: http://dx.doi.org/10.1038/nrm3767.

[49] Courtin, P., Monnet, V., and Rul, F. "Cell-wall proteinases PrtS and PrtB have a different role in Streptococcus thermophilus/Lactobacillus bulgaricus mixed cultures in milk". In: *Microbiology* 148.11 (2002), pp. 3413–3421. ISSN: 13500872. DOI: 10.1099/00221287-148-11-3413.

[50] Coyte, Katharine Z., Schluter, Jonas, and Foster, Kevin R. "The ecology of the microbiome: Networks, competition, and stability." In: *Science (New York, N.Y.)* 350.6261 (2015), pp. 663–6. ISSN: 1095-9203. DOI: 10.1126/science.aad2602. arXiv: 1011.1669.

[51] Crittenden, R. G., Martinez, N. R., and Playne, M. J. "Synthesis and utilisation of folate by yoghurt starter cultures and probiotic bacteria". In: *International Journal of Food Microbiology* 80.3 (2003), pp. 217–222. ISSN: 01681605. DOI: 10.1016/S0168-1605(02)00170-8.

[52] Crocetti R., Gregory et al. "Glycogen-accumulating organisms in laboratory-scale and full-scale wastewater treatment processes". In: *Microbiology* 148.11 (2002), pp. 3353–3364. ISSN: 13500872. DOI: 10.1099/00221287-148-11-3353.

[53]   Cronin, U. P. and Wilkinson, M. G. "The potential of flow cytometry in the study of Bacillus cereus". In: *Journal of Applied Microbiology* 108.1 (2010), pp. 1–16. ISSN: 13645072. DOI: 10.1111/j.1365-2672.2009.04370.x.

[54]   Crown, Scott B. and Antoniewicz, Maciek R. "Parallel labeling experiments and metabolic flux analysis: Past, present and future methodologies". In: *Metabolic Engineering* 16.1 (2013), pp. 21–32. ISSN: 10967176. DOI: 10.1016/j.ymben.2012.11.010. URL: http://dx.doi.org/10.1016/j.ymben.2012.11.010.

[55]   Crown, Scott B., Long, Christopher P., and Antoniewicz, Maciek R. "Optimal tracers for parallel labeling experiments and13C metabolic flux analysis: A new precision and synergy scoring system". In: *Metabolic Engineering* 38 (2016), pp. 10–18. ISSN: 10967184. DOI: 10.1016/j.ymben.2016.06.001. URL: http://dx.doi.org/10.1016/j.ymben.2016.06.001.

[56]   D'Souza, Glen et al. "Ecology and evolution of metabolic cross-feeding interactions in bacteria". In: *Natural Product Reports* 35.5 (2018), pp. 455–488. ISSN: 14604752. DOI: 10.1039/c8np00009c.

[57]   Dai, Zongjie and Nielsen, Jens. "Advancing metabolic engineering through systems biology of industrial microorganisms". In: 36 (Dec. 2015), pp. 8–15. ISSN: 18790429. DOI: 10.1016/j.copbio.2015.08.006.

[58]   Daims, Holger, Taylor, Michael W., and Wagner, Michael. "Wastewater treatment: a model system for microbial ecology". In: *Trends in Biotechnology* 24.11 (2006), pp. 483–489. ISSN: 01677799. DOI: 10.1016/j.tibtech.2006.09.002.

[59]   Damkohler, G. "Einflusse der Stromung, Diffusion und des Warmeuberganges auf die Leistung von Reaktionsofen". In: *Z.Elektroch.Bd.* 43.12 (1937), pp. 1–13. ISSN: 0005-9021.

[60]   Dandoy, Damien et al. "The fast milk acidifying phenotype of Streptococcus thermophilus can be acquired by natural transformation of the genomic island encoding the cell-envelope proteinase PrtS". In: *Microbial Cell Factories* 10.SUPPL. 1 (2011), pp. 1–9. ISSN: 14752859. DOI: 10.1186/1475-2859-10-S1-S21.

[61]   Davies, Julian. "Specialized microbial metabolites: Functions and origins". In: *Journal of Antibiotics* 66.7 (2013), pp. 361–364. ISSN: 00218820. DOI: 10.1038/ja.2013.61. URL: http://dx.doi.org/10.1038/ja.2013.61.

[62]   De Brabandere, Anne G. and De Baerdemaeker, Josse G. "Effects of process conditions on the pH development during yogurt fermentation". In: *Journal of Food Engineering* 41.3 (1999), pp. 221–227. ISSN: 0260-8774. DOI: https://doi.org/10.

1016/S0260-8774(99)00096-5. URL: `http://www.sciencedirect.com/science/article/pii/S0260877499000965`.

[63] Delvigne, Frank et al. "Taking control over microbial populations: Current approaches for exploiting biological noise in bioprocesses". In: *Biotechnology Journal* 12.7 (2017), pp. 1–17. ISSN: 18607314. DOI: `10.1002/biot.201600549`.

[64] Demain, Arnold L. and Adrio, Jose L. "Contributions of microorganisms to industrial biology". In: *Molecular Biotechnology* 38.1 (Jan. 2008), pp. 41–55. ISSN: 10736085. DOI: `10.1007/s12033-007-0035-z`.

[65] Derzelle, Sylviane et al. "Proteome analysis of Streptococcus thermophilus grown in milk reveals pyruvate formate-lyase as the major upregulated protein". In: *Applied and Environmental Microbiology* 71.12 (2005), pp. 8597–8605. ISSN: 00992240. DOI: `10.1128/AEM.71.12.8597-8605.2005`.

[66] Douwenga, Sieze, Janssen, Patrick, and Teusink, Bas. "A centrifugation-based clearing method allows high-throughput acidification and growth-rate measurements in milk". In: *Journal of Dairy Science* (2021). ISSN: 0022-0302. DOI: `10.3168/jds.2020-20108`. URL: `http://dx.doi.org/10.3168/jds.2020-20108`.

[67] Eigel, W. N. et al. "Nomenclature of Proteins of Cow's Milk: Fifth Revision". In: *Journal of Dairy Science* 67.8 (1984), pp. 1599–1631. ISSN: 00220302. DOI: `10.3168/jds.S0022-0302(84)81485-X`.

[68] El Kafsi, H. et al. "Lactobacillus delbrueckii ssp. lactis and ssp. bulgaricus: a chronicle of evolution in action". In: *BMC Genomics* 15 (2014), p. 407. ISSN: 1471-2164. DOI: `10.1186/1471-2164-15-407`.

[69] Even, Sergine, Lindley, Nic D., and Cocaign-Bousquet, Muriel. "Transcriptional, translational and metabolic regulation of glycolysis in Lactococcus lactis subsp. cremoris MG 1363 grown in continuous acidic cultures". In: *Microbiology* 149.7 (2003), pp. 1935–1944. ISSN: 13500872. DOI: `10.1099/mic.0.26146-0`.

[70] Even, Sergine et al. "Dynamic response of catabolic pathways to autoacidification in Lactococcus lactis: transcript profiling and stability in relation to metabolic and energetic constraints". In: *Molecular Microbiology* 45.4 (2002), pp. 1143–1152. ISSN: 0950-382X. DOI: `10.1046/j.1365-2958.2002.03086.x`. URL: `https://doi.org/10.1046/j.1365-2958.2002.03086.x`.

[71] Farias, Daniele and Maugeri Filho, Francisco. "Co-culture strategy for improved 2G bioethanol production using a mixture of sugarcane molasses and bagasse hydrolysate as substrate". In: *Biochemical Engineering Journal* 147.January (2019),

pp. 29–38. ISSN: 1873295X. DOI: 10.1016/j.bej.2019.03.020. URL: https://doi.org/10.1016/j.bej.2019.03.020.

[72] Faust, Karoline and Raes, Jeroen. "Microbial interactions: From networks to models". In: *Nature Reviews Microbiology* 10.8 (2012), pp. 538–550. ISSN: 17401526. DOI: 10.1038/nrmicro2832. URL: http://dx.doi.org/10.1038/nrmicro2832.

[73] Felton, Edward et al. "Heterotypic Cell Pair Co-culturing on Patterned Microarrays". In: *Bone* 23.1 (2014), pp. 1–7. ISSN: 15378276. DOI: 10.1039/c2lc40349h. Heterotypic. URL: https://www.ncbi.nlm.nih.gov/pmc/articles/PMC3624763/pdf/nihms412728.pdf.

[74] Ferenci, Thomas. "Trade-off Mechanisms Shaping the Diversity of Bacteria". In: *Trends in Microbiology* (2016). ISSN: 18784380. DOI: 10.1016/j.tim.2015.11.009.

[75] Ferrari, Belinda C., Binnerup, Svend J., and Gillings, Michael. "Microcolony cultivation on a soil substrate membrane system selects for previously uncultured soil bacteria". In: *Applied and Environmental Microbiology* 71.12 (2005), pp. 8714–8720. ISSN: 00992240. DOI: 10.1128/AEM.71.12.8714-8720.2005.

[76] Flint, Harry J. et al. "The role of the gut microbiota in nutrition and health". In: *Nature Reviews Gastroenterology and Hepatology* 9.10 (2012), pp. 577–589. ISSN: 17595045. DOI: 10.1038/nrgastro.2012.156. URL: http://dx.doi.org/10.1038/nrgastro.2012.156.

[77] Foucaud, C. and Poolman, B. "Lactose transport system of Streptococcus thermophilus. Functional reconstitution of the protein and characterization of the kinetic mechanism of transport". In: *J Biol Chem* 267.31 (1992), pp. 22087–94. ISSN: 0021-9258 (Print) 0021-9258.

[78] Fox, P. F. et al. *Dairy Chemistry and Biochemistry*. 2015. DOI: 10.1007/978-3-319-14892-2.

[79] Frick, Oliver and Wittmann, Christoph. "Characterization of the metabolic shift between oxidative and fermentative growth in Saccharomyces cerevisiae by comparative 13C flux analysis". In: *Microbial Cell Factories* 4 (2005). ISSN: 14752859. DOI: 10.1186/1475-2859-4-30.

[80] Friedman, Jonathan, Higgins, Logan M., and Gore, Jeff. "Community structure follows simple assembly rules in microbial microcosms". In: *Nature Ecology and Evolution* 1.5 (2017), pp. 1–7. ISSN: 2397334X. DOI: 10.1038/s41559-017-0109. URL: http://dx.doi.org/10.1038/s41559-017-0109.

[81] Gaggia, Francesca et al. "The role of protective and probiotic cultures in food and feed and their impact in food safety". In: *Trends in Food Science and Technology* 22 (2011), S58–S66. ISSN: 0924-2244. DOI: `https://doi.org/10.1016/j.tifs.2011.03.003`. URL: `http://www.sciencedirect.com/science/article/pii/S0924224411000409`.

[82] Ganesan, Vijaydev et al. "Heterologous biosynthesis of natural product naringenin by co-culture engineering". In: *Synthetic and Systems Biotechnology* 2.3 (2017), pp. 236–242. ISSN: 2405805X. DOI: `10.1016/j.synbio.2017.08.003`. URL: `https://doi.org/10.1016/j.synbio.2017.08.003`.

[83] Garault, Peggy et al. "Branched-chain amino acids and purine biosynthesis: Two pathways essential for optimal growth of Streptococcus thermophilus in milk". In: *Lait* 81.1-2 (2001), pp. 83–90. ISSN: 00237302. DOI: `10.1051/lait:2001114`.

[84] García Martín, Héctor et al. "A Method to Constrain Genome-Scale Models with13C Labeling Data". In: *PLoS Computational Biology* 11.9 (2015), pp. 1–34. ISSN: 15537358. DOI: `10.1371/journal.pcbi.1004363`.

[85] Gebreselassie, Nikodimos A. and Antoniewicz, Maciek R. "13C-metabolic flux analysis of co-cultures: A novel approach". In: *Metabolic Engineering* 31 (2015), pp. 132–139. ISSN: 10967184. DOI: `10.1016/j.ymben.2015.07.005`.

[86] Geinitz, Bertram et al. "Noninvasive tool for optical online monitoring of individual biomass concentrations in a defined coculture". In: *Biotechnology and Bioengineering* 117.4 (2020), pp. 999–1011. ISSN: 10970290. DOI: `10.1002/bit.27256`.

[87] Gentes, Marie-Claude, St-Gelais, Daniel, and Turgeon, Sylvie L. "Exopolysaccharide-milk protein interactions in a dairy model system simulating yoghurt conditions". In: *Dairy Science and Technology* 93.3 (Mar. 2013), pp. 255–271. DOI: `10.1007/s13594-013-0121-x`.

[88] Germerodt, Sebastian et al. "Pervasive Selection for Cooperative Cross-Feeding in Bacterial Communities". In: *PLoS Computational Biology* 12.6 (2016), pp. 1–21. ISSN: 15537358. DOI: `10.1371/journal.pcbi.1004986`.

[89] Ghosh, Amit et al. "A peptide-based method for 13C Metabolic Flux Analysis in microbial communities". In: *PLoS computational biology* 10.9 (Sept. 2014). Ed. by Christos A. Ouzounis, e1003827. ISSN: 15537358. DOI: `10.1371/journal.pcbi.1003827`. URL: `http://dx.plos.org/10.1371/journal.pcbi.1003827`.

[90] Ghoul, Melanie and Mitri, Sara. "The Ecology and Evolution of Microbial Competition". In: (2016). ISSN: 18784380. DOI: `10.1016/j.tim.2016.06.011`.

[91] Gilbert, Christophe et al. "A new cell surface proteinase: Sequencing and analysis of the prtB gene from Lactobacillus delbrueckii subsp. bulgaricus". In: *Journal of Bacteriology* 178.11 (1996), pp. 3059–3065. ISSN: 00219193. DOI: `10.1128/jb.178.11.3059-3065.1996`.

[92] Giri, Samir, Shitut, Shraddha, and Kost, Christian. "Harnessing ecological and evolutionary principles to guide the design of microbial production consortia". In: *Current Opinion in Biotechnology* 62 (2020), pp. 228–238. ISSN: 18790429. DOI: `10.1016/j.copbio.2019.12.012`. URL: `https://doi.org/10.1016/j.copbio.2019.12.012`.

[93] Giri, Samir et al. "Defining Division of Labour in Microbial Communities". In: *Journal of Molecular Biology* (June 2019). ISSN: 0022-2836. DOI: `10.1016/J.JMB.2019.06.023`. URL: `https://www.sciencedirect.com/`.

[94] Goel, Anisha et al. "Standardized Assay Medium To Measure Lactococcus lactis Enzyme Activities while Mimicking Intracellular Conditions". In: *Applied and Environmental Microbiology* 78.1 (2012), pp. 134–143. ISSN: 1098-5336. DOI: `10.1128/aem.05276-11`. URL: `https://aem.asm.org/content/aem/78/1/134.full.pdf`.

[95] Goers, Lisa, Freemont, Paul, and Polizzi, Karen M. "Co-culture systems and technologies: taking synthetic biology to the next level". In: *Journal of The Royal Society Interface* 11.96 (2014), p. 20140065. DOI: `10.1098/rsif.2014.0065`. eprint: `https://royalsocietypublishing.org/doi/pdf/10.1098/rsif.2014.0065`. URL: `https://royalsocietypublishing.org/doi/abs/10.1098/rsif.2014.0065`.

[96] Gordon, William G, Semmett, William F, and Bender, Maurice. "Amino Acid Composition of γ-Casein". In: *Journal of the American Chemical Society* 75.7 (Apr. 1953), pp. 1678–1679. ISSN: 0002-7863. DOI: `10.1021/ja01103a048`. URL: `https://doi.org/10.1021/ja01103a048`.

[97] Gordon, William G et al. "Amino Acid Composition of α-Casein and β-Casein2". In: *Journal of the American Chemical Society* 71.10 (Oct. 1949), pp. 3293–3297. ISSN: 0002-7863. DOI: `10.1021/ja01178a006`. URL: `https://doi.org/10.1021/ja01178a006`.

[98] Gottstein, Willi et al. "Constraint-based stoichiometric modelling from single organisms to microbial communities". In: *Journal of the Royal Society Interface* 13.124 (2016). ISSN: 17425662. DOI: `10.1098/rsif.2016.0627`.

[99] Goward, C R et al. "The purification and characterization of glucokinase from the thermophile Bacillus stearothermophilus". In: *Biochemical Journal* 237.2 (July 1986), pp. 415–420. DOI: `10.1042/bj2370415`.

[100] Grobben, G. J. et al. "Production of extracellular polysaccharides by Lactobacillus delbrueckii ssp. bulgaricus NCFB 2772 grown in a chemically defined medium". In: *Journal of Applied Bacteriology* 79.1 (1995), pp. 103–107. ISSN: 13652672. DOI: `10.1111/j.1365-2672.1995.tb03130.x`.

[101] Großkopf, Tobias and Soyer, Orkun S. "Synthetic microbial communities". In: *Current Opinion in Microbiology* 18.1 (2014), pp. 72–77. ISSN: 18790364. DOI: `10.1016/j.mib.2014.02.002`. URL: `http://dx.doi.org/10.1016/j.mib.2014.02.002`.

[102] Guchte, M. van de et al. "The complete genome sequence of Lactobacillus bulgaricus reveals extensive and ongoing reductive evolution". In: *Proceedings of the National Academy of Sciences* 103.24 (2006), pp. 9274–9279. ISSN: 0027-8424. DOI: `10.1073/pnas.0603024103`. URL: `http://www.pnas.org/cgi/doi/10.1073/pnas.0603024103`.

[103] Gunasekera, T. S., Veal, D. A., and Attfield, P. V. "Potential for broad applications of flow cytometry and fluorescence techniques in microbiological and somatic cell analyses of milk". In: *International Journal of Food Microbiology* 85.3 (2003), pp. 269–279. ISSN: 01681605. DOI: `10.1016/S0168-1605(02)00546-9`.

[104] Gunasekera, Thusitha S., Attfield, Paul V., and Veal, Duncan A. "A flow cytometry method for rapid detection and enumeration of total bacteria in milk". In: *Applied and Environmental Microbiology* 66.3 (2000), pp. 1228–1232. ISSN: 00992240. DOI: `10.1128/AEM.66.3.1228-1232.2000`.

[105] Hanemaaijer, Mark et al. "Model-based quantification of metabolic interactions from dynamic microbial-community data". In: *PLoS ONE* 12.3 (2017), pp. 1–19. ISSN: 19326203. DOI: `10.1371/journal.pone.0173183`.

[106] Hanemaaijer, Mark et al. "Systems modeling approaches for microbial community studies: from metagenomics to inference of the community structure". In: *Frontiers in Microbiology* 6.March (2015), pp. 1–12. ISSN: 1664-302X. DOI: `10.3389/fmicb.2015.00213`. URL: `http://www.frontiersin.org/Systems_Microbiology/10.3389/fmicb.2015.00213/abstract`.

[107] Hanemaaijer, Mark Jacobus. "Exploring the potential of metabolic models for the study of microbial ecosystems. PhD Thesis, Vrije University Amsterdam". In:

(2016). URL: https://research.vu.nl/en/publications/exploring-the-potential-of-metabolic-models-in-the-study-of-micro.

[108] Hanly, Timothy J and Henson, Michael A. "Dynamic metabolic modeling of a microaerobic yeast co-culture: predicting and optimizing ethanol production from glucose/xylose mixtures". In: *Biotechnology for Biofuels* 6.1 (Apr. 2013), p. 44. ISSN: 1754-6834. DOI: 10.1186/1754-6834-6-44. URL: http://biotechnologyforbiofuels.biomedcentral.com/articles/10.1186/1754-6834-6-44.

[109] Hanly, Timothy J. and Henson, Michael A. "Dynamic flux balance modeling of microbial co-cultures for efficient batch fermentation of glucose and xylose mixtures". In: *Biotechnology and Bioengineering* 108.2 (2011), pp. 376–385. ISSN: 00063592. DOI: 10.1002/bit.22954.

[110] Hanly, Timothy J., Urello, Morgan, and Henson, Michael A. "Dynamic flux balance modeling of S. cerevisiae and E. coli co-cultures for efficient consumption of glucose/xylose mixtures". In: *Applied Microbiology and Biotechnology* 93.6 (2012), pp. 2529–2541. ISSN: 01757598. DOI: 10.1007/s00253-011-3628-1.

[111] Hao, Pei et al. "Complete Sequencing and Pan-Genomic Analysis of Lactobacillus delbrueckii subsp. bulgaricus Reveal Its Genetic Basis for Industrial Yogurt Production". In: *PLoS ONE* 6.1 (Jan. 2011). Ed. by Niyaz Ahmed, e15964. DOI: 10.1371/journal.pone.0015964. URL: https://doi.org/10.1371/journal.pone.0015964.

[112] Hendersion, John and Brooks, Anne. "Improved Amino Acid Methods using Agilent ZORBAX Eclipse Plus C18 Columns for a Variety of Agilent LC Instrumentation and Separation Goals". In: *Agilent Technologies* (2010), pp. 1–16. URL: https://www.agilent.com/Library/applications/5990-4547EN.pdf.

[113] Hennig, Stefan, Rodel, Gerhard, and Ostermann, Kai. "Artificial cell-cell communication as an emerging tool in synthetic biology applications". In: *Journal of Biological Engineering* 9.1 (2015), pp. 1–12. ISSN: 17541611. DOI: 10.1186/s13036-015-0011-2. arXiv: 1005.1986. URL: http://dx.doi.org/10.1186/s13036-015-0011-2.

[114] Hernandez-Valdes, Jhonatan A. et al. "Enhancement of amino acid production and secretion by Lactococcus lactis using a droplet-based biosensing and selection system". In: *Metabolic Engineering Communications* 11.May (2020), e00133. ISSN:

22140301. DOI: `10.1016/j.mec.2020.e00133`. URL: `https://doi.org/10.1016/j.mec.2020.e00133`.

[115] Herve-Jimenez, Luciana et al. "Physiology of Streptococcus thermophilus during the late stage of milk fermentation with special regard to sulfur amino-acid metabolism". In: *Proteomics* 8.20 (2008), pp. 4273–4286. ISSN: 16159853. DOI: `10.1002/pmic.200700489`.

[116] Herve-Jimenez, Luciana et al. "Postgenomic analysis of Streptococcus thermophilus cocultivated in milk with Lactobacillus delbrueckii subsp. bulgaricus: Involvement of nitrogen, purine, and iron metabolism". In: *Applied and Environmental Microbiology* 75.7 (2009), pp. 2062–2073. ISSN: 00992240. DOI: `10.1128/AEM.01984-08`.

[117] Herzog, Jan et al. "Novel synthetic co-culture of Acetobacterium woodii and Clostridium drakei using CO2 and in situ generated H2 for the production of caproic acid via lactic acid". In: *Engineering in Life Sciences* December 2021 (2022), pp. 1–13. ISSN: 16182863. DOI: `10.1002/elsc.202100169`.

[118] Hesselman, Matthijn C. et al. "A multi-platform flow device for microbial (co-) cultivation and microscopic analysis". In: *PLoS ONE* 7.5 (2012). ISSN: 19326203. DOI: `10.1371/journal.pone.0036982`.

[119] Hetenyi, Kata, Nemeth, Aron, and Sevella, Bela. "Role of pH-regulation in lactic acid fermentation: Second steps in a process improvement". In: *Chemical Engineering and Processing: Process Intensification* 50.3 (2011), pp. 293–299. ISSN: 02552701. DOI: `10.1016/j.cep.2011.01.008`.

[120] Heyse, Jasmine et al. "Coculturing bacteria leads to reduced phenotypic heterogeneities". In: *bioRxiv* 85.0 (2018), pp. 1–13. ISSN: 10985336. DOI: `10.1128/AEM.02814-18`.

[121] Hickey, M. W., Hillier, A. J., and Jago, G. R. "Transport and metabolism of lactose, glucose, and galactose in homofermentative lactobacilli". In: *Applied and Environmental Microbiology* 51 (4 1986). ISSN: 00992240. DOI: `10.1128/aem.51.4.825-831.1986`.

[122] Hoefnagel, Marcel H N et al. "Metabolic engineering of lactic acid bacteria , the combined approach : kinetic modelling , metabolic control and experimental analysis". In: 2002 (2002), pp. 1003–1013.

[123] Hofer, Katharina. *Heat Inactivation of Lactic Acid Bacteria. Student thesis, Institute of Biochemical Engineering, University Stuttgart.* 2020.

[124] Hols, Pascal et al. "Conversion of Lactococcus lactis from homolactic to homoalanine fermentation through metabolic engineering". In: *Nature Biotechnology* 17.6 (1999), pp. 588–592. ISSN: 10870156. DOI: 10.1038/9902.

[125] Hols, Pascal et al. "New insights in the molecular biology and physiology of Streptococcus thermophilus revealed by comparative genomics". In: *FEMS Microbiology Reviews* 29.3 (2005), pp. 435–463. DOI: https://doi.org/10.1016/j.fmrre.2005.04.008. eprint: https://onlinelibrary.wiley.com/doi/pdf/10.1016/j.fmrre.2005.04.008. URL: https://onlinelibrary.wiley.com/doi/abs/10.1016/j.fmrre.2005.04.008.

[126] Hoops, S. et al. "COPASI–a COmplex PAthway SImulator". In: *Bioinformatics* 22.24 (2006), pp. 3067–74. ISSN: 1367-4803. DOI: 10.1093/bioinformatics/btl485.

[127] Horobin, Richard W., Stockert, Juan C., and Rashid-Doubell, Fiza. "Fluorescent cationic probes for nuclei of living cells: Why are they selective? A quantitative structure-activity relations analysis". In: *Histochemistry and Cell Biology* 126.2 (Aug. 2006), pp. 165–175. ISSN: 09486143. DOI: 10.1007/s00418-006-0156-7.

[128] Hu, Yue and Li, You. "Soybean peptides promote yoghurt fermentation and quality". In: *Biotechnology Letters* 2 (2020). ISSN: 1573-6776. DOI: 10.1007/s10529-020-02912-2. URL: https://doi.org/10.1007/s10529-020-02912-2.

[129] Hundsdorfer, Lara. *Applied mathematics for the description of stability and labeling dynamics in mixed cultures. Student thesis, Institute of Biochemical Engineering, University Stuttgart.* Bachelor Thesis. Stuttgart, 2019.

[130] Hutkins, R. W. "Microbiology and Technology of Fermented Foods". In: *Microbiology and Technology of Fermented Foods* (2007), pp. 1–473. DOI: 10.1002/9780470277515.

[131] Hutkins, Robert W. and Nannen, Nancy L. "pH Homeostasis in Lactic Acid Bacteria". In: *Journal of Dairy Science* 76.8 (1993). ISSN: 00220302. DOI: 10.3168/jds.S0022-0302(93)77573-6.

[132] Hyun, Jung Kim et al. "Defined spatial structure stabilizes a synthetic multispecies bacterial community". In: *Proceedings of the National Academy of Sciences* 105.47 (2008), pp. 18188–18193. ISSN: 0027-8424. DOI: 10.1073/pnas.0807935105. arXiv: arXiv:1408.1149. URL: http://www.pnas.org/cgi/doi/10.1073/pnas.0807935105.

[133] Jagmann, Nina and Philipp, Bodo. "Design of synthetic microbial communities for biotechnological production processes". In: *Journal of Biotechnology* 184 (2014), pp. 209–218. ISSN: 18734863. DOI: `10.1016/j.jbiotec.2014.05.019`. URL: `http://dx.doi.org/10.1016/j.jbiotec.2014.05.019`.

[134] Jamshidi, Neema and Palsson, B. "Mass action stoichiometric simulation models: Incorporating kinetics and regulation into stoichiometric models". In: *Biophysical Journal* 98.2 (2010), pp. 175–185. ISSN: 15420086. DOI: `10.1016/j.bpj.2009.09.064`.

[135] Johansen, Eric. "Use of Natural Selection and Evolution to Develop New Starter Cultures for Fermented Foods". In: *Annual Review of Food Science and Technology* 9 (2018), pp. 411–428. ISSN: 19411421. DOI: `10.1146/annurev-food-030117-012450`.

[136] Johns, Nathan I. et al. "Principles for designing synthetic microbial communities". In: *Current Opinion in Microbiology* 31 (2016), pp. 146–153. ISSN: 18790364. DOI: `10.1016/j.mib.2016.03.010`. arXiv: `15334406`. URL: `http://dx.doi.org/10.1016/j.mib.2016.03.010`.

[137] Jones, J. Andrew et al. "Experimental and computational optimization of an Escherichia coli co-culture for the efficient production of flavonoids". In: *Metabolic Engineering* 35 (2016), pp. 55–63. ISSN: 10967184. DOI: `10.1016/j.ymben.2016.01.006`.

[138] Junghans, Lisa et al. "From nutritional wealth to autophagy: In vivo metabolic dynamics in the cytosol, mitochondrion and shuttles of IgG producing CHO cells". In: *Metabolic Engineering* 54 (March 2019), pp. 145–159. ISSN: 10967184. DOI: `10.1016/j.ymben.2019.02.005`. URL: `https://doi.org/10.1016/j.ymben.2019.02.005`.

[139] Kailasapathy, Kasipathy. "Chemical Composition, Physical, and Functional Properties of Milk and Milk Ingredients". In: *Dairy Processing and Quality Assurance* (2016), pp. 77–105.

[140] Kanehisa, M. "Toward understanding the origin and evolution of cellular organisms". In: *Protein Sci* 28.11 (2019), pp. 1947–1951. ISSN: 0961-8368 (Print) 0961-8368. DOI: `10.1002/pro.3715`.

[141] Kanehisa, M. and Goto, S. "KEGG: kyoto encyclopedia of genes and genomes". In: *Nucleic Acids Res* 28.1 (2000), pp. 27–30. ISSN: 0305-1048 (Print) 0305-1048. DOI: `10.1093/nar/28.1.27`.

[142] Kanehisa, M. et al. "New approach for understanding genome variations in KEGG". In: *Nucleic Acids Res* 47.D1 (2019), pp. D590–d595. ISSN: 0305-1048 (Print) 0305-1048. DOI: `10.1093/nar/gky962`.

[143] Khandelwal, Ruchir A et al. "Community flux balance analysis for microbial consortia at balanced growth." In: *PloS one* 8.5 (2013), e64567. ISSN: 1932-6203. DOI: `10.1371/journal.pone.0064567`. arXiv: `arXiv:1011.1669v3`. URL: `http://journals.plos.org/plosone/article?id=10.1371/journal.pone.0064567`.

[144] Kleerebezem, Robbert and Loosdrecht, Mark CM van. "Mixed culture biotechnology for bioenergy production". In: *Current Opinion in Biotechnology* 18.3 (2007), pp. 207–212. ISSN: 09581669. DOI: `10.1016/j.copbio.2007.05.001`. arXiv: `arXiv:1011.1669v3`.

[145] Kliche, T et al. "Screening for proteolytically active lactic acid bacteria and bioactivity of peptide hydrolysates obtained with selected strains". In: (2017), pp. 7621–7633. DOI: `10.1007/s00253-017-8369-3`.

[146] Konstantinidis, Dimitrios et al. "Adaptive laboratory evolution of microbial cocultures for improved metabolite secretion". In: (2021), pp. 1–20. DOI: `10.15252/msb.202010189`.

[147] Kostal, Vratislav. "Susan Müller, Thomas Bley (Eds.): High resolution microbial single cell analytics". In: *Analytical and Bioanalytical Chemistry* 402.2 (2012), pp. 561–562. ISSN: 1618-2650. DOI: `10.1007/s00216-011-5502-5`. URL: `https://doi.org/10.1007/s00216-011-5502-5`.

[148] Krumpochova, Petra. *Metabolomics : From Method Development to System Biology. VU Amsterdam, PhD Thesis.* 2019.

[149] Kudo, H. and Sasaki, Y. "Intracellular pH Determination for the Study of Acid Tolerance of Lactic Acid Bacteria". In: *Methods Mol Biol* 1887 (2019), pp. 33–41. ISSN: 1064-3745. DOI: `10.1007/978-1-4939-8907-2\textunderscore4`.

[150] Kunji, Edmund R.S. "The proteolytic systems of lactic acid bacteria". In: *Antonie van Leeuwenhoek, International Journal of General and Molecular Microbiology* 70.2-4 (1996), pp. 187–221. ISSN: 00036072. DOI: `10.1007/BF00395933`.

[151] Kylilis, Nicolas et al. "Tools for engineering coordinated system behaviour in synthetic microbial consortia". In: *Nature Communications* 9.1 (2018). ISSN: 20411723. DOI: `10.1038/s41467-018-05046-2`. URL: `http://dx.doi.org/10.1038/s41467-018-05046-2`.

[152] Lahmann, Patrick et al. *RedCom: A strategy for reduced metabolic modeling of complex microbial communities and its application for analyzing experimental datasets from anaerobic digestion.* Vol. 15. 2. 2019, e1006759. DOI: `10.1371/journal.pcbi.1006759`.

[153] Le Bras, G., Deville-Bonne, D., and Garel, J. R. "Purification and properties of the phosphofructokinase from Lactobacillus bulgaricus. A non-allosteric analog of the enzyme from Escherichia coli". In: *Eur J Biochem* 198.3 (1991), pp. 683–7. ISSN: 0014-2956 (Print) 0014-2956. DOI: `10.1111/j.1432-1033.1991.tb16067.x`.

[154] Lee, Kelvin H. "Proteomics: a technology-driven and technology-limited discovery science". In: *Trends in Biotechnology* 19.6 (June 2001), pp. 217–222. ISSN: 0167-7799. DOI: `10.1016/S0167-7799(01)01639-0`. URL: `https://doi.org/10.1016/S0167-7799(01)01639-0`.

[155] Lee, Y., Nielsen, J., and Stephanopoulos, G. "Industrial Biotechnology: Microorganisms". In: *John Wiley and Sons* (2016). ISSN: 978-3-527-34179-5.

[156] Letort, C. and Juillard, V. "Development of a minimal chemically-defined medium for the exponential growth of Streptococcus thermophilus". In: *Journal of Applied Microbiology* 91.6 (2001), pp. 1023–1029. ISSN: 13645072. DOI: `10.1046/j.1365-2672.2001.01469.x`.

[157] Levenspiel, Octave. "Tracer Technology". In: *Journal of Chemical Information and Modeling* 53.9 (2019), pp. 1689–1699. ISSN: 1098-6596. arXiv: `arXiv:1011.1669v3`.

[158] Lewandowski, I et al. "Bioeconomy: Shaping the Transition to a Sustainable, Biobased Economy; Primary Production". In: (2018). Ed. by Iris Lewandowski, pp. 97–178.

[159] Li, Chenlin and Fang, Herbert H. P. "Fermentative Hydrogen Production From Wastewater and Solid Wastes by Mixed Cultures". In: *Critical Reviews in Environmental Science and Technology* 37.1 (2007), pp. 1–39. ISSN: 1064-3389. DOI: `10.1080/10643380600729071`. URL: `http://www.tandfonline.com/doi/abs/10.1080/10643380600729071`.

[160] Li, Sining et al. "Changes in Proteolysis in Fermented Milk Produced by Streptococcus thermophilus in Co-Culture with Lactobacillus plantarum or Bifidobacterium animalis subsp. Lactis during Refrigerated Storage". In: *Molecules* 24.20 (2019). ISSN: 14203049. DOI: `10.3390/molecules24203699`.

[161] Liebermeister, Wolfram and Klipp, Edda. "Bringing metabolic networks to life: convenience rate law and thermodynamic constraints". In: *Theoretical biology and*

medical modelling 3 (2006), pp. 41–41. ISSN: 1742-4682. DOI: 10.1186/1742-4682-3-41. URL: https://pubmed.ncbi.nlm.nih.gov/17173669%20https://www.ncbi.nlm.nih.gov/pmc/articles/PMC1781438/.

[162] Liu, Enuo et al. "A model of proteolysis and amino acid biosynthesis for Lactobacillus delbrueckii subsp. bulgaricus in whey". In: *Current Microbiology* 65.6 (2012), pp. 742–751. ISSN: 03438651. DOI: 10.1007/s00284-012-0214-4.

[163] Liu, Enuo et al. "Acquisition of amino acids by Lactobacillus delbrueckii subsp. bulgaricus 2038 when grown in the presence of casein". In: *International Dairy Journal* 35.2 (Apr. 2014), pp. 145–152. DOI: 10.1016/j.idairyj.2013.11.006. URL: https://doi.org/10.1016/j.idairyj.2013.11.006.

[164] Liu, Enuo et al. "Amino Acid Biosynthesis and Proteolysis in Lactobacillus bulgaricus Revisited : A Genomic Comparison". In: 2012.September (2012), pp. 61–77.

[165] Liu, Enuo et al. "Amino Acid Biosynthesis and Proteolysis in *Lactobacillus Bulgaricus* Revisited: A Genomic Comparison". In: *Computational Molecular Bioscience* 02.03 (2012), pp. 61–77. DOI: 10.4236/cmb.2012.23006. URL: https://doi.org/10.4236/cmb.2012.23006.

[166] Liu, Enuo et al. "Relationship between Lactobacillus bulgaricus and Streptococcus thermophilus under whey conditions: Focus on amino acid formation". In: *International Dairy Journal* 56 (2016), pp. 141–150. ISSN: 09586946. DOI: 10.1016/j.idairyj.2016.01.019. URL: http://dx.doi.org/10.1016/j.idairyj.2016.01.019.

[167] Liu, Mengjin et al. "The proteolytic system of lactic acid bacteria revisited: A genomic comparison". In: *BMC Genomics* 11.1 (2010), pp. 5–8. ISSN: 14712164. DOI: 10.1186/1471-2164-11-36.

[168] Locey, Kenneth J. and Lennon, Jay T. "Scaling laws predict global microbial diversity". In: *Proceedings of the National Academy of Sciences of the United States of America* 113.21 (2016), pp. 5970–5975. ISSN: 10916490. DOI: 10.1073/pnas.1521291113.

[169] Loghmani, Seyed Babak et al. "All Driven by Energy Demand? Integrative Comparison of Metabolism of Enterococcus faecalis Wildtype and a Glutamine Synthase Mutant". In: *Microbiology Spectrum* 10.2 (Apr. 2022). ISSN: 21650497. DOI: 10.1128/spectrum.02400-21.

[170] Luzia, Laura et al. "pH dependencies of glycolytic enzymes of yeast under *in vivo*-like assay conditions". In: *The FEBS Journal* 289.19 (May 2022), pp. 6021–6037. DOI: 10.1111/febs.16459. URL: https://doi.org/10.1111/febs.16459.

[171] Lyons, Nicholas A. and Kolter, Roberto. "On the evolution of bacterial multicellularity". In: *Current Opinion in Microbiology* 24 (2015), pp. 21–28. ISSN: 18790364. DOI: 10.1016/j.mib.2014.12.007. arXiv: 15334406. URL: http://dx.doi.org/10.1016/j.mib.2014.12.007.

[172] Madrid, R E and Felice, C J. "Microbial Biomass Estimation". In: *Critical Reviews in Biotechnology* 25.3 (Jan. 2005), pp. 97–112. ISSN: 0738-8551. DOI: 10.1080/07388550500248563. URL: https://doi.org/10.1080/07388550500248563.

[173] Mahon, Matthew John. "pHluorin2: an enhanced, ratiometric, pH-sensitive green florescent protein". In: *Advances in Bioscience and Biotechnology* 02.03 (2011), pp. 132–137. DOI: 10.4236/abb.2011.23021. URL: https://doi.org/10.4236/abb.2011.23021.

[174] Mainka, Thomas et al. "Soft sensor-based monitoring and efficient control strategies of biomass concentration for continuous cultures of Haloferax mediterranei and their application to an industrial production chain". In: *Microorganisms* 7.12 (Dec. 2019). ISSN: 20762607. DOI: 10.3390/microorganisms7120648.

[175] Maloney, P. C. "Membrane H+ conductance of Streptococcus lactis". In: *Journal of bacteriology* 140.1 (1979), pp. 197–205. ISSN: 0021-9193 1098-5530. URL: https://pubmed.ncbi.nlm.nih.gov/40951,%20https://www.ncbi.nlm.nih.gov/pmc/articles/PMC216796/.

[176] Manor, Ohad, Levy, Roie, and Borenstein, Elhanan. "Mapping the inner workings of the microbiome: Genomic- and metagenomic-based study of metabolism and metabolic interactions in the human microbiome". In: 20.5 (Nov. 2014), pp. 742–752. ISSN: 19327420. DOI: 10.1016/j.cmet.2014.07.021.

[177] Mar, Mette J et al. "Biotechnology for Biofuels Synergy at work : linking the metabolism of two lactic acid bacteria to achieve superior production of 2 - butanol". In: *Biotechnology for Biofuels* (2020), pp. 1–10. ISSN: 1754-6834. DOI: 10.1186/s13068-020-01689-w. URL: https://doi.org/10.1186/s13068-020-01689-w.

[178] Marco, Maria L. et al. "Health benefits of fermented foods: microbiota and beyond". In: *Current Opinion in Biotechnology* 44 (2017), pp. 94–102. ISSN: 18790429. DOI: 10.1016/j.copbio.2016.11.010.

[179] Markakiou, Sofia et al. "Harnessing the metabolic potential of Streptococcus thermophilus for new biotechnological applications". In: *Current Opinion in Biotechnology* 61 (2020), pp. 142–152. ISSN: 18790429. DOI: 10.1016/j.copbio.2019.12.019. URL: https://doi.org/10.1016/j.copbio.2019.12.019.

[180] Matuszczyk, Jens Christoph et al. "Compartment-specific metabolomics for CHO reveals that ATP pools in mitochondria are much lower than in cytosol". In: *Biotechnology Journal* 10 (10 2015). ISSN: 18607314. DOI: 10.1002/biot.201500060.

[181] McCarty, Nicholas S. and Ledesma-Amaro, Rodrigo. "Synthetic Biology Tools to Engineer Microbial Communities for Biotechnology". In: *Trends in Biotechnology* 37.2 (2019), pp. 181–197. ISSN: 18793096. DOI: 10.1016/j.tibtech.2018.11.002. URL: https://doi.org/10.1016/j.tibtech.2018.11.002.

[182] Mcclelland, R G and Pinder, A C. "Detection of Salmonella typhimunrum in Dairy Products with Flow Cytometry and Monoclonal Antibodies". In: (1994), pp. 4255–4262. URL: https://journals.asm.org/journal/aem.

[183] McClements, David Julian and Grossmann, Lutz. "A brief review of the science behind the design of healthy and sustainable plant-based foods". In: *npj Science of Food* 5.1 (2021). ISSN: 23968370. DOI: 10.1038/s41538-021-00099-y. URL: http://dx.doi.org/10.1038/s41538-021-00099-y.

[184] Mendes. "Transcriptome-based characterization of interactions between Saccharomyces cerevisiae and Lactobacillus delbrueckii subsp. bulgaricus in lactose-grown chemostat cocultures". In: *Applied and Environmental Microbiology* 79.19 (2013), pp. 5949–5961. ISSN: 00992240. DOI: 10.1128/AEM.01115-13.

[185] Mercade, Myriam, Duperray, Florence, and Loubiére, Pascal. "Energetic analysis of cultures of Lactobacillus delbrueckii subsp. bulgaricus: identification of the type of control between catabolism and anabolism". In: *Le Lait* 84.1-2 (Nov. 2003), pp. 39–47. DOI: 10.1051/lait:2003032.

[186] Mercade, Myriam, Lindley, Nic, and Loubiere, Pascal. "Metabolism of Lactococcus lactis subsp. cremoris MG 1363 in acid stress conditions". In: *International journal of food microbiology* 55 (May 2000), pp. 161–5. DOI: 10.1016/S0168-1605(00)00190-2.

[187] Millat, Thomas et al. "Integrative modelling of pH-dependent enzyme activity and transcriptomic regulation of the acetone-butanol-ethanol fermentation of *Clostridium acetobutylicum* in continuous culture". In: *Microbial Biotechnology* 6.5 (Jan.

2013), pp. 526–539. DOI: 10.1111/1751-7915.12033. URL: https://doi.org/10.1111/1751-7915.12033.

[188]   Minden, Steven et al. "Monitoring Intracellular Metabolite Dynamics in Saccharomyces cerevisiae during Industrially Relevant Famine Stimuli". In: *Metabolites* 12.3 (2022), pp. 1–24. ISSN: 22181989. DOI: 10.3390/metabo12030263.

[189]   Minty, Jeremy J. et al. "Design and characterization of synthetic fungal-bacterial consortia for direct production of isobutanol from cellulosic biomass". In: *Proceedings of the National Academy of Sciences* 110.36 (2013), pp. 14592–14597. ISSN: 0027-8424. DOI: 10.1073/pnas.1218447110. URL: http://www.pnas.org/lookup/doi/10.1073/pnas.1218447110.

[190]   Muller, Susanne. *Biomass measurement of Lactobacillus delbrueckii subsp. bulgaricus and Streptococcus thermophilus in milk analog medium by flow cytometry. Student thesis, Institute of Biochemical Engineering, University Stuttgart.* Bachelor Thesis. 2020.

[191]   Muller, Tobias et al. "Synthetic mutualism in engineered E. coli mutant strains as functional basis for microbial production consortia". In: *Engineering in Life Sciences* March (2022), pp. 1–14. ISSN: 16182863. DOI: 10.1002/elsc.202100158.

[192]   Nai, Corrado and Meyer, Vera. "From Axenic to Mixed Cultures: Technological Advances Accelerating a Paradigm Shift in Microbiology". In: *Trends in Microbiology* 26.6 (June 2018), pp. 538–554. ISSN: 18784380. DOI: 10.1016/j.tim.2017.11.004. URL: https://www.sciencedirect.com/science/article/pii/S0966842X17302536?via%3Dihub#.

[193]   Neves, A. R. et al. "Is the glycolytic flux in Lactococcus lactis primarily controlled by the redox charge? Kinetics of NAD(+) and NADH pools determined in vivo by 13C NMR". In: *J Biol Chem* 277.31 (2002), pp. 28088–98. ISSN: 0021-9258 (Print) 0021-9258. DOI: 10.1074/jbc.M202573200.

[194]   Nguyen, Tien-Thanh et al. "Homodimeric -galactosidase from Lactobacillus delbrueckii subsp. bulgaricus DSM 20081: expression in Lactobacillus plantarum and biochemical characterization". In: *Journal of agricultural and food chemistry* 60.7 (2012), pp. 1713–1721. ISSN: 1520-5118 0021-8561. DOI: 10.1021/jf203909e. URL: https://pubmed.ncbi.nlm.nih.gov/22283494%20https://www.ncbi.nlm.nih.gov/pmc/articles/PMC3284191/.

[195]   Nicolae, Averina et al. "Non-stationary 13C metabolic flux analysis of Chinese hamster ovary cells in batch culture using extracellular labeling highlights metabolic re-

versibility and compartmentation". In: *BMC Systems Biology* 8 (1 2014), pp. 1–15. ISSN: 17520509. DOI: `10.1186/1752-0509-8-50`.

[196] Niedenführ, Sebastian, Wiechert, Wolfgang, and Nöh, Katharina. "How to measure metabolic fluxes: A taxonomic guide for 13C fluxomics". In: *Current Opinion in Biotechnology* 34 (2015), pp. 82–90. ISSN: 18790429. DOI: `10.1016/j.copbio.2014.12.003`.

[197] Noack, Stephan and Baumgart, Meike. "Communities of Niche-Optimized Strains: Small-Genome Organism Consortia in Bioproduction". In: *Trends in Biotechnology* (Aug. 2018). ISSN: 0167-7799. DOI: `10.1016/J.TIBTECH.2018.07.011`. URL: `https://www.sciencedirect.com/`.

[198] Noack, Stephan et al. "Stationary versus non-stationary 13C-MFA: A comparison using a consistent dataset". In: *Journal of Biotechnology* 154.2-3 (2011), pp. 179–190. ISSN: 01681656. DOI: `10.1016/j.jbiotec.2010.07.008`.

[199] Noble, William S. "What is a support vector machine?" In: *Nature Biotechnology* 24 (2006). URL: `http://www.nature.com/naturebiotechnology`.

[200] Nöh, Katharina and Wiechert, Wolfgang. "The benefits of being transient: Isotope-based metabolic flux analysis at the short time scale". In: *Applied Microbiology and Biotechnology* 91.5 (2011), pp. 1247–1265. ISSN: 01757598. DOI: `10.1007/s00253-011-3390-4`.

[201] O'Brien, Edward J., Monk, Jonathan M., and Palsson, Bernhard O. "Using genome-scale models to predict biological capabilities". In: *Cell* 161.5 (2015), pp. 971–987. ISSN: 10974172. DOI: `10.1016/j.cell.2015.05.019`. arXiv: `15334406`. URL: `http://dx.doi.org/10.1016/j.cell.2015.05.019`.

[202] O'Brien, Edward J. et al. "Genome-scale models of metabolism and gene expression extend and refine growth phenotype prediction". In: *Molecular Systems Biology* (2013). ISSN: 17444292. DOI: `10.1038/msb.2013.52`.

[203] Oberhardt, Matthew A., Palsson, Bernhard, and Papin, Jason A. "Applications of genome-scale metabolic reconstructions". In: *Molecular Systems Biology* 5.320 (2009), pp. 1–15. ISSN: 17444292. DOI: `10.1038/msb.2009.77`.

[204] Oliveira, Ricardo Pinheiro de Souza et al. "Co-metabolic models of Streptococcus thermophilus in co-culture with Lactobacillus bulgaricus or Lactobacillus acidophilus". In: *Biochem. Eng. J.* 62 (2012), pp. 62–69. DOI: `http://dx.doi.org/10.1016/j.bej.2012.01.004`. URL: `http://www.sciencedirect.com/science/article/pii/S1369703X12000101`.

[205] Orth, Jeffrey D., Thiele, Ines, and Palsson, Bernhard O. "What is flux balance analysis?" In: *Nature Biotechnology* 28.3 (2010), pp. 245–248. ISSN: 10870156. DOI: 10.1038/nbt.1614. arXiv: NIHMS150003. URL: http://dx.doi.org/10.1038/nbt.1614.

[206] Otto, R et al. "The Relation between Growth-Rate and Electrochemical Proton Gradient of Streptococcus-Cremoris". In: *Fems Microbiology Letters* 16.1 (1983), pp. 69–74.

[207] Pachapur, Vinayak Laxman et al. "Biological hydrogen production using co-culture versus mono-culture system". In: *Environmental Technology Reviews* 4.1 (2015), pp. 55–70. ISSN: 21622523. DOI: 10.1080/21622515.2015.1068381. URL: https://doi.org/10.1080/21622515.2015.1068381.

[208] Pande, Samay et al. "Fitness and stability of obligate cross-feeding interactions that emerge upon gene loss in bacteria". In: *ISME Journal* (2014). ISSN: 17517370. DOI: 10.1038/ismej.2013.211. arXiv: NIHMS150003.

[209] Paricharttanakul, N. M. et al. "Kinetic and structural characterization of phosphofructokinase from Lactobacillus bulgaricus". In: *Biochemistry* 44.46 (2005), pp. 15280–6. ISSN: 0006-2960 (Print) 0006-2960. DOI: 10.1021/bi051283g.

[210] Park, Enoch Y., Naruse, Kazuya, and Kato, Tatsuya. "One-pot bioethanol production from cellulose by co-culture of Acremonium cellulolyticus and Saccharomyces cerevisiae". In: *Biotechnology for Biofuels* 5.1 (2012), p. 64. ISSN: 1754-6834. DOI: 10.1186/1754-6834-5-64. URL: Biotechnology%20for%20Biofuels.

[211] Pasolli, Edoardo et al. "Large-scale genome-wide analysis links lactic acid bacteria from food with the gut microbiome". In: *Nature Communications* 11 (1 2020), pp. 1–12. ISSN: 20411723. DOI: 10.1038/s41467-020-16438-8. URL: http://dx.doi.org/10.1038/s41467-020-16438-8.

[212] Pastink, Margreet I. et al. "Genome-scale model of Streptococcus thermophilus LMG18311 for metabolic comparison of lactic acid bacteria". In: *Applied and Environmental Microbiology* (2009). ISSN: 00992240. DOI: 10.1128/AEM.00138-09.

[213] Patil, Sayali S., Kumar, Martin S., and Ball, Andrew S. "Microbial community dynamics in anaerobic bioreactors and algal tanks treating piggery wastewater". In: *Applied Microbiology and Biotechnology* 87.1 (2010), pp. 353–363. ISSN: 01757598. DOI: 10.1007/s00253-010-2539-x.

[214] Pedregosa, Fabian et al. "Scikit-learn: Machine Learning in Python". In: *J. Mach. Learn. Res.* 12.null (2011), pp. 2825–2830. ISSN: 1532-4435.

[215] Pessione, Alessandro, Lamberti, Cristina, and Pessione, Enrica. "Proteomics as a tool for studying energy metabolism in lactic acid bacteria". In: *Molecular BioSystems* 6.8 (2010), p. 1419. DOI: 10.1039/c001948h.

[216] Pfizenmaier, Jennifer, Matuszczyk, Jens Christoph, and Takors, Ralf. "Changes in intracellular ATP-content of CHO cells as response to hyperosmolality". In: *Biotechnology Progress* 31 (5 2015). ISSN: 15206033. DOI: 10.1002/btpr.2143.

[217] Pfizenmaier, Jennifer and Takors, Ralf. "Host Organisms: Mammalian Cells". In: *Industrial Biotechnology* (2016). DOI: 10.1002/9783527807796.ch17.

[218] Pfizenmaier, Jennifer et al. "Hyperosmotic stimulus study discloses benefits in ATP supply and reveals miRNA/mRNA targets to improve recombinant protein production of CHO cells". In: *Biotechnology Journal* 11 (8 2016). ISSN: 18607314. DOI: 10.1002/biot.201500606.

[219] Pham, Van H.T. and Kim, Jaisoo. "Cultivation of unculturable soil bacteria". In: *Trends in Biotechnology* 30.9 (2012), pp. 475–484. ISSN: 01677799. DOI: 10.1016/j.tibtech.2012.05.007. URL: http://dx.doi.org/10.1016/j.tibtech.2012.05.007.

[220] Poolman, B. et al. "Lactose transport system of Streptococcus thermophilus: a hybrid protein with homology to the melibiose carrier and enzyme III of phosphoenolpyruvate-dependent phosphotransferase systems". In: *J Bacteriol* 171.1 (1989), pp. 244–53. ISSN: 0021-9193 (Print) 0021-9193.

[221] Portner, R. and Markl, H. "Dialysis cultures". In: *Applied Microbiology and Biotechnology* 50.4 (1998), pp. 403–414. ISSN: 01757598. DOI: 10.1007/s002530051312.

[222] Props, Ruben et al. "Measuring the biodiversity of microbial communities by flow cytometry". In: Ackermann 2015 (2016), pp. 1376–1385. DOI: 10.1111/2041-210X.12607.

[223] Pugliese, Alessandro et al. "Physical characterization of whole and skim dried milk powders". In: *Journal of Food Science and Technology* 54.11 (2017), pp. 3433–3442. ISSN: 09758402. DOI: 10.1007/s13197-017-2795-1.

[224] Radke-Mitchell, Lyn C. and Sandine, W. E. "Influence of Temperature on Associative Growth of Streptococcus thermophilus and Lactobacillus bulgaricus". In: *Journal of Dairy Science* 69.10 (1986), pp. 2558–2568. ISSN: 00220302. DOI: 10.3168/jds.S0022-0302(86)80701-9.

[225] Rajagopal, S. N. and Sandine, W. E. "Associative Growth and Proteolysis of Streptococcus thermophilus and Lactobacillus bulgaricus in Skim Milk". In: *Journal of*

Dairy Science 73.4 (1990), pp. 894–899. ISSN: 00220302. DOI: `10.3168/jds.S0022-0302(90)78745-0`.

[226] Ramos, João R. C. et al. "A dynamic model linking cell growth to intracellular metabolism and extracellular by-product accumulation". In: *Biotechnology and Bioengineering* 117.5 (Feb. 2020), pp. 1533–1553. DOI: `10.1002/bit.27288`. URL: `https://doi.org/10.1002/bit.27288`.

[227] Rappé, Michael S and Giovannoni, Stephen J. "The Uncultured Microbial Majority". In: *Annual Review of Microbiology* 57.1 (Oct. 2003), pp. 369–394. ISSN: 0066-4227. DOI: `10.1146/annurev.micro.57.030502.090759`. URL: `https://doi.org/10.1146/annurev.micro.57.030502.090759`.

[228] Rateb, Mostafa E. et al. "Induction of diverse secondary metabolites in Aspergillus fumigatus by microbial co-culture". In: *RSC Advances* 3.34 (2013), pp. 14444–14450. ISSN: 20462069. DOI: `10.1039/c3ra42378f`.

[229] Ratzke, Christoph, Barrere, Julien, and Gore, Jeff. "Strength of species interactions determines biodiversity and stability in microbial communities". In: *Nature Ecology and Evolution* (2020), pp. 1–8. ISSN: 2397-334X. DOI: `10.1038/s41559-020-1099-4`. URL: `http://www.nature.com/articles/s41559-020-1099-4`.

[230] Rau, Martin H. and Zeidan, Ahmad A. "Constraint-based modeling in microbial food biotechnology". In: *Biochemical Society Transactions* 46.2 (Apr. 2018), pp. 249–260. ISSN: 14708752. DOI: `10.1042/BST20170268`.

[231] Rau, Martin H. et al. "Genome-Scale Metabolic Modeling Combined with Transcriptome Profiling Provides Mechanistic Understanding of Streptococcus thermophilus CH8 Metabolism". In: *Applied and Environmental Microbiology* (Aug. 2022). Ed. by Danilo Ercolini. ISSN: 0099-2240. DOI: `10.1128/aem.00780-22`. URL: `https://journals.asm.org/doi/10.1128/aem.00780-22`.

[232] Rault, Aline, Bouix, Marielle, and Béal, Catherine. "Dynamic analysis of Lactobacillus delbrueckii subsp. bulgaricus CFL1 physiological characteristics during fermentation". In: *Applied Microbiology and Biotechnology* 81.3 (2008), pp. 559–570. ISSN: 1432-0614. DOI: `10.1007/s00253-008-1699-4`. URL: `https://doi.org/10.1007/s00253-008-1699-4`.

[233] Rault, Aline, Bouix, Marielle, and Béal, Catherine. "Fermentation pH influences the physiological-state dynamics of Lactobacillus bulgaricus CFL1 during pH-controlled culture". In: *Applied and environmental microbiology* 75.13 (2009), pp. 4374–4381. ISSN: 1098-5336 0099-2240. DOI: `10.1128/AEM.02725-08`. URL: `https://pubmed.`

ncbi . nlm . nih . gov / 19429565 % 20https : / / www . ncbi . nlm . nih . gov / pmc /
articles/PMC2704822/.

[234]   Reed, Jennifer L. and Palsson, Bernhard. "Thirteen years of building constraint-based in silico models of Escherichia coli". In: *Journal of Bacteriology* 185.9 (2003), pp. 2692–2699. ISSN: 00219193. DOI: 10.1128/JB.185.9.2692-2699.2003.

[235]   Rodriguez-Serrano, Gabriela Mariana et al. "Proteolytic system of streptococcus thermophilus". In: *Journal of Microbiology and Biotechnology* 28.10 (2018), pp. 1581–1588. ISSN: 17388872. DOI: 10.4014/jmb.1807.07017.

[236]   Rose, Dyson et al. "Nomenclature of the Proteins of Cow's Milk: Third Revision". In: *Journal of Dairy Science* 53.1 (1970), pp. 1–17. ISSN: 00220302. DOI: 10.3168/jds.S0022-0302(70)86141-0. URL: http://dx.doi.org/10.3168/jds.S0022-0302(70)86141-0.

[237]   Rubbens, Peter et al. "Flow Cytometric Single-Cell Identification of Populations in Synthetic Bacterial Communities". In: (2017), pp. 1–19. DOI: 10.1371/journal.pone.0169754.

[238]   Rubbens, Peter et al. "Stripping flow cytometry: How many detectors do we need for bacterial identification?" In: *Cytometry Part A* 91.12 (2017), pp. 1184–1191. ISSN: 15524930. DOI: 10.1002/cyto.a.23284.

[239]   Rühl, Martin, Hardt, Wolf Dietrich, and Sauer, Uwe. "Subpopulation-specific metabolic pathway usage in mixed cultures as revealed by reporter protein-based 13C analysis". In: *Applied and Environmental Microbiology* 77.5 (2011), pp. 1816–1821. ISSN: 00992240. DOI: 10.1128/AEM.02696-10.

[240]   Russell, James B and Diez-Gonzalez, Francisco. "The Effects of Fermentation Acids on Bacterial Growth". In: *Advances in Microbial Physiology* 39 (1998), pp. 228–234. ISSN: 00652911. DOI: 10.1016/s0065-2911(08)60017-x.

[241]   Russell, James B. and Diez-Gonzalez, Francisco. "The Effects of Fermentation Acids on Bacterial Growth". In: *Advances in Microbial Physiology*. Elsevier, 1997, pp. 205–234. DOI: 10.1016/s0065-2911(08)60017-x.

[242]   Sabra, Wael and Zeng, An Ping. "Mixed microbial cultures for industrial biotechnology: Success, chance, and challenges". In: 1 (2014), pp. 205–238. DOI: 10.1201/b17828-9.

[243]   Sabra, Wael et al. "Biosystems analysis and engineering of microbial consortia for industrial biotechnology". In: *Engineering in Life Sciences* 10.5 (2010), pp. 407–421. ISSN: 16180240. DOI: 10.1002/elsc.201000111.

[244] Sánchez, Álvaro et al. "Directed Evolution of Microbial Communities". In: *Annual Review of Biophysics* 50 (2021), pp. 323–341. ISSN: 19361238. DOI: 10.1146/annurev-biophys-101220-072829. URL: https://ecoevorxiv.org/gsz7j/.

[245] Sańchez, Claudia et al. "Contribution of Citrate Metabolism to the Growth of *Lactococcus lactis* CRL264 at Low pH". In: *Applied and Environmental Microbiology* 74.4 (Feb. 2008), pp. 1136–1144. DOI: 10.1128/aem.01061-07. URL: https://doi.org/10.1128/aem.01061-07.

[246] Sassi, Hosni et al. "Segregostat: a novel concept to control phenotypic diversification dynamics on the example of Gram-negative bacteria". In: *Microbial Biotechnology* 12.5 (2019), pp. 1064–1075. ISSN: 17517915. DOI: 10.1111/1751-7915.13442.

[247] Schädel, Friederike and Franco-Lara, Ezequiel. "Rapid sampling devices for metabolic engineering applications". In: 83.2 (May 2009), pp. 199–208. ISSN: 01757598. DOI: 10.1007/s00253-009-1976-x.

[248] Schaub, Jochen et al. "Integrated sampling procedure for metabolome analysis". In: *Biotechnology Progress* 22.5 (2006), pp. 1434–1442. ISSN: 87567938. DOI: 10.1021/bp050381q.

[249] Schindelin, Johannes et al. "Fiji: an open-source platform for biological-image analysis." In: *Nature methods* 9 (7 June 2012), pp. 676–682. ISSN: 1548-7105. DOI: 10.1038/nmeth.2019.

[250] Schlembach, Ivan et al. "Measurement Techniques to Resolve and Control Population Dynamics of Mixed-Culture Processes". In: *Trends in Biotechnology* (2021), pp. 1–17. ISSN: 18793096. DOI: 10.1016/j.tibtech.2021.01.006. URL: https://doi.org/10.1016/j.tibtech.2021.01.006.

[251] Schmidt, Julia K. et al. "A novel concept combining experimental and mathematical analysis for the identification of unknown interspecies effects in a mixed culture". In: *Biotechnology and Bioengineering* 108.8 (2011), pp. 1900–1911. ISSN: 00063592. DOI: 10.1002/bit.23126.

[252] Schmidt, Radomir et al. "Long-term use of cover crops and no-till shift soil microbial community life strategies in agricultural soil". In: *PLoS ONE* 13.2 (2018), pp. 1–19. ISSN: 19326203. DOI: 10.1371/journal.pone.0192953.

[253] Schneider, Caroline A, Rasband, Wayne S, and Eliceiri, Kevin W. "NIH Image to ImageJ: 25 years of image analysis." In: *Nature methods* 9 (7 July 2012), pp. 671–675. ISSN: 1548-7105. DOI: 10.1038/nmeth.2089.

[254] Schopping, Marie et al. "Identifying the essential nutritional requirements of the the probiotic bacteria Bifidobacterium animalis and Bifidobacterium longum using genome-scale modeling". In: *npj Systems Biology and Applications* (2021), pp. 1–15. DOI: 10.1038/s41540-021-00207-4.

[255] Schroeckh, V. et al. "Intimate bacterial-fungal interaction triggers biosynthesis of archetypal polyketides in Aspergillus nidulans". In: *Proceedings of the National Academy of Sciences* 106.34 (2009), pp. 14558–14563. ISSN: 0027-8424. DOI: 10.1073/pnas.0901870106. arXiv: arXiv:1408.1149. URL: http://www.pnas.org/cgi/doi/10.1073/pnas.0901870106.

[256] Schwentner, Andreas et al. "Metabolic engineering to guide evolution – Creating a novel mode for L-valine production with Corynebacterium glutamicum". In: *Metabolic Engineering* 47.March (2018), pp. 31–41. ISSN: 10967184. DOI: 10.1016/j.ymben.2018.02.015. URL: https://doi.org/10.1016/j.ymben.2018.02.015.

[257] Sender, Ron, Fuchs, Shai, and Milo, Ron. "Revised Estimates for the Number of Human and Bacteria Cells in the Body". In: *PLoS Biology* 14.8 (Aug. 2016). ISSN: 15457885. DOI: 10.1371/journal.pbio.1002533.

[258] Settachaimongkon, Sarn et al. "Influence of different proteolytic strains of Streptococcus thermophilus in co-culture with Lactobacillus delbrueckii subsp. bulgaricus on the metabolite profile of set-yoghurt". In: *International Journal of Food Microbiology* 177 (2014), pp. 29–36. ISSN: 0168-1605. DOI: https://doi.org/10.1016/j.ijfoodmicro.2014.02.008. URL: https://www.sciencedirect.com/science/article/pii/S0168160514000804.

[259] Shabala, L. et al. "Listeria innocua and Lactobacillus delbrueckii subsp. bulgaricus employ different strategies to cope with acid stress". In: *Int J Food Microbiol* 110.1 (2006), pp. 1–7. ISSN: 0168-1605 (Print) 0168-1605. DOI: 10.1016/j.ijfoodmicro.2006.01.026.

[260] Shaikh, Afshan S. et al. "Isotopomer distributions in amino acids from a highly expressed protein as a proxy for those from total protein". In: *Analytical Chemistry* 80.3 (2008), pp. 886–890. ISSN: 00032700. DOI: 10.1021/ac071445+.

[261] Shong, Jasmine, Jimenez Diaz, Manuel Rafael, and Collins, Cynthia H. "Towards synthetic microbial consortia for bioprocessing". In: *Current Opinion in Biotechnology* 23.5 (2012), pp. 798–802. ISSN: 09581669. DOI: 10.1016/j.copbio.2012.02.001. URL: http://dx.doi.org/10.1016/j.copbio.2012.02.001.

[262] Siegumfeldt, H., Björn Rechinger, K., and Jakobsen, M. "Dynamic changes of intracellular pH in individual lactic acid bacterium cells in response to a rapid drop in extracellular pH". In: *Applied and environmental microbiology* 66.6 (2000), pp. 2330–2335. ISSN: 0099-2240 1098-5336. DOI: 10.1128/aem.66.6.2330-2335.2000. URL: https://pubmed.ncbi.nlm.nih.gov/10831407%20https://www.ncbi.nlm.nih.gov/pmc/articles/PMC110524/.

[263] Siegumfeldt, Henrik, Rechinger, K., and Jakobsen, Mogens. "Use of fluorescence ratio imaging for intracellular pH determination of individual bacterial cells in mixed cultures". In: *Microbiology (Reading, England)* 145 (Pt 7) (1999), pp. 1703–9. DOI: 10.1099/13500872-145-7-1703.

[264] Sieuwerts, Sander et al. "Mixed-Culture transcriptome analysis reveals the molecular basis of mixed-culture growth in Streptococcus thermophilus and Lactobacillus bulgaricus". In: *Applied and Environmental Microbiology* 76.23 (2010), pp. 7775–7784. ISSN: 00992240. DOI: 10.1128/AEM.01122-10.

[265] Sieuwerts, Sander et al. "Unraveling microbial interactions in food fermentations: From classical to genomics approaches". In: *Applied and Environmental Microbiology* 74.16 (2008), pp. 4997–5007. ISSN: 00992240. DOI: 10.1128/AEM.00113-08.

[266] Singh, Asha, Christensen, Thomas, and Panoutsou, Calliope. "Policy review for biomass value chains in the European bioeconomy". In: *Global Transitions* 3 (2021), pp. 13–42. ISSN: 25897918. DOI: 10.1016/j.glt.2020.11.003. URL: https://doi.org/10.1016/j.glt.2020.11.003.

[267] Smid, Eddy J. and Lacroix, Christophe. "Microbe-microbe interactions in mixed culture food fermentations". In: *Current Opinion in Biotechnology* 24.2 (2013), pp. 148–154. ISSN: 09581669. DOI: 10.1016/j.copbio.2012.11.007. URL: http://dx.doi.org/10.1016/j.copbio.2012.11.007.

[268] Somerville, Vincent et al. "Use and limitations of genome-scale metabolic models in food microbiology". In: *Current Opinion in Food Science* 43 (2022), pp. 225–231. ISSN: 22147993. DOI: 10.1016/j.cofs.2021.12.010. URL: https://doi.org/10.1016/j.cofs.2021.12.010.

[269] Stevens, Kelly A. and Jaykus, Lee Ann. "Bacterial separation and concentration from complex sample matrices: A review". In: *Critical Reviews in Microbiology* 30.1 (2004), pp. 7–24. ISSN: 1040841X. DOI: 10.1080/10408410490266410.

[270] Stiles, Michael E and Holzapfel, Wilhelm H. "Lactic acid bacteria of foods and their current taxonomy". In: *International Journal of Food Microbiology* 36.1 (1997),

pp. 1–29. ISSN: 0168-1605. DOI: `https://doi.org/10.1016/S0168-1605(96)01233-0`. URL: `https://www.sciencedirect.com/science/article/pii/S0168160596012330`.

[271] Stolyar, Sergey et al. "Metabolic modeling of a mutualistic microbial community". In: *Molecular Systems Biology* 3.92 (2007), pp. 1–14. ISSN: 17444292. DOI: `10.1038/msb4100131`. arXiv: `NIHMS150003`.

[272] Straathof, Adrie J.J. et al. "Grand Research Challenges for Sustainable Industrial Biotechnology". In: *Trends in Biotechnology* 37.10 (2019), pp. 1042–1050. ISSN: 18793096. DOI: `10.1016/j.tibtech.2019.04.002`. URL: `https://doi.org/10.1016/j.tibtech.2019.04.002`.

[273] Streit, Wolfgang R, Daniel, Rolf, and Jaeger, Karl-Erich. "Prospecting for biocatalysts and drugs in the genomes of non-cultured microorganisms". In: *Current Opinion in Biotechnology* 15.4 (2004), pp. 285–290. ISSN: 0958-1669. DOI: `https://doi.org/10.1016/j.copbio.2004.05.006`. URL: `https://www.sciencedirect.com/science/article/pii/S0958166904000771`.

[274] Suk, Ahn Woo and Antoniewicz, Maciek R. "Parallel labeling experiments with [1,2-13C]glucose and [U-13C]glutamine provide new insights into CHO cell metabolism". In: *Metabolic Engineering* 15 (1 2013), pp. 34–47. ISSN: 10967184. DOI: `10.1016/j.ymben.2012.10.001`. URL: `http://dx.doi.org/10.1016/j.ymben.2012.10.001`.

[275] Takors, Ralf. "Kommentierte Formelsammlung Bioverfahrenstechnik". In: *Springer Spektrum Berlin, Heidelberg* (2014). DOI: `https://doi.org/10.1007/978-3-642-41903-4`.

[276] Tan, Yikun and Liao, James C. "Metabolic ensemble modeling for strain engineers". In: *Biotechnology Journal* 7.3 (2012), pp. 343–353. DOI: `https://doi.org/10.1002/biot.201100186`. URL: `https://onlinelibrary.wiley.com/doi/abs/10.1002/biot.201100186`.

[277] Tang, Yinjie J. et al. "Engineering microbial consortia by division of labor". In: *Microbial Cell Factories* (2019), pp. 1–11. ISSN: 1475-2859. DOI: `10.1186/s12934-019-1083-3`. URL: `https://link.springer.com/article/10.1186/s12934-019-1083-3?utm_source=researcher_appandutm_medium=referralandutm_campaign=MKEF_USG_Researcher_inbound`.

[278] Tanouchi, Yu, Smith, Robert P., and You, Lingchong. "Engineering microbial systems to explore ecological and evolutionary dynamics". In: *Current Opinion in*

Biotechnology 23.5 (2012), pp. 791–797. ISSN: 09581669. DOI: `10.1016/j.copbio.2012.01.006`. URL: `http://dx.doi.org/10.1016/j.copbio.2012.01.006`.

[279] Tatenhove-Pel, Rinke J. van et al. "Microdroplet screening and selection for improved microbial production of extracellular compounds". In: *Current Opinion in Biotechnology* 61 (2020), pp. 72–81. ISSN: 18790429. DOI: `10.1016/j.copbio.2019.10.007`. URL: `https://doi.org/10.1016/j.copbio.2019.10.007`.

[280] Teleki, A. et al. "Robust identification of metabolic control for microbial L-methionine production following an easy-to-use puristic approach". In: *Metabolic Engineering* 41.February (2017), pp. 159–172. ISSN: 10967184. DOI: `10.1016/j.ymben.2017.03.008`. URL: `http://dx.doi.org/10.1016/j.ymben.2017.03.008`.

[281] Teleki, Attila. "Systembiologische Untersuchungen zur Optimierung mikrobieller Produzenten schwefelhaltiger Aminosäuren. Dissertation, Institute of Biochemical Engineering, University Stuttgart, 2016". In: ().

[282] Teleki, Attila, Sánchez-Kopper, Andrés, and Takors, Ralf. "Alkaline conditions in hydrophilic interaction liquid chromatography for intracellular metabolite quantification using tandem mass spectrometry". In: *Analytical Biochemistry* 475 (2015). isobar: gleiche Nukleonenanzahl, bei unterschiedlichen protonen und neutronen., pp. 4–13. ISSN: 10960309. DOI: `10.1016/j.ab.2015.01.002`. URL: `http://dx.doi.org/10.1016/j.ab.2015.01.002`.

[283] Templeton, Neil et al. "Peak antibody production is associated with increased oxidative metabolism in an industrially relevant fed-batch CHO cell culture". In: *Biotechnology and Bioengineering* 110 (7 2013). ISSN: 00063592. DOI: `10.1002/bit.24858`.

[284] Tesfaye Damtew, Endale and Gebre, Aregay Berhe. "Journal of Environmental and Analytical Toxicology Chemical Composition and Heavy Metals Analysis of Raw Cow's Milk". In: 10 (2020), pp. 1–5. ISSN: 2161-0525.

[285] Teusink, Bas, Bachmann, Herwig, and Molenaar, Douwe. "Systems biology of lactic acid bacteria: A critical review". In: *Microb Cell Fact* 10.Suppl 1 (2011), S11. ISSN: 14752859. DOI: `10.1186/1475-2859-10-S1-S11`. URL: `http://www.microbialcellfactories.com/content/10/S1/S11%20http://www.ncbi.nlm.nih.gov/pubmed/21995498`.

[286] Teusink, Bas and Molenaar, Douwe. "Systems biology of lactic acid bacteria: For food and thought". In: *Current Opinion in Systems Biology* 6 (2017), pp. 7–13. ISSN: 24523100. DOI: `10.1016/j.coisb.2017.07.005`. URL: `https://doi.org/10.1016/j.coisb.2017.07.005`.

[287] Teusink, Bas and Smid, Eddy J. "Modelling strategies for the industrial exploitation of lactic acid bacteria". In: *Nature Reviews Microbiology* 4.1 (2006), pp. 46–56. ISSN: 17401526. DOI: `10.1038/nrmicro1319`.

[288] Thommes, Meghan et al. "Designing Metabolic Division of Labor in Microbial Communities". In: *mSystems* 4.2 (2019). ISSN: 2379-5077. DOI: `10.1128/msystems.00263-18`.

[289] Tringe, Susannah Green and Rubin, Edward M. "Metagenomics: DNA sequencing of environmental samples". In: *Nature Reviews Genetics* 6.11 (2005), pp. 805–814. ISSN: 1471-0064. DOI: `10.1038/nrg1709`. URL: `https://doi.org/10.1038/nrg1709`.

[290] Ulmer, Andreas et al. "A Two-Compartment Fermentation System to Quantify Strain-Specific Interactions in Microbial Co-Cultures". In: *Bioengineering* 10.1 (2023). ISSN: 2306-5354. DOI: `10.3390/bioengineering10010103`. URL: `https://www.mdpi.com/2306-5354/10/1/103`.

[291] Ulmer, Andreas et al. "Differential Amino Acid Uptake and Depletion in Mono-Cultures and Co-Cultures of Streptococcus thermophilus and Lactobacillus delbrueckii subsp. bulgaricus in a Novel Semi-Synthetic Medium". In: *Microorganisms* 10.9 (2022). ISSN: 2076-2607. DOI: `10.3390/microorganisms10091771`. URL: `https://www.mdpi.com/2076-2607/10/9/1771`.

[292] Ustunol, Z. "Development and Manufacture of Yogurt and Other Functional Dairy Products (2010), edited by F. Yildiz, CRC Press (Taylor and Francis Group), Boca Raton, Florida, USA. ISBN 978-1-4200-8207-4." In: *International Journal of Dairy Technology* 66.2 (2013), pp. 300–301. DOI: `https://doi.org/10.1111/1471-0307.12031`. URL: `https://onlinelibrary.wiley.com/doi/abs/10.1111/1471-0307.12031`.

[293] Varma, Amit and Palsson, Bernhard O. "Metabolic capabilities of escherichia coli. II. Optimal growth patterns". In: 165.4 (1993), pp. 503–522. ISSN: 00225193. DOI: `10.1006/jtbi.1993.1203`.

[294] Veal, D. A. et al. "Fluorescence staining and flow cytometry for monitoring microbial cells". In: *Journal of Immunological Methods* 243.1-2 (2000), pp. 191–210. ISSN: 00221759. DOI: `10.1016/S0022-1759(00)00234-9`.

[295] Vinnakota, Kalyan, Kemp, Melissa L., and Kushmerick, Martin J. "Dynamics of Muscle Glycogenolysis Modeled with pH Time Course Computation and pH-

Dependent Reaction Equilibria and Enzyme Kinetics". In: *Biophysical Journal* 91.4 (Aug. 2006), pp. 1264–1287. DOI: 10.1529/biophysj.105.073296.

[296] Vos, W. M. de and Vaughan, E. E. "Genetics of lactose utilization in lactic acid bacteria". In: *FEMS Microbiol Rev* 15.2-3 (1994), pp. 217–37. ISSN: 0168-6445 (Print) 0168-6445. DOI: 10.1111/j.1574-6976.1994.tb00136.x.

[297] Vos, Willem M. de. "Metabolic engineering of sugar catabolism in lactic acid bacteria". In: *Lactic Acid Bacteria: Genetics, Metabolism and Applications* (1996), pp. 127–146. DOI: 10.1007/978-94-009-1774-3-8.

[298] Wang, Xiaonan et al. "Developing E. coli-E. coli co-cultures to overcome barriers of heterologous tryptamine biosynthesis". In: *Metabolic Engineering Communications* 10.October 2019 (2020), e00110. ISSN: 22140301. DOI: 10.1016/j.mec.2019.e00110. URL: https://doi.org/10.1016/j.mec.2019.e00110.

[299] Wang, Yingying et al. "Past, present and future applications of flow cytometry in aquatic microbiology". In: *Trends in Biotechnology* 28.8 (2010), pp. 416–424. ISSN: 01677799. DOI: 10.1016/j.tibtech.2010.04.006.

[300] Wang, Zhong, Gerstein, Mark, and Snyder, Michael. "RNA-Seq: A revolutionary tool for transcriptomics". In: 10.1 (Jan. 2009), pp. 57–63. ISSN: 14710056. DOI: 10.1038/nrg2484.

[301] Warburg, Otto. "On the origin of cancer cells". In: *Science* 123 (3191 1956). ISSN: 00368075. DOI: 10.1126/science.123.3191.309.

[302] Weeke, Sebastian. *Assessment of a rapid sampling procedure for metabolic analysis of Corynebacterium glutamicum Statement of Authorship. Student Thesis, University Stuttgart.* 2017.

[303] Welch, B. L. "The Generalization of 'Student's' Problem when Several Different Population Variances are Involved". In: *Biometrika* 34 (1/2 1947). ISSN: 00063444. DOI: 10.2307/2332510.

[304] Welman, A D and Maddox, I S. "Fermentation performance of an exopolysaccharide-producing strain of Lactobacillus delbrueckii subsp. bulgaricus". In: *Journal of Industrial Microbiology and Biotechnology* 30.11 (Nov. 2003), pp. 661–668. ISSN: 1367-5435. DOI: 10.1007/s10295-003-0095-4. eprint: https://academic.oup.com/jimb/article-pdf/30/11/661/34737234/jimb0661.pdf. URL: https://doi.org/10.1007/s10295-003-0095-4.

[305]   Wen, Zhiqiang et al. "Enhanced solvent production by metabolic engineering of a twin-clostridial consortium". In: *Metabolic Engineering* 39.August 2016 (2017), pp. 38–48. ISSN: 10967184. DOI: `10.1016/j.ymben.2016.10.013`.

[306]   West, Stuart A. et al. "The social lives of microbes". In: *Annual Review of Ecology, Evolution, and Systematics* 38 (2007), pp. 53–77. ISSN: 1543592X. DOI: `10.1146/annurev.ecolsys.38.091206.095740`.

[307]   Whitney, Robert Mc L. et al. "Nomenclature of the Proteins of Cow's Milk: Fourth Revision". In: *Journal of Dairy Science* 59.5 (1976), pp. 795–815. ISSN: 00220302. DOI: `10.3168/jds.S0022-0302(76)84280-4`.

[308]   Wides, Aryeh and Milo, Ron. "Understanding the Dynamics and Optimizing the Performance of Chemostat Selection Experiments". In: (2018).

[309]   Wiechert, Wolfgang. "13 C Metabolic Flux Analysis". In: *Metabolic engineering* 3 (3 2001), pp. 195–206. ISSN: 10967176. DOI: `10.1006/mben.2001.0187`.

[310]   Wiechert, Wolfgang and Nöh, Katharina. "Isotopically non-stationary metabolic flux analysis: Complex yet highly informative". In: *Current Opinion in Biotechnology* 24.6 (2013), pp. 979–986. ISSN: 09581669. DOI: `10.1016/j.copbio.2013.03.024`.

[311]   Wijaya, Andy Wiranata et al. "Compartment-specific metabolome labeling enables the identification of subcellular fluxes that may serve as promising metabolic engineering targets in CHO cells". In: *Bioprocess and Biosystems Engineering* 44.12 (2021), pp. 2567–2578. ISSN: 16157605. DOI: `10.1007/s00449-021-02628-1`. URL: `https://doi.org/10.1007/s00449-021-02628-1`.

[312]   Winden, Wouter A. Van et al. "Metabolic-flux analysis of Saccharomyces cerevisiae CEN.PK113-7D based on mass isotopomer measurements of 13C-labeled primary metabolites". In: *FEMS Yeast Research* 5 (6-7 2005). ISSN: 15671356. DOI: `10.1016/j.femsyr.2004.10.007`.

[313]   Wintermute, Edwin H. and Silver, Pamela A. "Dynamics in the mixed microbial concourse". In: *Genes and Development* 24.23 (2010), pp. 2603–2614. ISSN: 08909369. DOI: `10.1101/gad.1985210`.

[314]   Wintermute, Edwin H. and Silver, Pamela A. "Emergent cooperation in microbial metabolism". In: *Molecular Systems Biology* 6.407 (2010), pp. 1–7. ISSN: 17444292. DOI: `10.1038/msb.2010.66`. URL: `http://dx.doi.org/10.1038/msb.2010.66`.

[315] Wittig, Ulrike et al. "SABIO-RK—database for biochemical reaction kinetics". In: *Nucleic Acids Research* 40.D1 (2011), pp. D790–D796. ISSN: 0305-1048. DOI: 10.1093/nar/gkr1046. URL: https://doi.org/10.1093/nar/gkr1046.

[316] Woolston, Benjamin M., Edgar, Steven, and Stephanopoulos, Gregory. "Metabolic engineering: Past and future". In: *Annual Review of Chemical and Biomolecular Engineering* 4.March (2013), pp. 259–288. ISSN: 19475438. DOI: 10.1146/annurev-chembioeng-061312-103312.

[317] Wu, Gang et al. "Metabolic Burden: Cornerstones in Synthetic Biology and Metabolic Engineering Applications". In: *Trends in Biotechnology* 34.8 (2016), pp. 652–664. ISSN: 18793096. DOI: 10.1016/j.tibtech.2016.02.010. URL: http://dx.doi.org/10.1016/j.tibtech.2016.02.010.

[318] Wuyts, Sander et al. "Applications of plant-based fermented foods and their microbes". In: *Current Opinion in Biotechnology* 61 (2020), pp. 45–52. ISSN: 18790429. DOI: 10.1016/j.copbio.2019.09.023. URL: https://doi.org/10.1016/j.copbio.2019.09.023.

[319] Xu, Peng. "Dynamics of microbial competition, commensalism, and cooperation and its implications for coculture and microbiome engineering". In: *Biotechnology and Bioengineering* (2020). ISSN: 10970290. DOI: 10.1002/bit.27562.

[320] Yang, Zheng Rong. "Biological applications of support vector machines". In: *Brief Bioinform.* 5 (2004). DOI: 10.1093/bib/5.4.328. URL: https://academic.oup.com/bib/article/5/4/328/265877.

[321] Young, Jamey D. "INCA: A computational platform for isotopically non-stationary metabolic flux analysis". In: *Bioinformatics* 30.9 (2014), pp. 1333–1335. ISSN: 14602059. DOI: 10.1093/bioinformatics/btu015.

[322] Zamboni, Nicola. "13C metabolic flux analysis in complex systems". In: *Current Opinion in Biotechnology* 22.1 (2011), pp. 103–108. ISSN: 09581669. DOI: 10.1016/j.copbio.2010.08.009. arXiv: NIHMS150003. URL: http://dx.doi.org/10.1016/j.copbio.2010.08.009.

[323] Zengler, Karsten and Palsson, Bernhard O. "A road map for the development of community systems (CoSy) biology". In: *Nature Reviews Microbiology* 10.5 (2012), pp. 366–372. ISSN: 17401526. DOI: 10.1038/nrmicro2763. URL: http://dx.doi.org/10.1038/nrmicro2763.

[324] Zhang, Haoran and Stephanopoulos, Gregory. "Co-culture engineering for microbial biosynthesis of 3-amino-benzoic acid in Escherichia coli". In: *Biotechnology Journal* 11.7 (2016), pp. 981–987. ISSN: 18607314. DOI: `10.1002/biot.201600013`.

[325] Zhang, Haoran and Wang, Xiaonan. "Modular co-culture engineering, a new approach for metabolic engineering". In: *Metabolic Engineering* 37 (2016), pp. 114–121. ISSN: 10967184. DOI: `10.1016/j.ymben.2016.05.007`. arXiv: `NIHMS150003`. URL: `http://dx.doi.org/10.1016/j.ymben.2016.05.007`.

[326] Zhang, Shu et al. "Interkingdom microbial consortia mechanisms to guide biotechnological applications". In: *Microbial Biotechnology* (2018). ISSN: 17517915. DOI: `10.1111/1751-7915.13300`. URL: `http://doi.wiley.com/10.1111/1751-7915.13300`.

[327] Zhang, Xiaolin and Reed, Jennifer L. "Adaptive evolution of synthetic cooperating communities improves growth performance". In: *PLoS ONE* 9.10 (2014). ISSN: 19326203. DOI: `10.1371/journal.pone.0108297`.

[328] Zhao, Zheng et al. "Isotopic non-stationary 13C gluconate tracer method for accurate determination of the pentose phosphate pathway split-ratio in Penicillium chrysogenum". In: *Metabolic Engineering* 10 (3-4 2008). ISSN: 10967176. DOI: `10.1016/j.ymben.2008.04.003`.

[329] Zheng, Huajun et al. "In silico analysis of amino acid biosynthesis and proteolysis in Lactobacillus delbrueckii subsp. bulgaricus 2038 and the implications for bovine milk fermentation". In: *Biotechnology Letters* 34.8 (2012), pp. 1545–1551. ISSN: 1573-6776. DOI: `10.1007/s10529-012-1006-4`. URL: `https://doi.org/10.1007/s10529-012-1006-4`.

[330] Zhou, Kang et al. "Distributing a metabolic pathway among a microbial consortium enhances production of natural products". In: *Nature Biotechnology* 33.4 (2015), pp. 377–383. ISSN: 15461696. DOI: `10.1038/nbt.3095`. arXiv: `15334406`. URL: `http://dx.doi.org/10.1038/nbt.3095`.

[331] Zhu, Linjiang et al. "Engineering the robustness of industrial microbes through synthetic biology". In: *Trends in Microbiology* 20.2 (2012), pp. 94–101. ISSN: 0966842X. DOI: `10.1016/j.tim.2011.12.003`. URL: `http://dx.doi.org/10.1016/j.tim.2011.12.003`.

[332] Ziesack, Marika et al. "Engineered Interspecies Amino Acid Cross-Feeding Increases Population Evenness in a Synthetic Bacterial Consortium". In: *mSystems* 4.4 (2019), pp. 1–15. ISSN: 2379-5077. DOI: `10.1128/msystems.00352-19`.

[333]   Zomorrodi, Ali R. and Segre, Daniel. "Synthetic Ecology of Microbes: Mathematical Models and Applications". In: *Journal of Molecular Biology* 428.5 (2016), pp. 837–861. ISSN: 10898638. DOI: `10.1016/j.jmb.2015.10.019`. URL: `http://dx.doi.org/10.1016/j.jmb.2015.10.019`.

[334]   Zuroff, Trevor R., Xiques, Salvador Barri, and Curtis, Wayne R. "Consortia-mediated bioprocessing of cellulose to ethanol with a symbiotic Clostridium phytofermentans/yeast co-culture". In: *Biotechnology for Biofuels* 6.1 (2013), pp. 1–12. ISSN: 17546834. DOI: `10.1186/1754-6834-6-59`.

Appendix A

Differential amino acid uptake and depletion in mono-cultures and co-cultures of *Streptococcus thermophilus* and *Lactobacillus delbrueckii* subsp. *bulgaricus* in a novel semi-synthetic medium

Reprinted from Ulmer et al. (2022) with permission of MDPI Microorganisms.

Article

Differential Amino Acid Uptake and Depletion in Mono-Cultures and Co-Cultures of *Streptococcus thermophilus* and *Lactobacillus delbrueckii* subsp. *bulgaricus* in a Novel Semi-Synthetic Medium

Andreas Ulmer [1] , Florian Erdemann [1], Susanne Mueller [1], Maren Loesch [1], Sandy Wildt [1], Maiken Lund Jensen [2], Paula Gaspar [2], Ahmad A. Zeidan [2] and Ralf Takors [1,*]

1 Institute of Biochemical Engineering, University of Stuttgart, 70569 Stuttgart, Germany
2 Systems Biology, R&D Discovery, Chr. Hansen A/S, 2970 Hørsholm, Denmark
* Correspondence: takors@ibvt.uni-stuttgart.de

Abstract: The mechanistic understanding of the physiology and interactions of microorganisms in starter cultures is critical for the targeted improvement of fermented milk products, such as yogurt, which is produced by *Streptococcus thermophilus* in co-culture with *Lactobacillus delbrueckii* subsp. *bulgaricus*. However, the use of complex growth media or milk is a major challenge for quantifying metabolite production, consumption, and exchange in co-cultures. This study developed a synthetic medium that enables the establishment of defined culturing conditions and the application of flow cytometry for measuring species-specific biomass values. Time courses of amino acid concentrations in mono-cultures and co-cultures of *L. bulgaricus* ATCC BAA-365 with the proteinase-deficient *S. thermophilus* LMG 18311 and with a proteinase-positive *S. thermophilus* strain were determined. The analysis revealed that amino acid release rates in co-culture were not equivalent to the sum of amino acid release rates in mono-cultures. Data-driven and pH-dependent amino acid release models were developed and applied for comparison. Histidine displayed higher concentrations in co-cultures, whereas isoleucine and arginine were depleted. Amino acid measurements in co-cultures also confirmed that some amino acids, such as lysine, are produced and then consumed, thus being suitable candidates to investigate the inter-species interactions in the co-culture and contribute to the required knowledge for targeted shaping of yogurt qualities.

Keywords: microbial interactions; co-culture; *Lactobacillus bulgaricus*; *Streptococcus thermophilus*; milk; amino acid metabolism; metabolite exchange; flow cytometry; pH-dependent modeling; proteolytic activity

1. Introduction

Dairy products have been a part of the human diet since ancient times [1]. Detailed identification and analysis of fermented milk products began in the twentieth century [2]. Efforts are ongoing to develop tools to examine lactic acid bacteria [3–6]. Yogurt, which is currently an important part of the cuisine of many cultures, will be a critical dietary component in the future. Therefore, the identification and determination of novel co-culture compositions that impart improved technological and organoleptic properties are active areas of research in the food industry [7]. *Streptococcus thermophilus* and *Lactobacillus delbrueckii* subsp. *bulgaricus* are the key species that drive yogurt production [2].

To meet the changing market demands, there is a need to understand the interaction between *S. thermophilus* and *L. bulgaricus* during milk fermentation and to make use of this knowledge to design improved food products [8]. Despite significant progress in the past, the current state of understanding still shows white spots [2].

In the last 15 years, metabolomics [9,10] and transcriptomics [11–13] have been widely applied to understand the physiology of *S. thermophilus* and *L. bulgaricus* in mono-culture and co-culture. Previous studies provide insights into the metabolites exchanged between the strains and elucidated the characteristic gene expression patterns. However, these datasets have provided a limited scope to assign contextual functionalities to metabolites [12–14].

Screening various combinations of *S. thermophilus* and *L. bulgaricus* strains in co-cultures is a time-consuming and costly process. Thus, only a small subset of all possible combinations and conditions has been investigated. To overcome this limitation, mathematical modeling approaches, such as community flux balance analysis, have been used to predict the performance of co-cultures [15]. Although the mathematical modeling approach enables the estimation of flux distributions in underdetermined systems, a minimum number of experimental measurements is required to limit the solution space. Additionally, the stoichiometry of interactions must be understood for the application of mathematical approaches. Both constraints require reliable and representative experimental datasets as a prerequisite for flux balance modeling [16].

Understanding of the complex metabolic interactions between *S. thermophilus* and *L. bulgaricus*, including the exchange of peptides and amino acids, is currently limited [2]. One key feature is the strong proteolytic activity of *L. bulgaricus*, which enhances the production of peptides and amino acids that become available for *S. thermophilus*, enabling growth [13]. However, some *S. thermophilus* strains exhibit proteolytic activity. Consequently, the question that arises is whether and what differences in this inter-species interaction exist when proteolytic and non-proteolytic *S. thermophilus* are combined with *L. bulgaricus* in co-cultures.

Acidification, a marker for lactic acid formation, may serve as an easy-to-follow readout once mono-cultures and co-cultures can be cultured under comparable conditions. Limited information is available on amino acid production and consumption [9] and potential amino acid depletion, which may trigger amino acid biosynthesis [12,13].

Milk is traditionally used as a growth medium for *S. thermophilus* and *L. bulgaricus* cultivations in the production of yogurt. *S. thermophilus* and *L. bulgaricus* produce lactic acid from lactose, which imparts an acidic taste and inhibits the growth of microbes, including *S. thermophilus* and *L. bulgaricus* [17,18]. However, milk composition is highly variable. Furthermore, milk comprises several complex ingredients that interfere with the sensitivity of analytical methods, such as high-performance liquid chromatography (HPLC) and mass spectrometry. Additionally, the acidification of milk leads to an increase in viscosity, which impairs the sensitivity of the analytical methods [19].

To overcome these intrinsic analytical barriers, this study developed a synthetic medium supplemented with amino acids (SMaa) to allow the growth of *S. thermophilus* and *L. bulgaricus* in mono-cultures, which enabled the analysis of individual growth characteristics. The synthetic medium may be supplemented with casein (SMcas) instead of amino acids to investigate the proteolytic abilities of *S. thermophilus* and *L. bulgaricus* in mono-cultures. The medium allows for investigation of the interactions between *S. thermophilus* and *L. bulgaricus* by excluding individual components that are likely to be exchanged. An important effect of the symbiotic relationship between *S. thermophilus* and *L. bulgaricus* is the faster acidification during milk fermentation [13]. Therefore, this study investigated this feature by co-cultivating the strains in SMcas.

This study presents a new medium and comparable datasets of *S. thermophilus* and *L. bulgaricus* in mono-culture and co-culture conditions, providing useful insights into essential amino acid production and consumption. Our results demonstrate that the patterns and levels of amino acid release and consumption in co-cultures are different from those of mono-cultures. These findings are essential for data-driven modeling and testing hypotheses on the induction of basic regulatory mechanisms in cells.

2. Materials and Methods

2.1. Strains and Cultivation Conditions

Lactobacillus delbrueckii subsp. *bulgaricus* strains (LB.1 = ATCC BAA-365, LB.2, LB.3, and LB.4) were provided by Chr. Hansen A/S and stored at $-70\,^\circ$C in Man–Rogosa–Sharpe (MRS) (69966 MRS Broth, Sigma-Aldrich Chemie GmbH, Steinheim, Germany) containing 20% (*v/v*) glycerol. For cultivation, the total cell suspension in the cryotube (1 mL) was transferred into 15 mL of MRS supplemented with 14.3 g L^{-1} lactose and incubated for 6–8 h at $40\,^\circ$C [20–23]. After washing twice with 0.9% NaCl solution, the cell pellet was resuspended in 200 µL of 0.9% NaCl to inoculate the preculture containing SMaa. The preculture was cultured at $40\,^\circ$C and gently stirred with a 10 mm magnetic bar at 400 rpm for 14–18 h until the pH was between 5 and 6.

Streptococcus thermophilus strains (ST.1, ST.2, ST.3, and ST.4 = LMG 18311) were provided by the industrial partner (Chr. Hansen) and stored at $-70\,^\circ$C in M17 (56156 M-17 Broth, Sigma-Aldrich Chemie GmbH, Steinheim, DE, USA) containing 20% (*v/v*) glycerol. The cells in the cryotube were washed twice with 0.9% NaCl solution. Then, the cell pellet was resuspended in 200 µL of 0.9% NaCl to inoculate the preculture containing SMaa. The preculture was cultured at $40\,^\circ$C and gently stirred with a 10 mm magnetic bar at 400 rpm for 2–6 h until the pH was between 5 and 6.

Calculated amounts of biomass from *L. bulgaricus* and *S. thermophilus* precultures were washed twice with 0.9% NaCl solution and the cell pellets were resuspended in 200 µL 0.9% NaCl to inoculate the main culture. The main culture was carried out in SMaa or SMcas as indicated in Table 1.

Table 1. Composition of synthetic medium (SM).

Category	Compound	Concentration [g L^{-1}]	CAS Number
-	Di-potassium hydrogen phosphate	2.5	7758-11-4
	Potassium dihydrogen phosphate	3	7778-77-0
	Sodium acetate	1	127-09-3
	Ammonium citrate tribasic	0.6	3458-72-8
	Manganese sulfate monohydrate	0.02	10034-96-5
	Iron(II) sulfate heptahydrate	0.00132	7782-63-0
	Calcium chloride dihydrate	0.08745	10035-04-8
	Tween 80	1 mL L^{-1}	9005-65-6
	D-Lactose monohydrate	15.75	10039-26-6
	Magnesium sulfate heptahydrate	0.2	10034-99-8
	Urea	0.12	57-13-6
nucleobases	Adenine	0.01	73-24-5
	Guanine	0.01	73-40-5
	Uracil	0.01	66-22-8
	Xanthine	0.01	69-89-6
vitamins	Biotin	0.0002	58-85-5
	Folic acid	0.0002	59-30-3
	Pyridoxal hydrochloride	0.001	65-22-5
	Riboflavin	0.0005	83-88-5
	Thiamine chloride hydrochloride	0.0005	67-03-8
	Nicotinamide	0.0005	98-92-0
	Cyanocobalamin	0.0005	68-19-9
	4-Aminobenzoic acid	0.0005	150-13-0
	D-Pantothenic acid hemicalcium salt	0.004	137-08-6
	DL-6,8-thioctic acid	0.0005	1077-28-7

Table 1. *Cont.*

Category	Compound	Concentration [g L^{-1}]	CAS Number
trace elements	Ammonium molybdate tetrahydrate	0.0000037	12054-85-2
	Cobalt(II) chloride hexahydrate	0.000007	7791-13-1
	Boric acid	0.000025	10043-35-3
	Copper(II) sulfate pentahydrate	0.0000025	7758-99-8
	Zinc sulfate heptahydrate	0.0000029	7446-20-0
amino acids	L-Alanine	0.1	56-41-7
	L-Arginine	0.317	74-79-3
	L-Asparagine monohydrate	0.343	5794-13-8
	L-Aspartic acid	0.499	56-84-8
	L-Cysteine hydrochloride monohydrate	0.3	7048-04-6
	L-Glutamic acid	0.331	56-86-0
	L-Glutamine	0.29	56-85-9
	Glycine	0.16	56-40-6
	L-Histidine monohydrochloride monohydrate	0.273	5934-29-2
	L-Isoleucine	0.361	73-32-5
	L-Leucine	0.6	61-90-5
	L-Lysine	0.351	56-87-1
	L-Methionine	0.119	63-68-3
	L-Phenylalanine	0.34	63-91-2
	L-Proline	0.921	147-85-3
	L-Serine	0.359	56-45-1
	L-Threonine	0.3	72-19-5
	L-Tryptophan	0.102	73-22-3
	L-Tyrosine	0.12	60-18-4
	L-Valine	0.468	72-18-4
casein	Casein	2	9005-46-3

The SM contains all listed compounds, except amino acids and casein. SM supplemented with amino acids (SMaa) contains all listed compounds, except casein. SM supplemented with casein (SMcas) contains all listed compounds, except amino acids.

The preculture (SMaa) and main culture (SMaa or SMcas) were cultured in crimp-top serum bottles, which were pretreated by flushing with 80% N_2 and 20% CO_2 for 10 min at 400 rpm. Growth was monitored by measuring the optical density (OD) ($\lambda = 600$ nm) using a photometer (Amersham Bioscience, Ultrospec 10 cell density meter) or flow cytometry.

2.2. Acidification Measurements

The pH was measured offline using a pH meter (SevenEasy^{TM}, Mettler Toledo, Columbus, OH, USA) connected to a pH electrode (InLab Semi-Micro, Mettler Toledo, Columbus, OH, USA).

2.3. Medium Preparation

2.3.1. Complex Media

MRS (69966 MRS Broth, Sigma-Aldrich Chemie GmbH, Steinheim, Germany) was dissolved in Milli-Q water and the pH of the medium was adjusted to 6.5 using 2 M NaOH. Then, the medium was filtered using a 0.22-μm filter (ROTILABO®, PVD, Carl Roth GmbH & Co. KG, Karlsruhe, Germany) and sterile polysorbate 80 (CAS-Nr.: 9005-65-6, Sigma-Aldrich Chemie GmbH, Steinheim, Germany) was added according to the manufacturer's instructions.

M17 (56156 M17 Broth, Sigma-Aldrich Chemie GmbH, Steinheim, DE, USA) was prepared following the manufacturer's instructions and autoclaved.

2.3.2. Semi-Synthetic Medium

A sterile $5\times$ basal solution containing di-potassium hydrogen phosphate, potassium dihydrogen phosphate, sodium acetate, ammonium citrate, manganese sulfate, iron(II) sulfate, and Tween 80 was prepared as indicated in Table 1. Sterile lactose, magnesium sulfate, urea, nucleobases, and amino acids were added to the solution. After the pH was set to 6.5 with 1 M HCl, trace elements, vitamins, calcium chloride, and casein were added. The serum bottle was sealed, crimped, and flushed with sterile 80% N_2 and 20% CO_2 for 10 min at 400 rpm.

The casein stock solution was prepared in a beaker containing glass beads (3 mm in diameter), which were covered with a thin layer of 200 μL of Tween 80. Next, 100 mL of water containing 0.26 g L^{-1} $CaCl_2$ was added, and the solution was stirred slowly overnight, followed by autoclaving for 5 min at 121 °C.

2.4. Cell Dry Weight (DW)

A glass vial (1 mL, VWR) was dried at 105 °C for at least 36 h, cooled at 20 °C for at least 1 h, and weighed. Aliquots of 1 mL of culture samples in SMaa were washed thrice with Milli-Q water (40 °C) in a 1.5-mL reaction tube (Eppendorf), resuspended in 300 μL of Milli-Q water, and transferred into a dried glass vial. The reaction tube was rinsed with 200 μL of Milli-Q water, and the water was transferred to the glass vial. The glass vial was dried at 105 °C for at least 36 h, cooled at 20 °C overnight in a desiccator, and weighed to calculate the cell dry weight. The correlation between optical density, flow cytometry data (events mL^{-1}), and cell dry weight (g_{DW} L^{-1}) was as follows: for LB.1, 1 g_{DW} L^{-1} = 0.17101671 × 10^{-7} * events mL^{-1} = 0.2527 × $OD_{600 \, nm}$; for ST.1, 1 g_{DW} L^{-1} = 0.01970622 × 10^{-7} * events mL^{-1} = 0.2075 × $OD_{600 \, nm}$; for ST.4. 1 g_{DW} L^{-1} = 0.043115 × 10^{-7} * events mL^{-1} = 0.243 × $OD_{600 \, nm}$.

2.5. Biomass Measurements Using Flow Cytometry

Samples for flow cytometry analysis were prepared as described previously [3]. The cell suspension (100 μL) was diluted 10-fold with Tris-HCl (1.3 M) EDTA (0.13 M) buffer (pH 8) and incubated for 10 min on a shaker (Eppendorf Thermomixer 5436, Hamburg, Germany) at 1200 rpm and 50 °C. Next, the cell suspension was incubated with $1\times$ SYBR™Green I nucleic acid gel stain concentrate (Thermo Fisher Scientific, Waltham, MA, USA) for at least 10 min at 20 °C in the dark. The sample was filtered through a filter (Partec CellTrics® 30 μM mesh filter size, Sysmex, Germany) into a polystyrene tube immediately before measurements and analyzed using a flow cytometer (BD Accuri™ C6; BD Bioscience, Franklin Lakes, NJ, USA) equipped with four fluorescence detectors (FL1 533/30 nm, FL2 585/40 nm, FL3 > 670 nm, and FL4 675/25 nm), two scatter detectors, a blue laser (488 nm), and a red laser (640 nm). Sterile Milli-Q water was used as the sheath fluid. The instrument performance was monitored weekly with BDTM CS&T RUO Beads. The threshold settings, FSC-H 500 and FL1-H 500, a limit of 25 μL, and the slow flow rate of 14 μL/min were used for the analysis of the samples.

The log-transformed FL1-A and FSC-H signals were used to enumerate the total number of events in a sample. The flow cytometry data of the first 10,000 events of the pure medium sample were used for a one-class support vector machine (SVM) classifier implemented in MATLAB® using the command 'fitcsvm' to identify and remove signal from medium in samples. Additionally, the lower background data were removed using a linear line as the gate, resulting in a cleaned dataset. Linear correlations between cleaned flow cytometric data and the dry weight of cells cultured in SMaa were fitted to the measured data from LB.1, ST1, and ST.4 cultures (Figure S8). To determine the transferability of the linear correlation between flow cytometric data and cell dry weight from cells cultured in SMaa to cells cultured in SMcas, a 1:1 mixture (*v/v*) of both samples was prepared and measured using flow cytometry. Additionally, each sample was individually analyzed using flow cytometry. The calculated sum of the number of cell events cultured in SMaa

and the number of cell events cultured in SMcas resulted in the same number of cell events in the measured mixture, indicating transferability (Figure S8).

Cell dry weight in co-cultures was calculated using the same method with determined transferability (Figure S9). The strain-specific cell events of *S. thermophilus* and *L. bulgaricus* in co-culture were estimated using manual classification or SVM classification depending on the pH of the sample (Figure S10). Manual classification was achieved by separating the flow cytometry data using a line (the log-transformed FSC-H signal was plotted against the log-transformed FL1-A signal and separated by a linear line). The data points above and below the line represent *L. bulgaricus* and *S. thermophilus*, respectively. Classification of strains in co-culture using SVM was achieved using the log-transformed FSC-H and FL1-A signals of mono-culture datasets. Background data were removed to optimize SVM parameters in MATLAB® using the command 'fitcsm' (Figure S11).

2.6. Quantification of Fermentation Products

The culture sample (0.5 mL) was centrifuged for 3 min at 20,000× *g* and 4 °C. The supernatant was stored at −70 °C.

Sugars (lactose, glucose, galactose) and organic acids (lactate, succinate, formate) were quantified using the Agilent 1200 series HPLC system equipped with an RI detector [24]. Before analysis, the supernatant was incubated with 4 M NH_3 and 1.2 M $MgSO_4$ solutions, followed by an incubation for 15 min with 0.1 M H_2SO_4 to precipitate phosphate. Isocratic separation was achieved using a Rezex ROA organic acid H (8%) column (300 × 7.8 mm, 8 µm; Phenomenex) protected by a Phenomenex guard carbo-H column (4 × 3.0 mm) at 50 °C. The HPLC conditions were as follows: mobile phase, 5 mM H_2SO_4 solution; constant flow rate, 0.4 mL min^{-1}. Absolute concentrations were obtained by standard-based external calibration, and rhamnose was used as an internal standard (1 g L^{-1}) to correct measurement variability.

Amino acid concentrations were determined by an Agilent 1200 series instrument (Agilent Technologies) [24]. Bicratic separation was achieved by an Agilent Zorbax Eclipse Plus C_{18} column (250 by 4.6 mm, 5 µm), which was protected by an Agilent Zorbax Eclipse Plus C_{18} guard column (12.5 by 4.6 mm, 5 µm). After automatic precolumn derivatization with *ortho*-phthaldialdehyde, fluorometric detection (excitation at 230 nm and emission at 450 nm) was carried out. The elution buffer consisted of a polar phase (10 mM Na_2HPO_4, 10 mM $Na_2B_4O_7$, 0.5 mM NaN_3, pH 8.2) and a nonpolar phase (45% [*v/v*] acetonitrile, 45% [*v/v*] methanol). The quantification of amino acids was achieved by standard-based external calibration, and 4-aminobutanoic acid was used as an internal standard at 100 µM to correct for analyte variability.

2.7. Total Amino Acid Composition in the Supernatant

The culture sample (0.3 mL) was centrifuged for 3 min at 20,000× *g* and 4 °C. The supernatant was stored at −70 °C. The supernatant (200 µL) was incubated with 300 µL of 32% HCl at 100 °C for 24 h, cooled at 20 °C for at least 1 h, slowly mixed with 490 µL of 6.23 M NaOH, and stored at −20 °C until quantification of amino acid concentrations by HPLC analysis.

2.8. Calculation of Amino Acid Production Rates

Individual biomass-specific amino acid production rates q_{aa} [mol g_{DW}^{-1} h^{-1}] were calculated for each amino acid in a differential manner at 1 h intervals. The average biomass c_x [g_{DW} L^{-1}] in the period Δt [h], and the net amount of produced amino acids Δc_{aa} [mol L^{-1}] (Equation (1)) were considered.

$$q_{aa} = \frac{\Delta c_{aa}}{\frac{c_{x_1}+c_{x_2}}{2}\cdot\Delta t} \tag{1}$$

2.9. Fitting of Gaussian Models to pH-Dependent Amino Acid Production Rate

The release of amino acids strongly relies on enzymatic proteolysis. As the proteolytic activity depends on various enzymes with each contributing to an individual optimum pH [25,26], integral activities may be described by the superposition of Gaussian activity distributions. However, exact values for pH optima were not available. Additionally, *de novo* biosynthesis may occur, albeit to a minor extent. Consequently, the Gaussian model was considered a suitable proxy for the observed amino acid 'production' profiles. Parameter regression was achieved by fitting the pH-dependent q_{aa} of the *L. bulgaricus* LB.1 mono-culture (Figure S13) using Equation (2) [27].

$$q_{aa} = \sum_{i=1}^{n} a_i e^{\left[-\left(\frac{pH-b_i}{c_i}\right)^2\right]} \tag{2}$$

where q_{aa} is the amino acid production rate [mol g_{DW}^{-1} h^{-1}]; n is the number of pH optima to fit; and a, b, and c are regression parameters coding for the shape of the curve. MATLAB® was used for fitting. The consideration of a single pH dependency is not always sufficient. Then, overlaying Gaussian models considering two pH optima were used to improve the model prediction quality (Figure S13).

2.10. Simulation of Amino Acid Concentrations

Changes of biomass, substrate, and product concentrations were described in a process model assuming batch operation modes by balancing biomass (Equation (3)), substrate (Equation (4)), and product (Equation (5)) within the system boundary.

$$\frac{dc_x}{dt} = \mu \cdot c_x \tag{3}$$

$$\frac{dc_s}{dt} = -q_s \cdot c_x \tag{4}$$

$$\frac{dc_p}{dt} = q_p \cdot c_x \tag{5}$$

The amino acid production kinetics were integrated into the process model to predict $c_{aa}(t)$. The simulation time steps Δt considered the mean pH and biomass values as indicated in Equation (6).

$$c_{aa} = q_{aa} \cdot c_x \cdot \Delta t = \sum_{i=1}^{n} a_i e^{\left[-\left(\frac{\frac{pH_1+pH_2}{2}-b_i}{c_i}\right)^2\right]} \cdot \frac{c_{x_1} + c_{x_2}}{2} \cdot \Delta t \tag{6}$$

The feasibility of this approach was demonstrated for the mono-culture of *L. bulgaricus* LB.1 (Figure S12).

2.11. Uncertainty Analysis

Metabolite concentrations, pH, OD, flow cytometric data, and dry weight values were analyzed using Microsoft® Excel. Mean and standard deviation were calculated using duplicates and triplicates (STABW.S) in Microsoft® Excel. All experimental results are expressed as the mean of three biological replicates with experimental errors unless otherwise stated.

3. Results

3.1. Medium Development

The main objectives for preparing the SMcas were as follows: (a) enabling the growth of both species in mono-culture, (b) enabling the growth of both species in co-culture, and (c) potential metabolites that may be exchanged [2,3,6,10,12–14,28,29] were excluded if growth was not affected. To obtain this medium, previously reported defined growth

medium compositions of *S. thermophilus* [30,31] and *L. bulgaricus* [21,32] were compiled, resulting in a long list of constituents. This list was further reduced to achieve a lean growth medium to fulfil the demands (a–c). Medium acidification, which mirrors growth-coupled lactate formation, was used as a readout to verify the ability of the strains to grow with different modifications in the medium. Oleic acid, pyruvic acid, formic acid, orotic acid, niacin, spermine, ascorbic acid, thioglycolate, and 2'-deoxyguanosine, which were used in the growth medium by Chervaux et al. [32] but not by Grobben et al. [21], were excluded from the medium because they are not essential for the growth of *L. bulgaricus*. Additionally, we evaluated whether the addition of orotic acid is essential since it was considered to be an important component of the growth medium by Otto et al. [30] and Letort et al. [31]. Growth analysis of *L. bulgaricus* and *S. thermophilus* in the medium lacking orotic acid revealed culture acidification. The omission of biotin, thiamine, aminobenzoic acid, and thioctic acid did not result in the acidification in *S. thermophilus* culture but promoted the acidification in *L. bulgaricus* culture. Furthermore, urea was not excluded from the medium because it has previously been established that it increases the buffer capacity of the medium [31] and provides carbon dioxide and ammonia [3].

Studies using SMcas revealed the ability of three proteinase-positive *S. thermophilus* (ST.1, ST.2, and ST.3) strains and the four *L. bulgaricus* strains to acidify the medium. The proteinase-negative *S. thermophilus* ST.4 was not able to acidify SMcas and required access to free amino acids provided in SMaa (Figure S1).

Protocooperation between *L. bulgaricus* and *S. thermophilus* in co-culture has industrial relevance [2]. Co-culture benefits from the rapid exchange of metabolites, leading to accelerated acidification [13]. The effect of this protocooperation in the co-culture was observed in SMcas in the form of a faster acidification rate and a lower final pH (Figure S2).

3.2. Growth and Amino Acid Release in L. bulgaricus Mono-Culture

L. bulgaricus hydrolyzes amino acids from casein through its cell wall proteinase PrtB, which is complemented by other intracellular and extracellular peptidase activities [12,13,33,34]. Therefore, peptides and free amino acids can be utilized by *S. thermophilus*. Furthermore, amino acid depletion may upregulate amino acid biosynthesis in co-cultures [12,13]. Hence, a key step in understanding cellular responses to extracellular amino acid depletion is to monitor amino acid release and uptake.

L. bulgaricus LB.1 was cultured in SMcas as a mono-culture. The biomass of the culture increased from 0.05 to 0.6 g_{DW} L^{-1}, whereas the pH decreased from 6.4 to 4.3 (Figure 1). Lactose was consumed, glucose was initially secreted (up to 1.4 mM) and then consumed, and galactose, lactate, formate, and succinate were produced (Figure S7) in the culture, indicating metabolic activity.

The following two patterns of amino acid release were observed (Figure 1): accumulation of alanine, serine, lysine, tyrosine, and valine from the beginning of culturing; other amino acids began to increase after 2 h. A previous study suggested that this lag time indicates cellular adaptation to casein through upregulation of proteolytic activity [9]. The initial release of tyrosine, arginine, serine, leucine, and valine indicates active proteolytic activity from the beginning of culturing as they might not be produced *de novo* from *L. bulgaricus* [13,35].

3.3. Growth and Amino Acid Release in Proteinase-Positive S. thermophilus Mono-Culture

The dynamics of amino acid release and uptake in the proteinase-positive *S. thermophilus* ST.1, amino acid concentrations were measured over a culturing period of 14 h (Figure 2). The following three distinct phases were identified: 0–5 h, increase of some amino acid concentrations but no change in biomass and pH; 5–10 h, acidification, biomass increase, and decrease of some amino acid concentrations while others kept increasing; 10–15 h, acidification, biomass decrease, and uptake and release of amino acids. The concentration of all analyzed amino acids increased at some time point. Additionally, the pH decreased from 6.6 to 4.7, whereas the biomass increased from 0.03 g_{DW} L^{-1} to

0.1 g_{DW} L^{-1} (Figure 2). Furthermore, 12 out of the 15 amino acids were consumed at some points in time. Moreover, the concentrations of some amino acids exhibited an oscillating release-consumption-release profile (e.g., serine and leucine). After 12 h, almost all lactose was consumed (30 mM), which was accompanied by the production of large amounts of glucose (22 mM) and lactate (30 mM) (Figure S3).
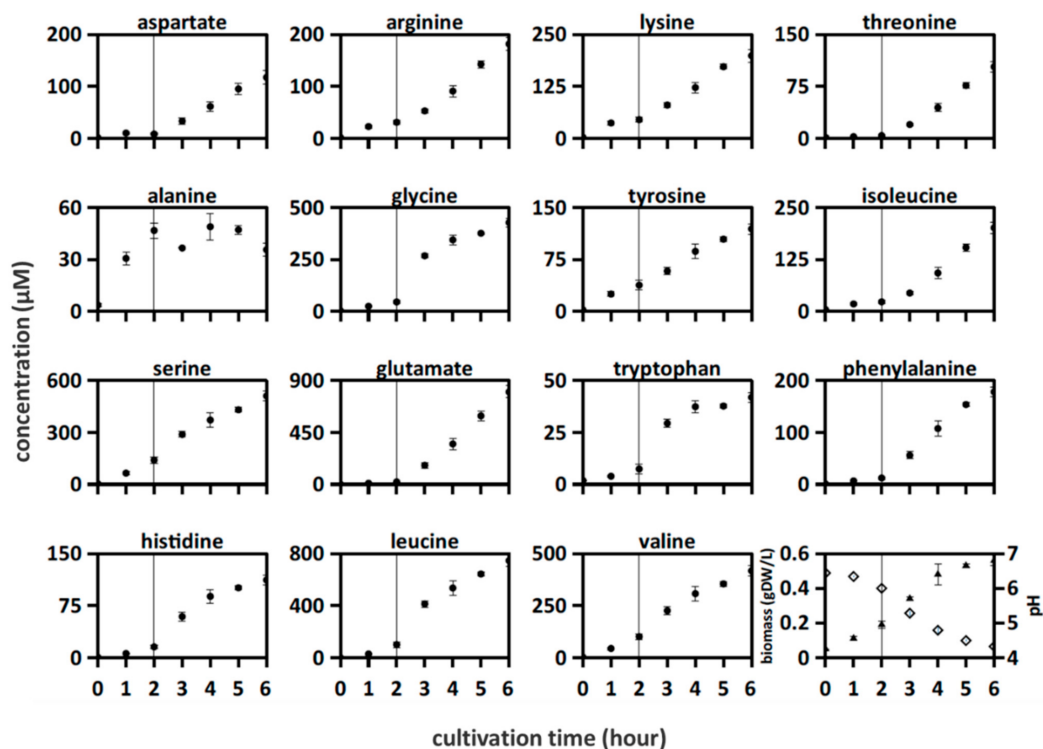

Figure 1. Amino acid concentrations were measured in *Lactobacillus bulgaricus* LB.1 culture in synthetic medium supplemented with casein (SMcas). The line indicates a change in increasing amino acid concentration profiles after 2 h. Downright: biomass (triangle) and pH (rhomb) measurements.

3.4. Growth and Amino Acid Release in the Co-Culture of Proteinase-Positive S. thermophilus and L. bulgaricus

Next, the amino acid concentrations in an *L. bulgaricus* LB.1—proteinase-positive *S. thermophilus* ST.1 co-culture were examined. The strains could grow in both SMcas (Figures 1 and 2) and SMaa (Figures S4 and S6), indicating their ability to utilize casein and free amino acids. As shown in Figure 3, the concentration of all amino acids increased during cultivation at some point. The concentrations of aspartate, arginine, lysine, alanine, and isoleucine began to decrease after approximately 2 h. Meanwhile, the decrease in glycine concentration was delayed until 4 h. The following two phases were observed in amino acid release (Figure 3), growth, and acidification (Figure 4): 0–4 h, pH decreased from 6.4 to 4.7 while the growth of both strains was weak (Figure 4); 4–7 h, the biomass of *L. bulgaricus* increased from 0.05 g_{DW} L^{-1} to 0.22 g_{DW} L^{-1}. Additionally, the consumption of 30 mM lactose, the production of 57 mM lactate, and the secretion (up to 10 mM) and uptake of glucose were observed (Figure S5).
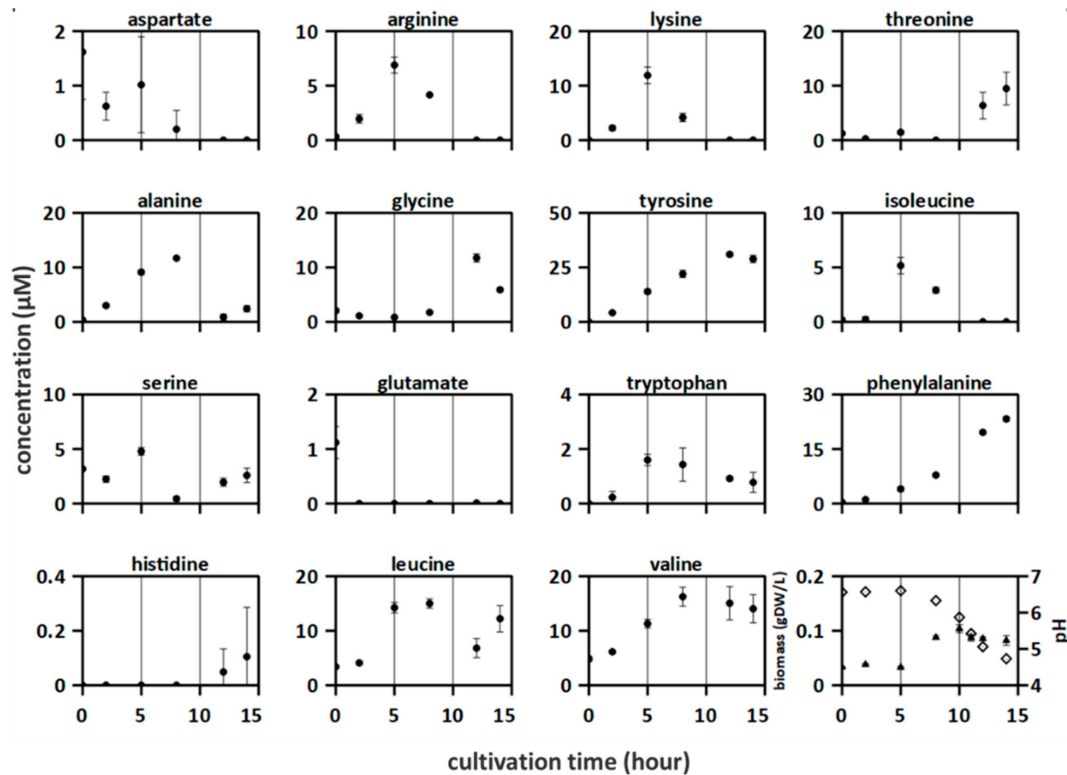
Figure 2. Amino acid concentrations were measured in proteinase-positive *S. thermophilus* ST.1 culture in synthetic medium supplemented with casein (SMcas). The lines indicate three phases according to the growth. Downright: biomass (triangle) and pH (rhomb) measurements.

3.5. Growth and Amino Acid Release in the Co-Culture of Proteinase-Negative S. thermophilus and L. bulgaricus

Next, the effects of replacement of proteinase-positive *S. thermophiles* ST.1 with proteinase-negative *S. thermophilus* ST.4 on the amino acid availability and the nutrient needs in the co-culture with *L. bulgaricus* LB.1 were examined. ST.4 could not grow in SMcas but could grow in SMaa (Figures S4 and S6). Therefore, a higher biomass fraction of *S. thermophilus* ST.4 was inoculated to avoid the anticipated overgrow of *L. bulgaricus*.

Figure 4B shows the following three phases: 0–2.5 h, increased biomass of *S. thermophilus* ST.4; 2.5–4 h, dominant growth of *L. bulgaricus* LB.1; 4–7 h, decreased biomass of *S. thermophilus* ST.4 even as *L. bulgaricus* LB.1 continued to grow. Hence, the presence of *L. bulgaricus* LB.1 enables the growth of *S. thermophilus* ST.4 in SMcas, which is consistent with previous findings [12]. Additionally, 25 mM of lactose was consumed and 58 mM of lactate was produced (Figure S5). Interestingly, lactose consumption severely slowed down after the growth stop of ST.4, while lactate formation continued. Furthermore, the concentrations of arginine (0–5 h), isoleucine (0–3 h), and lysine (0–7 h) decreased. Overall, the amino acid concentration in the proteinase-negative *S. thermophilus* ST.4—*L. bulgaricus* co-culture was lower than that in the proteinase-positive *S. thermophilus* ST.1—*L. bulgaricus* LB.1 co-culture.
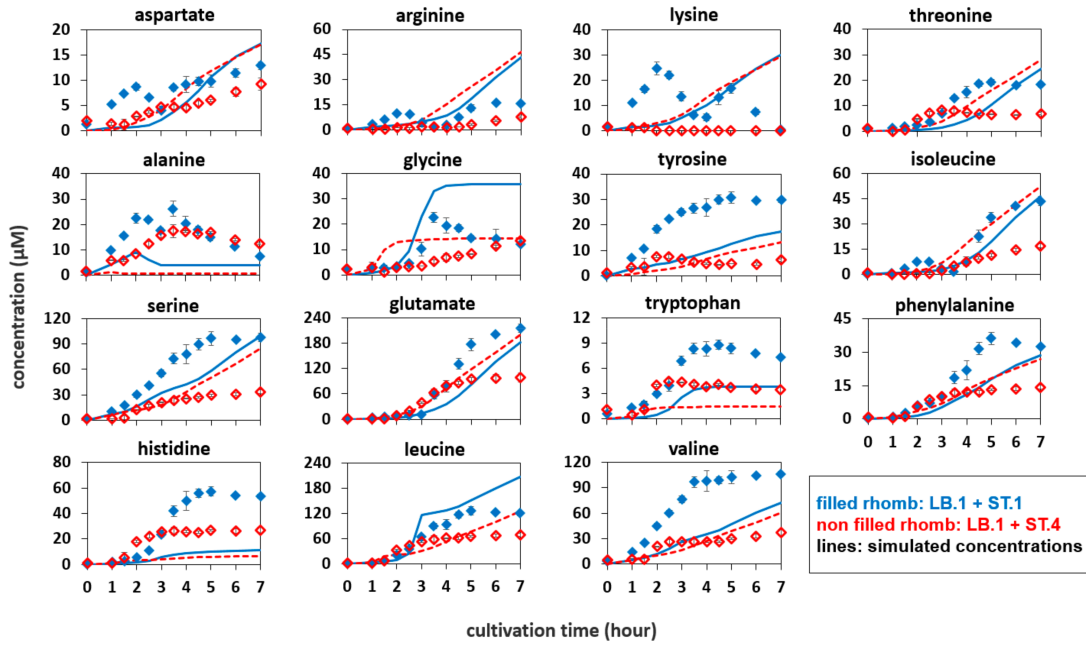
Figure 3. Amino acid concentrations in different co-cultures. (filled) *Lactobacillus bulgaricus* LB.1 co-cultured with proteinase-positive *Streptococcus thermophilus* ST.1 in synthetic medium supplemented with casein (SMcas). (non-filled) *L. bulgaricus* LB.1 co-cultured with proteinase-negative *S. thermophilus* ST.4 in SMcas. (line) Simulated amino acid concentration released from *L. bulgaricus* LB.1 in LB.1–ST.1 co-culture. (dashed line) Simulated amino acid concentration released from *L. bulgaricus* LB.1 in LB.1–ST.4 co-culture.
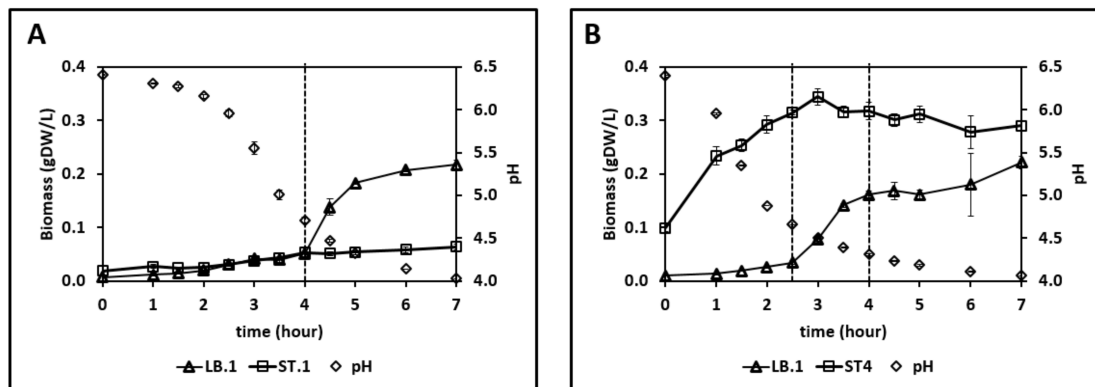
Figure 4. Strain-specific biomass profiles measured by flow cytometry and pH measurements in (**A**) LB.1–ST.1 (initial biomass fraction of 1:2 (LB:ST)) and (**B**) LB.1–ST.4 (initial biomass fraction 1:10 (LB:ST)) co-cultures in synthetic medium supplemented with casein (SMcas).

3.6. Simulation of Amino Acid Concentrations to Compare Mono- and Co-Culture Cultivations

To indicate the changes in the amino acid profile when *S. thermophilus* was added to the *L. bulgaricus* culture, a Gaussian model of amino acid release dependent on pH and

biomass was generated (see Methods). This model enables the simulation of the amount of amino acids released solely from *L. bulgaricus* in co-culture, which could not be identified in the mixed culture. Hence, the comparison between the simulation and measured data will indicate if the amino acid release activity differs between mono-culture and co-culture.

Amino acid profiles of *L. bulgaricus* mono-culture (Figure 1) were used to fit the Gaussian q_{aa} models. Figure 3 compares the simulated amino acid profiles of *L. bulgaricus* with the measured amino acid profiles of the co-cultures, reflecting the results of the mixed culture interaction.

Generally, the amino acid concentrations in the proteinase-positive *S. thermophilus* ST.1—*L. bulgaricus* co-culture were higher than those in the simulated amino acid time courses of *L. bulgaricus* in mono-culture, with the exception of glycine and leucine.

By way of analogy, Figure 3 shows the difference between the measured amino acid concentrations in the *S. thermophilus* ST.4—*L. bulgaricus* co-culture and the simulated amino acid concentrations released from *L. bulgaricus*. Here, most of the measured amino acid profiles, except for alanine, tryptophan, and histidine, were lower than those of the simulated courses. This indicates increased uptake of amino acids, likely via the proteinase-negative *S. thermophilus* ST.4, which can only feed on amino acids and peptides released from *L. bulgaricus* but not from casein.

4. Discussion

4.1. Amino Acids Are Consumed by L. bulgaricus and S. thermophilus

In this study, amino acids were consumed by *L. bulgaricus* and *S. thermophilus* cultured in SMcas in both mono-culture (Figures 1 and 2) and co-culture (Figure 3). This is in accordance with [22]. Amino acids were consumed even in the presence of peptide-bound amino acids (Table S1). For example, lysine was consumed in the *S. thermophilus* ST.1—*L. bulgaricus* LB.1 co-culture after 4 h (Figure 3), although at least 230 µM of lysine bound to proteins and peptides was available (Table S1).

This indicates that amino acid transporters are active and enable the strains to exchange amino acids that are produced through casein hydrolysis or biosynthesis [36,37]. Hence, it allows interaction [29,38,39]. Additionally, this enables the manipulation of *S. thermophilus* and *L. bulgaricus* cultivations in biotechnological processes by adding amino acids, such as lysine [40].

4.2. Amino Acids Can Accumulate in Cultivations with L. bulgaricus and S. thermophilus

L. bulgaricus LB.1 could accumulate all analyzed amino acids (Figure 1). Some of these amino acids accumulated from the beginning of culturing, indicating basal proteolytic activity although the strain was precultured under SMaa conditions. This suggests that *L. bulgaricus* LB.1 releases more amino acids from casein or/and produces amino acids than it is needed for growth and that amino acids become available for other strains [41]. The accumulation of amino acids indicates that extracellular peptidases are highly active [42], unusable amino acids are separated from peptides to gain posteriorly required amino acids, or proton-coupled amino acid secretion supports the maintenance of intracellular pH during acidification [43]. The poor release of amino acids in a *S. thermophilus* ST.1 cultivation reflects its low activity of peptidases [26,44].

4.3. Differences between Co-Cultures with Different S. thermophilus Strains

The proteinase-negative *S. thermophilus* ST.4—*L. bulgaricus* LB.1 co-culture yielded lower amino acid concentrations than the proteinase-positive *S. thermophilus* ST.1—*L. bulgaricus* LB.1 co-culture. This phenotype can be attributed to the increased growth of *S. thermophilus* ST.4 (Figure 4), which results in an enhanced demand for amino acids [45]. In addition, this observation is consistent with the lack of protease activity of *S. thermophilus* ST.4 (Figure 3). The depletion of arginine, lysine, and isoleucine observed in this study can upregulate peptidases or amino acid biosynthesis, which is consistent with the hypothesis of previous studies [9,12,13].

4.4. Co-Culture Is Not the Sum of Mono-Cultures

The proteinase-positive *S. thermophilus* ST.1—*L. bulgaricus* LB.1 co-culture yielded higher amino acid concentrations than the simulated concentration of amino acids released from only *L. bulgaricus* LB.1 (Figure 3). In particular, histidine was rarely released in the presumably histidine auxotroph *S. thermophilus* ST.1 mono-culture (Figure 2) [46] but was detected in high amounts in the *S. thermophilus* ST.1—*L. bulgaricus* LB.1 co-culture. The interaction between the two species may trigger metabolic changes in the strains, resulting in the rearrangement of metabolic fluxes [6,35,47]. Future studies must identify these co-culture triggers that serve as stimuli for basic metabolic adjustments.

The amount of amino acid released from the co-culture was higher than the individual sums of the amounts of amino acid released from the mono-cultures. This might be a consequence of an upregulated proteolytic system in *L. bulgaricus* LB.1 and *S. thermophilus* ST.1. Alternatively, individual biosynthetic pathways might be stimulated in co-culture but not in mono-culture [46,48]. Previous studies have alluded to the upregulation of histidine biosynthesis [12,13].

4.5. Stimulatory Effects of Branched-Chain Amino Acid (BCAA) Depletion

Previous studies have hypothesized that BCAA availability is limited in the *S. thermophilus*—*L. bulgaricus* co-cultures due to the upregulation of BCAA permease in *L. bulgaricus* [13] and BCAA biosynthesis in *S. thermophilus* [12,13,49]. In this study, the levels of isoleucine, but not those of valine or leucine, were temporarily depleted in the co-cultures (Figure 3). Furthermore, the release of BCAA in the *L. bulgaricus* LB.1 mono-culture was similar to that reported in a previous study [9], which revealed that the proteolytic activity of *L. bulgaricus* promotes the excess release of BCAA from casein. In the LB.1 mono-culture, the final concentration of isoleucine (200 μM) was lower than that of valine (417 μM) and leucine (746 μM). This indicated isoleucine as a potential candidate for depletion. Additionally, low concentrations of isoleucine (up to 5 μM), leucine (up to 15 μM), and valine (up to 16 μM) were observed in the protease-positive *S. thermophilus* ST.1 mono-culture, indicating its ability to release BCAA from casein or biosynthesize BCAA [36,46]. However, the levels of isoleucine, leucine, and valine were lower than those in *L. bulgaricus*. Hence, isoleucine depletion is plausible and may result in the upregulation of BCAA permease in *L. bulgaricus* and BCAA biosynthesis in *S. thermophilus*, respectively.

4.6. Arginine and Lysine Depletion in Co-Cultures

Arginine and lysine concentrations were limited in the proteinase-negative *S. thermophilus* ST.4—*L. bulgaricus* LB.1 co-culture and oscillated in the proteinase-positive *S. thermophilus* ST.1—*L. bulgaricus* LB.1 co-culture (Figure 3). Previous studies [12,13] have reported the upregulation of arginine biosynthesis in *S. thermophilus* co-cultured with *L. bulgaricus*. Hence, our results support the hypothesis that low arginine concentrations might influence physiological responses [50], such as the upregulation of arginine biosynthesis in *S. thermophilus*.

5. Conclusions

In this work, we developed a synthetic medium that supports the growth of the dairy organisms *S. thermophilus* and *L. bulgaricus* in mono- and co-culture, which enables the quantitative monitoring of growth as well as substrate consumption and metabolite production dynamics. Amino acid release profiles in co-culture were not the sum of amino acid release profiles in mono-cultures. Additionally, the amino acid release profiles were not similar in co-cultures with different strain combinations. Amino acid depletion was observed in *S. thermophilus*—*L. bulgaricus* co-cultures, which may provide an explanation for the induced expression of proteolytic enzymes.

The uptake of several amino acids was observed during growth. Knowledge of co-culture-specific consumption rates for peptide and amino acid uptake along with release rates of amino acids provides a tool for determining yogurt quality and useful insights

into cellular fitness for further strain and process optimization. Understanding cellular amino acid needs may enable a quantitative and detailed understanding of interactions in yogurt cultures.

References

1. Marco, M.L.; Heeney, D.; Binda, S.; Cifelli, C.J.; Cotter, P.D.; Foligné, B.; Gänzle, M.; Kort, R.; Pasin, G.; Pihlanto, A.; et al. Health Benefits of Fermented Foods: Microbiota and Beyond. *Curr. Opin. Biotechnol.* **2017**, *44*, 94–102. [CrossRef] [PubMed]
2. Markakiou, S.; Gaspar, P.; Johansen, E.; Zeidan, A.A.; Neves, A.R. Harnessing the Metabolic Potential of *Streptococcus thermophilus* for New Biotechnological Applications. *Curr. Opin. Biotechnol.* **2020**, *61*, 142–152. [CrossRef] [PubMed]
3. Arioli, S.; della Scala, G.; Remagni, M.C.; Stuknyte, M.; Colombo, S.; Guglielmetti, S.; de Noni, I.; Ragg, E.; Mora, D. *Streptococcus thermophilus* Urease Activity Boosts *Lactobacillus delbrueckii* subsp. *Bulgaricus Homolactic* Fermentation. *Int. J. Food Microbiol.* **2017**, *247*, 55–64. [CrossRef] [PubMed]
4. Blasche, S.; Kim, Y.; Mars, R.A.T.; Machado, D.; Maansson, M.; Kafkia, E.; Milanese, A.; Zeller, G.; Teusink, B.; Nielsen, J.; et al. Metabolic Cooperation and Spatiotemporal Niche Partitioning in a Kefir Microbial Community. *Nat. Microbiol.* **2021**, *6*, 196–208. [CrossRef] [PubMed]
5. Schöpping, M.; Gaspar, P.; Neves, A.R.; Fanzén, C.J.; Zeidan, A.A. Identifying the Essential Nutritional Requirements of the the Probiotic Bacteria *Bifidobacterium animalis* and *Bifidobacterium longum* Using Genome-Scale Modeling. *NPJ Syst. Biol. Appl.* **2021**, *7*, 1–15. [CrossRef]

6. Settachaimongkon, S.; Nout, M.J.R.; Antunes Fernandes, E.C.; Hettinga, K.A.; Vervoort, J.M.; van Hooijdonk, T.C.M.; Zwietering, M.H.; Smid, E.J.; van Valenberg, H.J.F. Influence of Different Proteolytic Strains of *Streptococcus thermophilus* in Co-Culture with *Lactobacillus delbrueckii* subsp. Bulgaricus on the Metabolite Profile of Set-Yoghurt. *Int. J. Food Microbiol.* **2014**, *177*, 29–36. [CrossRef]
7. Johansen, E. Use of Natural Selection and Evolution to Develop New Starter Cultures for Fermented Foods. *Annu. Rev. Food Sci. Technol.* **2018**, *9*, 411–428. [CrossRef]
8. Chandan, R.C.; Gandhi, A.; Shah, N.P. *Yogurt: Historical Background, Health Benefits, and Global Trade*; Elsevier Inc.: Amsterdam, The Netherlands, 2017. [CrossRef]
9. Liu, E.; Zheng, H.; Hao, P.; Konno, T.; Kume, H.; Oda, M.; Suzuki, K.; Ji, Z. Acquisition of Amino Acids by *Lactobacillus delbrueckii* subsp. Bulgaricus 2038 When Grown in the Presence of Casein. *Int. Dairy J.* **2014**, *35*, 145–152. [CrossRef]
10. de Souza Oliveira, R.P.; Torres, B.R.; Perego, P.; de Oliveira, M.N.; Converti, A. Co-Metabolic Models of *Streptococcus thermophilus* in Co-Culture with *Lactobacillus bulgaricus* or *Lactobacillus acidophilus*. *Biochem. Eng. J.* **2012**, *62*, 62–69. [CrossRef]
11. Herve-Jimenez, L.; Guillouard, I.; Guedon, E.; Gautier, C.; Boudebbouze, S.; Hols, P.; Monnet, V.; Rul, F.; Maguin, E. Physiology of *Streptococcus thermophilus* during the Late Stage of Milk Fermentation with Special Regard to Sulfur Amino-Acid Metabolism. *Proteomics* **2008**, *8*, 4273–4286. [CrossRef]
12. Herve-Jimenez, L.; Guillouard, I.; Guedon, E.; Boudebbouze, S.; Hols, P.; Monnet, V.; Maguin, E.; Rul, F. Postgenomic Analysis of *Streptococcus thermophilus* Cocultivated in Milk with *Lactobacillus delbrueckii* subsp. Bulgaricus: Involvement of Nitrogen, Purine, and Iron Metabolism. *Appl. Environ. Microbiol.* **2009**, *75*, 2062–2073. [CrossRef]
13. Sieuwerts, S.; Molenaar, D.; van Hijum, S.A.F.T.; Beerthuyzen, M.; Stevens, M.J.A.; Janssen, P.W.M.; Ingham, C.J.; de Bok, F.A.M.; de Vos, W.M.; van Hylckama Vlieg, J.E.T. Mixed-Culture Transcriptome Analysis Reveals the Molecular Basis of Mixed-Culture Growth in *Streptococcus thermophilus* and *Lactobacillus bulgaricus*. *Appl. Environ. Microbiol.* **2010**, *76*, 7775–7784. [CrossRef] [PubMed]
14. Mendes, F.; Sieuwerts, S.; de Hulster, E.; Almering, M.J.H.; Luttik, M.A.H.; Pronk, J.T.; Smid, E.J.; Bron, P.A.; Daran-Lapujadea, P. Transcriptome-Based Characterization of Interactions between *Saccharomyces cerevisiae* and *Lactobacillus delbrueckii* subsp. Bulgaricus in Lactose-Grown Chemostat Cocultures. *Appl. Environ. Microbiol.* **2013**, *79*, 5949–5961. [CrossRef] [PubMed]
15. Branco dos Santos, F.; de Vos, W.M.; Teusink, B. Towards Metagenome-Scale Models for Industrial Applications-the Case of *Lactic acid bacteria*. *Curr. Opin. Biotechnol.* **2013**, *24*, 200–206. [CrossRef] [PubMed]
16. Somerville, V.; Grigaitis, P.; Battjes, J.; Moro, F.; Teusink, B. Use and Limitations of Genome-Scale Metabolic Models in Food Microbiology. *Curr. Opin. Food Sci.* **2022**, *43*, 225–231. [CrossRef]
17. Chen, S.; Niu, H.; Wu, Y.; Sun, J.; Han, X.; Zhang, L. Influence of Lactic Acid on Cell Cycle Progressions in *Lactobacillus bulgaricus* During Batch Culture. *Appl. Biochem. Biotechnol.* **2021**, *193*, 912–924. [CrossRef]
18. Russell, J.B.; Diez-Gonzalez, F. The Effects of Fermentation Acids on Bacterial Growth. *Adv. Microb. Physiol.* **1998**, *39*, 228–234. [CrossRef]
19. Douwenga, S.; Janssen, P.; Teusink, B. A Centrifugation-Based Clearing Method Allows High-Throughput Acidification and Growth-Rate Measurements in Milk. *J. Dairy Sci.* **2021**, *8*, 8530–8540. [CrossRef]
20. Radke-Mitchell, L.; Sandine, W.E. Associative Growth and Differential Enumeration of *Streptococcus thermophilus* and *Lactobacillus bulgaricus*: A Review. *J. Food Prot.* **1984**, *47*, 245–248. [CrossRef]
21. Grobben, G.J.; Sikkema, J.; Smith, M.R.; de Bont, J.A.M. Production of Extracellular Polysaccharides by *Lactobacillus delbrueckii* ssp. Bulgaricus NCFB 2772 Grown in a Chemically Defined Medium. *J. Appl. Bacteriol.* **1995**, *79*, 103–107. [CrossRef]
22. Liu, E.; Zheng, H.; Shi, T.; Ye, L.; Konno, T.; Oda, M.; Shen, H.; Ji, Z.S. Relationship between *Lactobacillus bulgaricus* and *Streptococcus thermophilus* under Whey Conditions: Focus on Amino Acid Formation. *Int. Dairy J.* **2016**, *56*, 141–150. [CrossRef]
23. Radke-Mitchell, L.C.; Sandine, W.E. Influence of Temperature on Associative Growth of *Streptococcus thermophilus* and *Lactobacillus bulgaricus*. *J. Dairy Sci.* **1986**, *69*, 2558–2568. [CrossRef]
24. Buchholz, J.; Schwentner, A.; Brunnenkan, B.; Gabris, C.; Grimm, S.; Gerstmeir, R.; Takors, R.; Eikmanns, B.J.; Blombacha, B. Platform Engineering of *Corynebacterium glutamicum* with Reduced Pyruvate Dehydrogenase Complex Activity for Improved Production of L-Lysine, l-Valine, and 2-Ketoisovalerate. *Appl. Environ. Microbiol.* **2013**, *79*, 5566–5575. [CrossRef]
25. Kunji, E.R.S. The Proteolytic Systems of *Lactic acid bacteria*. *Antonie Van Leeuwenhoek Int. J. Gen. Mol. Microbiol.* **1996**, *70*, 187–221. [CrossRef]
26. Rodríguez-Serrano, G.M.; García-Garibay, J.M.; Cruz-Guerrero, A.E.; Gómez-Ruiz, L.D.C.; Ayala-Niño, A.; Castañeda-Ovando, A.; González-Olivares, L.G. Proteolytic System of *Streptococcus thermophilus*. *J. Microbiol Biotechnol.* **2018**, *28*, 1581–1588. [CrossRef]
27. Hetényi, K.; Németh, Á.; Sevella, B. Role of PH-Regulation in Lactic Acid Fermentation: Second Steps in a Process Improvement. *Chem. Eng. Processing: Process Intensif.* **2011**, *50*, 293–299. [CrossRef]
28. Crittenden, R.G.; Martinez, N.R.; Playne, M.J. Synthesis and Utilisation of Folate by Yoghurt Starter Cultures and Probiotic Bacteria. *Int. J. Food Microbiol.* **2003**, *80*, 217–222. [CrossRef]
29. Sieuwerts, S.; de Bok, F.A.M.; Hugenholtz, J.; van Hylckama Vlieg, J.E.T. Unraveling Microbial Interactions in Food Fermentations: From Classical to Genomics Approaches. *Appl. Environ. Microbiol.* **2008**, *74*, 4997–5007. [CrossRef]
30. Otto, R.; Tenbrink, B.; Veldkamp, H.; Konings, W.N. The Relation between Growth-Rate and Electrochemical Proton Gradient of Streptococcus-Cremoris. *FEMS Microbiol. Lett.* **1983**, *16*, 69–74. [CrossRef]

31. Letort, C.; Juillard, V. Development of a Minimal Chemically-Defined Medium for the Exponential Growth of *Streptococcus thermophilus*. *J. Appl. Microbiol.* **2001**, *91*, 1023–1029. [CrossRef]
32. Chervaux, C.; Ehrlich, S.D.; Maguin, E. Physiological Study of *Lactobacillus delbrueckii* subsp. Bulgaricus Strains in a Novel Chemically Defined Medium. *Society* **2000**, *66*, 5306–5311. [CrossRef]
33. Courtin, P.; Monnet, V.; Rul, F. Cell-Wall Proteinases PrtS and PrtB Have a Different Role in *Streptococcus thermophilus/Lactobacillus bulgaricus* Mixed Cultures in Milk. *Microbiology (N Y)* **2002**, *148*, 3413–3421. [CrossRef]
34. Liu, E.; Hao, P.; Konno, T.; Yu, Y.; Oda, M.; Zheng, H.; Ji, Z. Amino Acid Biosynthesis and Proteolysis in *Lactobacillus bulgaricus* Revisited: A Genomic Comparison. *Computat. Mol. Biosci.* **2012**, *2012*, 61–77. [CrossRef]
35. van de Guchte, M.; Penaud, S.; Grimaldi, C.; Barbe, V.; Bryson, K.; Nicolas, P.; Robert, C.; Oztas, S.; Mangenot, S.; Couloux, A.; et al. The Complete Genome Sequence of *Lactobacillus bulgaricus* Reveals Extensive and Ongoing Reductive Evolution. *Proc. Natl. Acad. Sci.* **2006**, *103*, 9274–9279. [CrossRef]
36. Hols, P.; Hancy, F.; Fontaine, L.; Grossiord, B.; Prozzi, D.; Leblond-Bourget, N.; Decaris, B.; Bolotin, A.; Delorme, C.; Ehrlich, S.D.; et al. New Insights in the Molecular Biology and Physiology of *Streptococcus thermophilus* Revealed by Comparative Genomics. *FEMS Microbiol. Rev.* **2005**, *29*, 435–463. [CrossRef]
37. Zheng, H.; Liu, E.; Hao, P. In Silico Analysis of Amino Acid Biosynthesis and Proteolysis in *Lactobacillus delbrueckii* subsp. Bulgaricus 2038 and the Implications for Bovine Milk Fermentation. *Biotechnol. Lett.* **2012**, *34*, 1545–1551. [CrossRef] [PubMed]
38. Smid, E.J.; Lacroix, C. Microbe-Microbe Interactions in Mixed Culture Food Fermentations. *Curr. Opin. Biotechnol.* **2013**, *24*, 148–154. [CrossRef]
39. Rau, M.H.; Gaspar, P.; Jensen, M.L.; Geppel, A.; Neves, A.R.; Zeidan, A.A. Genome-Scale Metabolic Modeling Combined with Transcriptome Profiling Provides Mechanistic Understanding of *Streptococcus thermophilus* CH8 Metabolism. *Appl. Environ. Microbiol.* **2022**, *88*, 1–18. [CrossRef] [PubMed]
40. Hu, Y.; Li, Y. Soybean Peptides Promote Yoghurt Fermentation and Quality. *Biotechnol. Lett.* **2020**, *42*, 1927–1937. [CrossRef]
41. Kliche, T.; Li, B.; Bockelmann, W.; Habermann, D.; Klempt, M.; de Vrese, M. Screening for Proteolytically Active *Lactic acid bacteria* and Bioactivity of Peptide Hydrolysates Obtained with Selected Strains. *Appl. Microbiol. Biotechnol.* **2017**, *101*, 7621–7633. [CrossRef] [PubMed]
42. Liu, E.; Zheng, H.; Hao, P.; Konno, T.; Yu, Y.; Kume, H.; Oda, M.; Ji, Z.S. A Model of Proteolysis and Amino Acid Biosynthesis for *Lactobacillus delbrueckii* subsp. Bulgaricus in Whey. *Curr. Microbiol.* **2012**, *65*, 742–751. [CrossRef] [PubMed]
43. Hutkins, R.W.; Nannen, N.L. pH Homeostasis in *Lactic acid bacteria*. *J. Dairy Sci.* **1993**, *76*, 2354–2365. [CrossRef]
44. Rajagopal, S.N.; Sandine, W.E. Associative Growth and Proteolysis of *Streptococcus thermophilus* and *Lactobacillus bulgaricus* in Skim Milk. *J. Dairy Sci.* **1990**, *73*, 894–899. [CrossRef]
45. Beshkova, D.M.; Simova, E.D.; Frengova, G.I.; Simov, Z.I.; Adilov, E.F. Production of Amino Acids by Yogurt Bacteria. *Biotechnol. Prog.* **1998**, *14*, 963–965. [CrossRef]
46. Pastink, M.I.; Teusink, B.; Hols, P.; Visser, S.; de Vos, W.M.; Hugenholtz, J. Genome-Scale Model of *Streptococcus thermophilus* LMG18311 for Metabolic Comparison of *Lactic acid bacteria*. *Appl. Environ. Microbiol.* **2009**, *75*, 3627–3633. [CrossRef] [PubMed]
47. Wintermute, E.H.; Silver, P.A. Dynamics in the Mixed Microbial Concourse. *Genes Dev.* **2010**, *24*, 2603–2614. [CrossRef]
48. Hao, P.; Zheng, H.; Yu, Y.; Ding, G.; Gu, W.; Chen, S.; Yu, Z.; Ren, S.; Oda, M.; Konno, T.; et al. Complete Sequencing and Pan-Genomic Analysis of *Lactobacillus delbrueckii* subsp. Bulgaricus Reveal Its Genetic Basis for Industrial Yogurt Production. *PLoS ONE* **2011**, *6*, e15964. [CrossRef]
49. Garault, P.; Letort, C.; Juillard, V.; Monnet, V. Branched-Chain Amino Acids and Purine Biosynthesis: Two Pathways Essential for Optimal Growth of *Streptococcus thermophilus* in Milk. *Lait* **2001**, *81*, 83–90. [CrossRef]
50. Arioli, S.; Roncada, P.; Salzano, A.M.; Deriu, F.; Corona, S.; Guglielmetti, S.; Bonizzi, L.; Scaloni, A.; Mora, D. The Relevance of Carbon Dioxide Metabolism in *Streptococcus thermophilus*. *Microbiology* **2009**, *155*, 1953–1965. [CrossRef]

Appendix B

A two-compartment fermentation system to quantify strain-specific interactions in microbial co-cultures

Article

A Two-Compartment Fermentation System to Quantify Strain-Specific Interactions in Microbial Co-Cultures

Andreas Ulmer [1], Stefan Veit [1], Florian Erdemann [1], Andreas Freund [1], Maren Loesch [1], Attila Teleki [1], Ahmad A. Zeidan [2] and Ralf Takors [1,*]

[1] Institute of Biochemical Engineering, University of Stuttgart, 70569 Stuttgart, Germany
[2] Systems Biology, R&D Discovery, Chr. Hansen A/S, 2970 Hørsholm, Denmark
*   Correspondence: takors@ibvt.uni-stuttgart.de

Abstract: To fulfil the growing interest in investigating microbial interactions in co-cultures, a novel two-compartment bioreactor system was developed, characterised, and implemented. The system allowed for the exchange of amino acids and peptides via a polyethersulfone membrane that retained biomass. Further system characterisation revealed a Bodenstein number of 18, which hints at backmixing. Together with other physical settings, the existence of unwanted inner-compartment substrate gradients could be ruled out. Furthermore, the study of Damkoehler numbers indicated that a proper metabolite supply between compartments was enabled. Implementing the two-compartment system (2cs) for growing *Streptococcus thermophilus* and *Lactobacillus delbrueckii* subs. *bulgaricus*, which are microorganisms commonly used in yogurt starter cultures, revealed only a small variance between the one-compartment and two-compartment approaches. The 2cs enabled the quantification of the strain-specific production and consumption rates of amino acids in an interacting *S. thermophilus*–*L. bulgaricus* co-culture. Therefore, comparisons between mono- and co-culture performance could be achieved. Both species produce and release amino acids. Only alanine was produced *de novo* from glucose through potential transaminase activity by *L. bulgaricus* and consumed by *S. thermophilus*. Arginine availability in peptides was limited to *S. thermophilus'* growth, indicating active biosynthesis and dependency on the proteolytic activity of *L. bulgaricus*. The application of the 2cs not only opens the door for the quantification of exchange fluxes between microbes but also enables continuous production modes, for example, for targeted evolution studies.

Keywords: microbial consortia; metabolomics; lactic acid bacteria; *Streptococcus thermophilus*; *Lactobacillus bulgaricus*; bioprocess engineering

1. Introduction

Interactions between bacteria are common in ecology [1,2] and involve complex mechanisms that are not yet fully understood [3]. Analysing these natural consortia is important because it improves our understanding of fundamental processes, such as bacterial communication [4]; enables community reshaping to gain health and environmental benefits [5]; and opens the door for the application of (synthetic) microbial consortia in biotechnological applications [6]. Consequently, thorough studies have been performed to investigate the application potential of interacting microbes [7,8], leading to the development of natural and synthetic co-cultures for industrial use [9–12].

Microbial interactions allow for a reduction in individual metabolic burden and are considered beneficial for metabolic productivity. For instance, one strain may provide essential nutritional components to another strain and vice versa [13]. Furthermore, the advantages of cofactor and precursor availability may be created for one microorganism if biosynthetic pathways are shared between two strains [14]. In some cases, increased enzyme activity is also observed [15]. Pande et al. [16] provided experimental evidence for the anticipated benefits and studied the growth performance of a synthetic co-culture

that relied on the exchange of essential amino acids. Indeed, the growth of the co-culture outperformed that of the mono-culture in the 24 h experiment. Furthermore, the co-culture was stable despite the presence of non-cooperating cells. Smartly sharing metabolic activity between mutually dependent strains yields improvements in biomass production [17–20].

Driven by the promising potential of microbial consortia for biotechnological applications, here, whether the toolbox for experimental analyses is already complete or should be complemented with novel devices to elucidate strain interactions inside consortia was evaluated. In particular, the following research trends are anticipated to benefit strongly from knowledge of quantitative exchange fluxes among interacting bacteria, which may be measurable in dedicated devices:

- Computational approaches are being steadily extended to unravel and predict interactions between bacteria [21–23]. To improve the simulation results, data from quantitative experiments providing strain-specific information—in particular, strain-specific growth rates, metabolite production, and consumption rates—are essential to validate model qualities, as indicated previously [24–28].
- Synthetic co-cultures should be rationally assembled to achieve the desired targets. This demands knowledge of individual uptake and production rates inside co-cultures for fine-tuning the metabolite exchange rates to prevent bottlenecks in supply and the accumulation of intermediates [29,30].
- Adaptive evolution experiments have been used to improve the performance of strains [31,32] and have been adapted for co-culture systems [33–35]. However, to select them for the jointly increased growth of co-cultures, individual adjustments may be necessary, such as the implementation of individual dilution rates to prevent overgrowth and washout scenarios.

Consequently, to meet the demands for strain-specific quantification in co-cultures and to extend co-culture cultivation techniques, several approaches have been developed in recent years:

One approach to obtaining strain-specific rates in co-cultures without disturbing metabolic activities is 13-C metabolic flux analysis [36]. To increase the accuracy of estimated fluxes in co-cultures, elegant methods have already been presented by Gebreselassie et al. [37] based on 13-C-labelled amino acids, and Ghosh et al. [38] used labelled peptides. These methods are restricted to specific metabolic networks or require specific experimental conditions. Interestingly, even higher flux-resolution patterns may be obtained when applying compartment-specific metabolomics [39]. These observations have shed some light on the potential to unravel exchange fluxes between interacting compartments, each hosting different species of a bacterial consortium.

Alternatively, strain-specific information may be obtained by separating the cells of a co-culture after harvesting. If the cell morphology differs significantly, centrifugation may be an appropriate separation approach [40]. However, this is a time-consuming procedure and is, consequently, prone to changes in intracellular states because of ongoing enzymatic activities [41]. The latter may be prevented by the application of proper cell inactivation technologies, which thus far are still missing. Furthermore, related approaches call for the individual development and optimisation of protocols, making them difficult to transfer to other co-cultures.

Other approaches utilise the spatial separation of interacting strains, as reviewed previously [42]. Often, such experimental settings are miniaturised, allowing the verification of multiple synthetic constructs in a parallel manner, thereby restricting sampling volumes. Examples include microfluidic systems [43–45] and cell culture plates [46]. Our own studies have indicated that a culture sample of approximately 100 µL is the minimal amount required to quantify the biomass correctly. An additional 100 µL of the supernatant is likely necessary to quantify the metabolites. Hence, the sophisticated and quantitative analysis of interacting cells requires larger reaction volumes than those provided by microfluidic and well-plate approaches. Alternatively, dialysis bioreactors [47] may be applied to cultivate co-cultures in two compartments. However, they incur rather high operational and

investment costs and may appear somewhat oversized for studying multiple co-cultures in parallel.

To address these limitations, this study aimed to develop a device for co-culture analysis that provides strain-specific information independent of metabolic activity and phenotype. Systematic strain evaluation was enabled by offering a sufficient sampling volume for extensive analysis, and the device was designed to allow quick assembly.

To this end, a compartmentalised fluid system that allowed the growth of two metabolite-exchanging strains was developed and applied. A strain-specific analysis of growth, production, consumption rates, and intracellular metabolite pools was undertaken. Reflecting the importance of co-cultures in yogurt production, the usability of the system was showcased by investigating the anaerobic interaction between *Streptococcus thermophilus* and *Lactobacillus delbrueckii* subs. *bulgaricus*.

The metabolic activities of the strains are linked to each other: the proteolytic system of *L. bulgaricus* comprises the extracellular proteinase PrtB [48] and intracellular peptidases [49], enabling the strain to gain amino acids from casein, which is likely the reason why the strain loses *de novo* biosynthetic capacities for many amino acids from sugar [50]. The proteinase-negative strain *S. thermophilus* benefits from this relationship as it consumes peptides and amino acids from *L. bulgaricus* [51,52]. The proteolytic system of *S. thermophilus* consists of intracellular and extracellular peptidases [53–55], which hydrolyse the peptides supplied by *L. bulgaricus*. Peptide and amino acid transporters have been predicted [53,56] and belong to the ABC binding cassette family [55]. Consequently, amino acids are released from *S. thermophilus*, as measured here [57–59]. These lactic acid bacteria are used in industrial processes, such as yogurt and bulk chemical production [60,61], but their interactions are not yet fully understood [54].

2. Materials and Methods

2.1. Medium Conditions

The synthetic medium (SM) for cultivation (Table S1 in Supplementary Materials) was chosen from a previous study [62]. SM containing lactose is indicated as SM + lactose, and SM containing glucose is indicated as SM + glucose. SM containing casein is denoted as SMcas, and SM containing amino acids is denoted as SMaa.

2.2. Strain Cultivation

L. delbrueckii subsp. *bulgaricus* ATCC BAA-365 and *S. thermophilus* LMG 18311 were received from Chr. Hansen A/S (Hørsholm, Denmark). Precultures and cultivations were performed in crimp-top serum bottles, as described previously [62]. If predefined dilutions were to be installed in cultivations using crimp-top serum bottles, the related medium was removed and replaced with fresh medium every hour.

For cultivations in two-compartment systems (2cs), precultures were prepared as previously described [62]. Calculated amounts of biomass from one or several precultures were washed twice with 0.9% NaCl solution, and the cell pellets were resuspended in the medium to inoculate each compartment.

2.3. Biomass Quantification via the Optical Density Method

Biomass was monitored by optical density (λ = 600 nm) using a photometer (Amersham Bioscience, Ultrospec 10 cell density meter) by applying the biomass/optical density correlation from a previous study [62]. The pH was measured off-line with a pH meter (SevenEasyTM; Mettler Toledo, Columbus, OH, USA) connected to a pH electrode (InLab Semi-Micro; Mettler Toledo, Columbus, OH, USA).

2.4. Biomass Quantification via Flow Cytometry

Samples were processed with Tris-HCl (1.3 M) EDTA (0.13 M) pH 8 buffer; stained with 1× SYBR™ Green I nucleic acid gel stain concentrate (Thermo Fisher Scientific, Waltham, MA, USA); analysed with the flow cytometer BD Accuri™ C6 (BD Biosciences-US) equipped

with four fluorescence detectors (FL1 533/30 nm, FL2 585/40 nm, FL3 > 670 nm, and FL4 675/25 nm), two scatter detectors, a blue laser (488 nm), and a red laser (640 nm); and correlated to biomass concentration c_x (g_{DW} L^{-1}), as described previously [62].

2.5. Membrane Unit

A membrane unit with two layers was built from polycarbonate to allow the integration of a polyethersulfone (PES; poly(oxy-1,4-phenylsulphonyl-1,4-phenyl)) membrane (pore size 0.2 µm, 15407-47-MIN; Sartorius, Goettingen, Germany) or a polyamide (PA) membrane (pore size 0.2 µm, 25007-47-N, Sartorius, Goettingen, Germany).

2.6. Vessel Bioreactor System

Two vessels (50 mL, 101116; Glasgeraetebau Ochs Laborfachhandel e.K., Bovenden, Germany) were connected to the membrane unit using Teflon tubes (inner diameter, 3 mm) and stirred. Each side was equipped with a mixing pump (Watson-Marlow 101U/R) to circulate the cultivation broth between the vessels and the membrane unit. The vessels and membrane units were maintained at 40 °C. The vessels and tubes were sterilised via autoclaving, and the membrane unit was sterilised via immersion in 70% (*v/v*) ethanol for 1 h. The sterile assembled vessel bioreactor system was filled with sterile medium as indicated and warmed up to the cultivation temperature. The biomass was then introduced, and samples were collected using a sterile needle and syringe at the vessel openings.

2.7. Tube Bioreactor System

The inlets and outlets of the membrane unit were connected to tubes equipped with a feed and harvest unit. The mixing pump (Watson-Marlow 101U/R) was equipped with a PharMed®-tube (Saint-Gobain, Courbevoie, France) with an outer diameter of 4.8 mm, inner diameter of 1.6 mm, and a length of 18 cm, resulting in a volume of 0.4 mL.

An additional connecting tube (Rotilo-silicon tube; Carl Roth GmbH + Co. KG, Karlsruhe, Germany) between the inlet and outlet had an inner diameter of 1.5 mm and a length of 31 cm, which resulted in a volume of 0.5 mL. The feed and harvest tubes had inner diameters of 1 mm.

The particles in the membrane unit were removed using 70% (*v/v*) ethanol followed by washing with sterile MilliQ water. The tubes and membranes were sterilised via autoclaving. After connecting the tubes and the membrane unit, the cells were seeded into the system by flushing the cell suspension through the feed until the air was removed. Subsequently, the membrane unit and tubes (without the tubes in the mixing pump) were immersed in water at 40 °C to ensure optimal cultivation conditions.

2.8. Continuous Cultivation in the Tube Bioreactor System

Each compartment in the tube bioreactor system was equipped with a feed inlet and an outlet to harvest the cultivation suspension for installing individual dilution rates. Syringe pumps (LA100; Landgraf Laborsysteme, Langenhagen, Germany) were used to ensure feeding to each compartment. To enable accurate harvesting, one outlet was equipped with a drawing syringe pump (LA100; Landgraf Laborsysteme, Langenhagen, Germany), whereas the other outlet allowed the free outflow of the cultivation medium. The harvest was collected for 1 h in an ice-cooled syringe or bottle. A new syringe and bottle were then connected to the harvest for the next sampling. The samples were analysed for biomass via flow cytometry or centrifuged (3 min, 14,000 rpm, 4 °C), and the supernatant was stored at −70 °C for further analysis.

2.9. Metabolite Balancing

Equation (1) depicts the mass balance for metabolite i which may enter one compartment via diffusion and feed (see Section 3.1.1.), may be produced (or consumed) in the reaction volume V_R, and leaves the compartment via efflux-indexed *production*. Consider-

ing equal reaction volumes in each compartment, Equation (2) (process model) was derived as follows:

$$\frac{dm_i}{dt} = \dot{m}_{i,feed} - \dot{m}_{i,out} + \dot{m}_{i,Diffusion} + \dot{m}_{i,production} \tag{1}$$

$$\frac{dc_i}{dt} = D \cdot (c_{i,feed} - c_i) + k_i \cdot \left(c_{i,connected\ compartment} - c_i \right) + Q_i \tag{2}$$

where m_i (kg) denotes the mass of metabolite I; t (h) denotes the time; c_i (mol L^{-1}) denotes the concentration of metabolite i in the balanced compartment; $c_{i,connected\ compartment}$ (mol L^{-1}) denotes the concentration of metabolite i in the connected compartment; D (h^{-1}) denotes the dilution rate; $c_{i,feed}$ (mol L^{-1}) denotes the concentration of metabolite i in the feed; k_i (h^{-1}) denotes the transport coefficient for diffusion in the membrane unit; and Q_i (mol L^{-1} h^{-1}) denotes the metabolic productivities (i.e., the production or consumption of metabolite i). As indicated, k_i denotes the trans-membrane transport coefficient resulting from the driving concentration profile between connected compartments.

To exploit the experimental data, Equation (2) was discretised for the time intervals $t_2 - t_1$. The metabolic productivity $Q_{i,1}$ in compartment 1 was calculated by Equation (3), and the metabolic productivity $Q_{i,2}$ in compartment 2 was calculated by Equation (4). Indexes *1*, *2*, t_1, and t_2 code for the compartments and time points (h), respectively.

$$Q_{i,1} = \frac{(c_{i,1,t_2} - c_{i,1,t_1})}{t_2 - t_1} - D_1 \cdot c_{i,1,feed} + D_1 \cdot \frac{(c_{i,1,t_1} + c_{i,1,t_2})}{2} - k_i \cdot \left(\frac{(c_{i,2,t_1} + c_{i,2,t_2})}{2} - \frac{(c_{i,1,t_1} + c_{i,1,t_2})}{2} \right) \tag{3}$$

$$Q_{i,2} = \frac{(c_{i,2,t_2} - c_{i,2,t_1})}{t_2 - t_1} - D_2 \cdot c_{i,2,feed} + D_2 \cdot \frac{(c_{i,2,t_1} + c_{i,2,t_2})}{2} - k_i \cdot \left(\frac{(c_{i,1,t_1} + c_{i,1,t_2})}{2} - \frac{(c_{i,2,t_1} + c_{i,2,t_2})}{2} \right) \tag{4}$$

Hence, the biomass-specific activity q_i (mol L^{-1} h^{-1} g$_{DW}^{-1}$) for amino acid i was calculated by dividing the metabolic productivity Q_i by the biomass c_x.

If 13-C-labelled amino acids were used, the related production and consumption terms Q_i^{13} were estimated as follows:

$$\frac{dc_{i,1}^{13}}{dt} = D_1 \cdot \left(c_{i,1,feed}^{13} - c_{i,1}^{13} \right) + k_i \cdot frac^{13} \cdot \left(c_{i,2}^{total} - c_{i,1}^{total} \right) + Q_{i,1}^{13} \tag{5}$$

where c^{13} denotes the concentration (mol L^{-1}) of the fully 13-C-labelled isotopologues; c^{total} denotes the total concentration of an amino acid irrelevant to its labelling pattern. For non-labelled amino acids, the sum of m + 0 plus the natural m + 1 background of isotopologues was considered. $frac^{13}$ (molar 13-C concentration divided by total molar concentration) denotes the fully 13-C-labeled isotopologue fraction of an amino acid pool either in compartment 1 (if $c_{i,1} > c_{i,2}$) or compartment 2 (if $c_{i,2} > c_{i,1}$).

2.10. Reaction Rate Constant of Metabolite Productivity

The consumption rate constant $k_{consumption,i}$ (h^{-1}) for amino acids was derived from the productivity Q_i for each amino acid concentration c_i according to Equation (6).

$$k_{consumption,i} = \frac{Q_i}{c_i} \tag{6}$$

2.11. Determination of Amino Acid Transport Coefficients in the Membrane Unit

To determine the transport coefficient k_i, the feed and harvest flows were disconnected, and compartment 1 was filled with 65 mL of various concentrations of amino acids (pH 6.5), whereas compartment 2 was filled with 65 mL of MilliQ water. A constant mixing pump rate of r_{pump} = 10 mL × min^{-1} was installed in each compartment. Samples (0.5 mL) were taken from each bioreactor after 0, 5, 10, 15, 20, 25, and 30 min or 0, 5, 15, and 30 min, and

amino acid concentrations were quantified using HPLC. The process model of Equation (2) is simplified to Equation (7) for compartment 1, and k_i was identified as the least-square estimate in MATLAB $^®$ (R2020a) (Code S1 in Supplementary Materials).

$$\frac{dc_{i,1}}{dt} = -\frac{dc_{i,2}}{dt} = k_i \cdot (c_{i,2} - c_{i,1}) \tag{7}$$

2.12. Determination of the Bodenstein Number

To determine the Bodenstein number (*Bo*) in the membrane unit, bromothymol blue solution with a pH of 7.5 (KK19.3; Carl Roth GmbH & Co. KG, Karlsruhe, Germany) was pumped through each side of the membrane unit at a typical cultivation mixing pump rate of 3.7 mL $\times$ min^{-1}. Subsequently, 15 μL of 2 M HCl tracer was pulsed into one side of the membrane unit, leading to a colour change.

The experiment was recorded using video. Then, one image of the outlet was decomposed into squares for colour analysis using "imread" from MATLAB $^®$. As the red *r*-values showed maximum variability, related intensities were applied for the mixing studies.

The average residence time (τ) and its variance (σ^2) were calculated after the pulse perturbation, as defined by a previous study [63]. To characterise the degree of mixing in the membrane unit, the *Bo* was extracted from τ and σ^2 (Equation (8)):

$$\frac{\sigma^2}{\tau^2} = \frac{2}{Bo} + \frac{8}{Bo^2} \tag{8}$$

2.13. Calculation of the Damkoehler Number

The Damkoehler number (*Da*) is a dimensionless mass balance that was adapted to indicate whether amino acid consumption in a compartment encountered limitations due to low amino acid supply by membrane transport [64]. Da_I (dimensionless) was calculated for each amino acid *I* in a compartment between two subsequent data points (t_1 and t_2) when amino acid consumption and transport in the membrane unit into the compartment were present. A homogeneous distribution of amino acids in the compartment was assumed. *Da* considered amino acid decrease by consumption (Q_i) and washout by dilution (*D*). An increase in amino acid concentration in a compartment was expected from transport across the membrane (see Section 3.6.6.). *Da* depicts the quotient between Q_i, *D* for washout, and the transport rate in the membrane unit for an amino acid *i* as follows:

$$Da_{i,t1-t2} = Da_{consumption} + Da_{dilution} = \frac{-Q_{i,t}}{k_i \cdot g_{i,t1-t2}} + \frac{D \cdot c_{i,t1-t2}}{k_i \cdot g_{i,t1-t2}} \tag{9}$$

Trans-compartment concentration gradients g_i (mol L^{-1}) were estimated by considering the arithmetic mean (Δc) of the concentrations between time points (t_1 and t_2) according to Equation (10).

$$g_i = \Delta c_{i,connected\ compartment,t_1-t2} - \Delta c_{i,t_1-t2} \tag{10}$$

The pool turnover rate ($k_{membrane\ unit}$ (h^{-1})) of metabolite pools in the membrane unit with the volume $V_{membrane\ unit}$ (L) imposed by the circulation of the fermentation broth with a mixing pump adjusted to the rate $r_{mixing\ pump}$ (L min^{-1}) was calculated as follows:

$$k_{membrane\ unit} = \frac{r_{mixing\ pump}}{V_{membrane\ unit}} \tag{11}$$

2.14. Quantification of Extracellular Metabolites

Sugar and lactate concentrations were measured with an isocratic Agilent 1200 series HPLC system (Agilent Technologies, Santa Clara, CA, USA) equipped with a Phenomenex guard carbo-H column (4 $\times$ 3.0 mm) and a Rezex ROA organic acid H (8%) column (300 $\times$ 7.8 mm, 8 μm; Phenomenex) maintained at 50 $°$C [62]. Separation was achieved with 5 mM H$_2$SO$_4$ with a constant flow rate of 0.4 mL min^{-1}. Samples were pretreated for

the precipitation of abundant phosphate by the addition of 4 M NH_3 and 1.2 M $MgSO_4$ solution followed by incubation with 0.1 M H_2SO_4. Absolute concentrations were obtained by standard-based external calibration and normalisation with L-rhamnose as the internal standard.

The amino acid concentrations were determined using an Agilent 1200 series instrument (Agilent Technologies, Santa Clara, CA, USA) [62]. Separation was achieved with an Agilent Zorbax Eclipse Plus C_{18} column (250 by 4.6 mm, 5 μm), which was protected by an Agilent Zorbax Eclipse Plus C_{18} guard column (12.5 by 4.6 mm, 5 μm), according to a previously established method [65]. After automatic pre-column derivatisation with ortho-phthaldialdehyde, fluorometric detection (excitation at 230 nm and emission at 450 nm) was performed. The elution buffer consisted of a polar phase (10 mM Na_2HPO_4, 10 mM $Na_2B_4O_7$, 0.5 mM NaN_3, and pH 8.2) and a non-polar phase (45% (*v/v*) acetonitrile and 45% (*v/v*) methanol). The quantification of amino acids was achieved via standard-based external calibration and using 4-aminobutanoic acid as an internal standard at 100 μM to correct for analyte variability.

2.15. Quantification of Extracellular and Intracellular Metabolites

For extracellular metabolite quantification via LC-MS/MS, the samples were centrifuged at 20,000× *g* for 3 min at 4 °C, and the supernatant was stored at −70 °C. The samples were then filtered (Centrifugation Units ROTI®Spin, MINI-3; Carl Roth GmbH & Co. KG, Karlsruhe, Germany) and mixed (1:1 *v/v*) with methanol to precipitate the remaining particles.

Biomass samples for intracellular metabolome analysis via LC-MS/MS were centrifuged at 4500× *g* for 3 min and 4 °C, washed with 0.9% (w/v) sodium chloride solution, centrifuged at 20,000× *g* for 3 min at 4 °C, and the pellet was stored at −70 °C. For metabolite extraction, the pellets were supplemented with 120 μL of 100 μM norvalin to correct for analyte variability, boiled at 95 °C for 4 min, and immediately centrifuged for 20 min at 20,000× *g* and 4 °C. The supernatants were filtered (Centrifugation Units ROTI®Spin, MINI-3; Carl Roth GmbH & Co. KG, Karlsruhe, Germany) and stored at −70 °C. The metabolite concentrations in the samples were measured using an Agilent 1200 HPLC system coupled with an Agilent 6410 B triple quadrupole mass spectrometer using an electrospray ion source. Chromatographic separation was achieved according to a previously described method [66]. The metabolite pool concentration was quantified by adding defined amounts of analyte standard to the reaction mixture. Data analysis was performed using MassHunter B.05.00 software (Agilent Technologies), and peaks of isotopologues containing 13-C were checked for interference by comparing samples of cultivation from 12-C and 13-C substrates.

2.16. Determination of Amino Acid Composition in Casein

First, 32% HCl (200 μL) was slowly added to casein solution (200 μL), vortexed, and incubated at 100 °C for 24 h. After cooling at 18 °C (1 h), 490 μL of 6.23 mM NaOH was slowly added. The samples were stored at −20 °C until HPLC was used to quantify the amino acid concentrations.

2.17. Uncertainty Analysis

The measured data were analysed using Microsoft Excel. The mean and standard deviation were calculated using duplicates and triplicates (STABW.S) using Microsoft Excel.

3. Results

3.1. Design of the Membrane Unit

3.1.1. Membrane Unit Characteristics

The channels in the membrane unit (see Materials) were located next to each other and were separated by the membrane (Figure 1). This setting enabled the diffusion of metabolites, such as amino acids, but retained the cells. The channel in the membrane unit

had a length of approximately 166 mm and volume of approximately 2.7 mL. The inserted membrane area was approximately 6.7×10^{-4} m^2.
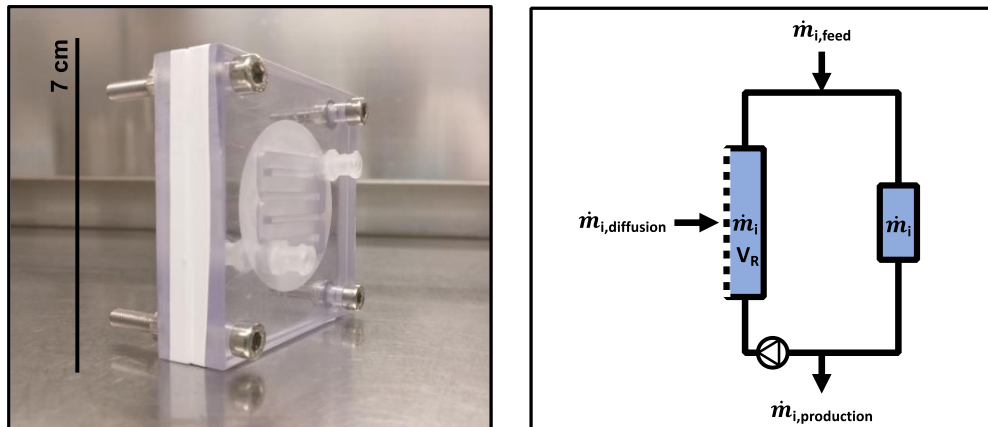

Figure 1. (**left**) Image of the membrane unit. The inlet and outlet of the channel were connected to vessels or tubes to allow the circulation of cells. Two polycarbonate elements were used to clamp a semi-permeable membrane that was aligned and fixed. (**right**) Mass balance of a compartment with inflow (feed), outflow (harvest), and diffusion flows in the membrane unit. The mixing pump allowed the circulation of the cultivation broth within the compartment.

3.1.2. Amino Acid Transport in the Membrane Unit

A PES or PA membrane was used to determine the amino acid transport coefficient (k_i) between the two vessels connected by the membrane unit. Three independent experiments were performed. Each experiment contained all of the amino acids. For each experiment, another initial amino acid concentration was set between 150 and 3200 μM (Table S2 in Supplementary Materials). The k_i for amino acid i was estimated based on all three experiments (for example, see $k_{alanine}$ in Figure S1 in Supplementary Materials). The membrane unit equipped with a PES membrane showed a higher mean transport coefficient ($k = 0.36 \pm 0.03$ h^{-1}) compared to a membrane unit equipped with a PA membrane ($k = 0.09 \pm 0.01$ h^{-1}) (Figure S2 in Supplementary Materials). Therefore, PES membranes were used in this study. Whether the power input by the mixing pump may bias k_i values by affecting the supply or removal of molecules in the membrane unit was considered. Given a mixing pump rate of $r_{pump} = 10$ mL $\times$ min^{-1}, the average pool turnover rate in the membrane unit was approximately $k_{membrane\ unit} = 222$ h^{-1} on one side of the membrane unit. Considering that the maximum transport coefficients were approximately $k = 0.4$ h^{-1}, the fraction of molecules exchanged by diffusion in the membrane unit was $f_{diffusion} = k/k_{membrane\ unit} = 0.02\%$. In other words, 99.98% of all the molecules in one compartment of the membrane unit was exchanged via pumping. Reducing r_{pump} to 3.7 mL $\times$ min^{-1} increased $f_{diffusion}$ to 0.05%, which was still considered to be a low value. Hence, the k_i was barely affected by the pumping rates used in this study.

3.2. Design of the 2cs

The presented 2cs was designed to investigate metabolic interactions in a co-culture. This system enabled the characterisation of individual strains by calculating strain-specific rates and quantifying intracellular metabolite pools. As shown in Figure 2, the experimental setup comprised a central membrane unit separating compartments 1 and 2 that may or may not embed an additional vessel section.
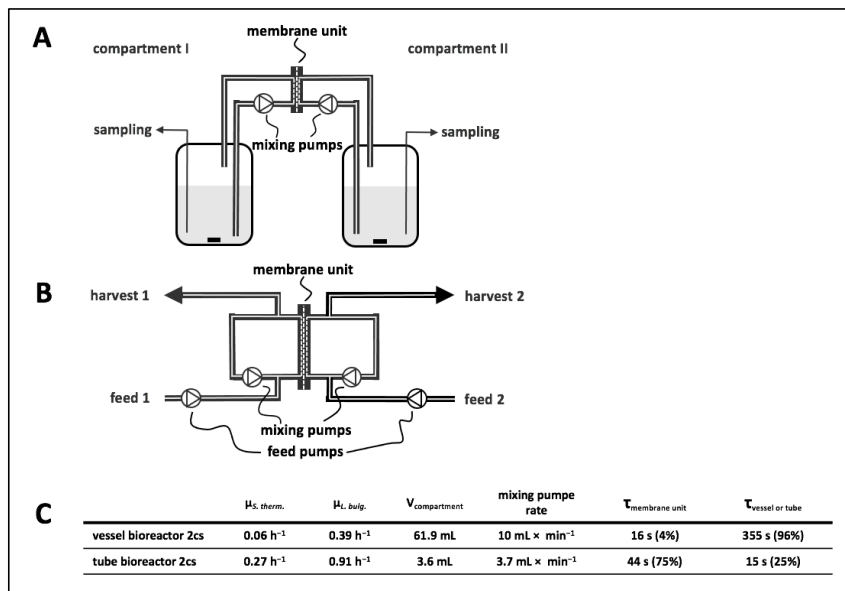
Figure 2. (**A**) Diagram of a vessel bioreactor system. The vessels were connected to the membrane unit, and circulation of medium in each compartment was achieved by mixing pumps. (**B**) Diagram of a tube bioreactor system. The inlets and outlets of the membrane unit were connected by tubes, and circulation of medium in each compartment was achieved by mixing pumps. Additionally, attached tubes for feeds and harvests allowed sampling and continuous cultivation by using feed pumps for each compartment. (**C**) Technical parameters and results of co-cultivations in respective two-compartment systems (2cs) with *Lactobacillus delbrueckii* subs. *bulgaricus* in synthetic medium (SM) containing casein and lactose and *Streptococcus thermophilus* in SM containing lactose. Strains were cultivated in co-culture in the 2cs, enabling exchange of metabolites, and strain-specific growth rates were determined from biomass measurements (Figures S4 and S5 in Supplementary Materials). V, volume.

3.3. Vessel Bioreactor System: Set-Up and Growth Experiment

The vessel bioreactor system comprised two vessels connected by a membrane unit. Each compartment was filled with 61.9 mL of cultivation broth (Figure 2A). To evaluate growth behaviour, compartment 1 was filled with SM + lactose and inoculated with *S. thermophilus*, whereas compartment 2 contained *L. bulgaricus* in SMcas + lactose. The biomass ratio in the 2cs at inoculation was 1:2.75 ($g_{DW}{}^{LB}$:$g_{DW}{}^{ST}$). This experimental setting was chosen to investigate whether the non-proteolytic *S. thermophilus* cultivated in compartment 1 benefited from metabolite exchange with the proteinase-positive *L. bulgaricus* cultivated in compartment 2. Notably, proteinase-negative *S. thermophilus* was not able to grow in SMcas + lactose as a pure culture (Figure S3 in Supplementary Materials). Consequently, the strain crucially relied on *L. bulgaricus*, which released amino acids and peptides from casein that further diffused through the membrane. Considering the geometries and mixing pump rate of 10 mL $\times$ min^{-1} in each compartment, the estimated cellular residence time was 355 s in the vessel and 16 s in the membrane unit.

Cultivation studies revealed a growth rate of $\mu = 0.39$ h^{-1} for *L. bulgaricus* and $\mu = 0.06$ h^{-1} for *S. thermophilus* (Figure S4 in Supplementary Materials). This observation is the first evidence that amino acids and peptides are released from *L. bulgaricus* and that they diffuse into compartments containing *S. thermophilus*. However, the growth of *S. thermophilus* is nutrient-limited.

3.4. Tube Bioreactor System

To increase the growth rate of *S. thermophilus*, the vessels were removed from the vessel bioreactor system, leading to a simplified tube bioreactor system design (Figure 2B). Accordingly, the compartment volume reduced from 61.9 to 3.6 mL, increasing the volume fraction in the membrane unit to 74% (instead of 4% in the vessel bioreactor system). By analogy, the membrane-to-compartment ratio improved from 11 m^{-1} in the vessel bioreactor system to 186 m^{-1} in the tube bioreactor system. In other words, the residence time of amino acids and peptides inside the membrane unit increased from 4% to 74% of the total cycling time.

Again, similar experimental conditions were chosen for the first vessel bioreactor system tests; namely, the cultivation of *S. thermophilus* in compartment 1 with SM + lactose and of *L. bulgaricus* in compartment 2 with SMcas + lactose. The mixing pump rate was reduced to 3.7 mL $\times$ min^{-1}. Dilution rates of $D = 0.14$ h^{-1} were installed in each compartment, resulting in mean residence times of 7.1 h per compartment. The feed medium was equivalent to the medium in the compartments (SM + lactose for feeding into compartment 1 and SMcas + lactose for feeding into compartment 2). The biomass ratio in the 2cs at inoculation was 1:0.7 (g$_{DW}$^{LB}:g$_{DW}$ST). As expected, the growth of *L. bulgaricus* and *S. thermophiles* was $\mu = 0.91$ h^{-1} and $\mu = 0.27$ h^{-1}, respectively (Figure S5 in Supplementary Materials). For both strains, the growth rates were higher than those in the studies using the vessel bioreactor system.

3.5. Comparison between Bacterial Growth in Serum Bottles and in the Tube Bioreactor System

To further characterise the growth of a co-culture in the tube bioreactor system (two-compartments), a crimp-top serum bottle (one-compartment) was additionally inoculated in parallel to the experiment described in Section 3.4. The crimp-top serum bottle contained SMcas + lactose (50 mL) inoculated with the same biomass concentrations of *S. thermophilus* and *L. bulgaricus* and was diluted at the same dilution rate of $D = 0.14$ h^{-1}. A defined volume was removed each hour and replaced with new SMcas + lactose medium, imitating the continuous process conditions in the tube bioreactor system described in Section 3.4.

Biomass was determined via flow cytometry at each harvest of the tube bioreactor system and in the crimp-top serum bottle. Then, the cell events of both compartments of the tube bioreactor system were summed up. It was not possible to measure the strain-specific biomass in a one-compartment bottle. As depicted in Figure S6 in Supplementary Materials, the growth of the co-culture in the one-compartment bottle approach was fairly similar to the added-up biomass course in the tube bioreactor system for the first 2 h. Then, exponential growth continued in the tube bioreactor system while the growth rate slowed down in the one-compartment system, finally leading to 3.2×10^7 cell events $\times$ mL^{-1} compared to 4.1×10^7 cell events $\times$ mL^{-1} in the tube bioreactor system. Apparently, the tube bioreactor system approach was beneficial for the growth of the co-culture.

3.6. Determination of Strain-Specific Rates in Co-Culture

To demonstrate the applicability of the tube bioreactor system for identifying exchange rates of metabolites, proteinase-negative *S. thermophilus* and proteinase-positive *L. bulgaricus* were cultivated using medium containing 13-C glucose in the tube bioreactor system. The goal of the experiments was to determine the strain-specific release and consumption of amino acids in the interacting co-culture. Furthermore, experiments were performed to determine whether the released amino acids originated from casein or were synthesised *de novo* from sugar.

3.6.1. Dynamic Cultivation Tests in the Tube Bioreactor System

L. bulgaricus was cultivated in one compartment of the tube bioreactor system containing SMcas + 13-C glucose. In the connected compartment, proteinase-negative *S. thermophilus* was cultivated in SM + 13-C glucose. The experiments were designed such

that dynamic growth conditions were set, which were individually adapted to the kinetics of each strain. The biomass ratio in the 2cs at inoculation was 1:4.4 (g_{DW}^{LB}:g_{DW}^{ST}). After 2 h of cultivation in the tube bioreactor system, the operational mode switched to continuous fermentation. Pumps feeding the medium with the same composition as the related compartment were started, together with the harvest pump. For the compartment with *S. thermophilus*, a dilution rate of $D = 0.34$ h^{-1} was set to avoid the anticipated overgrowth of the said strain with respect to *L. bulgaricus*. For the latter, a dilution rate of $D = 0.07$ h^{-1} was set to prevent fast washout. After 8 h, that is, 24 h after the start of the experiments, the biomass of each compartment was collected for intracellular metabolite analysis. During the continuous mode period, a mean growth rate of $\mu = 0.05$ h^{-1} for *S. thermophilus* and an intermediary maximum of $\mu = 0.1$ h^{-1} between 1 and 3 h were observed (Figure S7 in Supplementary Materials). This indicated the growth of *S. thermophilus*, which is only possible in the presence of amino acids or peptides supplied by *L. bulgaricus* (Figure S3 in Supplementary Materials). Therefore, amino acids and peptides must have diffused between the compartments and enriched the medium of *S. thermophilus* (Figure 3). Additionally, the pH dropped in the *S. thermophilus* compartment from 6.5 to 5.5, and lactate production was measured, which revealed the metabolic activity of *S. thermophilus*, *L. bulgaricus*, or both (Figure S8 in Supplementary Materials). Growth and pH were not measured in compartments containing *L. bulgaricus*. Throughout the continuous mode (8 h), *S. thermophilus* and *L. bulgaricus* were replaced 2.7- and 0.6-fold, respectively. In other words, the system did not run under a hydrodynamic steady state. Accordingly, the derived kinetics may serve as operational conditions, demonstrating the feasibility of this approach.
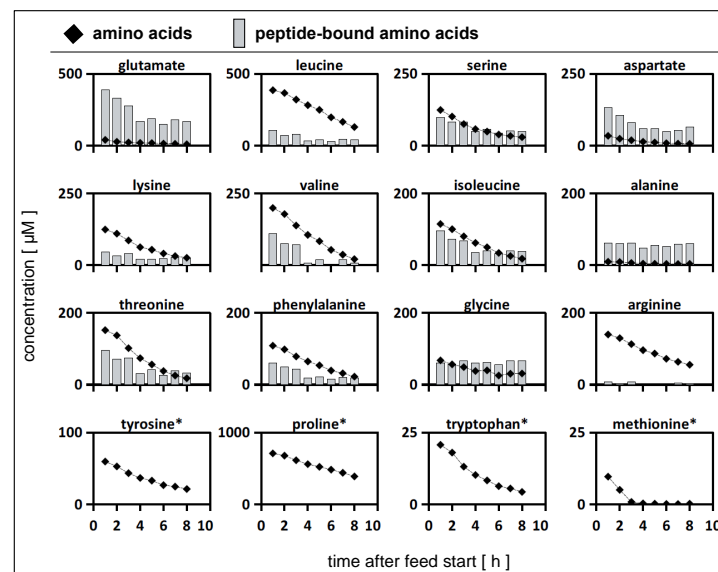

Figure 3. Amino acid profiles in the compartment containing *Streptococcus thermophilus* during co-cultivation with *Lactobacillus delbrueckii* subs. *bulgaricus* in the tube bioreactor system. (**rhomb**) Extracellular amino acid concentrations (μM) in the compartment containing *S. thermophilus* during the continuous mode. (**bars**) Extracellular peptide-bound amino acid concentrations (μM) in the compartment containing *S. thermophilus* during the continuous mode. *S. thermophilus* was cultivated in co-culture with *L. bulgaricus* in the tube bioreactor system containing synthetic medium (SM) with casein and glucose in the *L. bulgaricus* compartment and SM with glucose in the *S. thermophilus* compartment. * Profile data for these peptide-bound amino acids not measured.

3.6.2. Calculation of Strain-Specific Rates

In co-culture, proteinase-negative *S. thermophilus* consumed peptides and amino acids provided by *L. bulgaricus* to satisfy its nitrogen demand. A previous study using similar strains and experimental conditions [62] demonstrated that co-cultures of *L. bulgaricus* and *S. thermophilus* released and consumed amino acids (as aspartate, arginine, alanine, lysine, isoleucine, and glycine). Consequently, tracking these components may open the door for the identification of strain-specific dynamics and to gain further insight into the interactions of the strains.

The strength of the 2cs is that it allows the calculation of strain-specific amino acid rates by the individual analysis of sample concentrations (Table S3 in Supplementary Materials). As shown in Figure 4, positive values indicate amino acid release regardless of the precursor origin, that is, casein or glucose, whereas negative numbers correlate with amino acid consumption. By trend, both strains released amino acids during the first 3 h before metabolic productivity declined or even before consumption occurred. In particular, *L. bulgaricus* released amino acids (Table S3 in Supplementary Materials) based on its high proteolytic activity. Glutamate, aspartate, and alanine were only produced by *L. bulgaricus* and consumed by *S. thermophilus* during the first 3 h. Another exception was methionine, which was consumed by both strains in the continuous mode.
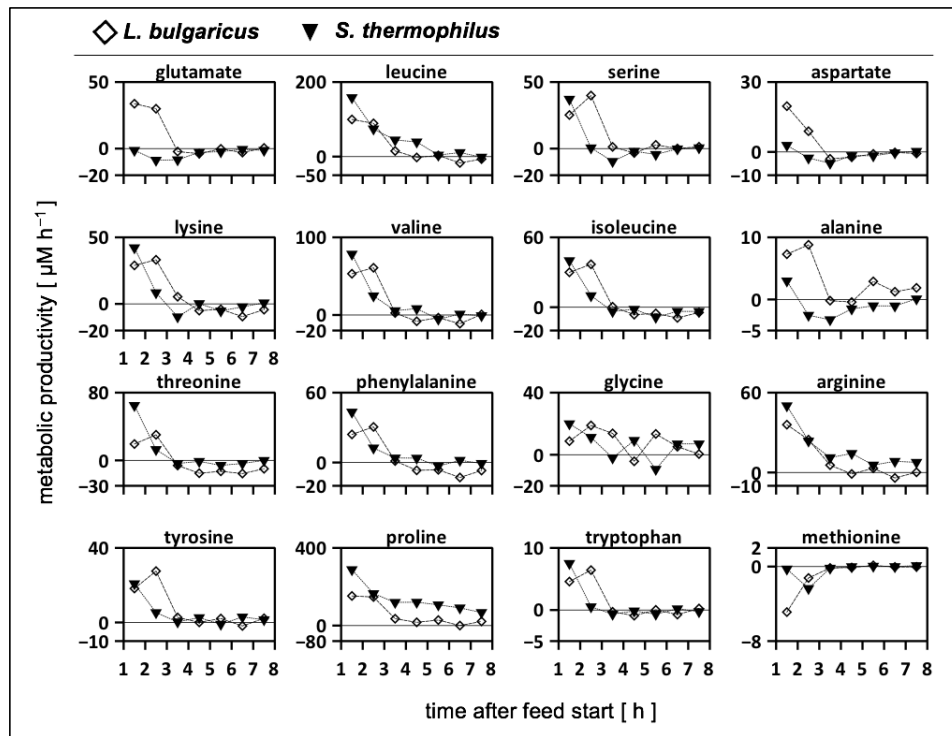

Figure 4. Metabolic productivity of *Lactobacillus delbrueckii* subs. *bulgaricus* (**rhomb**) and *Streptococcus thermophilus* (**triangle**) cultivated in the tube bioreactor system as a co-culture. Positive values indicate the release or production of amino acids; negative values indicate the uptake of amino acids. Strains were cultivated in a tube bioreactor system containing synthetic medium (SM) with casein and glucose in the *L. bulgaricus* compartment and SM with glucose in the *S. thermophilus* compartment. Amino acids were sorted in rows according to the mol-fraction in casein, except tyrosine, proline, tryptophan, and methionine.

3.6.3. Biomass-Specific Activity of *S. thermophilus* in Mono- and Co-Cultures

To gain a deeper understanding of amino acid metabolism in *S. thermophilus*, amino acid productivity has often been studied and modelled [52,67]. However, only strain- and biomass-specific measurements may enable detailed metabolic flux distributions in co-cultures [28], thereby linking mono- and co-culture models [68,69]. Figure 5 compares the amino acid productivity of *S. thermophilus* in a mono-culture grown on SMaa + lactose with the performance when co-cultivated with *L. bulgaricus* in the tube bioreactor system on SMcas + glucose (as shown in Figure 4). Most amino acids were released by *S. thermophilus* in the co-culture, indicating the uptake of peptides as well as intracellular and extracellular peptidase activity [56] compared to the mono-culture condition, where amino acids were almost entirely consumed. Similar to the mono-culture activities, glutamate and aspartate were consumed by *S. thermophilus* in the co-culture. This is remarkable, as peptide-bound glutamate and aspartate are available (Figure 3) but are not preferred. Apparently, *S. thermophilus* prefers consumption rather than replenishing its demand via the hydrolysis of peptides or interconversion through transaminases [70,71]. Methionine was consumed by *S. thermophilus* in the co-culture, but uptake was limited by low methionine concentrations (Figure 3), which might indicate an insufficient supply [67].
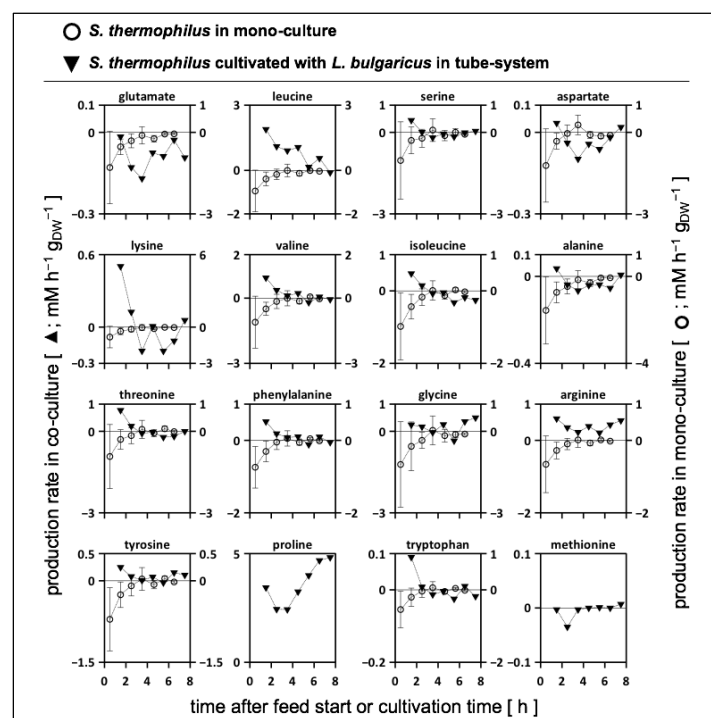

Figure 5. Biomass-specific activity of *Streptococcus thermophilus*. Amino acid production or consumption rates of *S. thermophilus* bridging amino acid productivity in mono-culture and co-culture. (**Filled**) *S. thermophilus* grown in co-culture with *Lactobacillus delbrueckii* subs. *bulgaricus*. Strains were cultivated in a tube bioreactor system containing synthetic medium (SM) with casein and glucose in the *L. bulgaricus* compartment and SM with glucose in the *S. thermophilus* compartment. (**Non-filled**) *S. thermophilus* grown in a crimp-top serum bottle containing SM with amino acids and lactose (modified from [62]). Amino acids were sorted in rows according to mol-fraction in casein, except tyrosine, proline, tryptophan, and methionine.

3.6.4. Analysis of Extracellular 13-C Alanine Enrichment

Concentrations of extracellular amino acid isotopologues were measured to determine the origin of the amino acids. Low fractions of labelled aspartate, tyrosine, and threonine were detected (< 1%). Only the alanine pool (mol L^{-1}) was enriched with up to 50% 13-C alanine (Figure 6), which was mirrored by intracellular labelling patterns in both strains (Figure S9 in Supplementary Materials). This observation highlighted the relevance of *de novo* alanine biosynthesis from (labelled) sugars. The strain-specific production and consumption rates for 13-C alanine were calculated (Equation (2)) using the process model (Figure 6A). Balancing revealed that alanine was produced *de novo* by *L. bulgaricus* at a maximum rate of 5 $\mu M \times h^{-1}$, whereas *S. thermophilus* mainly consumed the amino acids (Figure 6B).
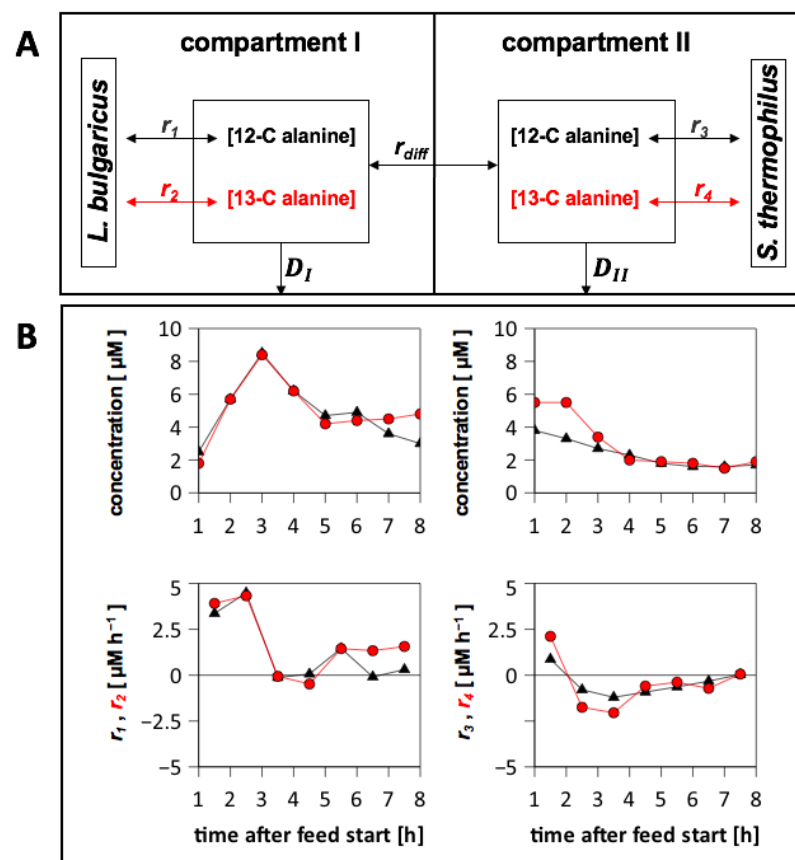
Figure 6. Alanine production and consumption of *Streptococcus thermophilus* and *Lactobacillus delbrueckii* subs. *bulgaricus* cultivated in the tube bioreactor system. (**A**) Illustration of alanine pools in the tube bioreactor system. r_1 and r_3 are the production and consumption rates of non-labelled alanine; r_2 and r_4 are the production and consumption rates of 13-C alanine; r_{diff} is the diffusion rate of alanine in the membrane unit according to concentration differences; and D is the dilution rate in compartment 1 or compartment 2. (**B**) Compartment 1 was filled with *L. bulgaricus* and synthetic medium (SM) with casein and 13-C glucose. Compartment 2 was filled with *S. thermophilus* and SM with 13-C glucose. Concentrations of non-labelled (**triangle**) and 13-C alanine (**circle**) were measured via LC-MS. Strain-specific rates were calculated by balancing each compartment. Positive rates: production; negative rates: consumption.

3.6.5. Alanine Exchange between the Compartments

The diffusion flux of 13-C alanine across the membrane was calculated. Figure S10 in Supplementary Materials shows a 13-C alanine flux from the compartment containing *L. bulgaricus* to the compartment containing *S. thermophilus* between 2 and 7 h. This indicated that *L. bulgaricus* provided *de novo*-produced alanine to *S. thermophilus* because *S. thermophilus* consumed alanine within this time range (Figure 6).

3.6.6. Calculation of Damkoehler Numbers

To further investigate the metabolite dynamics in the continuous experiments, Damkoehler numbers were calculated for each amino acid (Figure 7). In essence, the terms for amino acid consumption and washout were compared with trans-membrane amino acid transport rates, leading to $Da_{consumption}$ and $Da_{dilution}$, respectively (Table 1). Accordingly, $Da < 1$ indicated a faster amino acid supply than depletion, and this was the opposite for $Da > 1$, whereas $Da = 1$ represented an equilibrium between depletion and supply. The calculation of the Da terms $Da_{consumption}$ and $Da_{dilution}$ (Equation (9)) illustrated their individual importance for the total Da term.
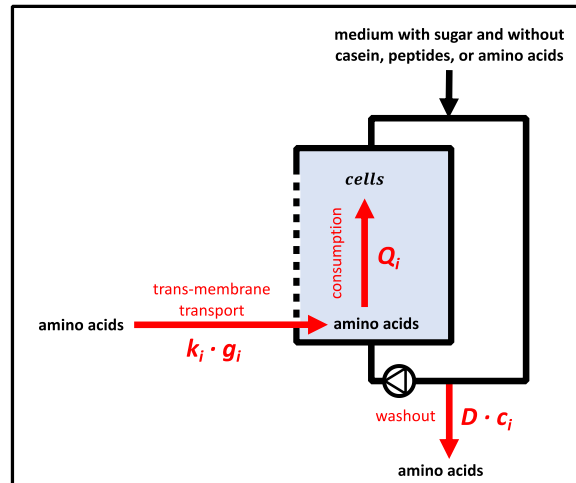

Figure 7. Illustration of terms to estimate the Damkoehler number (*Da*) during the continuous mode. Trans-membrane transport provided amino acids; *Streptococcus thermophilus* or *Lactobacillus delbrueckii* subs. *bulgaricus* consumed amino acids; and the continuous mode provoked amino acid washout. The initial concentration for some amino acids was above zero at the start of the continuous mode.

Table 1. Comparison of mass balance terms for amino acids in the compartment containing *Streptococcus thermophilus*.

mean amino acid consumption	$-Q_i$	3.0 ± 2.8 µM × h^{-1}
mean amino acid dilution	$D \times c_i$	11.4 ± 10.1 µM × h^{-1}
mean trans-membrane amino acid influx	$k_i \times g_i$	5.5 ± 3.8 µM × h^{-1}
mean change in amino acid concentration	dc_i/dt	13.5 ± 13.6 µM × h^{-1}
amino acid feed	$D \times c_{i,feed}$	0 µM × h^{-1} (feed medium without amino acids)
Damkoehler term for consumption	$Da_{consumption}$	0.6 ± 0.4
Damkoehler term for dilution	$Da_{dilution}$	2.3 ± 2.1
Damkoehler number	Da_{total}	2.9 ± 2.3

S. thermophilus was co-cultivated with *Lactobacillus delbrueckii* subs. *bulgaricus* in the tube bioreactor system containing synthetic medium (SM) with glucose in the *S. thermophilus* compartment and SM with casein and glucose in the *L. bulgaricus* compartment.

The analysis of Da_{total} time courses for the compartment containing *S. thermophilus* revealed that Da_{total} data were > 1 (Figure 8A) for all amino acids, irrespective of the time interval. By trend, the highest Da_{total} values were observed after 5 h, with alanine being the only exception. Consequently, most amino acids showed greater concentration decreases than their supply from the compartment containing *L. bulgaricus*. This scenario was only enabled by the already high concentrations of these amino acids within the compartments at the start of the continuous experiment (Figure 3). In the case of alanine, sugar-derived biosynthesis became more important as the experiment lasted longer. Figure 8B discloses the individual contributions of $Da_{dilution}$ and $Da_{consumption}$ for the calculation of the total Da number Da_{total} showcasing the compartment of *S. thermophilus*. $Da_{dilution}$ was larger than $Da_{consumption}$, outlining that the decrease in amino acid concentrations was predominately caused by the washout of amino acids (D = 0.34 h^{-1}) and not by their consumption ($k_{consumption}$ = 0.15 ± 0.16 h^{-1}) (Figure 7).
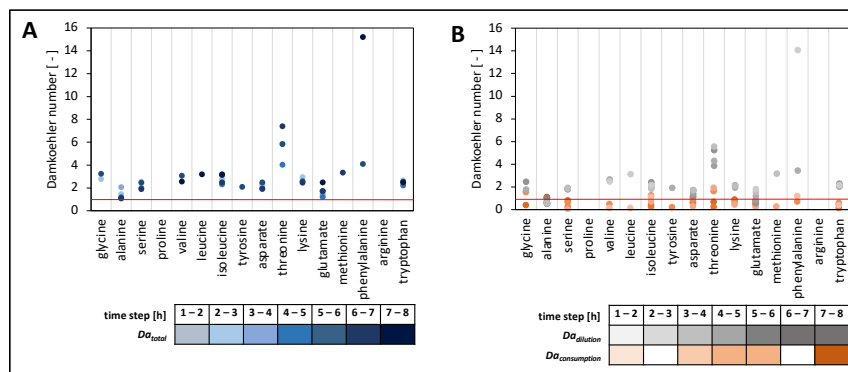

Figure 8. Damkoehler numbers (Da_I) of individual amino acids. (**A**) $Da_{total} = Da_{dilution} + Da_{consumption}$ in the compartment containing *Streptococcus thermophilus*. (**B**) $Da_{dilution} + Da_{consumption}$ separated in the compartment containing *S. thermophilus*. Strains were cultivated in the tube bioreactor system, and Da was calculated for each hour of continuous cultivation. Da numbers were only calculated if amino acid uptake was present within 1 h. The red line indicates Da = 1.

4. Discussion

4.1. Process Characterisation

The fluid behaviour in the membrane unit can be described by Bo = 18 (Figure S11 in Supplementary Materials). This indicated that axial molecular diffusion and additional backmixing effects were present [63]. Given that Bo represents the ratio between convective flow and axial backmixing (dispersion), one may estimate that a non-optimum plug-flow pattern exists inside the channels with approximately 5% backmixing. Backmixing increased the average residence time of elements inside the membrane unit. However, 5% is far too low to create substrate gradients inside the compartment, as consumption rates are much lower than the sum of trans-membrane transport (Table 1).

To investigate whether the diffusion process of metabolites in the membrane unit might result in limitations, such as the supply of amino acids from *L. bulgaricus* to *S. thermophilus*, Damkoehler numbers were estimated according to Equation (9). As almost all Da_{total} values were > 1, indicating stronger amino acid withdrawal than supply, cellular growth predominately relied on the amino acids that were released at the beginning of the continuous experiment or those that were already present before the start (Figure 3). However, the key readouts regarding amino acid dependencies could be deduced. Nevertheless, future experimental settings may reduce the dilution rate D as the key parameter for washout, which would significantly reduce the available amino acid amount per compartment (Figure 7).

4.2. Difference between Cultivation in the Serum Bottle and in the Tube Bioreactor System

The growth of the co-culture in the serum bottle and in the tube bioreactor system was compared to study the potential impacts of hampered cell-to-cell interactions. Metabolic interactions could be delayed because of diffusion-limited metabolite exchange, and missing cell-to-cell contact may create secondary responses [72]. Interestingly, 33% more cell events, that is, the proxy for cell growth, were found in the tube bioreactor system, which might have been the result of delayed acidification (Figure S6 in Supplementary Materials). Like amino acids, lactate needs to cross the membrane unit via diffusion, which decelerates acidification dynamics in the connected compartment while maintaining beneficial pH conditions for growth.

4.3. Strain-Specific Amino Acid Release and Consumption in the Tube Bioreactor System

Both strains released and consumed amino acids when cultivated in a tube bioreactor system in continuous mode (Figure 4). During the first 3 h, both strains mainly released amino acids. Subsequently, amino acids were released and consumed. Only methionine was entirely consumed during the continuous mode. These findings quantified, for the first time, to our knowledge, the amino acid production and consumption rates in an interacting co-culture of *L. bulgaricus* and *S. thermophilus* and highlighted their dynamics. Consequently, the amino acid transport demonstrated for both strains and their impact on proton gradient and energy metabolism must be taken into account to fully understand the cellular physiology in the co-culture [73]. The production and consumption of amino acids by both strains fulfilled the requirements for bidirectional amino acid exchange between the strains and allowed the manipulation of the co-culture by amino acid additions, such as methionine [67]. The amino acid consumption and production rates for *S. thermophilus* during co-cultivation with *L. bulgaricus* in the tube bioreactor system were compared with those of previously published data [62] for *S. thermophilus* during mono-culture growth (Figure 5). Basically, *S. thermophilus* released amino acids in co-culture to some extent (Figure 5), although these amino acids were available (Figure 3), indicating the uptake of peptides or amino acid synthesis (except glutamate, aspartate, and methionine). In contrast, *S. thermophilus* grown under mono-culture conditions only consumed amino acids (Figure 5). The dataset of this study confirmed the previously published simulated metabolic activities [67] of different *S. thermophilus* strains grown on various amino acid sources. The predicted amino acid fluxes were mostly within the same ranges as those presented in Figure 5. The measurements revealed the dynamics in the amino acid production and consumption of *S. thermophilus*, indicating the importance of extending the model when used for co-culture simulations [68,69,74].

Generally, the mutual release of almost all amino acids in an *L. bulgaricus*–*S. thermophilus* co-culture specified, for the first time, that both strains contribute to increasing amino acid concentrations in the medium and the enhanced current understanding of their metabolic activity. *L. bulgaricus* provided not only peptides but also—equally to *S. thermophilus*—amino acids to the co-culture, especially at the beginning of cultivation. At the end of the cultivation period, amino acid consumption occurred, indicating a switch between amino acid release and consumption.

Previous studies have revealed the upregulation of arginine biosynthesis genes in *S. thermophilus* [51,67,75], although arginine deficiency did not occur [67]. Consequently, here, it was hypothesised that arginine might serve as a precursor for ornithine or polyamine [67,75]. However, their low extracellular concentrations did not support the idea that arginine biosynthesis might have additional functions as a precursor [67]. The measurement of peptide-bound arginine in the compartment containing *S. thermophilus* revealed low arginine content (Figure 3). Thus, arginine upregulation may be caused by limiting arginine supply. In the compartment containing *S. thermophilus*, only 0.5% (after 8 h of continuous experiment) of all the analysed peptide-bound amino acids were arginine molecules (Figure 3). In contrast, the arginine fraction of casein represented 3% of the total casein-bound amino acids in a comparable experiment (Figure S12 in Supplementary Materials).

This observation may indicate that either *L. bulgaricus* prefers the release of peptides from casein with low arginine content or that *S. thermophilus* favours the consumption of arginine-containing peptides. In either case, *S. thermophilus* likely faced arginine limitations during co-cultivation with *L. bulgaricus*. This observation supports the findings of previous studies [51,75] where an upregulation of arginine biosynthesis occurred in *S. thermophilus*.

Because 13-C glucose was used as a substrate in the medium, it was possible to distinguish between non-labelled amino acids hydrolysed from casein and 13-C amino acids synthesised from glucose. Measurements of the extracellular medium indicated that alanine, aspartate, tyrosine, and threonine were produced *de novo* from glucose. However, only the alanine pool was enriched with high amounts of 13-C alanine (Figure 6). A higher 13-C alanine concentration was measured in the *L. bulgaricus* compartment than in the compartment containing *S. thermophilus*. Metabolite balancing revealed that *L. bulgaricus* produced 13-C alanine, while *S. thermophilus* consumed 13-C alanine (Figure 6). This supported the hypothesis that *L. bulgaricus* might have an alanine transaminase [49] providing alanine to supply *S. thermophilus* or even serving as a signal molecule for *S. thermophilus* to indicate the presence of *L. bulgaricus*.

5. Conclusions

A new compartmentalised cultivation system was developed and established to unclose strain-specific metabolomics and the subsequent calculation of the production and consumption rates of strains grown in co-culture. This enabled the generation of experimental data for sophisticated models that allow comprehensive insight into cellular processes in co-cultures at a strain-specific level. Although the cultivation system was characterised by the spatial separation of cells, the adequate exchange of molecules, such as peptides and amino acids, was enabled. The experimental setting provided a sufficient volume for comprehensive sampling. The small size of the system reduced the preparation time and cost. However, only anaerobic cultivations were installed, to date. It is noteworthy that fairly similar growth characteristics were achieved in the compartmentalised approach compared to the one-pot co-cultivation approach.

The functionality of the system was demonstrated using an *S. thermophilus*–*L. bulgaricus* co-culture, indicating that both strains released and consumed amino acids. In addition, cultivation was performed using 13-C glucose to quantify amino acid production and consumption rates, as well as the *de novo* biosynthesis of amino acids, indicating alanine transaminase activity in *L. bulgaricus* and exchange with *S. thermophilus*.

This setup allowed the characterisation of interacting microorganisms and clarified the interaction fluxes between them, allowing the rational design of co-cultures. Using the compartmentalised system for the continuous cultivation of co-cultures opens the field for advanced co-culturing; for example, by applying technology for targeted evolution studies.

References

1. West, S.A.; Diggle, S.P.; Buckling, A.; Gardner, A.; Griffin, A.S. The Social Lives of Microbes. *Annu. Rev. Ecol. Evol. Syst.* **2007**, *38*, 53–77. [CrossRef]
2. Lyons, N.A.; Kolter, R. On the Evolution of Bacterial Multicellularity. *Curr. Opin. Microbiol.* **2015**, *24*, 21–28. [CrossRef] [PubMed]
3. D'Souza, G.; Shitut, S.; Preussger, D.; Yousif, G.; Waschina, S.; Kost, C. Ecology and Evolution of Metabolic Cross-Feeding Interactions in Bacteria. *Nat. Prod. Rep.* **2018**, *35*, 455–488. [CrossRef] [PubMed]
4. Bassler, B.L. Small Talk: Cell-to-Cell Communication in Bacteria. *Cell* **2002**, *109*, 421–424. [CrossRef] [PubMed]
5. Ziesack, M.; Gibson, T.; Oliver, J.K.W.; Shumaker, A.M.; Hsu, B.B.; Riglar, D.T.; Giessen, T.W.; Di Benedetto, N.V.; Bry, L.; Way, J.C.; et al. Engineered Interspecies Amino Acid Cross-Feeding Increases Population Evenness in a Synthetic Bacterial Consortium. *mSystems* **2019**, *4*, e00352-19. [CrossRef]
6. Hennig, S.; Rödel, G.; Ostermann, K. Artificial Cell-Cell Communication as an Emerging Tool in Synthetic Biology Applications. *J. Biol. Eng.* **2015**, *9*, 13. [CrossRef]
7. Giri, S.; Shitut, S.; Kost, C. Harnessing Ecological and Evolutionary Principles to Guide the Design of Microbial Production Consortia. *Curr. Opin. Biotechnol.* **2020**, *62*, 228–238. [CrossRef]
8. Kleerebezem, R.; van Loosdrecht, M.C. Mixed Culture Biotechnology for Bioenergy Production. *Curr. Opin. Biotechnol.* **2007**, *18*, 207–212. [CrossRef]
9. Wintermute, E.H.; Silver, P.A. Emergent Cooperation in Microbial Metabolism. *Mol. Syst. Biol.* **2010**, *6*, 407. [CrossRef]
10. Brenner, K.; You, L.; Arnold, F.H. Engineering Microbial Consortia: A New Frontier in Synthetic Biology. *Trends Biotechnol.* **2008**, *26*, 483–489. [CrossRef]
11. Shong, J.; Jimenez Diaz, M.R.; Collins, C.H. Towards Synthetic Microbial Consortia for Bioprocessing. *Curr. Opin. Biotechnol.* **2012**, *23*, 798–802. [CrossRef] [PubMed]
12. McCarty, N.S.; Ledesma-Amaro, R. Synthetic Biology Tools to Engineer Microbial Communities for Biotechnology. *Trends Biotechnol.* **2019**, *37*, 181–197. [CrossRef] [PubMed]
13. Noack, S.; Baumgart, M. Communities of Niche-Optimized Strains: Small-Genome Organism Consortia in Bioproduction. *Trends Biotechnol.* **2018**, *37*, 126–139. [CrossRef]
14. Jones, J.A.; Vernacchio, V.R.; Sinkoe, A.L.; Collins, S.M.; Ibrahim, M.H.A.; Lachance, D.M.; Hahn, J.; Koffas, M.A.G. Experimental and Computational Optimization of an Escherichia Coli Co-Culture for the Efficient Production of Flavonoids. *Metab. Eng.* **2016**, *35*, 55–63. [CrossRef]
15. Zhou, K.; Qiao, K.; Edgar, S.; Stephanopoulos, G. Distributing a Metabolic Pathway among a Microbial Consortium Enhances Production of Natural Products. *Nat. Biotechnol.* **2015**, *33*, 377–383. [CrossRef]
16. Pande, S.; Merker, H.; Bohl, K.; Reichelt, M.; Schuster, S.; De Figueiredo, L.F.; Kaleta, C.; Kost, C. Fitness and Stability of Obligate Cross-Feeding Interactions That Emerge upon Gene Loss in Bacteria. *ISME J.* **2014**, *8*, 953–962. [CrossRef]
17. Zhang, H.; Wang, X. Modular Co-Culture Engineering, a New Approach for Metabolic Engineering. *Metab. Eng.* **2016**, *37*, 114–121. [CrossRef]
18. Tang, Y.J.; Fong, S.S.; Koffas, M.A.; Carr, R.R.; Zha, J.; Roell, G.W. Engineering Microbial Consortia by Division of Labor. *Microb. Cell Fact.* **2019**, *18*, 35. [CrossRef]

19. Giri, S.; Waschina, S.; Kaleta, C.; Kost, C. Defining Division of Labour in Microbial Communities. *J. Mol. Biol.* **2019**, *431*, 4712–4731. [CrossRef]

20. Thommes, M.; Wang, T.; Zhao, Q.; Paschalidis, I.C.; Segrè, D. Designing Metabolic Division of Labor in Microbial Communities. *mSystems* **2019**, *4*, e00263-18. [CrossRef]

21. Xu, P. Dynamics of Microbial Competition, Commensalism, and Cooperation and Its Implications for Coculture and Microbiome Engineering. *Biotechnol. Bioeng.* **2020**, *118*, 199–209. [CrossRef] [PubMed]

22. Germerodt, S.; Bohl, K.; Lück, A.; Pande, S.; Schröter, A.; Kaleta, C.; Schuster, S.; Kost, C. Pervasive Selection for Cooperative Cross-Feeding in Bacterial Communities. *PLoS Comput. Biol.* **2016**, *12*, e1004986. [CrossRef] [PubMed]

23. Lahmann, P.; Reichl, U.; Klamt, S.; Kohrs, F.; Bissinger, T.; Wendschuh, S.; Koch, S.; Benndorf, D. RedCom: A Strategy for Reduced Metabolic Modeling of Complex Microbial Communities and Its Application for Analyzing Experimental Datasets from Anaerobic Digestion. *PLoS Comput. Biol.* **2019**, *15*, e00263-18. [CrossRef]

24. Zengler, K.; Palsson, B.O. A Road Map for the Development of Community Systems (CoSy) Biology. *Nat. Rev. Microbiol.* **2012**, *10*, 366–372. [CrossRef] [PubMed]

25. Branco dos Santos, F.; de Vos, W.M.; Teusink, B. Towards Metagenome-Scale Models for Industrial Applications-the Case of Lactic Acid Bacteria. *Curr. Opin. Biotechnol.* **2013**, *24*, 200–206. [CrossRef] [PubMed]

26. Hanemaaijer, M.; Röling, W.F.M.; Olivier, B.G.; Khandelwal, R.A.; Teusink, B.; Bruggeman, F.J. Systems Modeling Approaches for Microbial Community Studies: From Metagenomics to Inference of the Community Structure. *Front. Microbiol.* **2015**, *6*, 213. [CrossRef] [PubMed]

27. Bajic, D.; Sanchez, A. The Ecology and Evolution of Microbial Metabolic Strategies. *Curr. Opin. Biotechnol.* **2020**, *62*, 123–128. [CrossRef]

28. Somerville, V.; Grigaitis, P.; Battjes, J.; Moro, F.; Teusink, B. Use and Limitations of Genome-Scale Metabolic Models in Food Microbiology. *Curr. Opin. Food Sci.* **2022**, *43*, 225–231. [CrossRef]

29. Wang, X.; Policarpio, L.; Prajapati, D.; Li, Z.; Zhang, H. Developing *E. Coli-E. Coli* Co-Cultures to Overcome Barriers of Heterologous Tryptamine Biosynthesis. *Metab. Eng. Commun.* **2020**, *10*, e00110. [CrossRef]

30. Ferenci, T. Trade-off Mechanisms Shaping the Diversity of Bacteria. *Trends Microbiol.* **2016**, *24*, 209–223. [CrossRef]

31. Bachmann, H.; Molenaar, D.; Branco Dos Santos, F.; Teusink, B. Experimental Evolution and the Adjustment of Metabolic Strategies in Lactic Acid Bacteria. *FEMS Microbiol. Rev.* **2017**, *41*, S201–S219. [CrossRef] [PubMed]

32. Schwentner, A.; Feith, A.; Münch, E.; Busche, T.; Rückert, C.; Kalinowski, J.; Takors, R.; Blombach, B. Metabolic Engineering to Guide Evolution—Creating a Novel Mode for L-Valine Production with Corynebacterium Glutamicum. *Metab. Eng.* **2018**, *47*, 31–41. [CrossRef] [PubMed]

33. Sánchez, Á.; Vila, J.C.C.; Chang, C.-Y.; Diaz-Colunga, J.; Estrela, S.; Rebolleda-Gomez, M. Directed Evolution of Microbial Communities. *Annu. Rev. Biophys.* **2021**, *50*, 323–341. [CrossRef] [PubMed]

34. Zhang, X.; Reed, J.L. Adaptive Evolution of Synthetic Cooperating Communities Improves Growth Performance. *PLoS ONE* **2014**, *9*, e108297. [CrossRef]

35. Konstantinidis, D.; Pereira, F.; Geissen, E.; Grkovska, K.; Kafkia, E.; Jouhten, P.; Kim, Y.; Devendran, S.; Zimmermann, M.; Patil, K.R. Adaptive Laboratory Evolution of Microbial Co-Cultures for Improved Metabolite Secretion. *Mol. Syst. Biol.* **2021**, *17*, e10189. [CrossRef]

36. Zamboni, N. 13C Metabolic Flux Analysis in Complex Systems. *Curr. Opin. Biotechnol.* **2011**, *22*, 103–108. [CrossRef]

37. Gebreselassie, N.A.; Antoniewicz, M.R. 13C-Metabolic Flux Analysis of Co-Cultures: A Novel Approach. *Metab. Eng.* **2015**, *31*, 132–139. [CrossRef]

38. Ghosh, A.; Nilmeier, J.; Weaver, D.; Adams, P.D.; Keasling, J.D.; Mukhopadhyay, A.; Petzold, C.J.; Martín, H.G. A Peptide-Based Method for 13C Metabolic Flux Analysis in Microbial Communities. *PLoS Comput. Biol.* **2014**, *10*, e1003827. [CrossRef]

39. Wijaya, A.W.; Ulmer, A.; Hundsdorfer, L.; Verhagen, N.; Teleki, A.; Takors, R. Compartment-Specific Metabolome Labeling Enables the Identification of Subcellular Fluxes That May Serve as Promising Metabolic Engineering Targets in CHO Cells. *Bioprocess Biosyst. Eng.* **2021**, *44*, 2567–2578. [CrossRef]

40. Stevens, K.A.; Jaykus, L.A. Bacterial Separation and Concentration from Complex Sample Matrices: A Review. *Crit. Rev. Microbiol.* **2004**, *30*, 7–24. [CrossRef]

41. Even, S.; Lindley, N.D.; Cocaign-Bousquet, M. Transcriptional, Translational and Metabolic Regulation of Glycolysis in Lactococcus Lactis Subsp. Cremoris MG 1363 Grown in Continuous Acidic Cultures. *Microbiology* **2003**, *149*, 1935–1944. [CrossRef] [PubMed]

42. Goers, L.; Freemont, P.; Polizzi, K.M. Co-Culture Systems and Technologies: Taking Synthetic Biology to the next Level. *J. R. Soc. Interface* **2014**, *11*, 20140065. [CrossRef] [PubMed]

43. Burmeister, A.; Hilgers, F.; Langner, A.; Westerwalbesloh, C.; Kerkhoff, Y.; Tenhaef, N.; Drepper, T.; Kohlheyer, D.; von Lieres, E.; Noack, S.; et al. A Microfluidic Co-Cultivation Platform to Investigate Microbial Interactions at Defined Microenvironments. *Lab Chip* **2019**, *19*, 98–110. [CrossRef] [PubMed]

44. Burmeister, A.; Grünberger, A. Microfluidic Cultivation and Analysis Tools for Interaction Studies of Microbial Co-Cultures. *Curr. Opin. Biotechnol.* **2020**, *62*, 106–115. [CrossRef]

45. Hesselman, M.C.; Odoni, D.I.; Ryback, B.M.; de Groot, S.; van Heck, R.G.A.; Keijsers, J.; Kolkman, P.; Nieuwenhuijse, D.; van Nuland, Y.M.; Sebus, E.; et al. A Multi-Platform Flow Device for Microbial (Co-) Cultivation and Microscopic Analysis. *PLoS ONE* **2012**, *7*, e36982. [CrossRef]

46. Hyun, J.K.; Boedicker, J.Q.; Jang, W.C.; Ismagilov, R.F. Defined Spatial Structure Stabilizes a Synthetic Multispecies Bacterial Community. *Proc. Natl. Acad. Sci. USA* **2008**, *105*, 18188–18193. [CrossRef]

47. Pörtner, R.; Märkl, H. Dialysis Cultures. *Appl. Microbiol. Biotechnol.* **1998**, *50*, 403–414. [CrossRef]

48. Courtin, P.; Monnet, V.; Rul, F. Cell-Wall Proteinases PrtS and PrtB Have a Different Role in *Streptococcus thermophilus/Lactobacillus bulgaricus* Mixed Cultures in Milk. *Microbiology* **2002**, *148*, 3413–3421. [CrossRef]

49. Liu, E.; Zheng, H.; Hao, P.; Konno, T.; Yu, Y.; Kume, H.; Oda, M.; Ji, Z.S. A Model of Proteolysis and Amino Acid Biosynthesis for Lactobacillus Delbrueckii Subsp. Bulgaricus in Whey. *Curr. Microbiol.* **2012**, *65*, 742–751. [CrossRef]

50. Liu, E.; Hao, P.; Konno, T.; Yu, Y.; Oda, M.; Zheng, H.; Ji, Z. Amino Acid Biosynthesis and Proteolysis in Lactobacillus Bulgaricus Revisited: A Genomic Comparison. *Sci. Res.* **2012**, *2012*, 61–77.

51. Sieuwerts, S.; Molenaar, D.; Van Hijum, S.A.F.T.; Beerthuyzen, M.; Stevens, M.J.A.; Janssen, P.W.M.; Ingham, C.J.; De Bok, F.A.M.; De Vos, W.M.; Van Hylckama Vlieg, J.E.T. Mixed-Culture Transcriptome Analysis Reveals the Molecular Basis of Mixed-Culture Growth in *Streptococcus thermophilus* and *Lactobacillus bulgaricus*. *Appl. Environ. Microbiol.* **2010**, *76*, 7775–7784. [CrossRef] [PubMed]

52. Pastink, M.I.; Teusink, B.; Hols, P.; Visser, S.; De Vos, W.M.; Hugenholtz, J. Genome-Scale Model of *Streptococcus thermophilus* LMG18311 for Metabolic Comparison of Lactic Acid Bacteria. *Appl. Environ. Microbiol.* **2009**, *75*, 3627–3633. [CrossRef] [PubMed]

53. Rodríguez-Serrano, G.M.; García-Garibay, J.M.; Cruz-Guerrero, A.E.; Gómez-Ruiz, L.D.C.; Ayala-Niño, A.; Castañeda-Ovando, A.; González-Olivares, L.G. Proteolytic System of *Streptococcus thermophilus*. *J. Microbiol. Biotechnol.* **2018**, *28*, 1581–1588. [CrossRef] [PubMed]

54. Markakiou, S.; Gaspar, P.; Johansen, E.; Zeidan, A.A.; Neves, A.R. Harnessing the Metabolic Potential of *Streptococcus thermophilus* for New Biotechnological Applications. *Curr. Opin. Biotechnol.* **2020**, *61*, 142–152. [CrossRef]

55. Alexandraki, V.; Kazou, M.; Blom, J.; Pot, B.; Papadimitriou, K.; Tsakalidou, E. Comparative Genomics of *Streptococcus thermophilus* Support Important Traits Concerning the Evolution, Biology and Technological Properties of the Species. *Front. Microbiol.* **2019**, *10*, 2916. [CrossRef]

56. Hols, P.; Hancy, F.; Fontaine, L.; Grossiord, B.; Prozzi, D.; Leblond-Bourget, N.; Decaris, B.; Bolotin, A.; Delorme, C.; Ehrlich, S.D.; et al. New Insights in the Molecular Biology and Physiology of *Streptococcus thermophilus* Revealed by Comparative Genomics. *FEMS Microbiol. Rev.* **2005**, *29*, 435–463. [CrossRef]

57. Li, S.; Tang, S.; He, Q.; Hu, J.; Zheng, J. Changes in Proteolysis in Fermented Milk Produced by *Streptococcus thermophilus* in Co-Culture with Lactobacillus Plantarum or *Bifidobacterium animalis* Subsp. Lactis during Refrigerated Storage. *Molecules* **2019**, *24*, 3699. [CrossRef]

58. Liu, E.; Zheng, H.; Shi, T.; Ye, L.; Konno, T.; Oda, M.; Shen, H.; Ji, Z.S. Relationship between *Lactobacillus bulgaricus* and *Streptococcus thermophilus* under Whey Conditions: Focus on Amino Acid Formation. *Int. Dairy J.* **2016**, *56*, 141–150. [CrossRef]

59. Letort, C.; Juillard, V. Development of a Minimal Chemically-Defined Medium for the Exponential Growth of *Streptococcus thermophilus*. *J. Appl. Microbiol.* **2001**, *91*, 1023–1029. [CrossRef]

60. Mar, M.J.; Andersen, J.M.; Kandasamy, V.; Liu, J.; Solem, C.; Jensen, P.R. Biotechnology for Biofuels Synergy at Work: Linking the Metabolism of Two Lactic Acid Bacteria to Achieve Superior Production of 2—Butanol. *Biotechnol. Biofuels* **2020**, *13*, 45. [CrossRef]

61. Teusink, B.; Molenaar, D. Systems Biology of Lactic Acid Bacteria: For Food and Thought. *Curr. Opin. Syst. Biol.* **2017**, *6*, 7–13. [CrossRef] [PubMed]

62. Ulmer, A.; Erdemann, F.; Mueller, S.; Loesch, M.; Wildt, S.; Jensen, M.L.; Gaspar, P.; Zeidan, A.A.; Takors, R. Differential Amino Acid Uptake and Depletion in Mono-Cultures and Co-Cultures of *Streptococcus thermophilus* and *Lactobacillus delbrueckii* Subsp. Bulgaricus in a Novel Semi-Synthetic Medium. *Microorganisms* **2022**, *10*, 1771. [CrossRef] [PubMed]

63. Levenspiel, O. Tracer Technology. *J. Chem. Inf. Model.* **2019**, *53*, 1689–1699.

64. Damköhler, G. Einflüsse Der Strömung, Diffusion Und Des Wärmeüberganges Auf Die Leistung von Reaktionsöfen. *Z. Elektroch. Bd.* **1937**, *43*, 1–13.

65. Henderson, J.W.; Brooks, A. Improved Amino Acid Methods Using Agilent ZORBAX Eclipse Plus C18 Columns for a Variety of Agilent LC Instrumentation and Separation Goals. *Agil. Technol.* **2010**, *5990-4547EN*, 1–16.

66. Teleki, A.; Sánchez-Kopper, A.; Takors, R. Alkaline Conditions in Hydrophilic Interaction Liquid Chromatography for Intracellular Metabolite Quantification Using Tandem Mass Spectrometry. *Anal. Biochem.* **2015**, *475*, 4–13. [CrossRef]

67. Rau, M.H.; Gaspar, P.; Jensen, M.L.; Geppel, A.; Neves, A.R.; Zeidan, A.A. Genome-Scale Metabolic Modeling Combined with Transcriptome Profiling Provides Mechanistic Understanding of *Streptococcus thermophilus* CH8 Metabolism. *Appl. Environ. Microbiol.* **2022**, *88*, e00780-22. [CrossRef]

68. Rau, M.H.; Zeidan, A.A. Constraint-Based Modeling in Microbial Food Biotechnology. In *Biochemical Society Transactions*; Portland Press Ltd.: London, UK, 2018; pp. 249–260. [CrossRef]

69. Gottstein, W.; Olivier, B.G.; Bruggeman, F.J.; Teusink, B. Constraint-Based Stoichiometric Modelling from Single Organisms to Microbial Communities. *J. R. Soc. Interface* **2016**, *13*, 20160627. [CrossRef]

70. Arioli, S.; Roncada, P.; Salzano, A.M.; Deriu, F.; Corona, S.; Guglielmetti, S.; Bonizzi, L.; Scaloni, A.; Mora, D. The Relevance of Carbon Dioxide Metabolism in *Streptococcus thermophilus*. *Microbiology* **2009**, *155*, 1953–1965. [CrossRef]

71. Arioli, S.; Monnet, C.; Guglielmetti, S.; Parini, C.; de Noni, I.; Hogenboom, J.; Halami, P.M.; Mora, D. Aspartate Biosynthesis Is Essential for the Growth of *Streptococcus thermophilus* in Milk, and Aspartate Availability Modulates the Level of Urease Activity. *Appl. Environ. Microbiol.* **2007**, *73*, 5789–5796. [CrossRef]

72. Bolotin, A.; Quinquis, B.; Renault, P.; Sorokin, A.; Ehrlich, S.D.; Kulakauskas, S.; Lapidus, A.; Goltsman, E.; Mazur, M.; Pusch, G.D.; et al. Complete Sequence and Comparative Genome Analysis of the Dairy Bacterium *Streptococcus thermophilus. Nat. Biotechnol.* **2004**, *22*, 1554–1558. [CrossRef] [PubMed]

73. Loghmani, S.B.; Zitzow, E.; Koh, G.C.C.; Ulmer, A.; Veith, N.; Großeholz, R.; Rossnagel, M.; Loesch, M.; Aebersold, R.; Kreikemeyer, B.; et al. All Driven by Energy Demand? Integrative Comparison of Metabolism of Enterococcus Faecalis Wildtype and a Glutamine Synthase Mutant. *Microbiol. Spectr.* **2022**, *10*, e02400-21. [CrossRef] [PubMed]

74. Khandelwal, R.A.; Olivier, B.G.; Röling, W.F.M.; Teusink, B.; Bruggeman, F.J. Community Flux Balance Analysis for Microbial Consortia at Balanced Growth. *PLoS ONE* **2013**, *8*, e64567. [CrossRef] [PubMed]

75. Herve-Jimenez, L.; Guillouard, I.; Guedon, E.; Boudebbouze, S.; Hols, P.; Monnet, V.; Maguin, E.; Rul, F. Postgenomic Analysis of *Streptococcus thermophilus* Cocultivated in Milk with *Lactobacillus delbrueckii* Subsp. Bulgaricus: Involvement of Nitrogen, Purine, and Iron Metabolism. *Appl. Environ. Microbiol.* **2009**, *75*, 2062–2073. [CrossRef] [PubMed]

Appendix C

Compartment-specific metabolome labeling enables the identification of subcellular fluxes that may serve as promising metabolic engineering targets in CHO cells

RESEARCH PAPER

Compartment-specific metabolome labeling enables the identification of subcellular fluxes that may serve as promising metabolic engineering targets in CHO cells

Andy Wiranata Wijaya[1] · Andreas Ulmer[1] · Lara Hundsdorfer[1] · Natascha Verhagen[1] · Attila Teleki[1] · Ralf Takors[1]

Abstract

^{13}C labeling data are used to calculate quantitative intracellular flux patterns reflecting in vivo conditions. Given that approaches for compartment-specific metabolomics exist, the benefits they offer compared to conventional non-compartmented ^{13}C flux studies remain to be determined. Using compartment-specific labeling information of IgG1-producing Chinese hamster ovary cells, this study investigated differences of flux patterns exploiting and ignoring metabolic labeling data of cytosol and mitochondria. Although cellular analysis provided good estimates for the majority of intracellular fluxes, half of the mitochondrial transporters, and NADH and ATP balances, severe differences were found for some reactions. Accurate flux estimations of almost all iso-enzymes heavily depended on the sub-cellular labeling information. Furthermore, key discrepancies were found for the mitochondrial carriers v_{AGC1} (Aspartate/Glutamate antiporter), v_{DIC} (Malate/H$^+$ symporter), and v_{OGC} (α-ketoglutarate/malate antiporter). Special emphasis is given to the flux of cytosolic malic enzyme (v_{ME}): it could not be estimated without the compartment-specific malate labeling information. Interesting enough, cytosolic malic enzyme is an important metabolic engineering target for improving cell-specific IgG1 productivity. Hence, compartment-specific ^{13}C labeling analysis serves as prerequisite for related metabolic engineering studies.

Abbreviations

^{13}C MFA	^{13}C metabolic flux analysis
CHO	Chinese hamster ovary
VCD	Viable cell density
PPP	Pentose phosphate pathway
CAC	Citric acid cycle
MID	Mass isotopomer distribution
MPC1/2	Mitochondrial pyruvate carrier
ME	Malic enzyme

Symbols

c_i	pmol L^{-1} Concentration of metabolite i
c_x	cell L^{-1} Viable cell density
dof	[-] Degree of freedom
E	[-] Expected MID measurement data
f_i	[-] Cytosolic fraction of metabolite i
$\mathbf{I}$	[-] Isotopomer distribution vector
$\mathbf{IMM}$	[-] Isotopomer mapping matrices
MID	[-] Mass isotopomer distribution
n	[-] Number of measurement data
O	[-] Observed MID simulation
$\mathbf{p}$	pmol cell^{-1} h^{-1} Vector containing estimated fluxes using mass-isotopomers data
p	[-] Number of fitted parameter
Q_i	pmol L^{-1} h^{-1} Feed-rate of metabolite i
q_i	pmol cell^{-1} h^{-1} Cell-specific rate of exo-metabolite i
$\mathbf{q_m}$	pmol cell^{-1} h^{-1} Vector containing measured extracellular rates
S	[-] Stoichiometric matrix of biochemical network
M	[-] Measurement information matrix

Andy Wiranata Wijaya and Andreas Ulmer were equally contributed for this work (first co-authorship).

✉ Ralf Takors
    ralf.takors@ibvt.uni-stuttgart.de

[1] Institute of Biochemical Engineering, University of Stuttgart, Allmandring 31, 70569 Stuttgart, Germany

| v_j | pmol cell^{-1} h^{-1} Intracellular flux of biochemical reaction j |
| $\mathbf{v}$ | pmol cell^{-1} h^{-1} Vector containing intracellular metabolic fluxes |

Greek symbols

α	[-] Statistical confidence interval
β	[-] Reversibility constant
σ	[-] Measurement standard deviation of MID
Θ	[-] Parameter

Indices

ex	[-] Compartment indication
feed	[-] Feed
in	[-] Compartment indication
i	[-] Compound/metabolite i
j	[-] Biochemical reactions j
meas	[-] Indication for measurement vector
net	[-] Indication for net fluxes
X	[-] Cells/biomass

Introduction

^{13}C metabolic flux analysis (^{13}C MFA) is a key tool for quantitative analysis in systems metabolic engineering. First, applications dealt with prokaryotic cells [1] but the technique was also applied for eukaryotes, such as yeast [2, 3], fungi [4], mammalian [5–8], and plant [9] cells. Among others, prokaryotes and eukaryotes differ in cellular compartmentation, which is particularly important when using ^{13}C MFA. In eukaryotes, compartmentation is essential since each cellular compartment fulfils different functions [10]. Even multi-compartment isozymes exist that serve different purposes. For example, Chinese hamster ovary (CHO) cells comprise cytosolic and mitochondrial malic enzymes (MEs) with different NAD$^+$ and NADP$^+$ regeneration capacities, thereby fulfilling diverse catabolic and anabolic needs [8].

Metabolic compartmentation must be considered when performing ^{13}C MFA [10]. There are two levels of complexity; on the one hand, subcellular metabolic models should be used to enable proper in silico predictions. On the other hand, in vivo compartment-specific metabolome data should be available to allow data-driven studies. Nicolae et al. and Pfizenmaier & Takors provided evidence for the importance of subcellular stoichiometric models for estimating fluxes in CHO cells [11, 12]. Regarding the latter, Matuszczyk et al. [13] applied compartment-specific metabolomics in CHO outlining that cytosolic ATP pools are considerably larger than their mitochondrial counterparts. Later, Junghans et al. [8] continued investigating mitochondrial and cytosolic metabolic patterns under different cultivation conditions. They found that pool sizes differed between cytosol and mitochondria for all conditions.

Given that subcellular metabolomics are very laborious [8, 13] the question arises what differences may occur if ^{13}C flux analysis is based on whole-cell metabolomics instead of compartment-specific measurements. In other words, whether the additional lab-efforts justify the information gain of subcellular studies.

Alternative approaches such as superimposing the patterns of two independent ^{13}C experiments using labeled glucose and labeled glutamine also aim to decipher subcellular flux distributions [6]. However, they rely on glutamine synthase deficient cells whereas the suggested subcellular metabolomics approach may be universally applicable.

Given that labeling dynamics in metabolite pools expressed by the ^{13}C labeling turn-over (τ_{13C}) are a key information for quantifying fluxes, influencing factors may be considered. Two factors, pool size of metabolite i and net labeling flux j through this pool exist [14]. Either factor may change when a system's analysis shifts from simplifying single to realistic multi-compartment analysis. Differences in τ_{13C} may occur originating from individual pool sizes and fluxes inside the compartments. In theory, the same metabolite in different compartment might present a different labeling dynamic providing that the metabolite turn-over time is different. Thus, resulting on a different labeling dynamics (τ_{13C}).

Exploiting the unique subcellular labeling dataset of Junghans et al. [8] this study investigated whether subcellular labeling information is crucial to obtain the correct compartment-specific flux patterns. Flux distributions considering and ignoring subcellular metabolite labeling were performed using CHO as the showcase. This study investigated whether significant differences exist using whole-cell and compartment-specific metabolic information.

Materials and methods

This study was based on published metabolome and ^{13}C isotopologue data [8]. In particular, the ^{13}C dataset covering the first 24 h was used to focus on the exponential growth phase.

Cell culture and experimental set-up

The CHO DP-12 cell line (ATCC® CRL-1445TM) was cultivated in a suspension with TC-42 medium (Xell AG, Bielefeld, Germany) supplemented with 42 mM D-glucose, 6 mM L-glutamine, and 200 mM methotrexate. Precultures were cultivated in pre-sterilized disposable shake flasks (Corning Inc., NY, USA) with culture volume ranging from 125 mL to 1 L at an initial viable cell density (VCD) of 0.4×10^6 cells/mL in a humidified shaking incubator (Infors HT Minitron,

Infors GmbH, Einsbach, Germany) at 37 °C, 150 rpm, and 5% saturated CO_2.

Bioreactor cultivations were performed in a two-fold parallel CellFerm Pro bioreactor system (DASGIP, Eppendorf, Germany) equipped with pitched blade impellers and a process control system. Bioreactor cultivations were started with a VCD of about 0.4×10^6 cells/mL, temperature was set to 37 °C and agitation to 150 rpm. In addition, the dissolved oxygen content was controlled using an amperometric electrode (Mettler-Toledo Inc., Columbus, OH, USA) at 40%. The pH was measured with a conventional pH probe (Mettler-Toledo Inc., Columbus, OH, USA) and maintained at 7.1 using 1 M Na_2CO_3 or CO_2 gassing. Carbon labeling experiments were performed in the same setup using [U-$^{13}C_6$]-D-glucose as a carbon tracer with an average isotopic ratio of 25% [U-$^{12}C_6$]- and 75% [U-$^{13}C_6$]-D-glucose. Experiments were performed as biological duplicates. In addition to carbon labeling experiments, bioreactor cultivations with [U-$^{12}C_6$]-D-glucose were performed using the same conditions for metabolome profiling.

Extracellular and intracellular analytics

VCD was monitored with a 12 h interval with Cedex XS, an offline cell counting system (Innovatis AG, Bielefeld, Germany). Extracellular D-glucose and L-lactate were monitored offline with LaboTRACE, an amperometric biosensor system (Trace Analytics GmbH, Braunschweig, Germany). Extracellular antibody (IgG1) concentrations were measured using ELISA as reported previously [15]. Extracellular amino acid concentrations were quantified with reversed-phase chromatography (Agilent 1200 Series, Agilent Technologies, Waldbronn, Germany) [8].

Sampling for metabolomics was performed using differential fast filtration [8, 13]. Then, processed samples were analyzed regarding metabolome quantification using an Agilent 1200 HPLC system coupled with an Agilent 6410B (Agilent Technologies, Waldbronn, Germany) triple quadrupole mass spectrometer equipped with an electrospray ion source. Analytical sample preparation and methodology were conducted as reported previously [8, 16].

^{13}C metabolic flux analysis

Isotopic non-stationary ^{13}C MFA was performed in MATLAB 2018a (The MathWorks, Inc., MA, USA). Before performing ^{13}C MFA, measured ^{13}C labeling distributions were corrected for natural stable isotope abundances [17]. Parameter optimization was conducted using MATLAB least square optimization *fmincon* function in combination with *GlobalSearch* and *MultiStart* algorithm in a multi-core

computing machine [18]. The first derivative of each isotopomer balance was solved using MATLAB Ordinary Differential Equations *ode15s* solver. The study used the metabolic and carbon-atom transition model in the previous study [8]. Details of the model are indicated in Table S1 (Supplementary Material S1) and are displayed in Fig. 1.

Metabolite balancing

The two-compartment CHO-cell model comprises the stoichiometric matrix S (Supplementary Material S1, Table S1) consisting of m metabolites and n reactions ($m \times n$). The following cell-specific rates [pmol cell^{-1} h^{-1}] were defined: q for cellular uptake and secretion rates, k as inter-compartment transport, and v as compartment-specific reaction. The balance of metabolite i participating in reaction j localized externally, in cytosol, or in mitochondria was described by Eqs. 1 and 2:

$$\frac{d_{C_{i,\text{ex}}}}{dt} = Q_{i,\text{feed}} + q_i c_X, \tag{1}$$

$$\frac{d_{c_{i,\text{in}}}}{dt} = \left(-q_i - k_i + \sum_{j=1}^{n} v_j\right) \cdot c_x = 0, \tag{2}$$

where c_i denotes the concentration of metabolite i [mol L^{-1}], c_x denotes VCD [cell L^{-1}], t denotes time [h], and $Q_{i,\text{feed}}$ denotes the feed-rate of metabolite i [pmol L^{-1} h^{-1}].

The process model describing the batch cultivation is given in Eq. 1 and allows the estimation of q for metabolite i by time-series analysis of extracellular concentrations c_i. Therefore, the metabolic steady-state was defined as mirrored in the constraint $\frac{d_{c,\text{intracellular}}}{dt} = 0$, which is a prerequisite for ^{13}C flux analysis. Both stationary and non-stationary labeling patterns were analyzed, originating from the metabolic steady-state condition.

Metabolic flux analysis

MFA was performed using the metabolic network S considering the following constraints: (i) pool sizes of cytosolic and mitochondrial metabolites were in a steady-state and (ii) the entire system was (over)-determined because of the ample ^{13}C labeling information. Fluxes were estimated according to:

$$v = \begin{pmatrix} S \\ M \end{pmatrix}^{-1} \begin{pmatrix} 0 \\ [\, q_{\text{meas}} \quad p \,] \end{pmatrix}, \tag{3}$$

where M is the measurement matrix containing the stoichiometric coefficients of q_{meas} (measured rates [pmol cell^{-1} h^{-1}]) and p contains the estimated fluxes using mass-isotopomer data [pmol cell^{-1} h^{-1}]).
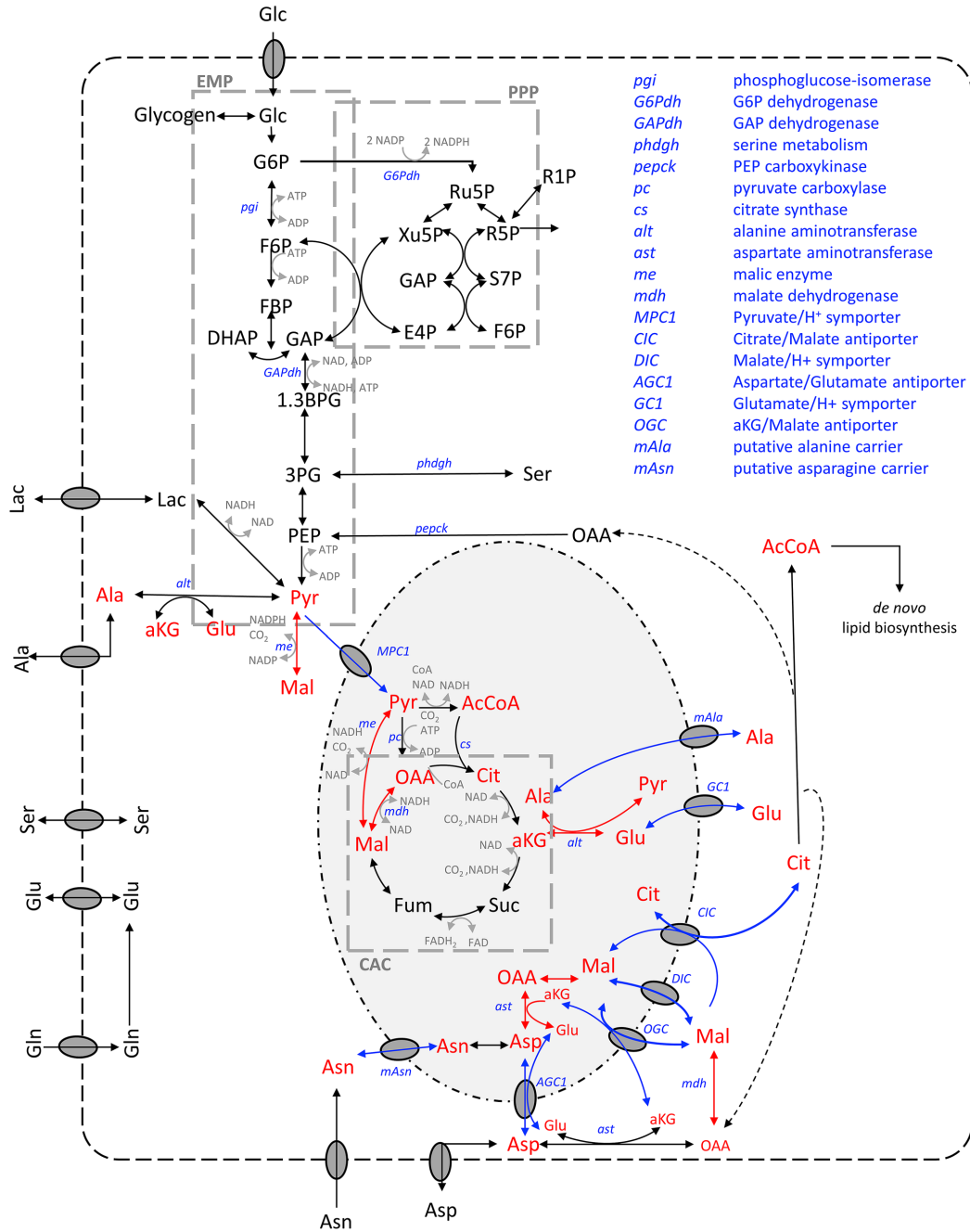
Fig. 1 Metabolic model of CHO cells used in this study (modified figure from Junghans et al. [8]). Arrow coloring indicates the localization of biochemical reactions as follows: black encodes single compartment; red encodes multi-compartments; and blue encodes inter-compartment transporters. In addition, multi-compartment metabolites are indicated in red (color figure online)

Isotopomer balancing and bidirectional reactions

Isotopomer balancing was applied to mathematically describe the incorporation of ^{13}C tracers into intracellular metabolite carbon skeletons [19, 20]. Isotopomer balances for intracellular metabolites are according to Eq. 4:

$$\frac{d(\mathbf{C_i I_i})}{dt} = \sum_{j=1}^{N} \left[\alpha \left(\begin{array}{c} 0 \\ \otimes \\ k=1 \end{array} \left(\sum_{m=1}^{n} \mathbf{IMM}_{k \to m} \right) \mathbf{I}_k \right) r_j + (1-\alpha)(v_i r_j \mathbf{I}_i) \right]$$

with

$$\alpha = \left\{ \begin{array}{l} 1, \text{if} v_{ij} > 0 \\ 0, \text{else} \end{array} \right. ,$$

$$(4)$$

where the isotopomer transition from reactant k to product m is described by $\mathbf{IMM}_{k \to m}$.

Furthermore, Eq. 5 was used to describe labeling dilution by extracellular pools (L-lactate, L-glutamate, L-aspartate, and L-alanine):

$$\frac{d(\mathbf{I}_{i,ex})}{dt} = \frac{1}{c_{i,ex}} \left[\overline{c_X} \left(\vec{q}_{i,ex} \cdot \mathbf{I}_{i,in} - \overleftarrow{q}_{i,ex} \cdot \mathbf{I}_{i,ex} \right) - \frac{dc_{i,ex}}{dt} \mathbf{I}_{i,ex} \right]$$

with

$$\vec{q}_{i,ex} = \beta_i \cdot q_{i,ex}^{net}$$

$$\overleftarrow{q}_{i,ex} = \vec{q}_{i,ex} - q_{i,ex}^{net}.$$

$$(5)$$

Exchange fluxes were defined for each reversible biochemical reaction [21, 22] according to Eq. 6:

$$\vec{v}_j = \beta_j \cdot v_j^{net}$$

$$\overleftarrow{v}_j = \vec{v}_j - v_j^{net}.$$

$$(6)$$

Parameter estimation and uncertainty

Parameter (flux) estimation was achieved by fitting the simulated mass isotopomer distribution (MID) to the measured in vivo MID as presented in Eq. 7:

$$\min f(\Phi) = \sum \left(\frac{MID_i^{sim} - MID_i^{exp}}{\sigma_i} \right)^2.$$

$$(7)$$

Cytosolic and mitochondrial MIDs were defined for subcellular studies. Non-compartmented analysis considered that no subcellular measurements were available. Instead, only entire cell labeling patterns should exist. Consequently, compartment-specific information was merged again, applying Eq. 8:

$$MID_i^{comb} = MID_i^{cyt} \cdot f + MID_i^{mit} \cdot (1-f),$$

$$(8)$$

where f denotes the molar fraction of metabolite i in the cytosol. During simulations, f was treated as an optimization parameter for those metabolites presented in both compartments; pyruvate, citrate, α-ketoglutarate, malate, alanine, aspartate, asparagine, and glutamine. Accordingly, f serves as an alternate indicator for the importance of considering compartments properly. Furthermore, flux estimation was achieved by fitting the measured non-compartment metabolome data with calculated MID using Eq. 9:

$$\min f(\Phi) = \sum \left(\frac{MID_i^{comb} - MID_i^{exp}}{\sigma_i} \right)^2.$$

$$(9)$$

A χ^2 statistical test was used to assess goodness of fit as described in Eq. 10:

$$\chi^2 = \sum \frac{\left(x^{sim} - x^{exp} \right)^2}{\sigma^2}$$

$$dof = (n-p)$$

$$\chi^2 \leq \chi^2_{(1-\alpha),dof}.$$

$$(10)$$

Parameter uncertainty is essential to evaluate the flux differences including versus excluding compartment-specific data. Conventional parameter uncertainty estimates make use of the local calculation of the Jacobian matrix as a linearized proxy for variance. However, this approach only shows poor performance if a complex and non-linear set of equations should be analyzed, as it is the case in this ^{13}C MFA study. Thus, confidence intervals of each parameter (fluxes) were estimated using the Chi-squared (χ^2) statistics, which works best for non-linear equations as demonstrated by Antoniewicz et al. [23]. The method relies on the assumption that the minimized variance-weighted sum of squared residuals is χ^2 distributed. Thus, the residual difference evaluating the global optimum and fixing one parameter is χ^2 distributed with one degree of freedom.

Statistical analysis

The significant differences between the two analyses were assessed using Welch's t-test for unequal variances [24].

Results

Prior to the ^{13}C MFA studies, a metabolic network model was formulated (Supplementary Material S1). First the structural identifiability and calculability of the network was assessed applying well established methodologies (Supplementary Material S4). Next, the identifiability of distinct
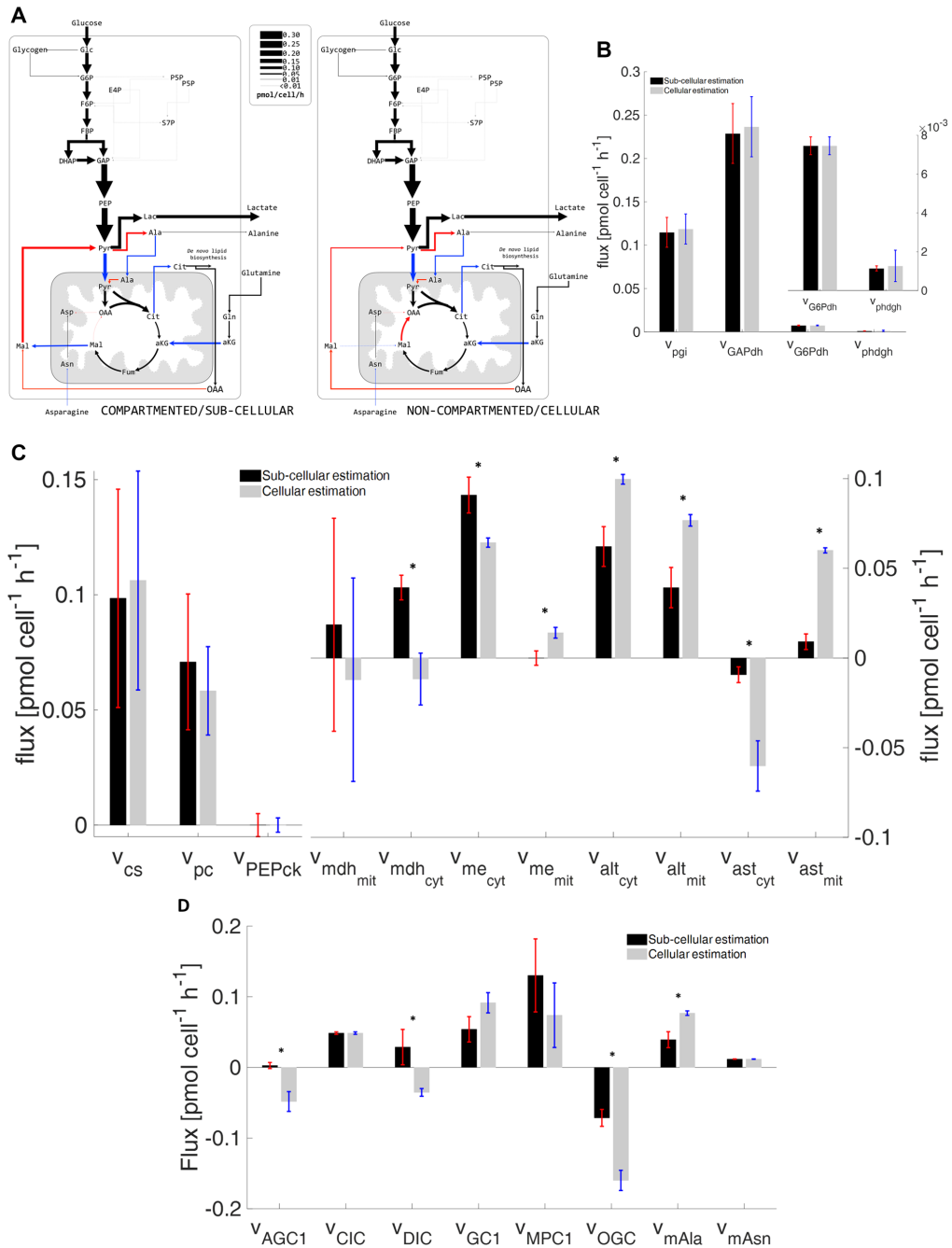
◄**Fig. 2** **A** Intracellular flux distribution estimated using compartment-specific (left) and non-compartmented data (right); **B** fluxes of biochemical reactions involving single-compartment metabolites; **C** fluxes of biochemical reactions involving multi-compartment metabolites; and **D** mitochondrial carrier fluxes estimated with compartment-specific and non-compartmented data (* indicates significance $p < 0.05$)

fluxes was checked by simulating intracellular ^{13}C labeling patterns assuming pool sizes measured by Junghans et al. [8]. Results presented in the Supplementary Material S4 indicate the good identifiability of intracellular fluxes which motivated us to continue the study by analyzing real labeling patterns and flux distributions.

In the study by Junghans et al. [8] CHO-DP12 cells were cultivated in a bioreactor to investigate three distinct growth scenarios; (I) exponential growth with no (carbon and nitrogen) limitation; (II) moderate growth with L-glutamine depletion and L-asparagine saturation; and (III) stationary phase with severe nitrogen limitation. However, the current study regarding the impact of subcellular ^{13}C data only covers the exponential growth phase during the first 24 h. This period is typically investigated in vitro because labeling and cultivation conditions can be controlled easily, giving accurate results regarding flux distributions and cell-specific productivities [5, 7]. Furthermore, additional cultivation study data investigating the same cell line and process conditions was used for broadening the data set of subcellular versus cellular ^{13}C metabolomics for flux analysis (see Supplementary Material S6). The summary of all estimated intracellular fluxes is provided in Supplementary Material S2.

Cell growth and carbon labeling studies

During the exponential growth phase, cells grew with 0.025 ± 0.001 h^{-1}. Carbon and nitrogen sources were constantly consumed, and metabolic byproducts were steadily released with constant specific rates (Supplementary Material S1, Table S2). D-Glucose was consumed as a major carbon source while L-glutamine and L-asparagine served as primary nitrogen sources. In addition, the Warburg effect [25] was observed, showing a glucose-to-lactate ratio of 0.93 mol$_{D-glucose}$/mol$_{L-lactate}$. ^{13}C carbon labeling was introduced by the addition of 75% [U-^{13}C$_6$]-D-glucose after 2.5 days, revealing no phenotypic changes, i.e., no alterations of cellular metabolism.

^{13}C metabolic flux analysis using compartment-specific metabolome data

^{13}C MFA was performed using compartment-specific metabolome data reflecting subcellular pools of cytosol and mitochondria together with isotopomer profiles of the said compartments. Flux estimations were performed at least 100 times with randomized input values and rational boundary values for each parameter (Supplementary Material S2). Finally, the chi-square tests achieved 228.87, which served the statistical constraint of 232.92 on a 95% significance level.

Glycolysis and PPP

High glycolytic (0.112 ± 0.017 pmol cell^{-1} h^{-1} of hexokinase) and extremely low PPP fluxes (0.008 ± 0.001 pmol cell^{-1} h^{-1} of G6P dehydrogenase) were found. The latter accounted for 6.68% of the D-glucose consumed. These observations are in agreement with the findings of Ahn & Antoniewicz [5], who performed ^{13}C MFA in adherent CHO-K1 cells. In addition, approximately 15% (0.016 ± 0.002 pmol cell^{-1} h^{-1}) of intracellular G6P was continuously in exchange with endogenous glycogen.

In vivo mitochondrial shuttle

Glycolytic carbon fueled into mitochondria via two transport mechanisms; 77% entered via the mitochondrial pyruvate carrier (MPC1/2) and 23% via a putative L-alanine transporter. MPC1/2 showed the highest mitochondrial transport activities while other transporters exchanged compounds for different purposes; (i) mitochondrial citrate carrier (citrate/malate antiporter; 0.049 ± 0.002 pmol cell^{-1} h^{-1}) served as a citrate exporter to provide cytosolic acetyl-CoA for the de novo lipid biosynthesis pathway; (ii) the malate-aspartate shuttle comprising 2-oxoglutarate carrier (α-ketoglutarate/mal antiporter) and aspartate-glutamate carrier (aspartate/glutamate antiporter), which is often described as an indirect NADH shuttle because imported malate is oxidized to oxaloacetate, releasing NADH, fulfilled a different function; malate was net exported from mitochondria to fuel cytosolic ME.

Cytosolic malic enzyme and NADPH production

NADPH is a key electron donor for anabolic pathways and is essential for monoclonal antibody biosynthesis. Ahn & Antoniewicz, Templeton et al. [5, 7] suggested MEs as key NADPH producers in CHO cells. This hypothesis was further confirmed via compartment-specific flux analysis by Junghans et al. [8]. Cytosolic ME (ME$_{cyt}$) was identified as

the primary provider serving NADPH needs. Compartment-specific ^{13}C MFA estimated that about 86% of the NADPH requirement was fulfilled by ME_{cyt} (0.09 ± 0.01 pmol cell^{-1} h^{-1}).

^{13}C Metabolic flux analysis using non-compartmented metabolome data

An additional ^{13}C MFA was performed to investigate the importance of distinct sub-cellular information to elucidate proper in vivo subcellular flux patterns. Analyzing the merged data (Eq. 6) via ^{13}C MFA yielded a Chi-squared value of 140.12 on the 95% confidence level, which was accepted as a good fit (with 154.30 as the χ^2 statistical threshold on 95% confidence interval).

This study was performed using the same model consisting of 42 intracellular biochemical reactions. Figure 2A provides the comparison of intracellular flux distributions estimated with (left) and without (right) sub-cellular information (Fig. 2A). The related single-compartment key fluxes and iso-enzymatic rates are depicted as bar plots in Fig. 2B, C. Notably, the term 'iso enzymes' encodes fluxes connecting the same substrates and products but localized in different compartments.

Biochemical reactions localized in a single compartment

Figure 2B, C left shows fluxes of biochemical reactions that exist in one compartment (cytosol or mitochondria) only. Most of them revealed similar results irrespective of whether compartment-specific information was used (black) or not (gray). Figure 2B demonstrates the case the metabolome pools and the respective fluxes were the same for both studies, yielding a similar τ_{13C}. This is also true for citrate synthase v_{CS}, although identifiability was poor. Similar results were observed for cytosolic-based reactions: pyruvate carboxylase (v_{pc}) and PEP carboxykinase (v_{pepck}) (Fig. 2C). These single-compartment reactions possessed the particularity of utilizing the same metabolites but in different compartments (Fig. 1). In this particular case, no statistically sound difference between v_{pc} and v_{pepck} was found, most likely because compartment-specific OAA values lacked.

Iso-enzymatic reactions localized in different compartments

Special emphasis is laid on the so-called iso-enzymatic reactions of Fig. 2C right that catalyze similar conversions in different compartments. The fluxes of malate dehydrogenase (v_{mdh}), ME (v_{me}), aspartate amino-transferases (v_{ast}), and alanine amino-transferases (v_{alt}) are localized in cytosol

and mitochondria, respectively. Of the eight iso-enzymes analyzed, seven conversion rates were significantly different. The only exception is the mitochondrial malate dehydrogenase ($v_{mdh,mit}$) which revealed statistical similarity although fluxes even reversed. On contrary, the cytosolic malate dehydrogenase ($v_{mdh,cyt}$) also disclosed flux reversion but with a sound statistical identifiability.

Non-compartmented data were not able to properly reflect real fluxes of the amino-transferases (v_{ast}), namely alanine amino-transferases (v_{alt}) and aspartate amino transferases (v_{ast}). The analysis of whole-cell data resulted in flux over-estimation compared to compartment-specific analysis. Notably, the substrate aspartate occurred in cytosol and mitochondria and is a key player of the aspartate-malate shuttle. Moreover, alanine was involved in the co-transport of glycolytic carbon into mitochondria with the MPC1/2. In this case, proper localization and labeling information of the compound is key to estimate fluxes correctly.

In addition, severe bias was observed for fluxes of both malic enzymes (v_{me}) as displayed in Fig. 2C right. By trend, ^{13}C flux estimations using non-compartmented data identified significantly lower (about 30%) cytosolic $v_{me,cyt}$ than the non-compartmented data. Regarding mitochondria, the opposite was found. The finding for v_{me} using non-compartmented data is consistent with the observations of Ahn & Antoniewicz, Templeton et al. [5, 7] who also performed ^{13}C MFA with cellular data. Importantly, cytosolic ME activity via $v_{me,cyt}$ was identified as a key supplier for NADPH needed for IgG production in CHO cells (Junghans et al. [8]).

Mitochondrial metabolite carriers

Comparing shuttle activities using sub-cellular and cellular labeling information reveals significant differences for half of the inter-compartment transporters, namely the aspartate/glutamate antiporter (v_{AGC1}), malate carrier (v_{DIC}), α-ketoglutarate/malate antiporter (v_{OGC}), and the putative alanine carrier (v_{mAla}) (Fig. 2D). Similar to the identification of aspartate amino-transferases, the proper identification of v_{AGC1} depends on the labeling turnover τ_{13C} of Asp in both compartments. Missing compartment-specific measurements lead to the different shuttle fluxes, which are also reflected in the biased flux v_{ast}. The same scenario also holds true for the putative alanine carrier (v_{mAla}) and the corresponding reactions (alanine amino-transferases; v_{alt}). Shuttle estimations regarding v_{DIC} and v_{OGC} using non-compartment-specific data contradict flux calculations using compartment-specific information estimation. The sub-cellular labeling information of malate is essential to get accurate flux estimates. Interestingly, the flux estimation of putative asparagine carrier (v_{mAsn}) was not biased by the use of whole-cell labeling data only. This may reflect that v_{mAsn} heavily depends on the

Table 1 Complete list of estimated and measured cytosolic fractions of subcellular metabolites used for 13C MFA

Metabolites	Cytosolic fraction (f)		
	Estimated	Measurement (Junghans et al. [8])	% difference (measurement as the reference value)
Mal	0.100	0.829	87.9
Pyr	0.910	0.838	8.59
aKG	0.100	0.714	85.99
Cit	0.995	0.489	103.48
Glu	0.373	0.827	54.90
Ala	0.100	0.840	88.1
Asn	0.717	0.805	10.48
Asp	0.500	0.809	38.20

measured L-asparagine uptake rate (q_{Asn}) irrespective of the existence of additional subcellular information.

Estimated cytosol–mitochondrial fraction (f factor)

Using Eq. 8, f factors were estimated for each metabolite and compared with the measurements of Junghans et al. [8] (Table 1). As indicated, all estimated cytosolic fractions (f) were poorly identified with pyruvate showing the smallest difference of 8.59% only. On average, 59.71% difference was found compared to the real labeling fraction. Notably, the best estimates of pyruvate and asparagine also enabled improved flux values for the corresponding biochemical reactions, e.g. $v_{MPC1/2}$, v_{pdh} for pyruvate, and v_{asns}, v_{mAsn} for asparagine.

Cellular NADH and NADPH production

Table 2 shows a comparison of NADH and NADPH production via compartment-specific analysis and neglection of sub-cellular data.

Neglecting sub-cellular data, NADPH production is underestimated by approximately 25%. This reflects the 30% underestimation of cytosolic v_{ME} when cellular and not subcellular data are used. In the case of NADH and ATP, the utilization of different datasets disclosed only minor

Table 2 Comparison of NADH, ATP, and NADPH net production rates in compartment-specific analysis and whole-cell analysis (values presented in pmol cell^{-1} h^{-1})

	NADH	ATP	NADPH
Compartment-specific	0.55692	0.22752	0.10577
Non-compartmented	0.60815	0.25914	0.07924

differences. NADH and ATP fluxes were overestimated by 9% and 14% for non-compartmented data, respectively.

Challenging the key statements by an additional data set

To investigate whether or not the observed flux characteristics may be specific for the data sets used, additional data of cultivations with the same cell line, cultivation conditions, and analytical tools was used. Figure S6-1:S6-3 (Supplementary Material S6) outlines that very similar key messages are obtained analyzing the new data set: Glycolytic fluxes are fairly similar irrespective whether subcellular or cellular ^{13}C metabolomics is used. On contrary, fluxes for cytosolic malate dehydrogenase and malic enzyme differ statistically significant depending on the granularity of metabolic labeling resolution. The same holds true for shuttle activities such as DIC, GC1, and OGC which is in agreement with the results derived from the other data sets.

Discussion

This study challenges the information gain when performing ^{13}C MFA with compartment-specific metabolome data compared to exploiting cellular labeling information not distinguishing between cytosol and mitochondria.

Figure 2 outlines the complexity of the interactions. A group of fluxes (v_{pgi}, v_{GAPdh} v_{G6Pdh}, and v_{phdgh}) located in a single compartment (here: cytosol) disclose equal values irrespective of the analytical approach selected. Interestingly, this also holds true for v_{cs}, located in mitochondria, primarily due to poor flux identifiability. Furthermore, v_{pepck} and v_{pc} revealed such high flux variances that no distinction could be found whether cellular or subcellular ^{13}C data were used. Apparently, both reactions depend on cytosolic (OAA$_{cyt}$) and mitochondrial oxaloacetate (OAA$_{mit}$). They act at the interphase of the two compartments and rely on proper sub-cellular measurement information (τ_{13C}) for correct identification. Distinct OAA measurements were not available in the current study due to challenging analytical access to the compound. Accordingly, flux estimations might be biased by the quality of OAA pool estimations.

In addition, some other fluxes should be interpreted with great care, too. This holds particularly true for mitochondrial malate dehydrogenase ($v_{mdh,mit}$) and the pyruvate carrier v_{MPC1}. Both disclose large error bars rendering a discrimination between cellular versus subcellular approaches hardly possible (Fig. 2C, D). Flux imprecisions reflect the lack of reliable CO$_2$ evolution rates (q_{CO_2}) and CO$_2$ labeling profiles.

The whole-cell (cellular) flux estimation failed to estimate the mitochondrial and cytosolic fluxes of the aminotransferases v_{alt} and v_{ast}. This may reflect that those fluxes

Fig. 3 Cell-specific production of monoclonal antibodies in CHO cells (modified from Junghans et al. [8])
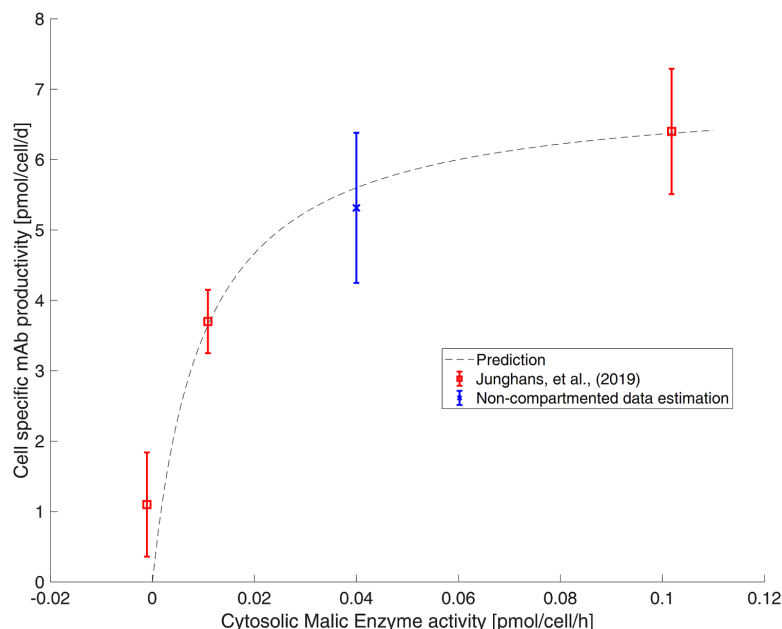
heavily depend on the compartment-specific labeling information of alanine and aspartate. Not providing this information by using whole-cell labeling data leads to the large discrepancies given in Fig. 2C.

Almost all mitochondrial carrier fluxes were poorly estimated when using non-compartmented data. Inaccurate estimations of v_{AGC1} and v_{mAla} are also reflected by the results of v_{ast} and v_{alt}. In addition, the poor estimation of the malate carriers v_{DIC} and v_{OGC} depended on v_{me}. In general, fluxes of transporters and bioreactions heavily relied on the labeling dynamics measured in the related metabolites. Regarding v_{MPC1}, the reduced shuttle activity based on non-compartmented data reflects the missing malate exported into cytosol (Fig. 2D).

To check whether the additional use of labeled glutamine [6] might have achieved similar subcellular flux resolutions as the compartment-specific analysis, simulations were performed using [U-^{13}C$_5$]-L-glutamine (Supplementary Material S3). Interestingly, without information about compartment-specific metabolomics, cytosolic ^{13}C signals obtained from simulations are pretty similar to those of the whole-cell. This is mainly due to the relatively low information gain with respect to the key mitochondrial metabolites malate and aspartate. Compartment-specific labeling information and turnover of the latter are decisive to resolve activities of mitochondrial transporters.

In general, most of the flux estimations using either non-compartmented or compartmented data led to similar values. Even global cell qualifications, such as rates of total ATP formation and NADH production, were similar. However, two main findings should be considered:

1. Often, cellular analysis achieved similar flux estimations as subcellular studies by fitting measured cytosolic labeling fractions for the sake of estimating pool sizes properly (Table 1). In other words, flux optimization algorithms adapted cytosolic and mitochondrial pool sizes to complement missing labeling information. However, the simulated pool size readouts were strongly misleading.
2. Among the fluxes with the largest discrepancies is the cytosolic ME v_{me}. Remarkably, this flux was found to be a promising metabolic engineering target to maximize the formation of heterologous proteins by improved NADPH supply [8]. Accordingly, exact estimation is a prerequisite for proper strain engineering. Figure 3 illustrates that even the result of non-compartment data analysis still fits to the subcellular kinetics published in Junghans et al. [8]. Whether or not experimentalists may have identified this enzyme as a metabolic engineering target remains open and is a matter of qualitative discussion rather than quantitative target identification [8].

To date, the compartment-specific analytical approach has shown its suitability for multiple metabolomic studies

investigating CHO cells under in vivo-like conditions [8, 15, 24–30]. The latter is enabled by fast and standardized metabolism inactivation. Furthermore, data quality essentially relies on the quantitative access to internal standards, such as G6P/F6P (in cytosolic space) and *cis*-aconitate (in mitochondrion) to correct for mitochondrial leakage. In general, fast metabolic inactivation, standardized sample processing and use of internal standards are prerequisites for any compartment-specific metabolomics approach that might be used in future applications.

Conclusions

Investigating the need for using subcellular ^{13}C labeling data, the study revealed that non-compartmented data enabled to identify most fluxes involving single compartment metabolites. Besides, half of the mitochondrial shuttle fluxes and global properties, such as ATP and NADH formation, were fairly well estimated without requiring further subcellular labeling information. However, there is a number of sensitive fluxes that could only be identified properly if compartment-specific pool information was used. Among those were mitochondrial shuttles that rely on alanine, aspartate and malate. Furthermore, key metabolic engineering targets, such as the cytosolic ME flux for NADPH formation, were severely underestimated using (total) cellular data. This may disguise their role as promising metabolic engineering target if non-compartmented pool analysis is performed, only. The finding underlines the necessity to apply subcellular data for flux estimation, not only to quantify cytosolic/mitochondrial shuttle activities but also to identify metabolic engineering targets and obtain valid values for real pool sizes.

Declarations

Conflict of interest The authors declare no financial or commercial conflict of interest.

References

1. Wiechert W (2001) ^{13}C metabolic flux analysis. Metab Eng 3(3):195–206
2. Frick O, Wittmann C (2005) Characterization of the metabolic shift between oxidative and fermentative growth in *Saccharomyces cerevisiae* by comparative 13C flux analysis. Microb Cell Fact 4(1):1–16
3. van Winden WA, van Dam JC, Ras C, Kleijn RJ, Vinke JL, van Gulik WM, Heijnen JJ (2005) Metabolic-flux analysis of *Saccharomyces cerevisiae* CEN. PK113–7D based on mass isotopomer measurements of 13C-labeled primary metabolites. FEMS Yeast Res 5(6–7):559–568
4. Zhao Z, Kuijvenhoven K, Ras C, van Gulik WM, Heijnen JJ, Verheijen PJ, van Winden WA (2008) Isotopic non-stationary ^{13}C gluconate tracer method for accurate determination of the pentose phosphate pathway split-ratio in *Penicillium chrysogenum*. Metab Eng 10(3–4):178–186
5. Ahn WS, Antoniewicz MR (2011) Metabolic flux analysis of CHO cells at growth and non-growth phases using isotopic tracers and mass spectrometry. Metab Eng 13(5):598–609
6. Ahn WS, Antoniewicz MR (2013) Parallel labeling experiments with [1,2–^{13}C] glucose and [U-^{13}C] glutamine provide new insights into CHO cell metabolism. Metab Eng 15:34–47
7. Templeton N, Dean J, Reddy P, Young JD (2013) Peak antibody production is associated with increased oxidative metabolism in an industrially relevant fed-batch CHO cell culture. Biotechnol Bioeng 110(7):2013–2024
8. Junghans L, Teleki A, Wijaya AW, Becker M, Schweikert M, Takors R (2019) From nutritional wealth to autophagy: *in vivo* metabolic dynamics in the cytosol, mitochondrion and shuttles of IgG producing CHO cells. Metab Eng 54:145–159
9. Allen DK, Shachar-Hill Y, Ohlrogge JB (2007) Compartment-specific labeling information in ^{13}C metabolic flux analysis of plants. Phytochemistry 68(16–18):2197–2210
10. Ahn WS, Antoniewicz MR (2012) Towards dynamic metabolic flux analysis in CHO cell cultures. Biotechnol J 7(1):61–74. https://doi.org/10.1002/biot.201100052
11. Nicolae A, Wahrheit J, Bahnemann J, Zeng AP, Heinzle E (2014) Non-stationary ^{13}C metabolic flux analysis of Chinese hamster ovary cells in batch culture using extracellular labeling highlights metabolic reversibility and compartmentation. BMC Syst Biol 8(1):50
12. Pfizenmaier J, Takors R (2017) Host organisms: mammalian cells. In: Industrial biotechnology, vol 2. pp 643–671
13. Matuszczyk JC, Teleki A, Pfizenmaier J, Takors R (2015) Compartment-specific metabolomics for CHO reveals that ATP pools in mitochondria are much lower than in cytosol. Biotechnol J 10(10):1639–1650
14. Buescher JM, Antoniewicz MR, Boros LG, Burgess SC, Brunengraber H, Clish CB et al (2015) A roadmap for interpreting ^{13}C metabolite labeling patterns from cells. Curr Opin Biotechnol 34:189–201

15. Pfizenmaier J, Matuszczyk JC, Takors R (2015) Changes in intracellular ATP-content of CHO cells as response to hyperosmolality. Biotechnol Prog 31(5):1212–1216

16. Teleki A, Sánchez-Kopper A, Takors R (2015) Alkaline conditions in hydrophilic interaction liquid chromatography for intracellular metabolite quantification using tandem mass spectrometry. Anal Biochem 475:4–13

17. Fernandez CA, Des Rosiers C, Previs SF, David F, Brunengraber H (1996) Correction of ^{13}C mass isotopomer distributions for natural stable isotope abundance. J Mass Spectrom 31(3):255–262

18. Agnarsson J, Sunde M, Ermilova I (2013) Parallel optimization in MATLAB. Project in Computational Science Report

19. Wiechert W, de Graaf AA (1997) Bidirectional reaction steps in metabolic networks: I. Modeling and simulation of carbon isotope labeling experiments. Biotechnol Bioeng 55(1):101–117

20. Schmidt K, Carlsen M, Nielsen J, Villadsen J (1997) Modeling isotopomer distributions in biochemical networks using isotopomer mapping matrices. Biotechnol Bioeng 55(6):831–840

21. Hofmann U, Maier K, Niebel A, Vacun G, Reuss M, Mauch K (2008) Identification of metabolic fluxes in hepatic cells from transient 13C-labeling experiments: Part I. Experimental observations. Biotechnol Bioeng 100(2):344–354

22. Schaub J, Mauch K, Reuss M (2008) Metabolic flux analysis in *Escherichia coli* by integrating isotopic dynamic and isotopic stationary 13C labeling data. Biotechnol Bioeng 99(5):1170–1185

23. Antoniewicz MR, Kelleher JK, Stephanopoulos G (2006) Determination of confidence intervals of metabolic fluxes estimated from stable isotope measurements. Metab Eng 8(4):324–337

24. Welch BL (1947) The generalization of student's' problem when several different population variances are involved. Biometrika 34(1/2):28–35

25. Warburg O (1956) On the origin of cancer cells. Science 123(3191):309–314

26. Pfizenmaier J, Junghans L, Teleki A, Takors R (2016) Hyperosmotic stimulus study discloses benefits in ATP supply and reveals miRNA/mRNA targets to improve recombinant protein production of CHO cells. Biotechnol J 11(8):1037–1047

27. Becker M, Junghans L, Teleki A, Bechmann J, Takors R (2019) The less the better: how suppressed base addition boosts production of monoclonal antibodies with Chinese Hamster Ovary cells. Front Bioeng Biotechnol 7:76

28. Becker M, Junghans L, Teleki A, Bechmann J, Takors R (2019) Perfusion cultures require optimum respiratory ATP supply to maximize cell-specific and volumetric productivities. Biotechnol Bioeng 116(5):951–960

29. Verhagen N, Wijaya AW, Teleki A, Fadhlullah M, Unsöld A, Schilling M et al (2020) Comparison of ʟ-tyrosine containing dipeptides reveals maximum ATP availability for ʟ-prolyl-ʟ-tyrosine in CHO cells. Eng Life Sci 20(9–10):384–394

30. Verhagen N, Teleki A, Heinrich C, Schilling M, Unsöld A, Takors R (2020) S-adenosylmethionine and methylthioadenosine boost cellular productivities of antibody forming Chinese hamster ovary cells. Biotechnol Bioeng 117(11):3239–3247

Appendix D

The pH-dependent lactose metabolism of *Lactobacillus delbrueckii* subsp. *bulgaricus*: an integrative view through a mechanistic computational model

The pH-dependent lactose metabolism of *Lactobacillus delbrueckii* subsp. *bulgaricus*: An integrative view through a mechanistic computational model

Tamara Bendig [a,1], Andreas Ulmer [b,1], Laura Luzia [c], Susanne Müller [b], Sven Sahle [a], Frank T. Bergmann [a], Maren Lösch [b], Florian Erdemann [b], Ahmad A. Zeidan [d], Sebastian N. Mendoza [c], Bas Teusink [c], Ralf Takors [b], Ursula Kummer [a,*], Ana Sofia Figueiredo [a,*]

[a] *BioQuant, Centre for Organismal Studies (COS), Heidelberg University, Heidelberg, Germany*
[b] *Institute of Biochemical Engineering, University of Stuttgart, Stuttgart, Germany*
[c] *Systems Biology Lab, Vrije Universiteit, Amsterdam, the Netherlands*
[d] *Systems Biology, R&D Discovery, Chr. Hansen A/S, Hørsholm, Denmark*

ARTICLE INFO

ABSTRACT

The fermentation process of milk to yoghurt using *Lactobacillus delbrueckii* subsp. *bulgaricus* in co-culture with *Streptococcus thermophilus* is hallmarked by the breakdown of lactose to organic acids such as lactate. This leads to a substantial decrease in pH - both in the medium, as well as cytosolic. The latter impairs metabolic activities due to the pH-dependence of enzymes, which compromises microbial growth. To quantitatively elucidate the impact of the acidification on metabolism of *L. bulgaricus* in an integrated way, we have developed a proton-dependent computational model of lactose metabolism and casein degradation based on experimental data. The model accounts for the influence of pH on enzyme activities as well as cellular growth and proliferation of the bacterial population. We used a machine learning approach to quantify the cell volume throughout fermentation. Simulation results show a decrease in metabolic flux with acidification of the cytosol. Additionally, the validated model predicts a similar metabolic behaviour within a wide range of non-limiting substrate concentrations. This computational model provides a deeper understanding of the intricate relationships between metabolic activity and acidification and paves the way for further optimization of yoghurt production under industrial settings.

1. Introduction

Lactobacillus delbrueckii subsp. *bulgaricus* is a homofermentative lactic acid bacterium (LAB) widely used in co-culture with *Streptococcus thermophilus* in the dairy industry. LAB catabolize carbohydrates such as lactose and glucose to mainly produce lactic acid as an end product of fermentation. The production of lactic acid leads to a remarkable pH drop in the medium (Russell and Diez-Gonzalez, 1997), while achieving the desired characteristics of yoghurt such as acidity, taste, and texture (Chen et al., 2017; Cheng, 2010; Gentès et al., 2013). Further, the resulting acidification inhibits the growth of competing bacteria, prevents spoilage, and prolongs the product shelf-life (Gaggia et al., 2011). However, bacteria vary in their ability to maintain growth under acidic stress. Coping with low pH is an essential aspect for survival and productivity, and consequently for the industrial use such as for the choice

of starter cultures or probiotics Hutkins and Nannen (1993). As a strategy to cope with low pH, *L. bulgaricus* reduces the cytosolic pH (pH$_c$) as a function of the extracellular pH (pH$_e$) (Siegumfeldt al., 1999; Shabala et al., 2006; Rault et al., 2008). However, the reduction in pH causes a decreased catabolic flux and increased rates for energy consumption, resulting in energy limiting growth conditions Mercade et al. (2003). In addition, an acidic pH$_e$ can lead to membrane damage Alakomi et al. (2000), affects growth rates (Chen et al., 2020; Mercade et al., 2000), viability, and reduces metabolic activities. *In vitro* studies of enzyme kinetics in *L. lactis* indicate that a reduction of one pH unit to 5 reduces the activity of glycolytic enzymes by around 50% Even et al. (2003). Regarding enzymes, the pH does not only alter the protonation state of the functional groups of enzymes, it also affects the equilibrium and kinetics for reactions including protons. For these reasons, it is essential to consider the pH dynamics when investigating the reaction

---

velocities and thermodynamics of metabolism in LAB. While pH is a key factor in metabolism, especially in environments which can reach a pH of 4 or lower De Brabandere and De Baerdemaeker (1999), it is often overlooked in models. To the authors' current knowledge, no prior computational models exist describing the lactose metabolism of *L. bulgaricus* using pH-dependent kinetics and suitable data is scarce. Some data exists, such as the change of pH_c in *L. bulgaricus* upon the impact of an abrupt decrease in extracellular pH_e (e.g., Siegumfeldt et al., 2000; Kudo and Sasaki, 2019). However, no study could be found explaining the development of pH_c throughout fermentation and especially not continuously between lag phase and stationary phase and in growing cells. Further, measuring pH_c during batch fermentation and in a changing pH environment experimentally pose challenges difficult to tackle with the available technology. Experimental methods require high cell densities Neves et al. (2002), staining Siegumfeldt et al. (2000) or the expression of genetic modified pH sensors Mahon (2011), which are not always compatible with the experimental design or even food industry regulations. Only a few models consider the effect of inherent acidification and metabolic processes in LAB (e.g., Åkerberg et al., , 1998; Andersen et al., 2009; Even et al., 2002), however, pH_c as a dynamic value impacting the activities of individual glycolytic enzymes has not been incorporated in such models. While pH_c-dependent enzyme kinetics are rarely considered in models of other organisms (Vinnakota et al., 2006; Luzia et al., 2022; Millat et al., 2013), such models highlight the importance of pH_c in metabolic regulation. Consequently, the influence of pH on glycolytic flux and its impact on growth behaviour is not fully elucidated yet. Understanding pH_c dynamics will contribute to strengthen our knowledge about lactose metabolism and the underlying reason for the incomplete lactose catabolism. Further, such models can be used to stir the fermentation product outcome in terms of acidity and residual lactose concentration. Systems biology approaches to model lactose fermentation with protons as species can help to shed light upon the processes behind lactic acid bacteria metabolism and its interdependence with pH dynamics.

In this work, we investigated the lactose metabolism of *L. bulgaricus* using a proton-dependent computational model. Protons were incorporated as a species in relevant reactions and thus, flux through glycolysis and the lactate dehydrogenase caused acidification and consequently decreasing values in pH_c and pH_e. We implemented pH_c into the enzyme kinetics of glycolytic reactions to simulate the impact of lower pH_c on the rate of the central carbon metabolism. In addition to the carbon metabolism, we added a simplified proteolytic system to the model, allowing to degrade casein into peptides and consequently amino acids. Amino acids can be metabolized to generate more metabolic energy and thus help to control pH_c Fernández and Zúñiga (2006). To implement the impact of growth changes throughout batch fermentation, we integrated a volume growth function into the kinetic model. Taken together, we present a proton dependent computational model with predictive power to provide new insights into the central carbon metabolism of *L. bulgaricus* and its intricate dependency with pH levels.

2. Results

In this work, we developed a model of *L. bulgaricus*, which links the extracellular pH (pH_e) with the cytosolic pH (pH_c) and its impact on glycolytic activity. The model can predict acidification profiles and residual amounts of lactose for various cultivation conditions. To accommodate the impact of pH on enzymatic activity, we constructed a kinetic model that includes the lactose metabolism of *L. bulgaricus*, as described in section 2.1. In section 2.1, we depict the measured substrate conversion of glycolytic enzymes across multiple pHs to couple pH_c and enzyme activities. We additionally developed a machine learning based image analysis approach to estimate cytosolic volume from flow cytometry measurements. The influence of pH on the enzyme kinetics and the increase in total cytosolic volume was integrated into the model in section 2.3. Section 2.4 describes further parameterization processes

and model validation with additional data sets not used for parameterization. Lastly, we used the model to predict the final pH of cultures at various lactose concentrations.

2.1. Setup of L. bulgaricus model reactions

The stoichiometric reactions required for the metabolism of lactose were selected based on literature. Our model consists of import reactions for the uptake of carbohydrates, the respective anaerobic catabolism and export of lactic acid, the degradation of casein to peptides and amino acids to generate energy and finally, a cytosolic buffer system to control cytosolic acidity. We grouped protonated and deprotonated species except for the buffer systems (eq. (2)).

Carbohydrate uptake. Our model includes two import systems for lactose (lcts_e): an antiporter with galactose (gal) and a symporter with protons (h_e) via the lactose permease LacS (LACS, TC: 2.A.2.2.1) (Welman and Maddox, 2003; Foucaud and Poolman, 1992; Hutkins, 2007). The symport reaction accounts for the kick start of lactose uptake while the antiport reaction is used predominantly to sustain the majority of lactose uptake in later stages Poolman et al. (1989). No functional phosphoenolpyruvate:lactose phosphotransferase system (PTS) for the lactose uptake was reported Hickey et al. (1986), therefore we omitted a phosphoenolpyruvate:lactose PTS. We integrated a reversible glucose uptake reaction with the phosphoenolpyruvate:glucose (pep:glu) PTS (GLUpts) Hickey et al. (1986) and two symport reactions exporting and importing equimolar amounts of glucose called GLUe and GLUi, respectively.

Lactose catabolism. The uptaken lactose is irreversibly split into glucose (glu) and galactose (gal) by the *β*-galactosidase LacZ (LACZ, EC: 3.2.1.23). This hydrolysis is non-competitively inhibited by glucose and galactose Nguyen et al. (2012), however, the competitive effect of glucose is rather negligible. Therefore, we did not implement the inhibitory effect of glucose and considered only the impact of galactose. The majority of galactose is extruded by LacS and the glucose moiety is further metabolized to pyruvate (pyr) by glycolytic enzymes and eventually reduced to lactate (de Vos and Vaughan, 1994; El Kafsi et al., 2014; Hickey et al., 1986).

Regarding glycolysis, glucose is degraded to lactate through eleven reactions, all modelled as pH_c-dependent. Further, we account for the regulatory mechanisms acting upon phosphofructokinase (EC: 2.7.1.11) and pyruvate kinase (EC: 2.7.1.40). Phosphofructokinase is inhibited by ADP and phosphoenolpyruvate (pep) Paricharttanakul et al. (2005). Pyruvate kinase is inhibited by fructose 1,6-bisphosphate (fdp) and activated by glucose 6-phosphate (g6p) and fructose 6-phosphate (f6p) Bras and Garel (1993) (see reaction PYK in Fig. 1). In the lower branch of glycolysis, pyruvate is oxidized to lactate (lac), which is excreted by a lactate-proton symporter LACt and a leak reaction, as the membrane is permeable to undissociated lactic acid Cássio et al. (1987). Undissociated lactic acid is present to a small extent at pH values between 5.5 and 6.5. NADP-dependent non-phosphorylating glyceraldehyde-3-phosphate dehydrogenase (EC: 1.2.1.9) was neglected in our model, as we could not observe any activity under our experimental setting (Fig. A.15). To include side branches of glycolysis related with catabolism, two sink reactions were implemented: one for fructose-1,6-diphosphate (fdp) and one for pyruvate (pyr).

Casein degradation and amino acid catabolism. *L. bulgaricus BAA-365* possesses a powerful proteolytic system to degrade casein into peptides and eventually amino acids (Liu et al., 2012, 2014). Albeit *L. bulgaricus BAA-365* has lost the arginine deiminase pathway and glutamate decarboxylase El Kafsi et al. (2014), some amino acids can be decarboxylated or catabolized and used in the carbon cycle, thus supplying additional ATP Pessione et al. (2010). For example, aspartate can be converted in two reactions to phosphoenolpyruvate, which can be used in glycolysis. Aspartate can be synthesized from other amino acids such as asparagine or glutamine (Zheng et al., 2012; Hao et al., 2011), making other amino acids available for ATP production as well. To
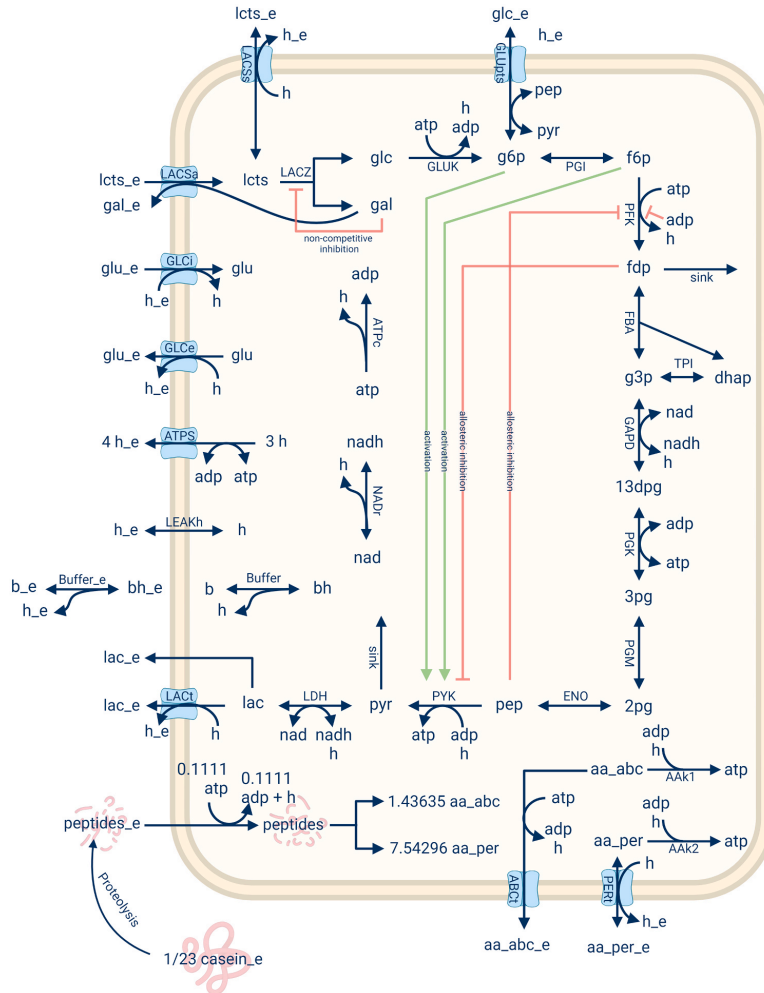
Fig. 1. Illustration of the reactions in the kinetic model. The model represents the relevant reactions for the glucose metabolism of *L. bulgaricus* ATCC BAA-365. The green arrows indicate an activating effect, and the red arrows represent an inhibitory impact of the compound. The cytosolic compartment is growing. The reactions to correct the concentrations of the three cytosolic buffers b, adenosine phosphates (ATP and ADP) and nicotinamide adenine dinucleotides (NAD$^+$ and NADH) by the growth rate were not implemented in the figure. The buffer system is depicted as one reaction in this figure, while it was modelled with three identical reactions with different pKs.

ensure that amino acids are available in our model, we implemented a simplified version of proteolysis, where casein is degraded into peptides followed by cytosolic breakdown into amino acids. At the end of the proteolytic pathway, the amino acids are catabolized in an irreversible reaction that generates ATP, as exemplarily shown in eq. (1).

$$aa + adp + h^+ \longrightarrow atp \tag{1}$$
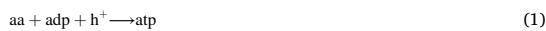
We lumped the amino acids into two groups based on the transport mechanisms described by Zheng et al. (2012): reversible transport via a permease or irreversible export by an ATP-binding cassette (ABC) transporter. Arginine, asparagine, aspartate, glutamate, glutamine, and glycine were included in the second group, and thus grouped as abc. Alanine, histidine, isoleucine, leucine, lysine, phenylalanine, serine, threonine, tryptophan, tyrosine, and valine were allowed to diffuse via permeases and were grouped as per. In this model, we did not include cysteine, serine and threonine. The stoichiometric coefficients for all reactions were calculated based on previously published data Ulmer et al. (2023) and a genome-scale metabolic reconstruction of *L. bulgaricus*. For each amino acid, we determined the experimental and

the predicted secretion rate. Then, we calculated experimental and predicted amino acid yields using the secretion rates and the specific growth rate predicted by the model (pFBA). The algorithm uses an iterative process to adjust the amino acid stoichiometry until the experimental and predicted yield match.

Cytosolic acidity control and buffer system. Weak organic acids, such as lactic acid, as well as other compounds are acting as an internal buffer system, which contribute to pH buffering. We generically consider this contribution by an estimated buffer capacity in the model. This lumped buffer capacity is modelled in a similar way as in the model of Andersen et al. (2009) and consists of a buffer system for the cytosolic and extracellular compartment, respectively. Each buffer system contains three stepwise distributed protonation reactions with different pKs. Every reaction is modelled using reversible mass action and consists of a buffer (bh), which can be deproned to the deprotonated buffer b and the proton h (eq. (2)). Additionally, a leak flux for protons was included in the model Maloney (1979), and implemented as a reversible flux of protons between the extracellular and cytosolic compartments.

$$b + h^+ \rightleftharpoons bh \tag{2}$$

2.2. pH-dependent enzyme activity and total cytosolic volume

pH-dependency of enzymes. In our model, the activities of every glycolytic enzyme with the addition of LACZ and LDH are modulated by pH_c. To achieve this, we fitted pH-dependent activity values we obtained from literature and experiments (Table. A.2) to a bell-shaped algebraic function (eq. (6)). The values determined in this work were obtained by measuring the substrate conversion rates of enzymes using cell lysate in *in vivo*-like buffer at pH 5.25, 5.5, 6.0, and 6.5. Although this pH range only allowed an extrapolation of the relative activity for pHs beyond this range, existing literature confirmed our work for PFK Le Bras et al. (1991) and PYK Bras and Garel (1993) in *L. bulgaricus* and for GAPD in *L. lactis* Even et al. (2003).

All enzymes showed the highest activity at a neutral pH around 7, and we consistently observed a substantial decrease in enzyme activity at lower pH values. The enzyme activity of most enzymes decreased at pH 6 by approximately 50% relative to activity at pH 7 (Fig. 2). It can be assumed that pH_c is maintained above 6 if the pH_e is higher than 5 Siegumfeldt et al. (2000).

Increase of cytosolic volume. As *L. bulgaricus* proliferates during the process of fermentation, the total volume in which lactose can be metabolized increases. For this reason, our model comprises a volume growth function describing the time-dependent volume changes of cytosol derived from biomass measurements. The cytosolic volume was fitted to eq. (3). The extracellular volume was assumed by subtracting the cytosolic volume from the total fermentation volume of 0.05 L (eq. (4)).

$$V_{t,c} = \frac{b \cdot t^n}{t^n + k^n} \tag{3}$$

$$V_{t,e} = 0.05 - V_{t,c} \tag{4}$$

2.3. Model construction

The metabolic network given in section 2.1 is translated into a kinetic model based on ordinary differential equations (ODEs). The reaction rates of enzymatically catalyzed reactions were predominantly described using convenience kinetics Liebermeister and Klipp (2006), as exemplarily shown in eq. (5) for a reversible reaction with one substrate S and one product P. Non-enzymatic reactions are implemented using mass action as rate law. The rate laws for all reactions can be found in Table A.5. The changes in apparent enzyme activity caused by pH were included by the pH-dependent algebraic function $F_{E,pH}$ (eq. (6)). A schematic overview of the model is given in Fig. 1.

$$S \underset{k_{-1}}{\overset{k_1}{\rightleftharpoons}} P, \quad v = F_{E,pH_c} \cdot \frac{(V_{max} \cdot k_{M,P}) \cdot ([S] \cdot k_{eq} - [P])}{k_{eq} \cdot (k_{M,S} \cdot k_{M,P} + [S] \cdot k_{M,P} + [P] \cdot k_{M,S})} \tag{5}$$

$$\text{with } F_{E,pH_c} = \left(\frac{k_{opt}}{1 + 10^{k1 - pH_c} + 10^{pH_c - k2}} \right)^n \tag{6}$$

2.4. Measurement and simulation of glycolytic metabolites

Parameter estimation. We cultivated *L. bulgaricus* in synthetic medium (SM) with casein to obtain time-dependent data for pH_e, lactose, glucose, galactose, lactate, and amino acids, as well as biomass measurements. This dataset, excluding biomass, was added to the parameter estimation task in COPASI Hoops et al. (2006) to estimate
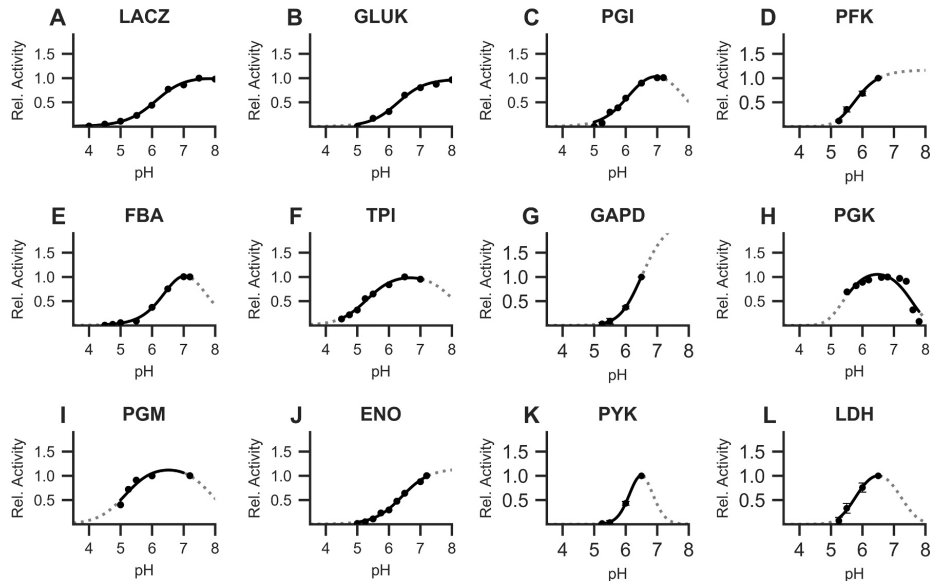

Fig. 2. Enzyme activities of the glycolytic enzymes report different pH dependencies. The activities of the respective enzymes in (D), (G), (K) and (L) were measured in *in vivo*-like assay buffer at pH 5.25, 5.5, 6.0, and 6.5. The other profiles were retrieved from literature. The black part of the curve lies within the range of measurements. The dotted grey lines are extrapolated based on the measured values fitted to an algebraic function. The activity of each pH profile was normalized to the highest value within the dataset. (A) β-galactosidase LACZ Nguyen et al. (2012), (B) Glucokinase GLUK Goward et al. (1986), (C) Glucose-6-phosphate isomerase PGI Even et al. (2003), (D) Phosphofructokinase PFK, (E) Fructose-1,6-bisphosphate aldolase FBA Even et al. (2003), (F) Triosephosphate isomerase TPI Even et al. (2003), (G) Glyceraldehyde-3-phosphate dehydrogenase GAPD, (H) Phosphoglycerate kinase PGK Bourniquel and Mollet (2002), (I) Phosphoglycerate mutase PGM Even et al. (2003), (J) Enolase ENO Even et al. (2003), (K) Pyruvate kinase PYK, (L) Lactate dehydrogenase LDH.

parameter values in our model. Having a well-parameterized model, we can estimate the dynamics of pH$_c$. The simulations with the parameterized model are in good agreement with the experimental data for lactose, lactate, galactose, and pH$_e$ (Fig. 3A, B, D, E) and fall within the experimental error. However, as indicated by the calculated error of the parameter estimation (see Table A.3), the data points of glucose are less well reproduced. The experimental data show an accumulation of glucose (Fig. 3C) to 1 mM within 2.5 h, followed by its consumption and decline to 0 mM. Within the next 20 h, the concentration increases again to 0.22 mM. While the simulated concentrations of glucose after 24 and 26 h are in agreement with the experimental data, the glucose accumulation within the first 2.5 h could not be reproduced by the model nor the ensemble of models (Fig. A.13 C). Instead of a single peak, the model displays oscillatory dynamics with peaks up to 0.5 mM glucose - less than half the concentration of the data. In general, we frequently observed oscillations as part of the resulting fits. Since oscillatory dynamics in the core metabolism of diverse organism is a common phenomenon (as reviewed e.g. in Hauser, 2022) and almost expected with the numbers of feedbacks involved, we did not select against such solutions and only used the goodness of the fit as criterion.

The model shows a continuous metabolization of lactose with an increase in the concentrations of lactate and galactose. The decrease of lactose can be divided into four stages (Fig. 3A). During the lag phase and the early exponential phase, lactose is consumed very slowly. Then, in the exponential phase, lactose is consumed with a high but oscillating rate, followed by a slightly lower rate with a linear consumption of extracellular lactose in the transition and early stationary phase. After approximately 10 h, a sudden stagnation in the concentrations of lactose, lactate, galactose, and in pH$_e$ becomes apparent. By the end of the time course, 30 mM of lactose were approximately consumed.

Glycolytic flux and cytosolic pH. This model incorporates dynamic changes in pH$_c$. Therefore, we measured substrate conversion rates *in vitro* in different pH environments (Fig. 2) and implemented pH-dependent kinetic equations (eq. (5) and (6)). The resulting parameterized model allows to gain a better understanding of the changes in pH$_c$ during cultivation and interdependence between pH$_c$, glycolytic flux, and carbohydrate metabolism. Hereafter, we will use the flux through the PYK as representative for the glycolytic flux because it is the

last step to pyruvate followed by lactate production.

Fig. 4A shows the change of pH$_c$ and glycolytic flux for PYK during a batch fermentation in SM with initially 45 mM lactose and casein. We identified four phases according to the growth curve (Fig. 4B): a lag phase (Fig. 4A, red) from 0 h to 1.3 h with almost no cytosolic acidification and no conversion of lactose, the exponential phase (Fig. 4A and B, white), accompanied with the majority of growth and the highest metatabolic flux shown by PYK up until 3.5 h, a transition phase (Fig. 4A, green) with a steady consumption of lactose until 9 h and a stationary phase until the end of the time course (Fig. 4A, blue). The time course of our model showed oscillations in metabolite concentrations and fluxes during exponential phase with increasing peaks reaching up to 0.2 mmol · min^{-1} for PYK. This increased metabolic activity causes a decreasing pH$_c$ from 7.6 and 6.3. The exponential phase also harbours the highest extracellular acidification rate (Fig. 3E) and biomass increase (Fig. 4B). With the end of the exponential phase, the oscillations disappear and the pH$_c$ further declines to 5.6 at 10 h, while the glycolytic flux regresses from 0.03 to 0.01 mmol · min^{-1} within 5.5 h. Interestingly, enzymes of the upper branch of glycolysis are strongly affected in their activity by the reduction in pH occurring during the exponential phase and demonstrated activity levels close to the lower points of the oscillations at the beginning of the transition phase. Enzymes of the lower branch such as PGK, PGM, PYK, and LDH are less affected and began the transition phase with activity levels around the upper extremes. This has the consequence that those enzymes could potentially maintain longer a higher activity albeit a further decline in pH$_c$ during the transition phase (Fig. A.7). Within the stationary phase, approx. 10 h after the start of fermentation, pH$_c$ sharply declines from pH 5.5–3.8 within 1.5 h (Fig. 4A), eventually matching pH$_e$. This decline in pH$_c$ inactivates all glycolytic enzymes (Fig. A.7) and thus ceases the glycolytic flux and the depletion of lactose stops. Concisely, Fig. 4A indicates three states for glycolytic activity: a high glycolytic flux at pH$_c$ above 6.5 during the exponential phase, a reduced glycolytic flux until pH 5.5 during the transition and early stationary phase, or no flux after pH$_c$ fell below pH 5.5 and converged to pH$_e$ in the later stationary phase.

Quantification of predictive power. To determine the predictive power of the model, the batch fermentation experiments were repeated
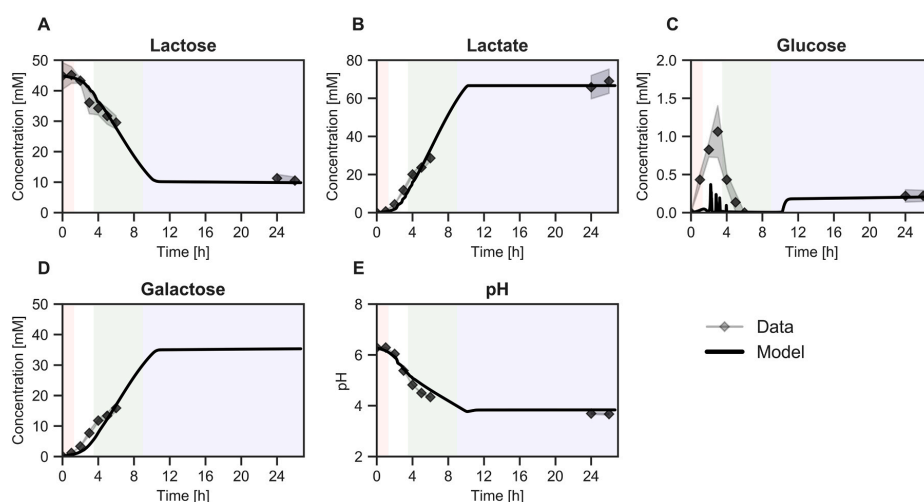

Fig. 3. Metabolic profiles of extracellular metabolites and pH. Shown are the experimental values (squares) of a batch fermentation in synthetic medium (SM) with an initial concentration of 45 mM lactose and 2 g/L casein measured in triplicate. The standard deviation is shown as a transparent error band. The calculated concentrations after the model was fit to the experimental data (solid line) of (**A**) extracellular lactose, (**B**) lactic acid, (**C**) glucose, (**D**) galactose, and (**E**) extracellular pH. Growth phases are color-coded in the background. Red: lag-phase, white: exponential phase, green: transition phase, blue: stationary phase.

Fig. 4. Glycolytic flux in dependence of cytosolic pH. (**A**) Simulated time course for the glycolytic flux, represented by the flux of PYK (blue), pH_c (red) and extracellular lactose (green). (**B**) Total intracellular volume in Litre (L) in dependence of model time. The solid line gives the model value while the dots represent the mean of three experimentally determined values. Growth phases are color-coded in the background. Red: lag-phase, white: exponential phase, green: transition phase, blue: stationary phase.
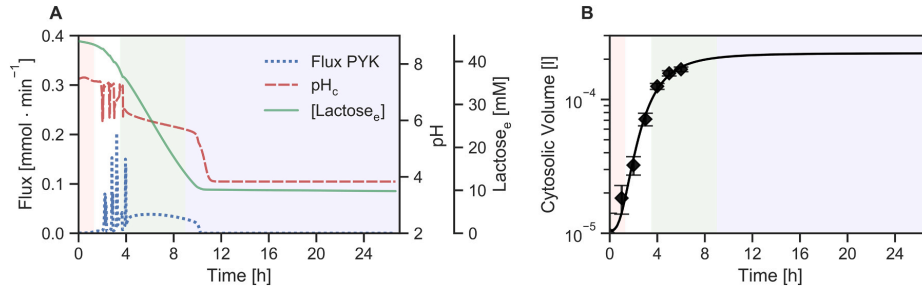
with altered concentrations of initial lactose. We increased the initial lactose concentration to 60 mM to investigate any effects of high lactose concentrations on lactate production and we decreased it to 30 mM to achieve complete consumption of lactose. Then, we used the parameter set of the previously parameterized model and adjusted only the initial values for lactose to the respective initial concentration of the experiments and compared the simulation outcomes to the experimental data as shown by the blue, black, and red curves in Fig. 5. The simulations predict a similar behavior in terms of dynamics for lactose, lactate, glucose, galactose, and pH_e as well as substrate limitation at less than 30 mM lactose. The model correctly predicts the final concentrations of lactose, lactate, galactose, and pH_e, however, the pH_e is slightly overestimated by 0.2 pH units for 30 mM initial lactose concentration. Differences between the simulated and the measured data set are only found for glucose (Fig. 5C), particularly the last two data points in the simulation with a high initial lactose concentration (60 mM). Overall, the model can simulate the correct acidification and metabolite profiles for all initial lactose concentrations, which supports its predictive power.

Prediction of pH as a results of various lactose concentrations. Our aim was to predict the final pH_e of cultivations with *L. bulgaricus*. Therefore, we developed and parameterized a model which could reproduce three experiments and used this model with a wide range of initial lactose concentrations to predict pH_e after 24 h. Fig. 6A shows the pH value after 24 h from simulations with initial lactose concentration from 0 to 80 mM. We found that an initial lactose concentrations above 40 mM result in final pH_e values between 4.0 and 3.8. A lower initial lactose concentration results in a higher pH as less lactose depletion occurs. As expected, to gain an excess of lactose above 1 mM after 24 h, the initial lactose concentration must be higher then 30 mM. If the initial lactose concentration is higher, lactose is not metabolized, causing a plateau in the final lactate concentrations at around 68 mM (Fig. 6B).

3. Discussion

In contrast to most other bacteria, LAB thrive in acidic environments. Fermentation processes by LAB can cause a dramatic drop in pH_e leading to outcompeting other microbes and preservation of foods. Although
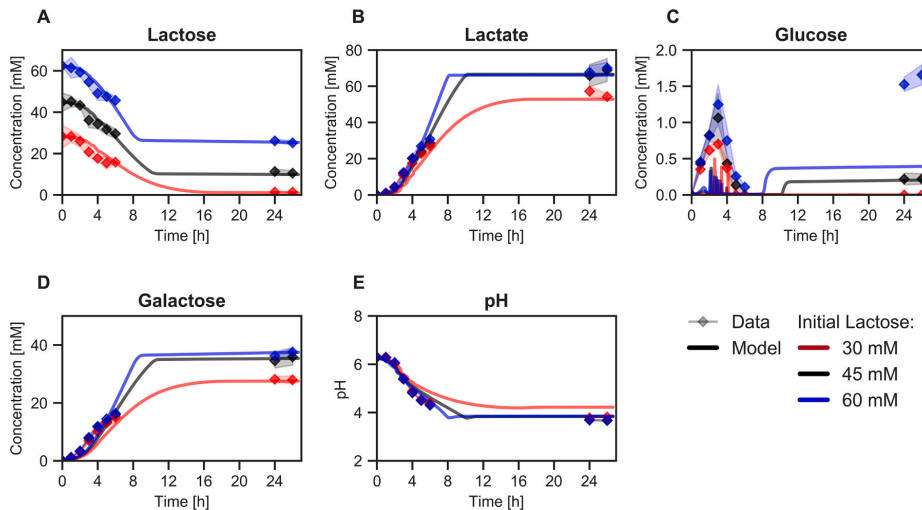

Fig. 5. Prediction of metabolic behavior with different initial concentrations of lactose at pH 6.3. The concentration of (**A**) extracellular lactose, (**B**) lactic acid, (**C**) glucose, (**D**) galactose, and (**E**) pH_e was measured at pH 6.3 with 30 mM (blue), 45 mM (red) and 60 mM (black) initial lactose concentration. The dots with the standard deviation shown as a transparent error band are the experimentally determined concentrations measured in biological triplicates. The lines are model predictions based on the parameterized model shown in Fig. 3.
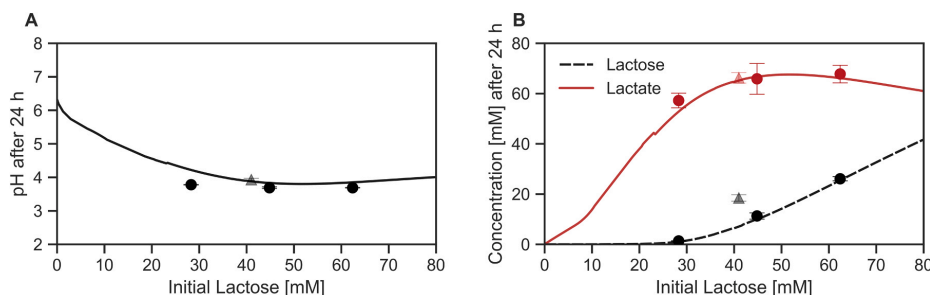
Fig. 6. Prediction of final pH, lactose concentration and lactate concentrations after 24 h with different initial concentrations of lactose. pH_e (**A**); extracellular lactose and extracellular lactic acid (**B**). The lines are model predictions based on the parameterized model shown in Fig. 3. The circles are the mean of three independent experiments with the respective standard deviation shown in Fig. 5. The results from a fourth experiment (grey or light red triangle) were added with a different experimental set-up (synthetic medium (SM) with 5 g/L casein instead of 2 g/L).

L. bulgaricus maintains a more alkaline cytosolic environment in comparison to the medium, its pH_c is decreasing in co-dependence to the environmental pH_e and can potentially reach values below 6 as the pH of the medium declines (Siegumfeldt et al., 1999; Shabala et al., 2006; Rault et al., 2008). As enzyme activities are pH-dependent, changes in pH_c affect the catabolic flux. The resulting impact is often neglected in metabolic models and including pH_c is a step towards more physiologically accurate approach to the study of metabolism and eventually the production of high-quality fermented dairy products.

General methodology In this study we introduced an approach to account for changes in cellular volume during batch cultivation. Since the total volume changes at least 10-fold, this drastically changes the uptake and release of metabolites and protons in the culture. To our knowledge, this is the first time that a mechanistic biochemical model of intracellular processes in microbial batch culture has been integrated with volume growth. Only in the context of vertebrate cells - human brain cells - we found one example integrating volume changes and intracellular behaviour Ramos et al. (2020). In addition, we included protons as an independent species in our model - something that has been done in the context of LABs before (e.g., Andersen et al., 2009), albeit rarely. Another new insight is further offered, as we took measured pH dependent enzyme activities into account, which hasn't been done before for studying batch cultures and LABs. Generally, we know of only one study on skeletal muscle metabolism Vinnakota et al. (2006) that takes measured pH dependencies of enzyme activities into account and one study that used simplified forms of computed pH dependency in a model of *Clostridium acetobutylicum* Millat et al. (2013). The drastic changes in pH during fermentation of LAB, and especially *L. bulgaricus*, emphasize the importance of considering pH and its impact on metabolism.

Modeling pH and its impact on metabolism During fermentation, protons are intrinsically produced in metabolic reactions e.g., upon the usage of ATP, while other reactions such as e.g., the pyruvate kinase consume protons. In our model, those protons are considered as an independent species, which can further impact enzyme activities due to pH-dependent V_{max} values. The pH-activity profiles shown in Fig. 2 which are affecting the V_{max}-values of glycolytic enzymes (eq. (6)), demonstrate, that the resulting changes in pH_c affect the activities of the different glycolytic enzymes in distinct ways. According to our data, enzymes in *L. bulgaricus* which are less sensitive to pH variation in terms of their activity are e.g., PGK, PGM, and especially TPI. TPI and PGM maintain around 10% of their activity even at pH 4.2 compared to pH 6.5, while the other enzymes function at approximately 2% (Fig. 2). Consequently, TPI and PGM are still potentially capable to maintain a high metabolic flux. In contrast, enzymes which catalyze the often flux controlling reactions are more affected by pH, such as PYK, GLUK, FBA, halting glycolysis at a lower pH_c. When pH_c reached values lower than

5.5, the glycolytic flux diminishes and even converges to 0 mmol · min^{-1}, if pH_c becomes lower than 5, as depict in Fig. 4A. The structure of the rate laws in our model is limited for pH-mediated changes in activity, however, neglecting effects of changing enzyme concentrations, since these are kept constant throughout simulation. The results of Even et al. (2003) suggest an increase in enzyme synthesis for many glycolytic enzymes at lower pH values for *L. lactis* in steady-state, indicating a compensation mechanism. So far, it is unclear in which manner *L. bulgaricus* changes enzyme concentrations during batch cultivation. Including the changes in enzyme concentration during acidification could help to increase the predictive power of the model further. Another way to improve the model to generate more realistic simulations and to increase its accuracy and predictive power is the integration of our kinetic model in the genome-scale model of *L. bulgaricus* - an approach which is currently under development.

pH_c and growth phases Maintaining glycolytic flux is necessary for bacterial growth and, ultimately, the survival of the population. Our model showed that *L. bulgaricus* can maintain a low glycolytic flux at acidic pH_c down to 5.5 and that the pH_c needs to be above 5.5 to enable enzyme activity and therefore, glycolytic flux. According to our model, the glycolytic flux was reduced from maximally 0.2 mmol · min^{-1} at the exponential phase to 0.03 mmol · min^{-1} at pH_c 6.3 and 0.01 mmol · min^{-1} pH_c 5.6 during the transition phase (Fig. 4A). pH_c values around 5.5 occurred at the stationary phase (Fig. 4A), before it finally converged to the level of pH_e. Those predictions are consistent with existing research indicating that lactic acid production diminishes rapidly at pH values below 6 in permeabilized cells Arioli et al. (2017) and pH_e 4.7 as the limit for growth Mercade et al. (2000). Fig. 4A revealed a drop in pH_c after 10 h, which stops the activity of all enzymes and explains the incomplete lactose depletion, while the 10-fold lower glycolytic flux during the transition phase can explain the diminishing lactose depletion rates and, lastly, growth arrest. However, the model predictions about the drop in pH_c at 10 h and the abruptness may be inaccurate, as we have a gap in data between 6 and 24 h due to the lack of such data reported in literature. Nevertheless, the model findings depict the observation that *L. bulgaricus* starts to fail maintaining the gradient between pH_c and pH_e shortly after the beginning of the stationary phase Rault et al. (2009). Our model could demonstrate how the continuous metabolic acidification leads to lower glycolytic flux and finally to the collapse of the pH gradient as well as the inactivation of cytosolic enzymes. Accurate predictions of this behaviour require time-course data of cytosolic metabolites and could further give insights into the impact of organic acid accumulation, which is also suspected to cause growth arrest (Carpenter and Broadbent, 2009; Sánchez et al., 2008).

Different lactose concentrations and their impact on metabolic behavior Another industrially relevant aspect in yoghurt making is the effect of substrate concentration on the product outcome, such as

product yield and acidity. To validate our model, we cultivated *L. bulgaricus* with different substrate concentrations and measured the pH_e, carbohydrates, and biomass. As shown in Fig. 5, the metabolic behaviour with different initial concentrations of lactose followed similar dynamics - in our model and in the experimental data. Regardless of the non-limiting substrate concentration, metabolic inhibition occurred, which suggests an internal effect. This internal effect can be explained by the diminishing pH_c depicted by our model. As our model reproduced the experimental data well without changing parameter values, we applied our model to a parameter scan with a range of initial lactose concentrations to simulate pH_e and remaining lactose concentration after 24 h of batch fermentation. The results in Fig. 6 point out that maximally 68 mM lactate were produced, independent of the initial lactose concentration. If more than 34 mM lactose were consumed, glycolytic intermediates accumulated inside the cell without being fully metabolized to lactate. This effect can also be seen in the predictions made by an ensemble of models (Fig. A.14B), showing that lactose is metabolized incompletely after 24 h for initial lactose concentrations higher than approximately 35 mM, without a further decrease in pH_e for most models within the ensemble. As the acidity of yoghurt is an essential parameter for taste and consumer acceptance, this model can be applied to optimize the fermentation condition to achieve a desired product outcome.

Conclusion In summary, our model allows the simulation of pH_c and the computation of biotechnologically relevant parameters such as external pH and residual lactose as a function of the initial lactose concentration. Moreover, this study provides valuable insights into how activity of enzymes and their inactivation by the internal pH_c changes the metabolic activity of the cell population. The model simulation illustrated that metabolic activity continuously acidifies the cytosol. Once a threshold of a pH_c below 5.5 is reached, the metabolic activity regressed rapidly, with the consequence of metabolic inactivation and growth arrest. Thus, the model can be used for the optimization of batch cultures of *Lactobacillus delbrueckii* subsp. *bulgaricus* and as starting point for more complex questions such as modeling a co-culture with *Streptococcus thermophilus* during yoghurt cultivation. This can lead to a deep understanding of growth inhibition under non-limiting substrate conditions and e.g., to obtain a milder yoghurt with a higher pH_e or less residual lactose for lactose intolerant customers.

4. Materials and methods

Strain and culture conditions. All experiments were conducted with *Lactobacillus delbrueckii* subsp. *bulgaricus* ATCC®BAA-365 in SM (Appendix A.1) under microaerophilic conditions (80% vol/vol N_2 and 20% vol/vol CO_2) as previously described in Ulmer et al. (2022) with deviations in the concentration of lactose monohydrate or substitution of the amino acids by casein as indicated in the respective experimental setup. The fermentation to measure extracellular metabolites was performed without pH control, using an initial pH of 6.3 and synthetic medium (SM) containing 2 g/L casein (Sigma-Aldrich Chemie GmbH, #9005–46–3, Steinheim, Germany) as a substitute for the amino acids, 43.85 mM lactose, a constant fermentation temperature of 40°C and stirring with 500 rpm.

Biomass and dry weight quantification The biomass was quantified using flow cytometry as described in Ulmer et al. (2022).

Optical density and correlation to total cellular volume. Growth was determined spectrophotometrically in SM containing amino acids and 15 g/L lactose by measuring the optical density at 600 nm in biological triplicates. To evaluate the cytosolic volume, ten images of the cell suspension per time point were captured in two biological replicates during the time course using a bright-field light microscope with a 400-fold magnification in Bürker-Türk counting chambers. The area occupied by cells per image was determined in Fiji (Version 1.52p, Schindelin et al., 2012; Schneider et al., 2012). Cell segmentation was performed using the machine learning tool Trainable Weka

Segmentation Arganda-Carreras et al. (2017) with default settings and the Particle Analyser implemented in Fiji. Only particles smaller than 10^{-7} mm^2 and a circularity lower than 0.7 were considered. The volume of all cells within the culture was calculated using eq. (7) assuming a cylindrical cell shape. The volume of each particle n was calculated as the product of the respective area A_n of particle n, π and the respective secondary axis of a fitted ellipse, depicting the width of the particle M_n. The volumes of all particles were summed up for each image k, representing the cellular volume in 2.5×10^{-4} mm^3 medium.

$$\sum\nolimits_{k=1}^{n} V_k = A_n \cdot \pi \cdot \frac{M_n}{4} \qquad (7)$$

The mean of two samples per time point with the 10 technical replicates per sample was used to calculate the volume. The linear relationship between OD_{600} and the total cytosolic volume shown in A.9 was used to convert OD_{600} values to cytosolic volume.

Quantification of metabolites. The concentrations of extracellular metabolites were measured using high-performance liquid chromatography (HPLC). The concentration of carbohydrates (lactose, glucose, galactose, lactate) was measured in cell-free supernatants using the Agilent 1200 series HPLC system with a RI detector. The isocratic separation was achieved by a Rezex ROA organic acid H (8%) column (300 by 7.8 mm, 8 μm; Phenomenex) protected by a Phenomenex guard carbo-H column (4×3.0 mm) maintained at 50°C. 5 mM H_2SO_4 was used as mobile phase with a constant flow rate of 0.4 mL min^{-1}. To precipitate phosphate, the supernatants were treated with 4 M NH_3 and 1.2 M $MgSO_4$ solutions and incubated with 0.1 M H_2SO_4 before the experiment. Rhamnose was used as internal standard at 1 g/L to correct for measurement variability. The quantification of amino acids was conducted with an Agilent 1200 series instrument (Agilent Technologies, Santa Clara, USA). Separation was achieved by an Agilent Zorbax Eclipse Plus C_{18} column (250×4.6 mm, 5 μm) which was protected by an Agilent Zorbax Eclipse Plus C_{18} guard column (12.5×4.6 mm, 5 μm). After automatic precolumn derivatization with ortho-phthaldialdehyde, fluorometric detection (excitation at 230 nm and emission at 450 nm) was carried out. The elution buffer consisted of a polar phase (10 mM Na_2HPO_4, 10 mM $Na_2B_4O_7$, 0.5 mM NaN_3, pH 8.2) and a nonpolar phase (45% vol/vol acetonitrile, 45% vol/vol methanol). Quantification of amino acids was achieved by using 4-aminobutanoic acid as internal standard at 100 μM to correct for analyte variability.

Preparation of cell extracts. The enzyme activity was assayed using a modified protocol by Goel et al. (2012) with cell pellets harvested in prior at mid-log phase and stored at -80°C until further use. The frozen pellet was resuspended in cell lysis buffer (50 mM HEPES (Sigma), pH 7.5, 2 mM $MgCl_2$ (Sigma) and 1x Halt™ Protease Inhibitor-Cocktail (Sigma) and disrupted with the the FastPrep-24™ 5 G cell homogenizer (MP Biomedicals) immediately according to Goel et al. (2012). Then, the cell extract was diluted with the same amount of cell lysis buffer and diluted with a serial dilution (1:2, 1:4, 1:8, 1:16, 1:32). The protein concentration was measured in three diluted cell extract samples using the bicinchoninic acid assay (Pierce™ BCA, Protein Assay Kit, Thermo Scientific, #23225) according to the manufacturer's instructions.

Evaluation of enzyme activity. The enzyme activity was measured by following spectrophotometrically changes in concentration of NAD(P)H at 340 nm. The method to determine the enzymatic activity was based on the protocols of Goel et al. (2012) with modifications. The enzyme activity was measured in *in vivo*-like assay buffer containing: 0.1 M MES (Applichem), 0.4 M glutamic acid potassium salt (Fluka), 0.05 M sodium chloride (Merck), 0.001 M K_3PO_4 (Fluka), 1:10-diluted metals given in Appendix A.1 and the respective reaction specific compounds stated in Table 1. The pH of each solution was adjusted to 5.25, 5.5, 6.0, and 6.5, respectively, at 30°C. The activities were measured in triplicates using excess amounts of substrate, co-substrate and, if required, coupling enzymes. To ensure non-rate-limiting conditions and to capture dilution rate where the enzyme activity scaled linearly with the enzyme concentration, the assay was performed using

Table 1
Reaction specific compounds for the *in vivo*-like assay buffer.

Enzyme	EC	Reaction Specific Compounds	Based on
PFK	2.7.1.11	ATP: 5 mM, NADH: 0.3 mM; MgSO4: 7 mM; Phosphocreatine: 80 mM; Creatine Kinase (EC: 2.7.3.2): 30 μg/mL, Aldolase (EC: 4.1.2.13): 2 U/mL; G3PDH (EC: 1.1.1.8): 4 U/mL, TPI (EC: 5.3.1.1): 5 U/mL. **Start:** F_6P: 20 mM	Paricharttanakul et al. (2005)
GAPD	1.2.1.12	ADP: 3 mM; NAD^+: 5 mM; KH_3PO_4: 50 mM; PGK (EC: 2.7.2.3): 14.5 U/mL; $MgSO_4$: 5 mM, Cysteine: 5 mM. **Start:** G3P: 10 mM	Goel et al. (2012)
PYK	2.7.1.40	ADP: 3 mM; NADH: 0.3 mM; $MgSO_4$: 5 mM; $F_{1,6}BP$: 5 mM; LDH (EC: 1.1.1.27): 10 U/mL. **Start:** PEP: 6 mM	Goel et al. (2012)
LDH	1.1.1.27	NADH: 0.3 mM; $F_{1,6}BP$: 3 mM; $MgSO_4$: 2 mM. **Start:** PYR: 20 mM	Goel et al. (2012)

The given concentrations refer to the final concentrations in the assay.

six different dilutions. The NAD(P)H formation or consumption as monitored at 340 nm using a Multiskan™ FC Microplate-Photometer (Thermo Scientific, #11590685). The data was evaluated in Python 3.7.1. The script determined the slope of the linear part of the progress curve over time and determined the range where the enzyme velocity scaled linear with the used amount of cell extract using the random sample consensus (RANSAC) algorithm Pedregosa et al. (2011) with a threshold of 20% of the median absolute deviation to determine outliers. The slope of the inliers was corrected by the base activity by subtracting the slope of the control without cell extract. The corrected slope was divided by the respective dilution and the mean of all corrected slopes of inliers was used as final value.

Computational approaches for model construction. The computational model was constructed using a system of ODEs. The model was build using COPASI 4.40 (Build 278) Hoops et al. (2006). The rate laws were formulated in accordance with Liebermeister and Klipp's convenience kinetics Liebermeister and Klipp (2006) and mass action. The reaction stoichiometries were taken from literature or KEGG (Kanehisa, 2019; Kanehisa et al., 2019; Kanehisa and Goto, 2000). The model was parameterized using parameter ranges for the parameter estimation task in COPASI corresponding to the minimum and maximum value of the respective glycolytic enzyme occurring in the class of bacteria in SABIO-RK Wittig et al. (2011) or from Bar-Even et al. (2011), if SABIO-RK had only a few listed values. Parameters were estimated with the Parameter Estimation Task in COPASI, using Particle Swarm (swarm size 50, standard deviation for an alternative ending of 10^{-6}), based on the experimental data. Equilibrium constants K_{eq} were estimated in a range between 0.5 and 100. The parameter ranges for transport reactions were divided by the initial cytosolic volume to allow for the scaling of the reactions to the smaller volume. Some parameter ranges were adjusted iteratively to fit the experimental data. The effect of the pH on the enzyme activities was included by adding a pH-dependent scaling factor to the respective rate laws by multiplying the V_{max} by the respective pH_c-dependent factor F_{E,pH_c} in eq. (6) as a Global Quantity. To ensure that the concentrations of ATP, ADP, NAD, NADH and the internal buffers b1, b2, b3 are not reduced by the growing internal volume, we added synthesis reactions, in which we multiplied the transient concentrations with the derivative of the volume growth function.

Determination of the buffer capacity. The parameters of the cytosolic buffer system were estimated by the parameter estimation function in COPASI. The buffer system was modeled employing the equations of Andersen et al. (2009), with the deviation that only three buffers for the cytosol and medium, respectively, were used. The initial values for all buffer systems were implemented with initial conditions for the protonated buffer bh to assure an equilibrium of the buffer compounds at time point 0 (eq. (8)).

$$[bh_0] = \frac{k_1 \cdot [h_0] \cdot [b_{total,0}]}{k_2 + k_1 \cdot [h_0]} \tag{8}$$

Retrieving pH profiles. In order to implement the effect of pH_c, the enzyme activity of every glycolytic enzyme is adjusted by pH_c using eq. (6) with pH as a function of the cytosolic concentration of protons (eq. (9)). The values for the pH profile was retrieved by experimental measurements as stated above or taken from literature. The reference of the pH profiles is given in Table A.2. All values were normalized to the maximal value in the respective data set. As the model was in mmol/L, the pH was calculated by eq. (9), respectively for the cytosolic and pH_e. The parameters of eq. (6) for every enzyme were estimated using the Parameter Estimation function in COPASI. Only literature pH profiles from enzymes with a sequence similarity in terms of chemical similarity of > 65 % was used. The sequence similarity was calculated by the alignment function of UniProt Bateman et al. (2020).

$$pH = -(log_{10}) \frac{[h]}{1000} \tag{9}$$

CRediT authorship contribution statement

UK, AAZ, BT and RT conceived the project, planned and supervised the work. ASF co-supervised the computational modeling. TB supported by SS, FTB and ASF performed the computational modeling. TB supported by LL also did the kinetic measurements of enzyme activities and determined the cell volume with the microscopy approach. AU, ML, SM, and FE performed the rest of the experimental work, such as the fermentation processes and analytics. TB, AU, ASF and UK wrote the ms. All authors read and commented the ms and approved the final version.

Declaration of Generative AI and AI-assisted technologies in the writing process

During the preparation of this work the authors used ChatGPT-3.5 as a writing assistant to enhance readability of some sentences. No research ideas or full sentences were copied from ChatGPT. After using this tool, the authors reviewed and edited the content as needed and take full responsibility for the content of the publication.

Declaration of Competing Interest

The authors declare that they have no known competing financial interests or personal relationships that could have appeared to influence the work reported in this paper.

Data availability

Data will be made available on request.

Acknowledgments

the kinetic model reactions is created with BioRender.com.

Appendix A. Supporting information

Supplementary data associated with this article can be found in the online version at doi:10.1016/j.jbiotec.2023.08.001.

References

Åkerberg, C., Hofvendahl, K., Zacchi, G., Hahn-Hägerdal, B., 1998. Modelling the influence of ph, temperature, glucose and lactic acid concentrations on the kinetics of lactic acid production by lactococcus lactis ssp. lactis atcc 19435 in whole-wheat flour. Appl. Microbiol. Biotechnol. 49 (6), 682–690. https://doi.org/10.1007/s002530051232.

Alakomi, H.L., Skyttä, E., Saarela, M., Mattila-Sandholm, T., Latva-Kala, K., Helander, I. M., 2000. Lactic acid permeabilizes gram-negative bacteria by disrupting the outer membrane. Appl. Environ. Microbiol. 66 (5), 2001–2005. https://doi.org/10.1128/aem.66.5.2001-2005.2000.

Andersen, A.Z., Carvalho, A.L., Neves, A.R., Santos, H., Kummer, U., Olsen, L.F., 2009. The metabolic ph response in lactococcus lactis: an integrative experimental and modelling approach. Comput. Biol. Chem. 33 (1), 71–83. https://doi.org/10.1016/j.compbiolchem.2008.08.001. ⟨http://www.sciencedirect.com/science/article/pii/S1476927108001096⟩.

Arganda-Carreras, I., Kaynig, V., Rueden, C., Eliceiri, K.W., Schindelin, J., Cardona, A., Sebastian Seung, H., 2017. Trainable weka segmentation: a machine learning tool for microscopy pixel classification. Bioinforma. (Oxf., Engl.) 33, 2424–2426. https://doi.org/10.1093/bioinformatics/btx180.

S. Arioli, G. DellaScala, M.C. Remagni, M. Stuknyte, S. Colombo, S. Guglielmetti, I. De Noni, E. Ragg, D. Mora, Streptococcus thermophilus urease activity boosts lactobacillus delbrueckii subsp. bulgaricus homolactic fermentation, International Journal of Food Microbiology 247 (2017)55–64.special Issue: CBL 20th edition: New challenges for research and industry.10.1016/j.ijfoodmicro.2016.01.006, ⟨https://www.sciencedirect.com/science/article/pii/S0168160516300071⟩.

Bar-Even, A., Noor, E., Savir, Y., Liebermeister, W., Davidi, D., Tawfik, D.S., Milo, R., 2011. The moderately efficient enzyme: evolutionary and physicochemical trends shaping enzyme parameters. Biochemistry 50 (21), 4402–4410. https://doi.org/10.1021/bi2002289.

Bateman, Alex, Martin, M.-J., Orchard, S., Magrane, M., Agivetova, R., Ahmad, S., Alpi, E., Bowler-Barnett, E.H., Britto, R., Bursteinas, B., Bye-A-Jee, H., Coetzee, R., Cukura, A., Silva, A.D., Denny, P., Dogan, T., Ebenezer, T., Fan, J., Castro, L.G., Garmiri, P., Georghiou, G., Gonzales, L., Hatton-Ellis, E., Hussein, A., Ignatchenko, A., Insana, G., Ishtiaq, R., Jokinen, P., Joshi, V., Jyothi, D., Lock, A., Lopez, R., Luciani, A., Luo, J., Lussi, Y., MacDougall, A., Madeira, F., Mahmoudy, M., Menchi, M., Mishra, A., Moulang, K., Nightingale, A., Oliveira, C.S., Pundir, S., Qi, G., Raj, S., Rice, D., Lopez, M.R., Saidi, R., Sampson, J., Sawford, T., Speretta, E., Turner, E., Tyagi, N., Vasudev, P., Volynkin, V., Warner, K., Watkins, X., Zaru, R., Zellner, H., Bridge, A., Poux, S., Redaschi, N., Aimo, L., Argoud-Puy, G., Auchincloss, A., Axelsen, K., Bansal, P., Baratin, D., Blatter, M.-C., Bolleman, J., Boutet, E., Breuza, L., Casals-Casas, C., de Castro, E., Echioukh, K.C., Coudert, E., Cuche, B., Doche, M., Dornevil, D., Estreicher, A., Famiglietti, M.L., Feuermann, M., Gasteiger, E., Gehant, S., Gerritsen, V., Gos, A., Gruaz-Gumowski, N., Hinz, U., Hulo, C., Hyka-Nouspikel, N., Jungo, F., Keller, G., Kerhornou, A., Lara, V., Mercier, P.L., Lieberherr, D., Lombardot, T., Martin, X., Masson, P., Morgat, A., Neto, T.B., Paesano, S., Pedruzzi, I., Pilbout, S., Pourcel, L., Pozzato, M., Pruess, M., Rivoire, C., Sigrist, C., Sonesson, K., Stutz, A., Sundaram, S., Tognolli, M., Verbregue, L., Wu, C.H., Arighi, C.N., Arminski, L., Chen, C., Chen, Y., Garavelli, J.S., Huang, H., Laiho, K., McGarvey, P., Natale, D.A., Ross, K., Vinayaka, C.R., Wang, Q., Wang, Y., Yeh, L.-S., Zhang, J., Ruch, P., Teodoro, D., 2020. UniProt: the universal protein knowledgebase in 2021. Nucleic Acids Res. 49 (D1), D480–D489. https://doi.org/10.1093/nar/gkaa1100.

Bourniquel, A.A., Mollet, B., 2002. Purification and characterization of the 3-phospho-glycerate kinase from the thermophile lactobacillus delbrueckii subsp. lactis. Int. Dairy J. 12 (9), 723–728. https://doi.org/10.1016/S0958-6946(02)00069-9. ⟨http://www.sciencedirect.com/science/article/pii/S0958694602000699⟩.

Bras, G.L., Garel, J., 1993. Pyruvate kinase from lactobacillus bulgaricus: possible regulation by competition between strong and weak effectors. Biochimie 75 (9), 797–802. https://doi.org/10.1016/0300-9084(93)90130-k.

Carpenter, C., Broadbent, J., 2009. External concentration of organic acid anions and ph: Key independent variables for studying how organic acids inhibit growth of bacteria in mildly acidic foods. J. Food Sci. 74, R12–R15. https://doi.org/10.1111/j.1750-3841.2008.00994.x.

Cássio, F., Leão, C., van Uden, N., 1987. Transport of lactate and other short-chain monocarboxylates in the yeast saccharomyces cerevisiae. Appl. Environ. Microbiol. 53 (3), 509–513. https://doi.org/10.1128/aem.53.3.509-513.1987.

Chen, C., Zhao, S., Hao, G., Yu, H., Tian, H., Zhao, G., 2017. Role of lactic acid bacteria on the yogurt flavour: a review. Int. J. Food Prop. 20 (sup1), S316–S330. https://doi.org/10.1080/10942912.2017.1295988.

Chen, S., Niu, H., Wu, Y., Sun, J., Han, X., Zhang, L., 2020. Influence of lactic acid on cell cycle progressions in lactobacillus bulgaricus during batch culture. Appl. Biochem. Biotechnol. https://doi.org/10.1007/s12010-020-03459-8.

Cheng, H., 2010. Volatile flavor compounds in yogurt: a review. Crit. Rev. Food Sci. Nutr. 50 (10), 938–950. https://doi.org/10.1080/10408390903044081.

De Brabandere, A.G., De Baerdemaeker, J.G., 1999. Effects of process conditions on the ph development during yogurt fermentation. J. Food Eng. 41 (3), 221–227. https://doi.org/10.1016/S0260-8774(99)00096-5. ⟨http://www.sciencedirect.com/science/article/pii/S0260877499000965⟩.

El Kafsi, H., Binesse, J., Loux, V., Buratti, J., Boudebbouze, S., Dervyn, R., Kennedy, S., Galleron, N., Quinquis, B., Batto, J.M., Moumen, B., Maguin, E., van de Guchte, M., 2014. Lactobacillus delbrueckii ssp. lactis and ssp. bulgaricus: a chronicle of evolution in action. BMC Genom. 15, 407. https://doi.org/10.1186/1471-2164-15-407.

Even, S., Lindley, N.D., Loubière, P., Cocaign-Bousquet, M., 2002. Dynamic response of catabolic pathways to autoacidification in lactococcus lactis: transcript profiling and stability in relation to metabolic and energetic constraints. Mol. Microbiol. 45 (4), 1143–1152. https://doi.org/10.1046/j.1365-2958.2002.03086.x.

Even, S., Lindley, N.D., Cocaign-Bousquet, M., 2003. Transcriptional, translational and metabolic regulation of glycolysis in lactococcus lactis subsp. cremoris mg 1363 grown in continuous acidic cultures. Microbiology 149 (Pt 7), 1935–1944. https://doi.org/10.1099/mic.0.26146-0.

Fernández, M., Zúñiga, M., 2006. Amino acid catabolic pathways of lactic acid bacteria. Crit. Rev. Microbiol. 32 (3), 155–183. https://doi.org/10.1080/10408410600880643.

Foucaud, C., Poolman, B., 1992. Lactose transport system of streptococcus thermophilus. functional reconstitution of the protein and characterization of the kinetic mechanism of transport. J. Biol. Chem. 267 (31), 22087–22094.

Gaggia, F., Di Gioia, D., Baffoni, L., Biavati, B., 2011. The role of protective and probiotic cultures in food and feed and their impact on food safety. Trends Food Sci. Technol. 22, S58–S66. https://doi.org/10.1016/j.tifs.2011.03.003. ⟨http://www.sciencedirect.com/science/article/pii/S0924224411000409⟩.

Gentès, M.-C., St-Gelais, D., Turgeon, S.L., 2013. Exopolysaccharide–milk protein interactions in a dairy model system simulating yoghurt conditions. Dairy Sci. Technol. 93 (3), 255–271. https://doi.org/10.1007/s13594-013-0121-x.

Goel, A., Santos, F., de Vos, W.M., Teusink, B., Molenaar, D., 2012. Standardized assay medium to measure lactococcus lactis enzyme activities while mimicking intracellular conditions. Appl. Environ. Microbiol. 78 (1), 134–143. https://doi.org/10.1128/aem.05276-11. ⟨https://aem.asm.org/content/aem/78/1/134.full.pdf⟩.

Goward, C.R., Hartwell, R., Atkinson, T., Scawen, M.D., 1986. The purification and characterization of glucokinase from the thermophile bacillus stearothermophilus. Biochem. J. 237 (2), 415–420. https://doi.org/10.1042/bj2370415.

Hao, P., Zheng, H., Yu, Y., Ding, G., Gu, W., Chen, S., Yu, Z., Ren, S., Oda, M., Konno, T., Wang, S., Li, X., Ji, Z.-S., Zhao, G., 2011. Complete sequencing and pan-genomic analysis of lactobacillus delbrueckii subsp. bulgaricus reveal its genetic basis for industrial yogurt production. PLoS ONE 6 (1), e15964. https://doi.org/10.1371/journal.pone.0015964.

Hauser, M.J., 2022. Synchronisation of glycolytic activity in yeast cells. Curr. Genet. 68 (1), 69–81.

Hickey, M.W., Hillier, A.J., Jago, G.R., 1986. Transport and metabolism of lactose, glucose, and galactose in homofermentative lactobacilli. Appl. Environ. Microbiol 51 (4), 825–831.

Hoops, S., Sahle, S., Gauges, R., Lee, C., Pahle, J., Simus, N., Singhal, M., Xu, L., Mendes, P., Kummer, U., 2006. Copasi–a complex pathway simulator. Bioinformatics 22 (24), 3067–3074. https://doi.org/10.1093/bioinformatics/btl485.

Hutkins, R.W., 2007. Microbiology and technology of fermented foods. Microbiol. Technol. Ferment. Foods 1–473. https://doi.org/10.1002/9780470277515.

Hutkins, R.W., Nannen, N.L., 1993. ph homeostasis in lactic acid bacteria1. J. Dairy Sci. 76 (8), 2354–2365. https://doi.org/10.3168/jds.S0022-0302(93)77573-6. ⟨http://www.sciencedirect.com/science/article/pii/S0022030293775736⟩.

Kanehisa, M., 2019. Toward understanding the origin and evolution of cellular organisms. Protein Sci. 28 (11), 1947–1951. https://doi.org/10.1002/pro.3715.

Kanehisa, M., Goto, S., 2000. Kegg: kyoto encyclopedia of genes and genomes. Nucleic Acids Res 28 (1), 27–30. https://doi.org/10.1093/nar/28.1.27.

Kanehisa, M., Sato, Y., Furumichi, M., Morishima, K., Tanabe, M., 2019. New approach for understanding genome variations in kegg. Nucleic Acids Res 47 (D1), D590–D595. https://doi.org/10.1093/nar/gky962.

Kudo, H., Sasaki, Y., 2019. Intracellular ph determination for the study of acid tolerance of lactic acid bacteria. Methods Mol. Biol. 1887, 33–41. https://doi.org/10.1007/978-1-4939-8907-2_4.

Le Bras, G., Deville-Bonne, D., Garel, J.R., 1991. Purification and properties of the phosphofructokinase from lactobacillus bulgaricus. a non-allosteric analog of the enzyme from escherichia coli. Eur. J. Biochem 198 (3), 683–687. https://doi.org/10.1111/j.1432-1033.1991.tb16067.x.

Liebermeister, W., Klipp, E., 2006. Bringing metabolic networks to life: convenience rate law and thermodynamic constraints. Theor. Biol. Med. Model. 3, 41. https://doi.org/10.1186/1742-4682-3-41. ⟨https://pubmed.ncbi.nlm.nih.gov/17173669⟩. https://www.ncbi.nlm.nih.gov/pmc/articles/PMC1781438/.

Liu, E., Hao, P., Konno, T., Yu, Y., Oda, M., Zheng, H., Ji, Z.-S., 2012. Amino acid biosynthesis and proteolysis in *Lactobacillus Bulgaricus* revisited: A genomic comparison. Comput. Mol. Biosci. 02 (03), 61–77. https://doi.org/10.4236/cmb.2012.23006.

E. Liu , H. Zheng , P. Hao , T. Konno , H. Kume , luyi Ye , M. Oda , K. Suzuki , Z.-S. Ji Acquisition of amino acids by lactobacillus delbrueckii subsp. bulgaricus 2038 when grown in the presence of casein, International Dairy Journal 35(2) (2014) 145–152.10.1016/j.idairyj.2013.11.006.

Luzia, L., Lao-Martil, D., Savakis, P., van Heerden, J., van Riel, N., Teusink, B., 2022. pH dependencies of glycolytic enzymes of yeast under in vivo -like assay conditions. FEBS J. 289 (19), 6021–6037. https://doi.org/10.1111/febs.16459.

Mahon, M.J., 2011. pHluorin2: an enhanced, ratiometric, pH-sensitive green florescent protein. Adv. Biosci. Biotechnol. 02 (03), 132–137. https://doi.org/10.4236/abb.2011.23021.

Maloney, P.C., 1979. Membrane h+ conductance of streptococcus lactis. J. Bacteriol. 140 (1), 197–205. ⟨https://pubmed.ncbi.nlm.nih.gov/40951⟩. https://www.ncbi.nlm.nih.gov/pmc/articles/PMC216796/.

Mercade, M., Lindley, N., Loubiere, P., 2000. Metabolism of lactococcus lactis subsp. cremoris mg 1363 in acid stress conditions. Int. J. Food Microbiol. 55, 161–165. https://doi.org/10.1016/S0168-1605(00)00190-2.

Mercade, M., Duperray, F., Loubiére, P., 2003. Energetic analysis of cultures of lactobacillus delbrueckii subsp. bulgaricus: identification of the type of control between catabolism and anabolism. Le. Lait. 84 (1–2), 39–47. https://doi.org/10.1051/lait:2003032.

Millat, T., Janssen, H., Bahl, H., Fischer, R.-J., Wolkenhauer, O., 2013. Integrative modelling of pH-dependent enzyme activity and transcriptomic regulation of the acetone-butanol-ethanol fermentation of *Clostridium acetobutylicum* in continuous culture. Microb. Biotechnol. 6 (5), 526–539. https://doi.org/10.1111/1751-7915.12033.

Neves, A.R., Ventura, R., Mansour, N., Shearman, C., Gasson, M.J., Maycock, C., Ramos, A., Santos, H., 2002. Is the glycolytic flux in lactococcus lactis primarily controlled by the redox charge? kinetics of nad(+) and nadh pools determined in vivo by ^{13}c nmr. J. Biol. Chem. 277 (31), 28088–28098. https://doi.org/10.1074/jbc.M202573200.

Nguyen, T.-T., Nguyen, H.A., Arreola, S.L., Mlynek, G., Djinović-Carugo, K., Mathiesen, G., Nguyen, T.-H., Haltrích, D., 2012. Homodimeric -galactosidase from lactobacillus delbrueckii subsp. bulgaricus dsm 20081: expression in lactobacillus plantarum and biochemical characterization. J. Agric. Food Chem. 60 (7), 1713–1721. https://doi.org/10.1021/jf203909e. ⟨https://pubmed.ncbi.nlm.nih.gov/22283494⟩. https://www.ncbi.nlm.nih.gov/pmc/articles/PMC3284191/.

Paricharttanakul, N.M., Ye, S., Menefee, A.L., Javid-Majd, F., Sacchettini, J.C., Reinhart, G.D., 2005. Kinetic and structural characterization of phosphofructokinase from lactobacillus bulgaricus. Biochemistry 44 (46), 15280–15286. https://doi.org/10.1021/bi051283g.

Pedregosa, F., Varoquaux, G., Gramfort, A., Michel, V., Thirion, B., Grisel, O., Blondel, M., Prettenhofer, P., Weiss, R., Dubourg, V., Vanderplas, J., Passos, A., Cournapeau, D., Brucher, M., Perrot, M., Duchesnay, E., 2011. Scikit-learn: machine learning in python. J. Mach. Learn. Res. 12 (null), 2825–2830.

Pessione, A., Lamberti, C., Pessione, E., 2010. Proteomics as a tool for studying energy metabolism in lactic acid bacteria. Mol. Biosyst. 6 (8), 1419. https://doi.org/10.1039/c001948h.

Poolman, B., Royer, T.J., Mainzer, S.E., Schmidt, B.F., 1989. Lactose transport system of streptococcus thermophilus: a hybrid protein with homology to the melibiose carrier and enzyme iii of phosphoenolpyruvate-dependent phosphotransferase systems. J. Bacteriol. 171 (1), 244–253.

Ramos, J.R.C., Rath, A.G., Genzel, Y., Sandig, V., Reichl, U., 2020. A dynamic model linking cell growth to intracellular metabolism and extracellular by-product accumulation. Biotechnol. Bioeng. 117 (5), 1533–1553. https://doi.org/10.1002/bit.27288.

Rault, A., Bouix, M., Béal, C., 2008. Dynamic analysis of lactobacillus delbrueckii subsp. bulgaricus cfl1 physiological characteristics during fermentation. Appl. Microbiol. Biotechnol. 81 (3), 559–570. https://doi.org/10.1007/s00253-008-1699-4.

Rault, A., Bouix, M., Béal, C., 2009. Fermentation ph influences the physiological-state dynamics of lactobacillus bulgaricus cfl1 during ph-controlled culture. Appl. Environ. Microbiol. 75 (13), 4374–4381. https://doi.org/10.1128/AEM.02725-08. ⟨https://pubmed.ncbi.nlm.nih.gov/19429565⟩. https://www.ncbi.nlm.nih.gov/pmc/articles/PMC2704822/.

Russell, J.B., Diez-Gonzalez, F., 1997. The effects of fermentation acids on bacterial growth. In: Advances in Microbial Physiology. Elsevier, pp. 205–234. https://doi.org/10.1016/s0065-2911(08)60017-x.

Sańchez, C., Neves, A.R., o Cavalheiro, J., dos Santos, M.M., Garciá-Quintańs, N., Lopéz, P., Santos, H., 2008. Contribution of citrate metabolism to the growth of *Lactococcus lactis* crl264 at low ph. Appl. Environ. Microbiol. 74 (4), 1136–1144. https://doi.org/10.1128/aem.01061-07.

Schindelin, J., Arganda-Carreras, I., Frise, E., Kaynig, V., Longair, M., Pietzsch, T., Preibisch, S., Rueden, C., Saalfeld, S., Schmid, B., Tinevez, J.-Y., White, D.J., Hartenstein, V., Eliceiri, K., Tomancak, P., Cardona, A., 2012. Fiji: an open-source platform for biological-image analysis. Nat. Methods 9, 676–682. https://doi.org/10.1038/nmeth.2019.

Schneider, C.A., Rasband, W.S., Eliceiri, K.W., 2012. Nih image to imagej: 25 years of image analysis. Nat. Methods 9, 671–675. https://doi.org/10.1038/nmeth.2089.

Shabala, L., McMeekin, T., Budde, B.B., Siegumfeldt, H., 2006. Listeria innocua and lactobacillus delbrueckii subsp. bulgaricus employ different strategies to cope with acid stress. Int J. Food Microbiol 110 (1), 1–7. https://doi.org/10.1016/j.ijfoodmicro.2006.01.026.

Siegumfeldt, H., Rechinger, K., Jakobsen, M., 1999. Use of fluorescence ratio imaging for intracellular ph determination of individual bacterial cells in mixed cultures. Microbiology 145 (Pt 7), 1703–1709. https://doi.org/10.1099/13500872-145-7-1703.

Siegumfeldt, H., Björn Rechinger, K., Jakobsen, M., 2000. Dynamic changes of intracellular ph in individual lactic acid bacterium cells in response to a rapid drop in extracellular ph. Appl. Environ. Microbiol. 66 (6), 2330–2335. https://doi.org/10.1128/aem.66.6.2330-2335.2000. ⟨https://pubmed.ncbi.nlm.nih.gov/10831407⟩. https://www.ncbi.nlm.nih.gov/pmc/articles/PMC110524/.

Ulmer, A, Erdemann, F., Mueller, S., Loesch, M., Wildt, S., Jensen, M.L., Gaspar, P., Zeidan, A.A., Takors, R., 2022. Differential amino acid uptake and depletion in mono-cultures and co-cultures of streptococcus thermophilus and lactobacillus delbrueckii subsp. bulgaricus in a novel semi-synthetic medium. Microorganisms 10 (9). https://doi.org/10.3390/microorganisms10091771. ⟨https://www.mdpi.com/2076-2607/10/9/1771⟩.

Ulmer, A., Veit, S., Erdemann, F., Freund, A., Loesch, M., Teleki, A., Zeidan, A.A., Takors, R., 2023. A two-compartment fermentation system to quantify strain-specific interactions in microbial co-cultures. Bioengineering 10 (1). https://doi.org/10.3390/bioengineering10010103. ⟨https://www.mdpi.com/2306-5354/10/1/103⟩.

Vinnakota, K., Kemp, M.L., Kushmerick, M.J., 2006. Dynamics of muscle glycogenolysis modeled with pH time course computation and pH-dependent reaction equilibria and enzyme kinetics. Biophys. J. 91 (4), 1264–1287. https://doi.org/10.1529/biophysj.105.073296.

de Vos, W.M., Vaughan, E.E., 1994. Genetics of lactose utilization in lactic acid bacteria. FEMS Microbiol Rev. 15 (2–3), 217–237. https://doi.org/10.1111/j.1574-6976.1994.tb00136.x.

Welman, A.D., Maddox, I.S., 2003. Fermentation performance of an exopolysaccharide-producing strain of Lactobacillus delbrueckii subsp. bulgaricus. J. Ind. Microbiol. Biotechnol. 30 (11), 661–668. https://doi.org/10.1007/s10295-003-0095-4.

Wittig, U., Kania, R., Golebiewski, M., Rey, M., Shi, L., Jong, L., Algaa, E., Weidemann, A., Sauer-Danzwith, H., Mir, S., Krebs, O., Bittkowski, M., Wetsch, E., Rojas, I., Müller, W., 2011. Sabio-rk—database for biochemical reaction kinetics. Nucleic Acids Res. 40 (D1), D790–D796. https://doi.org/10.1093/nar/gkr1046.

Zheng, H., Liu, E., Hao, P., Konno, T., Oda, M., Ji, Z.-S., 2012. In silico analysis of amino acid biosynthesis and proteolysis in lactobacillus delbrueckii subsp. bulgaricus 2038 and the implications for bovine milk fermentation. Biotechnol. Lett. 34 (8), 1545–1551. https://doi.org/10.1007/s10529-012-1006-4.

Appendix E

Supplements: Integration of proteomics and metabolomics into a genome-scale metabolic model of *Lactobacillus bulgaricus* identifies unique adaptations to protein-rich environment
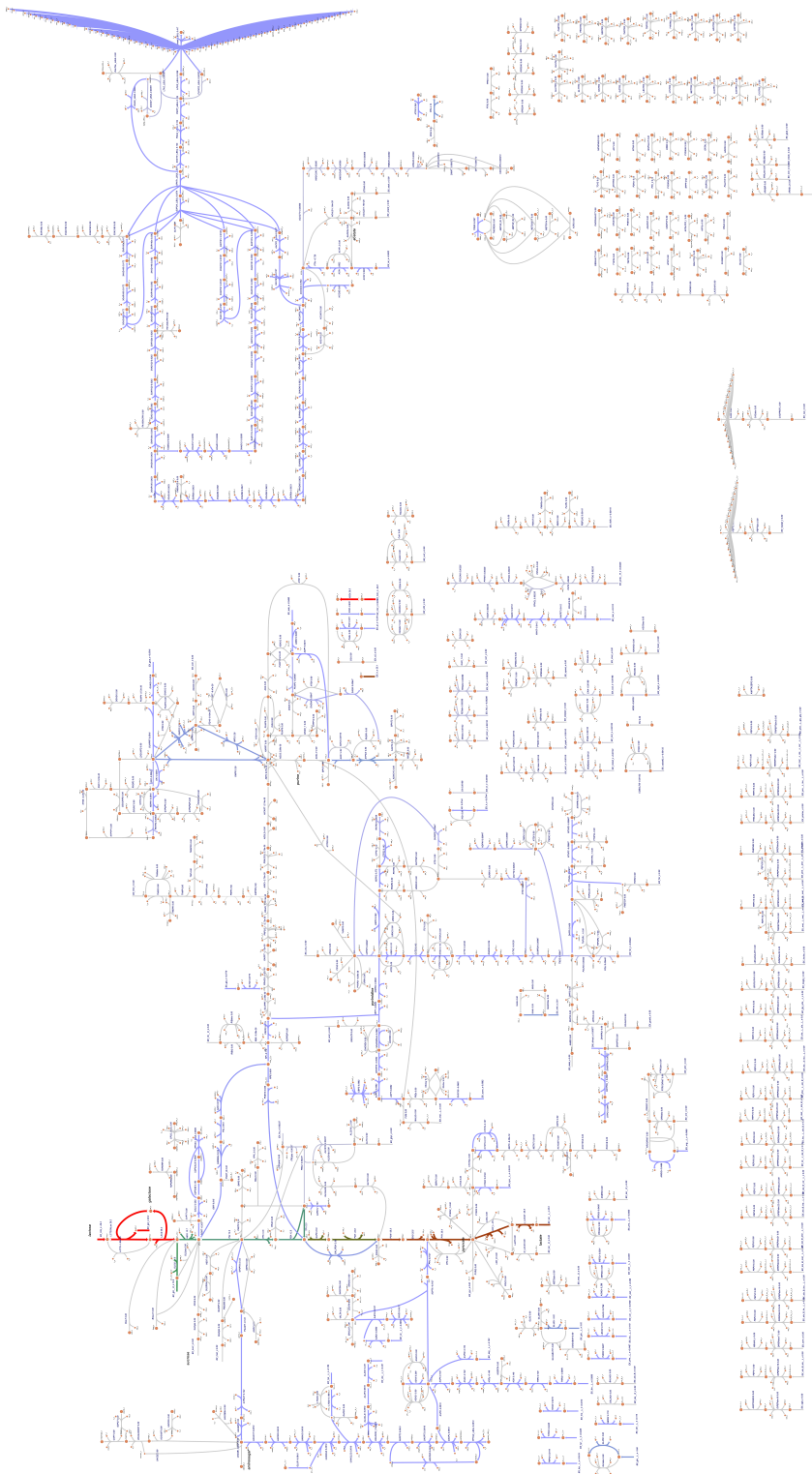
Figure E.1: Supplementary Material S1: Escher map for the entire GEM of *L. bulgaricus*
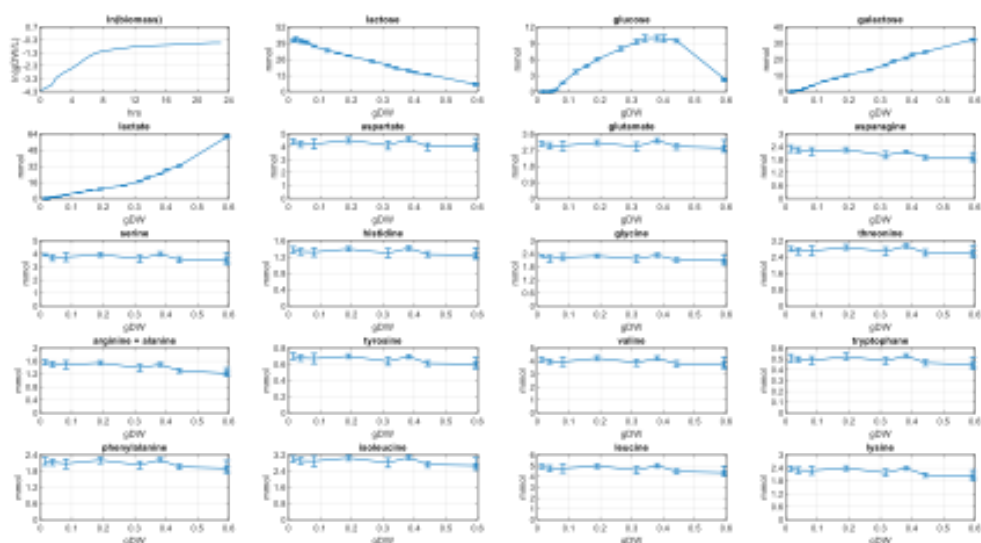
Figure E.2: Supplementary Figure S2. Concentration of metabolites plotted against biomass concentration, for *L. bulgaricus* growing on amino acids
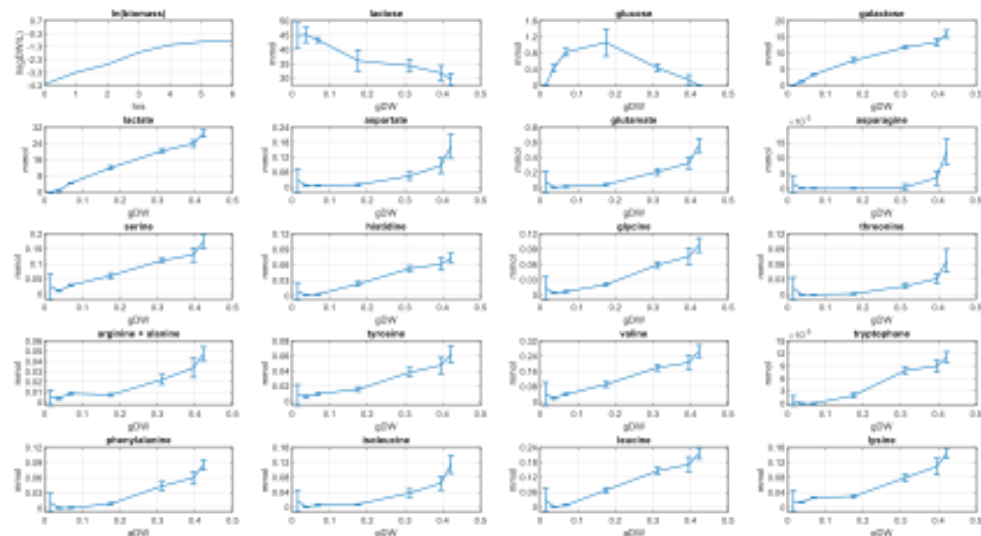

Figure E.3: Supplementary Figure S3. Concentration of metabolites plotted against biomass concentration, for *L. bulgaricus* growing on casein.